

XBeach skillbed report: XBeach 1.14 Halloween

status update trunk_default, revision 6057



XBeach skillbed report: XBeach 1.14 Halloween

status update trunk_default, revision 6057

Authors

Deltares

XBeach skillbed report: XBeach 1.14 Halloween

status update trunk_default, revision 6057

Client	
Contact	
Reference	
Keywords	XBeach, Surfbeat, Infragravity waves, Dune erosion, Non-hydrostatic wave model

Document control

Version	6057
Date	
Project number	
Document ID	XBeach
Pages	152
Status	Final

Author(s)

	XBeach team	

Summary

This document contains the XBeach testbed. The testbed includes implementations tests, but also validation tests related to the hydrodynamics and morphodynamics. The accuracy of the model is both validated with field measurements, laboratory experiments or analytical solutions.

Contents

Summary	4	
List of Tables	7	
List of Figures	10	
1	Introduction	17
1.1	Introduction to the XBeach model	17
1.2	Model approach and innovations	18
1.3	XBeach skillbed	19
2	Implementation tests	20
2.1	Curvilinear	20
2.2	Long wave propagation	21
2.3	1D wave runup (analytical solution)	23
2.4	Longcrested refraction2	24
2.5	Dambreak	25
2.5.1	1D dam break test	25
2.5.2	Tide	26
2.5.3	Blankenberge	27
2.6	River outflow	28
2.7	Drifters	29
2.8	Multiple sediment fractions	30
3	Hydrodynamic tests	32
3.1	Specific tests	32
3.2	2D wave runup	32
3.3	Surfbeat	34
3.3.1	High- and low-frequency wave transformation over barred beach	34
3.3.2	High- and low-frequency wave transformation over sloping beach	38
3.4	Nonhydrostatic	41
3.4.1	High- and low-frequency wave transformation over barred beach	41
3.4.2	High- and low-frequency wave transformation over fringing reef	44
3.4.3	Bichromatic waves	49
4	Hydrodynamic field cases	53
4.1	Ningaloo Reef	53
4.2	DELILAH	55
4.3	Schiermonnikoog	56
4.4	Saint-Trojan	61
5	Morphological laboratory tests	67
5.1	M1263 III: Delta Flume 1980-1981	69
5.2	DeltaflumeH298 (Revetments)	76
5.3	LIP11D: Delta Flume 1994	78
5.3.1	Detailed results	80
5.3.2	Bar evolution	82
5.4	Deltaflume H4731	83
5.5	Grosse Wellen Kanal 1998	85
5.6	M1797: Delta Flume 1981	91
5.7	H4357: Delta Flume 2006	92
5.7.0.1	Spectral shape	97

5.7.1	Double dune system	101
6	Field validation	103
6.1	Egmond	103
6.2	Vlaanderen	109
6.3	Vedersoe	112
6.4	Fire-Island	115
6.5	Langeoog	119
6.6	Holland 1976	122
6.7	Holland 1953	126
6.8	Erosion and overwash of Asseteague Island	128
6.9	Breach growth at Zwin	129
7	Specific functionalities	132
7.1	Gravel (XBeach-G)	132
7.2	Vegetation	133
8	References	135
A	Model Performance Statistics	141
A.1	Introduction	141
A.2	MPS parameters	141
A.3	Mean Error & Standard Deviation	141
A.4	Correlation coefficient	142
A.5	Relative Bias	142
A.6	Scatter Index	142
A.7	Brier Skill Score	142
A.8	Brier Skill Score (Murphy and Epstein, 1989)	143
B	Overview	145

List of Tables

2.1	The XBeach and analytical wave heights and wave lengths. The amplitude without reflection is computed for the period t=0 to t=600s. The amplitude for the standing wave pattern is computed for the period t=500 to t=1200. The amplitude is defined as the maximum water level/velocity in the domain for the given time period.	23
2.2	The maximum and minimum surface elevation and velocities in the runup.	24
3.1	Error statistics Zelt Case 1	34
3.2	The Boers (1996) wave conditions.	35
3.3	The statistical scores for the Boers experiments. The scatter index (SCI) and relative bias (rel. bias) are shown for the short-wave height, infragravity wave height and setup.	38
3.4	The statistical scores for the GLOBEX experiments. The scatter index (SCI) and relative bias (rel. bias) are shown for the short-wave height, infragravity wave height and setup.	41
3.5	The Boers (1996) wave conditions.	42
3.6	The statistical scores for the Boers experiments. The scatter index (SCI) and relative bias (rel. bias) are shown for the short-wave height, infragravity wave height and spectral period.	44
3.7	Specifics for considered test within XBeach testbed	45
3.8	The statistical scores for the Buckley experiments. The scatter index (SCI) and relative bias (rel. bias) are shown for the short-wave height, infragravity wave height and setup.	49
3.9	Wave conditions for the three tests (Van Noorloos, 2003) which are modelled with XBeach. f_1 and f_2 are the primary wave frequency, f_b is the bound wave frequency and kd the maximum normalized water depth	50
3.10	The statistical scores for the Van Noorloos experiments. The scatter index (SCI) and relative bias (rel. bias) are shown for the short-wave height, infragravity wave height and spectral period.	52
4.1		56
4.2	Goodness-of-fit (GoF) indicators for the modelled water depth [m] and the spectral significant wave height [m] for high frequency and infragravity waves compared to the measurements.	61
4.3	Goodness-of-fit (GoF) indicators for the modelled water depth [m] and the high- and low frequency wave heights [m] compared to the measurements at the PT1 to PT8 (seaward to landward side of measurement transect).	65
5.1	Overview of experiments	69
5.2	The computed and observed volume (V) and berm slopes (S) for Test-1. Volumes (V) are given in m^3/m . The relative error is expressed in a percentage. Both the relative error in terms of the same time (rel, t) and the final time are shown (rel).	71
5.3	The computed and observed volume (V) and berm slopes (S) for Test-2. Volumes (V) are given in m^3/m . The relative error is expressed in a percentage. Both the relative error in terms of the same time (rel, t) and the final time are shown (rel).	72
5.4	The computed and observed volume (V) and berm slopes (S) for Test-3. Volumes (V) are given in m^3/m . The relative error is expressed in a percentage. Both the relative error in terms of the same time (rel, t) and the final time are shown (rel).	73

5.5	The computed and observed volume (V) and berm slopes (S) for Test-4. Volumes (V) are given in m^3/m . The relative error is expressed in a percentage. Both the relative error in terms of the same time (rel, t) and the final time are shown (rel).	74
5.6	The computed and observed volume (V) and berm slopes (S) for Test-5. Volumes (V) are given in m^3/m . The relative error is expressed in a percentage. Both the relative error in terms of the same time (rel, t) and the final time are shown (rel).	75
5.7	M1263 III statistical scores.	76
5.8	Overview of experiments	77
5.9	The computed and observed volume (V) and berm slopes (S) for 2E. Volumes (V) are given in m^3/m . The relative error is expressed in a percentage. Both the relative error in terms of the same time (rel, t) and the final time are shown (rel).	80
5.10	Overview of experiments	82
5.11	The computed and observed volume (V) and berm slopes (S) for T14. Volumes (V) are given in m^3/m . The relative error is expressed in a percentage. Both the relative error in terms of the same time (rel, t) and the final time are shown (rel).	84
5.12	The computed and observed volume (V) and berm slopes (S) for A9. Volumes (V) are given in m^3/m . The relative error is expressed in a percentage. Both the relative error in terms of the same time (rel, t) and the final time are shown (rel).	86
5.13	The computed and observed volume (V) and berm slopes (S) for B2. Volumes (V) are given in m^3/m . The relative error is expressed in a percentage. Both the relative error in terms of the same time (rel, t) and the final time are shown (rel).	87
5.14	The computed and observed volume (V) and berm slopes (S) for C2. Volumes (V) are given in m^3/m . The relative error is expressed in a percentage. Both the relative error in terms of the same time (rel, t) and the final time are shown (rel).	88
5.15	The computed and observed volume (V) and berm slopes (S) for F1. Volumes (V) are given in m^3/m . The relative error is expressed in a percentage. Both the relative error in terms of the same time (rel, t) and the final time are shown (rel).	89
5.16	The computed and observed volume (V) and berm slopes (S) for H2. Volumes (V) are given in m^3/m . The relative error is expressed in a percentage. Both the relative error in terms of the same time (rel, t) and the final time are shown (rel).	90
5.17	Statistical scores for the Grosse Wellen Kanal experiments.	91
5.18	The computed and observed volume (V) and berm slopes (S) for T01. Volumes (V) are given in m^3/m . The relative error is expressed in a percentage. Both the relative error in terms of the same time (rel, t) and the final time are shown (rel).	91
5.19	Overview of experiments	92
5.20	The computed and observed volume (V) and berm slopes (S) for T01. Volumes (V) are given in m^3/m . The relative error is expressed in a percentage. Both the relative error in terms of the same time (rel, t) and the final time are shown (rel).	93
5.21	The computed and observed volume (V) and berm slopes (S) for T02. Volumes (V) are given in m^3/m . The relative error is expressed in a percentage. Both the relative error in terms of the same time (rel, t) and the final time are shown (rel).	94
5.22	The computed and observed volume (V) and berm slopes (S) for T03. Volumes (V) are given in m^3/m . The relative error is expressed in a percentage. Both the relative error in terms of the same time (rel, t) and the final time are shown (rel).	95
5.23	The computed and observed volume (V) and berm slopes (S) for T08. Volumes (V) are given in m^3/m . The relative error is expressed in a percentage. Both the relative error in terms of the same time (rel, t) and the final time are shown (rel).	96
5.24	Deltagoot 2006 statistical scores.	97
5.25	Wave dissipation parameter settings	97
6.1	A quantitative comparison of modelled and observed erosion volumes [m^3/m] and dune retreat [m] at 3m + NAP for all 7 profiles.	108

6.2	Dune erosion volume [m^3/m] and retreat distance [m] at 7 m +TAW for the Sint Nicholas storm in the XBeach simulation and the measured profiles for the 15 selected profiles along the Flemish coast.	111
6.3	A quantitative comparison of modelled and observed erosion volumes [m^3/m] and dune retreat [m] at 5m + MSL for both profiles	115
6.4	Modeled and measured erosion volumes [m^3/m] and retreat distances [m] at 3 m +NAVD88 in absolute values. NaN means that no dune retreat could be determined, i.e. the dune has breached.	117
6.5	A quantitative comparison of modelled and observed erosion volumes [m^3/m] and dune retreat [m] at 5 m +NHN for all 6 profiles	121
6.6	Dune erosion volume [m^3/m] and retreat distance [m] for the 1976 storm in the XBeach simulation and the measured profiles for the 30 profiles along the northern Dutch coast. The Veromeas of profiles with insufficient measured data is indicated with a NaN.	124
6.7	Hydrodynamic boundary conditions XBeach simulations	129
A.1	MPS parameters	141
A.2	Brier Skill Score quantification (Van Rijn <i>et al.</i> , 2003)	143
A.3	Brier Skill Score decomposition factors (Murphy and Epstein, 1989)	144
A.4	Brier Skill Score (Murphy and Epstein, 1989) quantification (Van Rijn <i>et al.</i> , 2003)	144
B.1	Status overview skillbed tests	145
B.1	Status overview skillbed tests	146
B.1	Status overview skillbed tests	147
B.1	Status overview skillbed tests	148
B.1	Status overview skillbed tests	149
B.1	Status overview skillbed tests	150
B.1	Status overview skillbed tests	151

List of Figures

2.1	Snapshot of the RMS wave height and the flow velocity field in the last time step	20
2.2	Mean values of the RMS wave height and the flow velocity field	21
2.3	Water levels and velocities from the start of the experiment until the wave just reaches the end of the flume. The amplitude of the analytical solution is shown with a red line.	22
2.4	Snapshots of water levels and velocities showing a standing wave pattern. The amplitude of the analytical solution is shown with a red line.	22
2.5	Snapshots of water level and velocity	24
2.6	Wave energy, direction and flow velocities for different sized of theta bins.	25
2.7	Refraction with different sizes of theta bins. The red dotted line indicates the solution according to Snel law.	25
2.8	The results of the 1D dam break test with dry bed after 5 seconds.	26
2.9	The results of the 1D dam break test with wet bed ($h=0.1\text{m}$) after 5 seconds.	26
2.10	The lower-left panel shows the tidal timeseries imposed to the offshore corners of the model (dots) and the generated waterlevels at these locations (lines). For six moments indicated with the black vertical lines, the flow field is shown in the upper panels.	27
2.11	The lower-left panel shows the tidal timeseries imposed to the offshore corners of the model (dots) and the generated waterlevels at these locations (lines). For six moments indicated with the black vertical lines, the flow field is shown in the upper panels.	28
2.12	Final bathymetry	29
2.13	Drifter paths after 50, 100, 150 and 450 seconds	29
2.14	Initial bathymetry and sediment distribution	30
2.15	Final bathymetry and sediment distribution	31
2.16	Profile development	31
3.1	Definition sketch of concave beach bathymetry	32
3.2	Normalized vertical runup in time (panel 1) and maximum and minimum values (panel 2)	34
3.3	Locations of surface elevation measurements	35
3.4	Wave hydrodynamics during experiment 1A. The observed short-wave height (dots) and observed infragravity wave height (triangles) are compared to the XBeach results (blue and red line) in the upper panel. The observed setup (dots) is compared to the setup computed with XBeach (blue line) in the second panel and the bathymetry is shown in the third panel.	36
3.5	Wave hydrodynamics during experiment 1B. The observed short-wave height (dots) and observed infragravity wave height (triangles) are compared to the XBeach results (blue and red line) in the upper panel. The observed setup (dots) is compared to the setup computed with XBeach (blue line) in the second panel and the bathymetry is shown in the third panel.	36
3.6	Wave hydrodynamics during experiment 1C. The observed short-wave height (dots) and observed infragravity wave height (triangles) are compared to the XBeach results (blue and red line) in the upper panel. The observed setup (dots) is compared to the setup computed with XBeach (blue line) in the second panel and the bathymetry is shown in the third panel.	37
3.7	Overview of the statistical scores of the Boers experiments. The relative error and scatter index for the short-wave height (upper panel), infragravity wave height (second panel) and setup (third panel) are shown for the different Boers experiments.	37

3.8	Elevation z versus cross-shore distance x in the Scheldegoot during the GLOBEX project. Here, $x = 0$ is the location of the wave-maker at rest, and $z = 0$ corresponds to the still water level. At $x = 84.6$ m the still water level intersected with the bed. The 190 dots are the positions of the wave gauges.	38
3.9	Wave hydrodynamics during experiment A1. The observed short-wave height (dots) and observed infragravity wave height (triangles) are compared to the XBeach results (blue and red line) in the upper panel. The observed setup (dots) is compared to the setup computed with XBeach (blue line) in the second panel and the bathymetry is shown in the third panel.	39
3.10	Wave hydrodynamics during experiment A2. The observed short-wave height (dots) and observed infragravity wave height (triangles) are compared to the XBeach results (blue and red line) in the upper panel. The observed setup (dots) is compared to the setup computed with XBeach (blue line) in the second panel and the bathymetry is shown in the third panel.	39
3.11	Wave hydrodynamics during experiment A3. The observed short-wave height (dots) and observed infragravity wave height (triangles) are compared to the XBeach results (blue and red line) in the upper panel. The observed setup (dots) is compared to the setup computed with XBeach (blue line) in the second panel and the bathymetry is shown in the third panel.	40
3.12	Overview of the statistical scores of the GLOBEX experiments. The relative error and scatter index for the short-wave height (upper panel), infragravity wave height (second panel) and setup (third panel) are shown for the different GLOBEX experiments.	40
3.13	Locations of surface elevation measurements	41
3.14	Wave hydrodynamics during test 1A. The top-left panel shows the model set-up. The other plots show the performance of XBeach (red) compared to the observations during the experiments (blue).	42
3.15	Wave hydrodynamics during test 1B. The top-left panel shows the model set-up. The other plots show the performance of XBeach (red) compared to the observations during the experiments (blue).	43
3.16	Wave hydrodynamics during test 1C. The top-left panel shows the model set-up. The other plots show the performance of XBeach (red) compared to the observations during the experiments (blue).	44
3.17	Schematic of the fringing reef showing the reef slope (1:5), reef flat length (14 m; 500-m field scale), beach slope (1:12), and instrument locations. Directional measurement sites have collocated water level and velocity measurements, whereas other nondirectional sites have only water level measurements. (b) An example of the wave setup profile in the vicinity of the reef crest, defining the still water depth h_0 and the total water depth.	45
3.18	Wave hydrodynamics during test 1. The top-left panel shows the model set-up. The other plots show the performance of XBeach (red) compared to the observations during the experiments (blue).	46
3.19	Wave hydrodynamics during test 2. The top-left panel shows the model set-up. The other plots show the performance of XBeach (red) compared to the observations during the experiments (blue).	47
3.20	Wave hydrodynamics during test 9. The top-left panel shows the model set-up. The other plots show the performance of XBeach (red) compared to the observations during the experiments (blue).	48
3.21	Wave hydrodynamics during test 12. The top-left panel shows the model set-up. The other plots show the performance of XBeach (red) compared to the observations during the experiments (blue).	49
3.22	The upper panel shows the measured (blue dots) and modeled (red line) total wave height. The lower panel shows the filtered bound long wave of the measurements (blue dots) and the XBeach results (red line).	50

3.23	The upper panel shows the measured (blue dots) and modeled (red line) total wave height. The lower panel shows the filtered bound long wave of the measurements (blue dots) and the XBeach results (red line).	51
3.24	The upper panel shows the measured (blue dots) and modeled (red line) total wave height. The lower panel shows the filtered bound long wave of the measurements (blue dots) and the XBeach results (red line).	51
4.1	Cross-shore profile of the bathymetry along the main measurement transect with instrument locations shown.	54
4.2	Comparison between the 1D model results (blue) and measured data (red) for the duration of the 5 day swell event. (a,f,k) are for instrument C1, (b,g,l) C3, (c,h,m) C4, (d,i,n) C5 and (e,j,o) C6. The peak of the storm is indicated by the red vertical line. Note the large reduction in vertical scale between C1 and the reef sites C3-C6.	54
4.3	Bias and RMS error from the 1D swell duration (5 day) model results compared with the measured data at each site, based on the short wave heights, IG wave heights, and mean water levels.	55
4.4	Bathymetry and measurement locations	55
4.5	Wave height transformation and flow velocities during the DELILAH field experiment 1990	56
4.6	Overview of the Schiermonnikoog study area. Right: elevation at and surrounding Schiermonnikoog (mosaic of the Vaklodingen of 2012-2015) and the location of the (offshore) hydraulic stations of RWS (black dots) and the transect (red line) with measurement equipment locations (red dots). Left: aerial photograph of the tail of Schiermonnikoog at 04-20-2014 (Google Earth). The coordinates are in meter (RD-new projection).	57
4.7	Cross-section with the modelled and measured water level and spectral significant wave height (H_{m0}) of high and low frequency waves during the storm peak (11-01-2015 13:00-13:30). The grey zone around the modelled $H_{m0,hf}$ indicates the minimum and maximum $H_{m0,hf}$. Note the difference between the modelled low frequency H_{m0} (no frequency domain filter) (black line) and the measured infragravity H_{m0} (0.005 and 0.05 Hz) at the point locations (grey-green dots).	59
4.8	Timeseries of measured and modelled water depth, short and infragravity spectral significant wave height including goodness-of-fit indicators for measurement location P1.	60
4.9	Scatter plot of the measured versus modelled water depth, spectral significant wave height (H_{m0}) of short waves (G) and infragravity waves (IG) for all measurement locations at Schiermonnikoog. The dashed line indicates a perfect fit, the continuous line represents a linear fit through the point cloud	60
4.10	Location of the Saint Trojan study area in the Bay of Biscay, with the Biscay buoy (OE) and Chassiron Meteorological station (OE). (b) Detailed bathymetry of the study area (m relative to mean sea level), showing the location of the offshore ADCP1 (OE) and the instrumented cross-shore profile (dashed line). The coordinates are in meter (Lambert-93 projection). Source: Bertin <i>et al.</i> (2020)	62
4.11	Cross-section at the transect location during storm peak (3rd of February 2017 at 8 AM) of the water level (upper panel), short-wave height (middle panel) and low-frequency (IG and VLF) wave height (middle panel). In blue the model results, and the observations are represented by circles. In grey the predicted minimum and maximum short-wave heights during the half hour around the peak of the storm.	63
4.12	Modeled (blue line) against observed (circles) water depth (top), short-wave height (middle) and low-frequency wave height (bottom) at PT3.	64

4.13	Modeled (blue line) against observed (circles) water depth (top), short-wave height (middle) and low-frequency wave height (bottom) at PT7.	65
4.14	Observed versus predicted (left) water levels, (middle) short-wave height $H_{m0,HF}$ and (right) low-frequency wave-height $H_{m0,LF}$.	66
5.1	Dune retreat indicator. See the Appendix for the definition of this indicator.	68
5.2	Definition of erosion volume. See the Appendix for the definition of this indicator.	68
5.3	Berm slope indicator. See the Appendix for the definition of this indicator.	68
5.4	Boundary conditions for test 3. The storm development is shown for the water level (upper panel), the wave height (second panel) and the peak period (lower panel) as a function of time.	70
5.5	Boundary conditions for test 4. The storm development is shown for the water level (upper panel), the wave height (second panel) and the peak period (lower panel) as a function of time.	70
5.6	Comparisons of profiles from experiment Test-1 for different moments in time. Observed profiles are shown with a dashed line and the XBeach profiles with a solid line. The storm surge level is shown with a black dashed line.	71
5.7	Temporal development of the relative error for the three indicators.	71
5.8	Comparisons of profiles from experiment Test-2 for different moments in time. Observed profiles are shown with a dashed line and the XBeach profiles with a solid line. The storm surge level is shown with a black dashed line.	72
5.9	Temporal development of the relative error for the three indicators.	72
5.10	Comparisons of profiles from experiment Test-3 for different moments in time. Observed profiles are shown with a dashed line and the XBeach profiles with a solid line. The storm surge level is shown with a black dashed line.	73
5.11	Temporal development of the relative error for the three indicators.	73
5.12	Comparisons of profiles from experiment Test-4 for different moments in time. Observed profiles are shown with a dashed line and the XBeach profiles with a solid line. The storm surge level is shown with a black dashed line.	74
5.13	Temporal development of the relative error for the three indicators.	74
5.14	Comparisons of profiles from experiment Test-5 for different moments in time. Observed profiles are shown with a dashed line and the XBeach profiles with a solid line. The storm surge level is shown with a black dashed line.	75
5.15	Temporal development of the relative error for the three indicators.	75
5.16	Overview of the statistical scores for M1263 experiments.	76
5.17	Profile development during test T1	77
5.18	Profile development during test T2	78
5.19	Profile development during test T3	78
5.20	Comparisons of profiles from experiment LIP 2E for different moments in time. Observed profiles are shown with a dashed line and the XBeach profiles with a solid line. The storm surge level is shown with a black dashed line.	79
5.21	Temporal development of the relative error for the three indicators.	80
5.22	Computed and observed short wave height transformation, infragravity wave height transformation and mean water level (upper panel) for test 2E. The lower panel shows the initial and final computed profiles.	81
5.23	Erosion pattern and volumes and retreat distance during test 2E	81
5.24	Erosion volumes as a function of time for test E2	82
5.25	Morphodynamics during test 1B	83
5.26	Morphodynamics during test 1C	83
5.27	Comparison of profile during experiment T14 Observed profiles are shown with a dashed line and the XBeach profiles with a solid line. The storm surge level is shown with a black dashed line.	84
5.28	Temporal development of the relative error for the three indicators.	84

5.29	Comparisons of profiles from experiment A9 for different moments in time. Observed profiles are shown with a dashed line and the XBeach profiles with a solid line. The storm surge level is shown with a black dashed line.	85
5.30	Temporal development of the relative error for the three indicators.	86
5.31	Comparisons of profiles from experiment B2 for different moments in time. Observed profiles are shown with a dashed line and the XBeach profiles with a solid line. The storm surge level is shown with a black dashed line.	86
5.32	Temporal development of the relative error for the three indicators.	87
5.33	Comparisons of profiles from experiment C2 for different moments in time. Observed profiles are shown with a dashed line and the XBeach profiles with a solid line. The storm surge level is shown with a black dashed line.	87
5.34	Temporal development of the relative error for the three indicators.	88
5.35	Comparisons of profiles from experiment F1 for different moments in time. Observed profiles are shown with a dashed line and the XBeach profiles with a solid line. The storm surge level is shown with a black dashed line.	88
5.36	Temporal development of the relative error for the three indicators.	89
5.37	Comparisons of profiles from experiment H2 for different moments in time. Observed profiles are shown with a dashed line and the XBeach profiles with a solid line. The storm surge level is shown with a black dashed line.	89
5.38	Temporal development of the relative error for the three indicators.	90
5.39	GWK overview	90
5.40	Comparison of profile during experiment T01. Observed profiles are shown with a dashed line and the XBeach profiles with a solid line. The storm surge level is shown with a black dashed line.	91
5.41	Temporal development of the relative error for the three indicators.	92
5.42	Comparisons of profiles from experiment T01 for different moments in time. Observed profiles are shown with a dashed line and the XBeach profiles with a solid line. The storm surge level is shown with a black dashed line.	93
5.43	Temporal development of the relative error for the three indicators.	93
5.44	Comparisons of profiles from experiment T02 for different moments in time. Observed profiles are shown with a dashed line and the XBeach profiles with a solid line. The storm surge level is shown with a black dashed line.	94
5.45	Temporal development of the relative error for the three indicators.	94
5.46	Comparisons of profiles from experiment T03 for different moments in time. Observed profiles are shown with a dashed line and the XBeach profiles with a solid line. The storm surge level is shown with a black dashed line.	95
5.47	Temporal development of the relative error for the three indicators.	95
5.48	Comparisons of profiles from experiment T08 for different moments in time. Observed profiles are shown with a dashed line and the XBeach profiles with a solid line. The storm surge level is shown with a black dashed line.	96
5.49	Temporal development of the relative error for the three indicators.	96
5.50	Overview of statistical scores for the Deltagoot 2006 experiments.	97
5.51	Profile development during test DP01	98
5.52	Profile development during test DP02	98
5.53	Erosion pattern and volumes and retreat distance during test DP01	98
5.54	Erosion pattern and volumes and retreat distance during test DP02	99
5.55	Hydrodynamics during test DP01	99
5.56	Hydrodynamics during test DP02	100
5.57	Velocities during test DP01	100
5.58	Velocities during test DP02	101
5.59	Profile development during test T04	102
5.60	Erosion pattern and volumes and retreat distance during test T04	102
5.61	Hydrodynamics during test T04	102

6.1	Location of study site (left panel). The beach poles form an alongshore reference line, with the km number referring to the distance to the zero point at the northern end of the Holland coast. The origin of the local coordinate system used (right panel) here is beach pole 41.25, with positive x and y in the seaward and southern direction, respectively. The crosses (x) indicate the different pressure sensors.	104
6.2	Observed water levels (black circles) against the modelled water levels (orange) for all pressure sensors. The panel in the middle shows the location of the pressure sensors, and the surrounding subpanels follow the order from North to South (top to bottom) and from sea (left) to the beach (right).	105
6.3	Observed short-wave heights (black circles) against the modelled short-wave heights (orange) for all pressure sensors. The panel in the middle shows the location of the pressure sensors, and the surrounding subpanels follow the order from North to South (top to bottom) and from sea (left) to the beach (right).	106
6.4	Observed infragravity wave heights (black circles) against the modelled infragravity wave heights (orange) for all pressure sensors. The panel in the middle shows the location of the pressure sensors, and the surrounding subpanels follow the order from North to South (top to bottom) and from sea (left) to the beach (right).	107
6.5	XBeach results for cross-shore transect 0 at Egmond aan Zee. Initial bed levels are depicted by the black dotted line, observed post-storm bed levels by the black solid line and XBeach model results are presented in red. The modelled dune erosion is shown by the red shaded area.	108
6.6	XBeach results for cross-shore transect -1755 at Egmond aan Zee. Initial bed levels are depicted by the black dotted line, observed post-storm bed levels by the black solid line and XBeach model results are presented in red. The modelled dune erosion is shown by the red shaded area.	109
6.7	Overview of the Belgian coastline with the location of the analyzed cross-shore profiles measured before and after the Sint Nicholas storm and the water level (WL) and wave measurement locations used for this case.	110
6.8	Cross-section profile nr. 119 before and after the Sint Nicholas storm based on the measurements and XBeach, including dune erosion volumes and retreat distances. Bottom: entire XBeach profile, top: zoom of beach and dune profile.	112
6.9	Location of the study area near Vedersoe (Denmark). The two different transects considered in this study are located close to each other, but different morphological behaviour is observed. Source: Kystdirektoratet (2021)	113
6.10	XBeach results for cross-shore transect Vedersoe 01 Initial bed levels are depicted by the black dashed line, observed post-storm bed levels by the black solid line and XBeach model results are presented in red. The modelled dune erosion is shown by the red shaded area, whereas the observed dune erosion is depicted with the grey shaded area.	114
6.11	XBeach results for cross-shore transect Vedersoe 02. Initial bed levels are depicted by the black dashed line, observed post-storm bed levels by the black solid line and XBeach model results are presented in red. The modelled dune erosion is shown by the red shaded area, whereas the observed dune erosion is depicted with the grey shaded area.	115
6.12	Left: Model domain extent of the nested regional D-Flow FM/SWAN model (in grey) and the XBeach model (in red): Wilderness breach. Right: observed pre-(top) and post-(middle) bathymetry and sedimentation/erosion (bottom).	116
6.13	XBeach results for cross-shore transect 005 at Fire Island. Initial bed levels are depicted by the black dotted line, observed post-storm bed levels by the black solid line and XBeach model results are presented in red. The modelled dune erosion is shown by the red shaded area.	117

6.14	XBeach results for cross-shore transect 305 at Fire Island. Initial bed levels are depicted by the black dotted line, observed post-storm bed levels by the black solid line and XBeach model results are presented in red. The modelled dune erosion is shown by the red shaded area.	118
6.15	XBeach results for cross-shore transect 405 at Fire Island. Initial bed levels are depicted by the black dotted line, observed post-storm bed levels by the black solid line and XBeach model results are presented in red. The modelled dune erosion is shown by the red shaded area.	119
6.16	Location of the study site in Langeoog, Germany and location of the XBeach model. Model input bathymetry (right panel) with the location of the beach nourishment and the six transects A to F. Source: Hillmann and Frederiksen (2021)	120
6.17	XBeach results for cross-shore transect A at Langeoog. Initial bed levels are depicted by the black dotted line, observed post-storm bed levels by the black solid line and XBeach model results are presented in red. The modelled dune erosion is shown by the red shaded area.	121
6.18	XBeach results for cross-shore transect D at Langeoog. Initial bed levels are depicted by the black dotted line, observed post-storm bed levels by the black solid line and XBeach model results are presented in red. The modelled dune erosion is shown by the red shaded area.	122
6.19	Indication of assessed coastal profiles in red, from 568 in the north to 7100 in the south.	123
6.20	Cross-section for JarKus profile 648 before and after the 1976 storm based on the measurements and XBeach, including dune erosion volumes and retreat distances.	125
6.21	Cross-section for JarKus profile 5000 before and after the 1976 storm based on the measurements and XBeach, including dune erosion volumes and retreat distances.	125
6.22	Cross-section for JarKus profile 7100 before and after the 1976 storm based on the measurements and XBeach, including dune erosion volumes and retreat distances.	126
6.23	Overview of the extent of the southern part of the Dutch coast (Hoek van Holland to IJmuiden) and the location of the ERA5 data.	127
6.24	Pre and post storm surge profile as computed by XBeach. Upper frame shows the dune erosion section, the lower frame shows the entire XBeach profile.	128
6.25	Pre-storm profiles (black dotted line), measured post-storm profiles (black solid line) and modelled post-storm profiles (red solid line). Upper left panel: profile A. Upper right panel: profile B1. Lower left panel: profile B2. Lower right panel: profile C. The seaward side is on the left in all panels. Note that the measured post-storm profiles contain only the sea surface and emerged topography and no submerged topography.	129
6.26	Growth of breach width	131
6.27	Breach width related to water level and flow velocities	131
7.1	Profile development for Slapton Sands	132
7.2	Profile development for Chesil Beach	133
7.3	Profile development for test E10 of the Bardex experiment	133
7.4	Significant high-frequency (sea-swell) and low-frequency (infragravity) wave height computed with XBeach nonhydrostatic (top panel) and surfbeat mode (middle panel) without (black) and with vegetation (orange) for case 4 reported by Lovas (2000). Measurements are indicated with the black and grey symbols (respectively, without and with vegetation)	134

1 Introduction

1.1 Introduction to the XBeach model

The devastating effects of hurricanes on low-lying sandy coasts, especially during the 2004 and 2005 seasons have pointed at an urgent need to be able to assess the vulnerability of coastal areas and (re-)design coastal protection for future events, and also to evaluate the performance of existing coastal protection projects compared to 'do-nothing' scenarios. In view of this the Morphos-3D project was initiated by USACE-ERDC, bringing together models, modelers and data on hurricane winds, storm surges, wave generation and nearshore processes. As part of this initiative an open-source program, XBeach for eXtreme Beach behaviour, has been developed to model the nearshore response to hurricane impacts. The model includes wave breaking, surf and swash zone processes, dune erosion, overwashing and breaching (Roelvink *et al.*, 2009).

Existing tools to assess dune erosion under extreme storm conditions assume alongshore uniform conditions and have been applied successfully along relatively undisturbed coasts (Vellinga, 1986; Steetzel, 1993; Nishi and Kraus, 1996; Larson *et al.*, 2004), but are inadequate to assess the more complex situation where the coast has significant alongshore variability. This variability may result from anthropogenic causes, such as the presence of artificial inlets, sea walls, and revetments, but also from natural causes, such as the variation in dune height along the coast or the presence of rip channels and shoals on the shoreface (Thornton *et al.*, 2007). A particularly complex situation is found when barrier islands protect storm impact on the main land coast. In that case the elevation, width and length of the barrier island, as well as the hydrodynamic conditions (surge level) of the back bay should be taken into account to assess the coastal response. Therefore, the assessment of storm impact in these more complex situations requires a two-dimensional process-based prediction tool, which contains the essential physics of dune erosion and overwash, avalanching, swash motions, infragravity waves and wave groups.

With regard to dune erosion, the development of a scarp and episodic slumping after undercutting is a dominant process (Van Gent *et al.*, 2008). This supplies sand to the swash and surf zone that is transported seaward by the backwash motion and by the undertow; without it the upper beach scours down and the dune erosion process slows down considerably. One-dimensional (cross-shore) models such as DUROSTA (Steetzel, 1993) focus on the underwater offshore transport and obtain the supply of sand by extrapolating these transports to the dry dune. Overton and Fisher (1988), Nishi and Kraus (1996) focus on the supply of sand by the dune based on the concept of wave impact. Both approaches rely on heuristic estimates of the runup and are well suited for 1D application but difficult to apply in a horizontally 2D setting. Hence, a more comprehensive modelling of the swash motions is called for.

Swash motions are up to a large degree a result from wave-group forcing of infragravity waves (Tucker, 1954). Depending on the beach configuration and directional properties of the incident wave spectrum both leaky and trapped infragravity waves contribute to the swash spectrum (Huntley *et al.*, 1981). Raubenheimer and Guza (1996) show that incident band swash is saturated, infragravity swash is not, therefore infragravity swash is dominant in storm conditions. Models range from empirical formulations (e.g. Stockdon *et al.*, 2006) through

analytical approaches (Schaeffer, 1994; Erikson *et al.*, 2005) to numerical models in 1D (e.g. List, 1992; Roelvink, 1993b) and 2DH (e.g. Van Dongeren *et al.*, 2003; Reniers *et al.*, 2004a, 2006). 2DH wavegroup resolving models are well capable of describing low-frequency motions. However, for such a model to be applied for swash, a robust drying/flooding formulation is required.

1.2

Model approach and innovations

Our aim is to model processes in different regimes as described by Sallenger (2000). He defines an Impact Level to denote different regimes of impact on barrier islands by hurricanes, which are the 1) swash regime, 2) collision regime, 3) overwash regime and 4) inundation regime. The approach we follow to model the processes in these regimes is described below.

To resolve the swash dynamics the model employs a novel 2DH description of the wave groups and accompanying infragravity waves over an arbitrary bathymetry (thus including bound, free and refractively trapped infragravity waves). The wave-group forcing is derived from the time-varying wave-action balance (e.g. Phillips, 1977) with a dissipation model for use in combination with wave groups (Roelvink, 1993a). A roller model (Svendsen, 1984; Nairn *et al.*, 1990; Stive and De Vriend, 1994) is used to represent momentum stored in surface rollers which leads to a shoreward shift in wave forcing.

The wave-group forcing drives infragravity motions and both longshore and cross-shore currents. Wave-current interaction within the wave boundary layer results in an increased wave-averaged bed shear stress acting on the infragravity waves and currents (e.g. Soulsby *et al.*, 1993, and references therein). To account for the randomness of the incident waves the description by Feddersen *et al.* (2000) is applied which showed good skill for longshore current predictions using a constant drag coefficient (Ruessink *et al.*, 2001).

During the swash and collision regime the mass flux carried by the waves and rollers returns offshore as a return flow or a rip-current. These offshore directed flows keep the erosion process going by removing sand from the slumping dune face. Various models have been proposed for the vertical profile of these currents (see Reniers *et al.*, 2004b, for a review). However, the vertical variation is not very strong during extreme conditions and has been neglected for the moment.

Surf and swash zone sediment transport processes are very complex, with sediment stirring by a combination of short-wave and long-wave orbital motion, currents and breaker-induced turbulence. However, intra-wave sediment transports due to wave asymmetry and wave skewness are expected to be relatively minor compared to long-wave and mean current contributions (Van Thiel de Vries *et al.*, 2008). This allows for a relatively simple and transparent formulation according to Soulsby & Van Rijn (Soulsby, 1997) in a shortwave averaged but wave-group resolving model of surf zone processes. This formulation has been applied successfully in describing the generation of rip channels (Damgaard *et al.*, 2002; Reniers *et al.*, 2004a) and barrier breaching (Roelvink *et al.*, 2003).

In the collision regime, the transport of sediment from the dry dune face to the wet swash, i.e. slumping or avalanching, is modeled with an avalanching model accounting for the fact that saturated sand moves more easily than dry sand, by introducing both a critical wet slope and dry slope. As a result slumping is

predominantly triggered by a combination of infragravity swash runup on the previously dry dune face and the (smaller) critical wet slope.

During the overwash regime the flow is dominated by lowfrequency motions on the time scale of wave groups, carrying water over the dunes. This onshore flux of water is an important landward transport process where dune sand is being deposited on the island and within the shallow inshore bay as overwash fans (e.g. Leatherman *et al.*, 1977; Wang and Horwitz, 2007). To account for this landward transport some heuristic approaches exist in 1D, e.g. in the SBeach overwash module (Larson *et al.*, 2004) which cannot be readily applied in 2D. Here, the overwash morphodynamics are taken into account with the wave-group forcing of low-frequency motions in combination with a robust momentum-conserving drying/flooding formulation (Stelling and Duinmeijer, 2003) and concurrent sediment transport and bed-elevation changes.

Breaching of barrier islands occurs during the inundation regime, where a new channel is formed cutting through the island. Visser (1998) presents a semi-empirical approach for breach evolution based on a schematic uniform cross-section. Here a generic description is used where the evolution of the channel is calculated from the sediment transports induced by the dynamic channel flow in combination with avalanche-triggered bank erosion.

1.3 XBeach skillbed

The XBeach code and related functionalities develop fast. As a result there is a need from modelers and code developers to develop a tool that gives insight in the effect of code developments on model performnace. The XBeach skillbed tries to fulfill this need by running a range of tests including analytical solutions, laboratory tests and practical field cases.

2 Implementation tests

This chapter contains test to check certain aspects of XBeach.

2.1 Curvilinear

In this test a curvi-linear grid is applied to simulate waves and hyrdodynamics around a virtual island. The island is circular with a linear sloping profile. The lower half of the offshore boundary generates bichromatic waves that partly refract towards the island, but also passes the island. The waves passing the island leave the model through the upper half of the offshore boundary. Reflections at the offshore boundary are minimal due to the 2D weakly-reflective boundary condition used (Van Dongeren and Svendsen, 1997).

Figure 2.2 shows the RMS wave height (color) and the flow velocity field (arrows) around the island in the last time step. Figure 2.2 shows the same parameters, but in this case the overall mean values are presented.

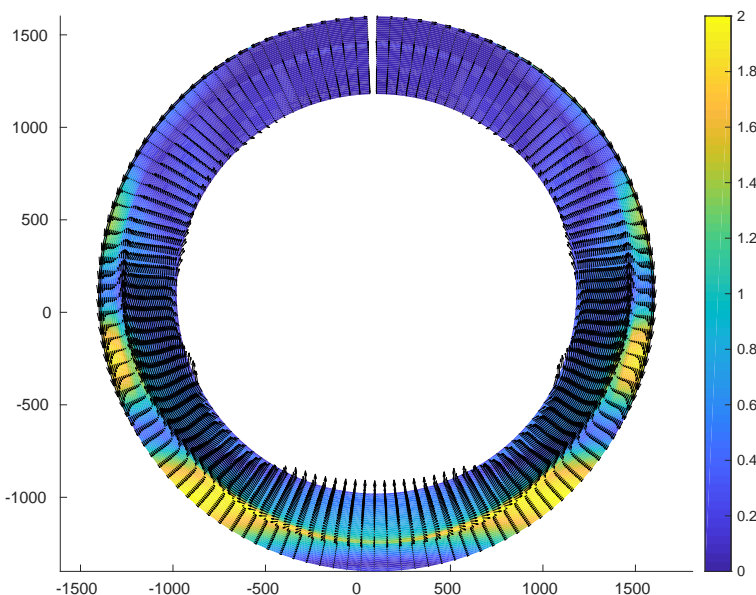


Figure 2.1 Snapshot of the RMS wave height and the flow velocity field in the last time step

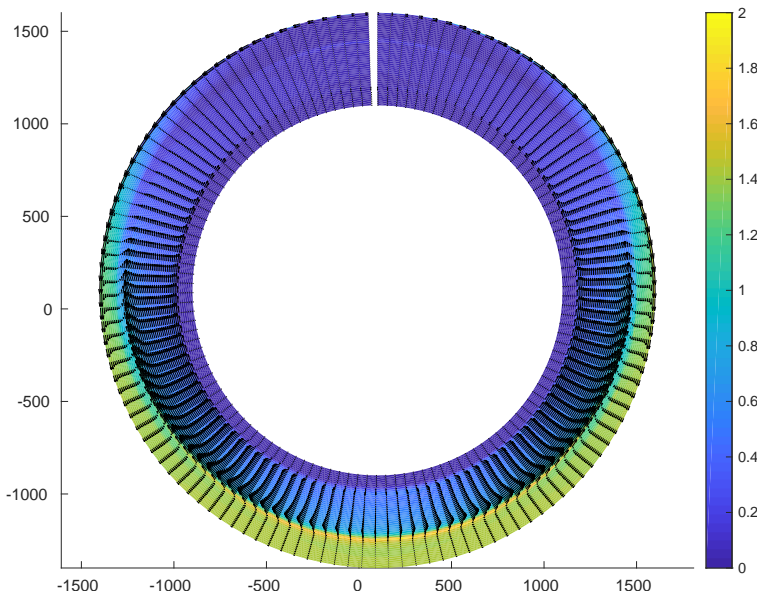


Figure 2.2 Mean values of the RMS wave height and the flow velocity field

2.2

Long wave propagation

The purpose of the this test is to check whether the NSWE numerical scheme is not too dissipative and that it does not create large errors in propagation speed.

A long wave with a small amplitude of 0.01 m and period of 80 s is sent into a domain with a length of 1 km, a depth of 5 m and a grid size of 5 m. Since only long waves are modelled a grid size of 5 m can be applied (more than 100 points per wave length). At the end, a fully reflecting wall is imposed. The wave length in this case should be $\sqrt{g \cdot d} \cdot T = \sqrt{9.81 \cdot 5} \cdot 80 = 560m$. The velocity amplitude should be $\sqrt{g/h} \cdot A = \sqrt{9.81/5} \cdot 0.01 = 0.014m$, because the these waves are shallow water waves. After the wave has reached the wall, a standing wave with double amplitude should be created.

The computed surface elevation and velocity snapshots before the waves reach the end of the domain is shown in [Figure 2.3](#). The surface elevation and velocity snapshots with the standing wave pattern are shown in [Figure 2.4](#). The computed and analytical wave amplitudes and wave lengths are shown in [Table 2.1](#). Note that the maximum velocity and surface elevation amplitude is found at the wall.

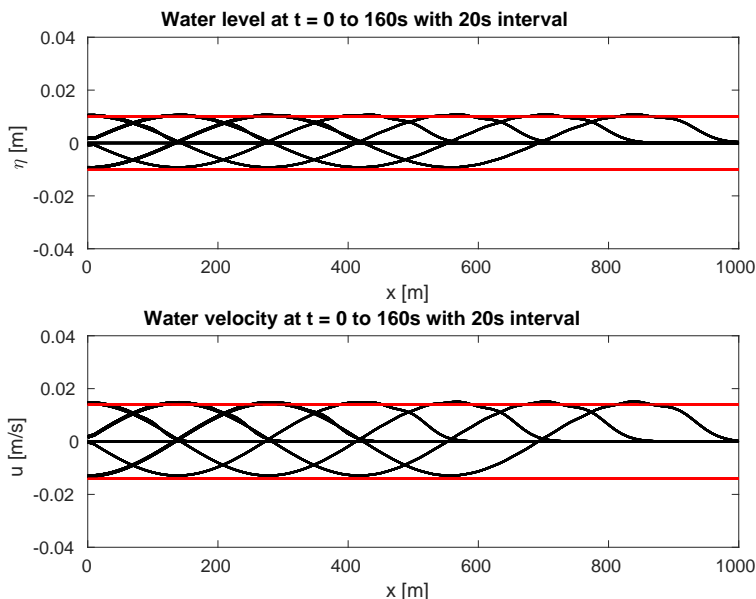


Figure 2.3 Water levels and velocities from the start of the experiment until the wave just reaches the end of the flume. The amplitude of the analytical solution is shown with a red line.

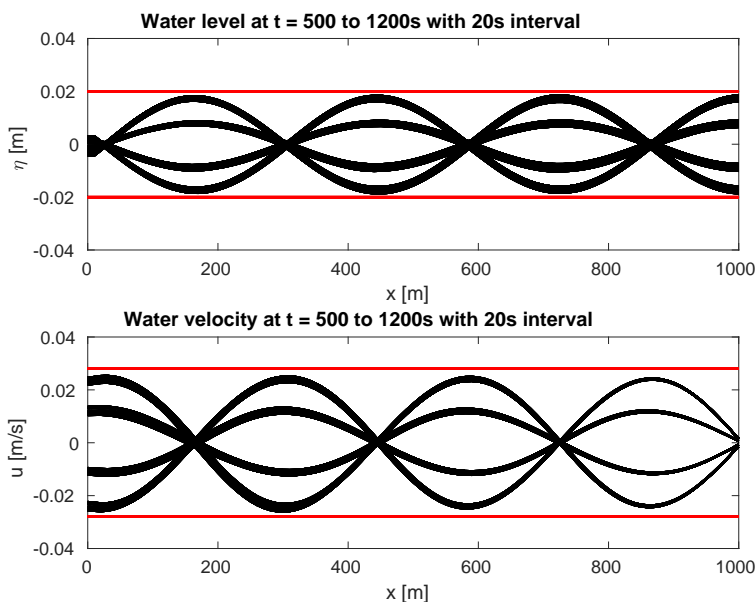


Figure 2.4 Snapshots of water levels and velocities showing a standing wave pattern. The amplitude of the analytical solution is shown with a red line.

Table 2.1 The XBeach and analytical wave heights and wave lengths. The amplitude without reflection is computed for the period $t=0$ to $t=600s$. The amplitude for the standing wave pattern is computed for the period $t=500$ to $t=1200$. The amplitude is defined as the maximum water level/velocity in the domain for the given time period.

	Amplitude [m]	Amplitude (Stand- ing wav) [m]	velocitie ampli- tude [m/s]	Velocitie ampli- tude (Stand- ing wave) [m/s]	Wave length [m]
XBeach	0.011	0.020	0.015	0.028	560.000
Analytical solution	0.010	0.020	0.014	0.028	560.000

2.3

1D wave runup (analytical solution)

The purpose of this test is to check the ability of the model to represent runup and rundown of non-breaking long waves. To that end, a comparison was made with the analytical solution of the non-linear shallow water equation (NSWE) by Carrier and Greenspan (1958), which describes the motion of harmonic, non-breaking long waves on a plane sloping beach without friction.

A free long wave with a wave period of 32 seconds and wave amplitude of half the wave breaking amplitude ($a_{in} = 0.5 \cdot a_{br}$) propagates over a beach with constant slope equal to 1:25. The wave breaking amplitude is computed as

$$a_{br} = 1/\sqrt{128} \cdot \pi^3 \cdot s^{2.5} \cdot T^{2.5} \cdot g^{1.25} \cdot h_0^{-0.25} = 0.0307m, \text{ where } s \text{ is the beach slope, } T \text{ is the wave period and } h_0 \text{ is the still water depth at the seaward boundary.}$$

The grid is non uniform and consists of 160 grid points. The grid size Δx is decreasing in shoreward direction and is proportional to the (free) long wave celerity ($\sqrt{g \cdot h}$). The minimum grid size in shallow water was set at $\Delta x = 0.1m$.

A comparison of surface elevation and velocity snapshots is shown in Figure 2.5. The maximum and minimum values of the analytical solution and the XBeach computations are shown in Table 2.2

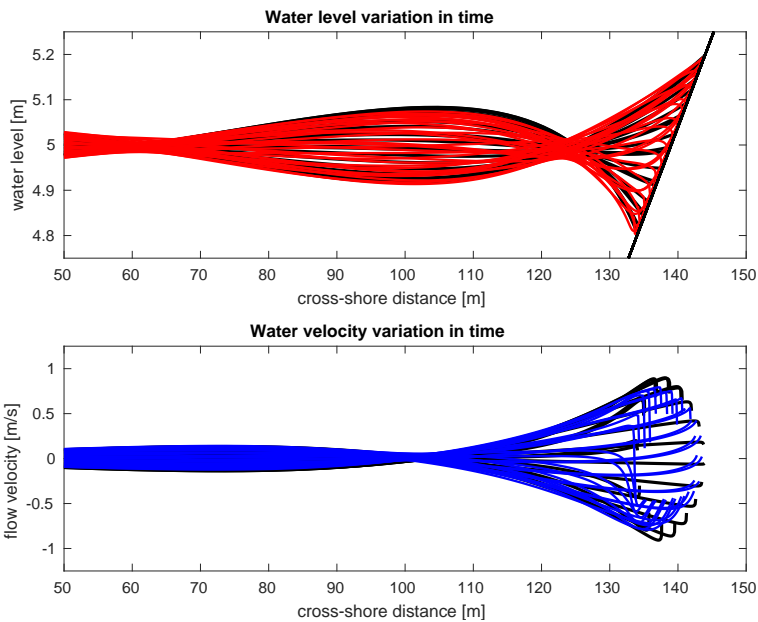


Figure 2.5 Snapshots of water level and velocity

Table 2.2 The maximum and minimum surface elevation and velocities in the runup.

	$\max(\eta)$ [m]	$\min(\eta)$ [m]	$\max(u)$ [m/s]	$\min(u)$ [m/s]
XBeach	5.20	4.80	0.90	-0.91
Analytical solution	5.19	4.80	0.79	-0.79

2.4 Longcrested refraction2

This test is to check the refraction behaviour of longcrested waves, which are simulated using instat=stat and m=1000. Four cases are generated and compared: directional bins of 2.5, 5 and 10 degrees and a single bin. In all cases the incident wave angle is 60 degrees and theta grid runs from -10 to 90 degrees. The results are compared among themselves and, for the wave direction, with Snel's law and with mean direction computed by integrating $c_\theta/c_{g,x}$ over x. The results all agree within approx. one degree, which is considered satisfactory. Note that the longshore current does not exhibit any negative velocities, as was noticed when the refraction is not computed correctly.

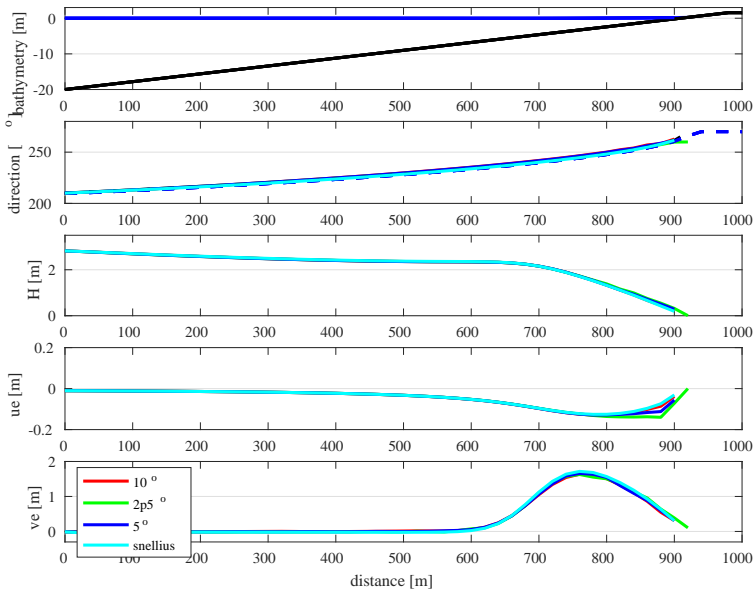


Figure 2.6 Wave energy, direction and flow velocities for different sized of theta bins.

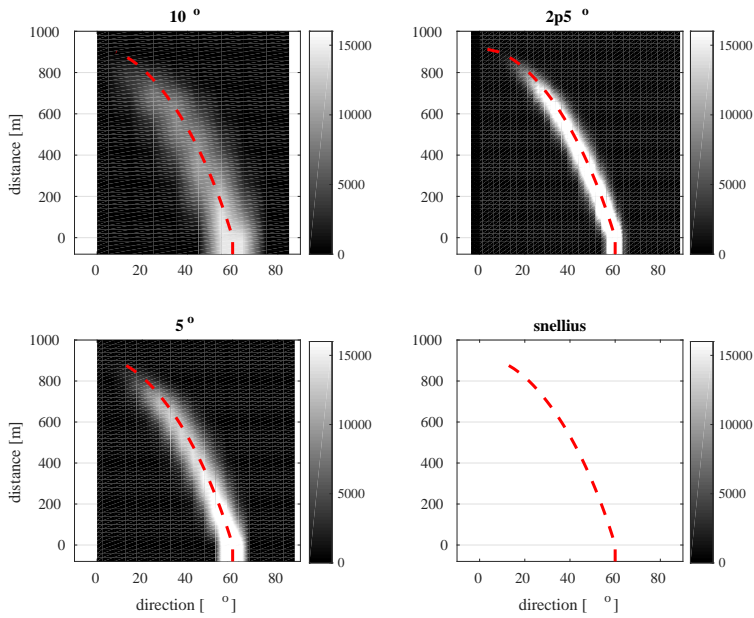


Figure 2.7 Refraction with different sizes of theta bins. The red dotted line indicates the solution according to Snel law.

2.5

Dambreak

2.5.1

1D dam break test

The 1D dam break test is a classic test to verify whether the advection scheme is momentum conservative or not. The upstream water level is set to 1m, and the downstream water level respectively 0m and 0.1m for the dry and wet bed cases. The initial velocities are set to zero and the release of the water is instantaneous.

The dry bed case was first studied by Ritter (1892) and later by Stelling and Duinmeijer (2003). The analytic solutions are based on Chanson (2006) and Kroon (2009). The results shown are with a grid size of 0.1m, no friction and after 5 seconds.

The surfbeat (hydrostatic) as well as the non-hydrostatic results are shown. XBeach non-hydrostatic uses another advection scheme. The difficult part to correctly reproduce is the tip of the shock wave, where deviations with the analytical solutions are often found.

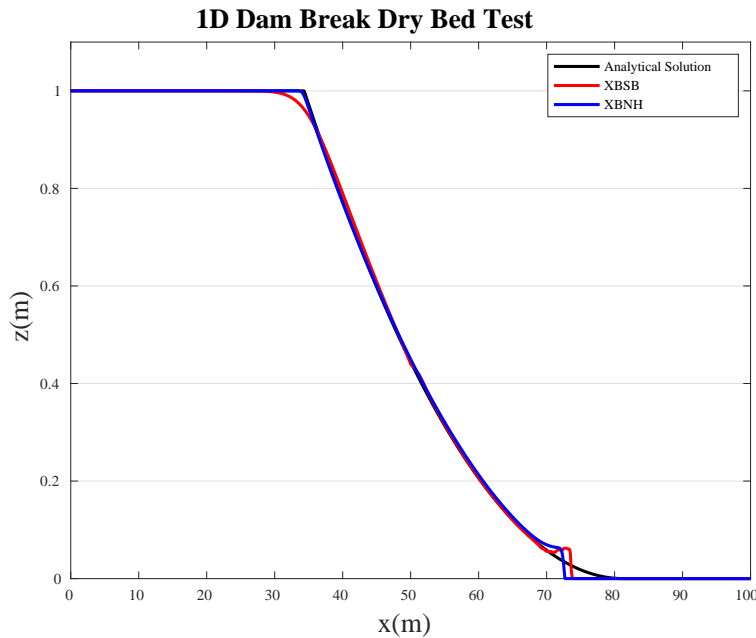


Figure 2.8 The results of the 1D dam break test with dry bed after 5 seconds.

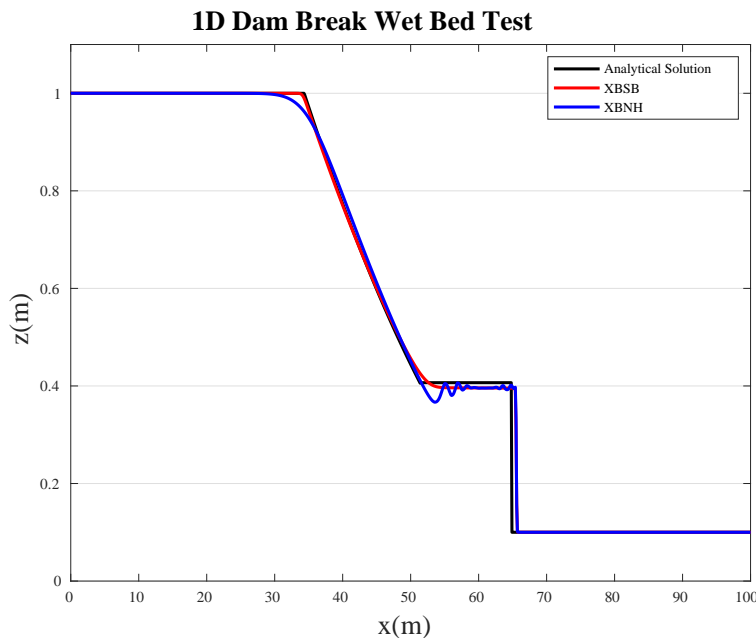


Figure 2.9 The results of the 1D dam break test with wet bed ($h=0.1m$) after 5 seconds.

2.5.2 Tide

This test was set up to verify the capability of XBeach to model tidal elevation and longshore currents in a small model, based on water level time series at the seaward corner points, which have a small time shift. The current pattern should spin up in a longshore uniform pattern and remain longshore uniform at all times. In the figure velocity patterns at six times during a one-day simulation are shown. Also the input

timeseries of water levels at the corners (dots) can be compared with the model water level time series, which should closely follow the input but may have a small delay depending on the type of boundary condition chosen (abs_1d, abs_2d or waterlevel) and on settings of epsi (-1 in this case) and cats (5). In this case without wave forcing, the abs_2d boundary type does not perform well; water levels do not match the input. This is probably due to the absence of waves. With abs_1d the results as in the reference figure are shown.

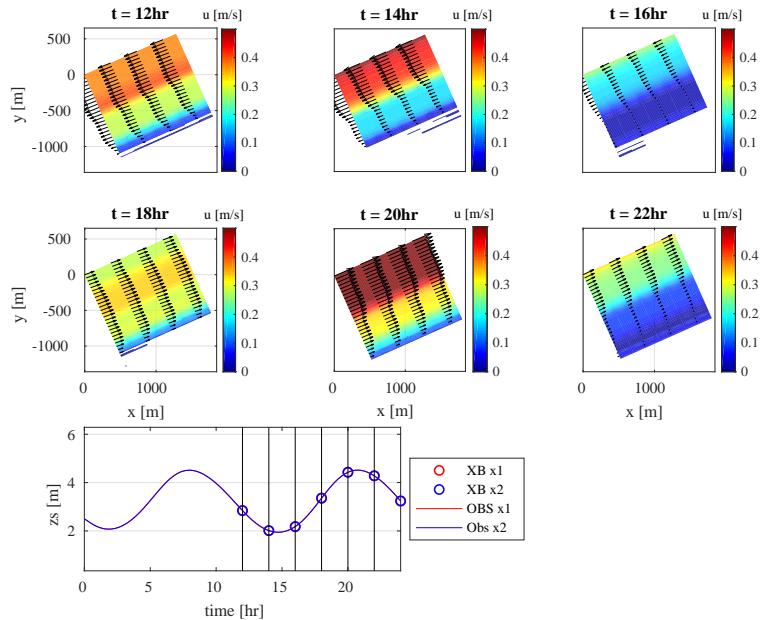


Figure 2.10 The lower-left panel shows the tidal timeseries imposed to the offshore corners of the model (dots) and the generated waterlevels at these locations (lines). For six moments indicated with the black vertical lines, the flow field is shown in the upper panels.

2.5.3

Blankenberge

This represents a realistic test model of the coast and port of Blankenberge on the Belgian coast, in a model set up by IMDC and Flanders Hydraulics. The model experienced bad tidal currents; after fixing this problem the accompanying figure show smooth and realistic current patterns with a nearshore current dominated by wave-driven currents (instationary, JONSWAP-type, with waves from 270 degrees, so a large angle to the coast. In this case the abs_2d boundary option does not pose a problem to the tidal forcing. In the present setup we run it with theta bins of 20 degrees.

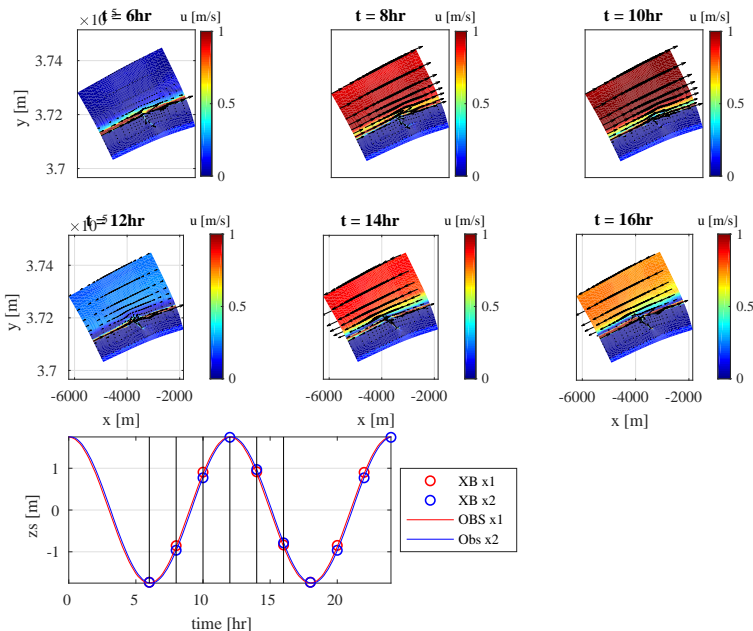


Figure 2.11 The lower-left panel shows the tidal timeseries imposed to the offshore corners of the model (dots) and the generated waterlevels at these locations (lines). For six moments indicated with the black vertical lines, the flow field is shown in the upper panels.

2.6

River outflow

The river outflow case is meant to test XBeach for the combined effects of a river outflow and a steady wave-driven longshore current on the sediment transport and the morphological evolution. Though purely hypothetical, this case contains many salient features of real-life applications, such as longshore currents through open side-boundaries and exchange of water and sand through a gap in a closed boundary. Thus, the formulation of open boundary conditions is also tested here.

The initial topography consists of a plane beach (slope 1:50), which is interrupted by a 75 m wide river mouth with a water outflow of $150 \text{ m}^3/\text{s}$. The bottom contours are straight and parallel to the shoreline, except for a shallow submerged channel in line with the river.

The computational grid is rectangular, with 56 nodes in the x-direction (cross-shore) and 111 nodes in the y-direction (longshore), with a uniform grid spacing of 15 m. The waves are irregular and long-crested, with a root-mean-square height of 2m at a water depth of 13.5m. The direction of wave incidence is 30 degrees with respect to the shore-normal. The peak wave period is 8s. The bed material is uniform sand of 250, with a settling velocity of 0.031m/s.

In this figure the bathymetry is shown after approximately 4 days; arrows indicate the sediment transport vectors. plotted for every cross-shore cell and every third longshore cell. When functioning correctly, we see a channel that has turned towards the north and straight contour lines downstream of the channel.

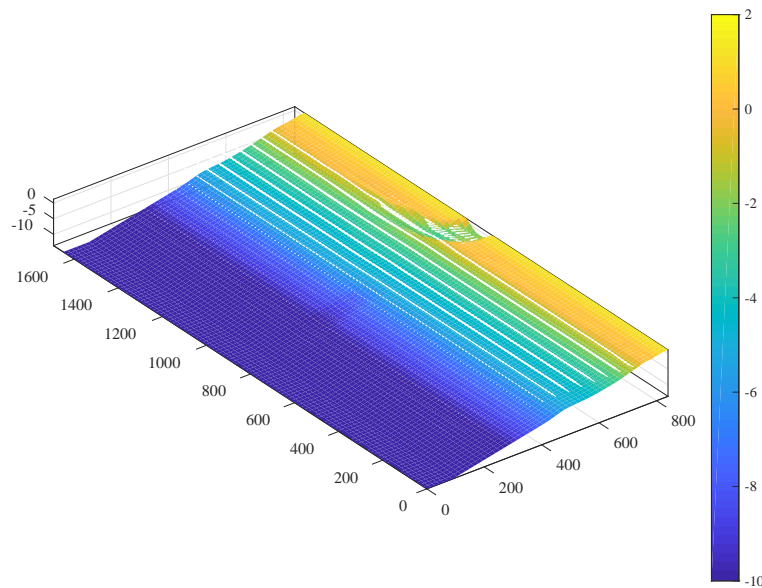


Figure 2.12 Final bathymetry

2.7

Drifters

This purely hypothetical test combines three specific functionalities of XBeach: curvilinear grids, discharges and drifters. The model is basically an odd-shaped bathtub with a single discharge location at the left boundary. The bathtub is filled by the discharged water, indicated by the increasing water levels (colored background). The bathtub is approximately 70m x 70m. Considering that, the discharge of $50\text{m}^3/\text{s}$ is rather large. Every 10 seconds, two drifters are released just before the discharge opening. One of the two drifters is released at the upper boundary of the opening, the other at the lower boundary. The entire path a single drifter has followed at a certain moment in time is plotted in Figure 2.13. Two large eddies driven by the large discharge are revealed by these paths.

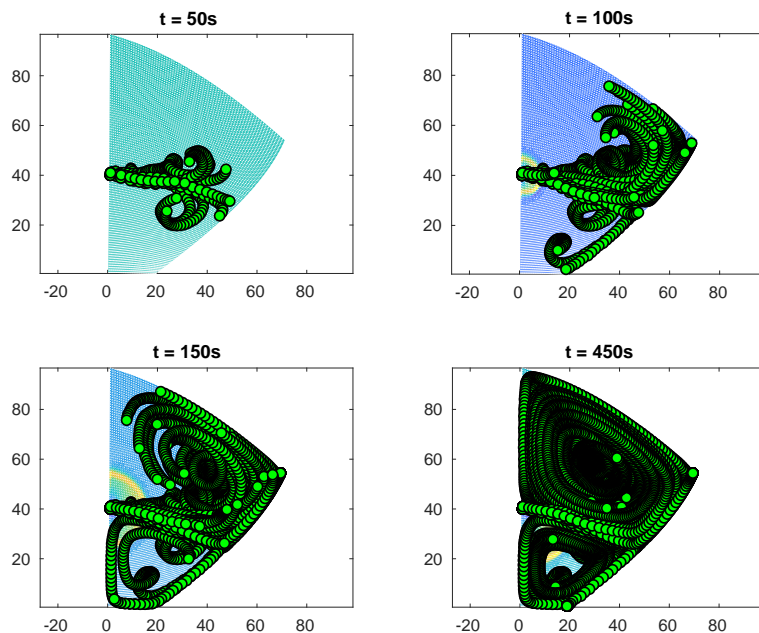


Figure 2.13 Drifter paths after 50, 100, 150 and 450 seconds

2.8

Multiple sediment fractions

The purpose of this simulation is to ensure the multiple sediment fractions model in XBeach performs as expected. In this test, the Deltaflume 2006 T01 test is recreated with two types of sand with different colours, red and blue. The sand is initially placed in a zebra-stripe pattern in the profile. The properties of both types of sand such as the grain size and mobility are the same as the sand used in the Deltaflume experiment. For the test to be successful, the following conditions should be met:

- 1 The simulated final profile should be the same as the final profile in the original Deltaflume 2006 T01 test.
- 2 The two sediment types should mix and form layers over each other (yellow).

The figures [Figure 2.14](#) and [Figure 2.15](#) show the initial and final distribution of red and blue sediment in the profile near the dune face. The red and blue lines in the same figure show the sediment concentration of each sediment type in the water column. If the simulation is successful, the red and blue sediment will be well mixed on the foreshore and fresh blue sediment will be deposited over the red sediment at the dune foot as the dune face retreats. The concentration of blue sediment in the water column should be higher than the concentration of red sediment in the water in areas where only blue sediment is available in the top layer of the bed. The red line in [Figure 2.16](#) shows the predicted dune face retreat and bed level change in the XBeach multiple-sediment model. The black line in the same figure represents the corresponding measured final profile. If the simulation has been successful, the red and black line will align reasonably well. The results of this simulation should be compared to the Deltaflume 2006 T01 test described earlier in this report.

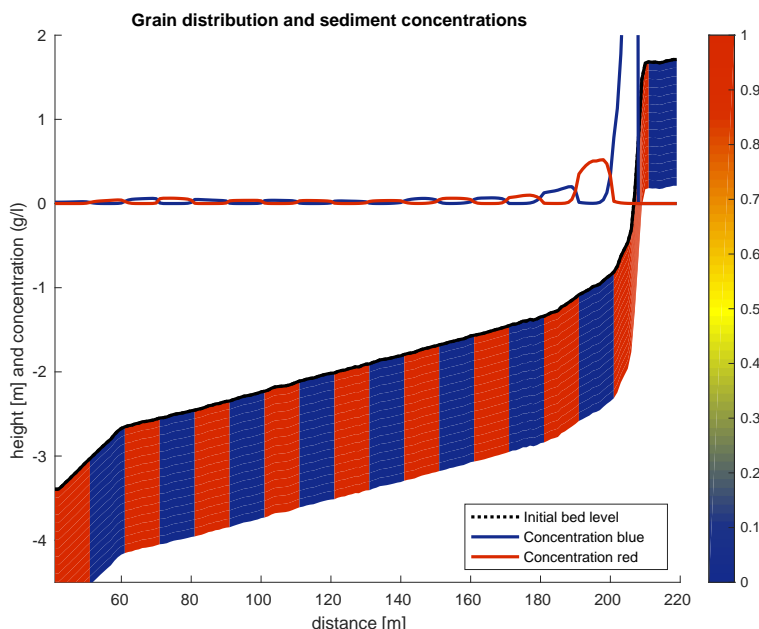


Figure 2.14 Initial bathymetry and sediment distribution

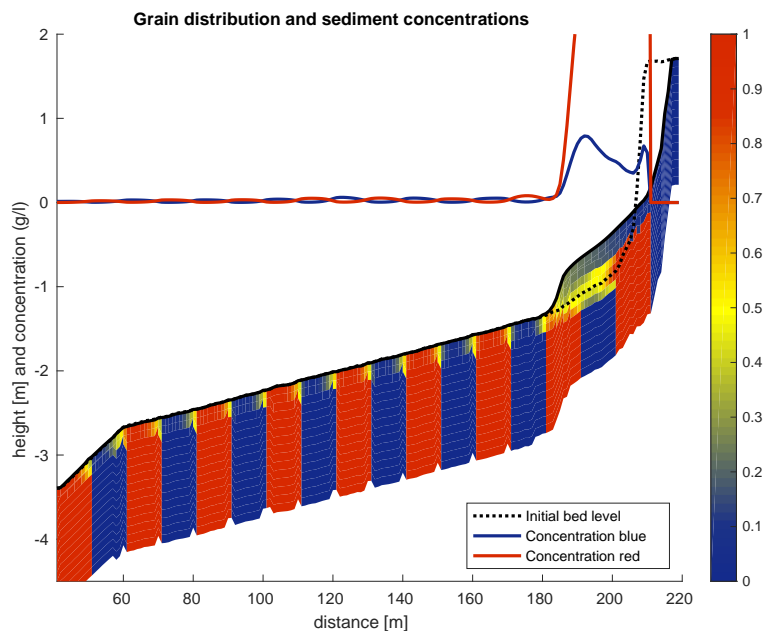


Figure 2.15 Final bathymetry and sediment distribution

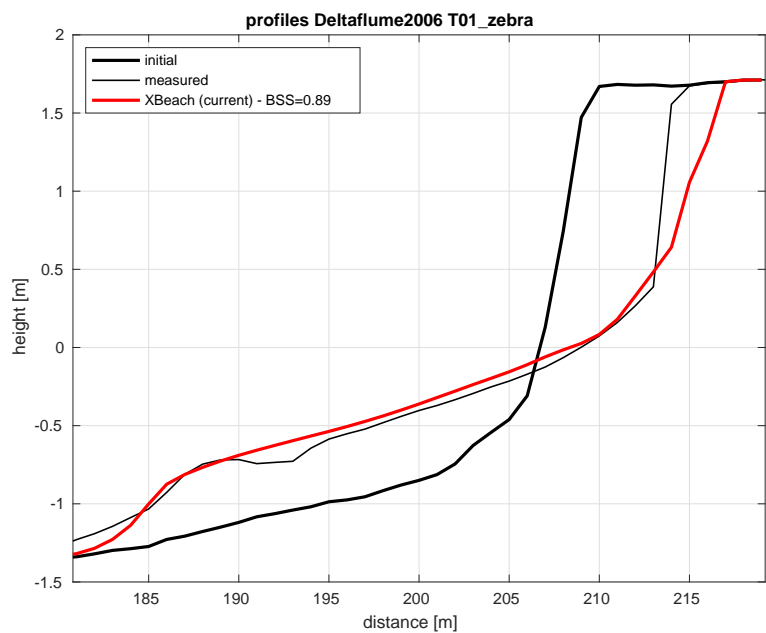


Figure 2.16 Profile development

3 Hydrodynamic tests

Morphodynamics start with hydrodynamics. In this chapter the hydrodynamic results of XBeach are discussed. All tests are run without the morphological module and the analysis is focussed on the wave propagation and transformation computed by XBeach.

3.1 Specific tests

3.2 2D wave runup

The verification cases so far considered solely the cross-shore dimension and assumed a longshore uniform coast. In the following case the potential of the model to predict coastal and dune erosion in situations that include the two horizontal dimensions is further examined. A first step towards a 2DH response is to verify that the 2DH forcing by surge run-up and run-down is accurately modelled by testing not against Zelt (1986), but actually Özkan-Haller and Kirby (1997). The reason is that Zelt modeled the NSW equations including some dispersive and dissipative terms, which the present model does not include. For that reason, we compared the model to the results of Özkan-Haller and Kirby (1997) who modeled the NSW equations using a Fourier-Chebyshev Collocation method, which does not have any numerical dissipation or dispersion errors. They use a moving, adapting grid with a fixed Δy (which is equal to the present model's Δy in this comparison) but with a spatially and temporally varying Δx so that the grid spacing in x near the shoreline is very small. In the present model Δx is set equal to Δy , which means that we can expect to have less resolution at the shoreline than Özkan-Haller and Kirby (1997).

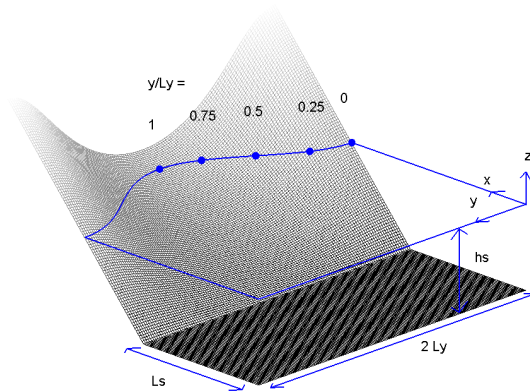


Figure 3.1 Definition sketch of concave beach bathymetry

Figure 3.1 shows the definition sketch of the concave beach bathymetry in the present coordinate system, converted from the original system by Zelt (1986). The bathymetry consists of a flat bottom part and a beach part with a sinusoidally varying slope. For

Zelt (1986)'s fixed parameter choice of $\sqrt{\beta} = \frac{h_s}{L_y} = \frac{4}{10\pi}$, the bathymetry is given by

$$h = \begin{cases} h_s & , \quad x \leq L_s \\ h_s - \frac{0.4(x-L_s)}{3-\cos(\frac{\pi y}{L_y})} & , \quad x > L_s \end{cases}$$

where h_s is the shelf depth, L_s is the length of the shelf in the modeled domain and L_y is the length scale of the longshore variation of the beach. This results in a beach slope of $h_x = \frac{1}{10}$ in the center of the bay and of $h_x = \frac{1}{5}$ normal to the "headlands". In the following we chose $L_y = 8 m$, which determines $h_s = 1.0182 m$. We set $L_s = L_y$. Different values for L_s only cause phase shifts in the results, but no qualitative difference, so this parameter is not important in this problem. Also indicated in the figure are the five stations where the vertical run-up (the surface elevation at the shoreline) will be measured.

At the offshore ($x = 0$) boundary we specify an incoming solitary wave, which in dimensional form reads

$$\zeta_i(t) = \alpha h_s \operatorname{sech}^2 \left(\sqrt{\frac{3g}{4h_s}} \alpha (1 + \alpha) (t - t_o) \right)$$

which is similar to Zelt (1986)'s Eq. (5.3.7). The phase shift t_o is chosen such that the surface elevation of the solitary wave at $t = 0$ is 1% of the maximum amplitude. The only parameter yet to be chosen is α . We will compare our model to Zelt's case of $\alpha = \frac{H}{h_s} = 0.02$, where H is the offshore wave height. Zelt found that the wave broke for a value of $\alpha = 0.03$, so the present test should involve no breaking, but has a large enough nonlinearity to exhibit a pronounced two-dimensional run-up.

Any outgoing waves will be absorbed at the offshore boundary by the absorbing-generating boundary condition. At the lateral boundaries $y = 0$ and $y = 2 L_y$ we specify a no-flux (wall) boundary condition following Zelt (1986). The model equations used in this test are the nonlinear shallow water equations without forcing or friction. The numerical parameters are $\Delta x = \Delta y = \frac{1}{8} m$ with a Courant number $\nu = 0.7$.

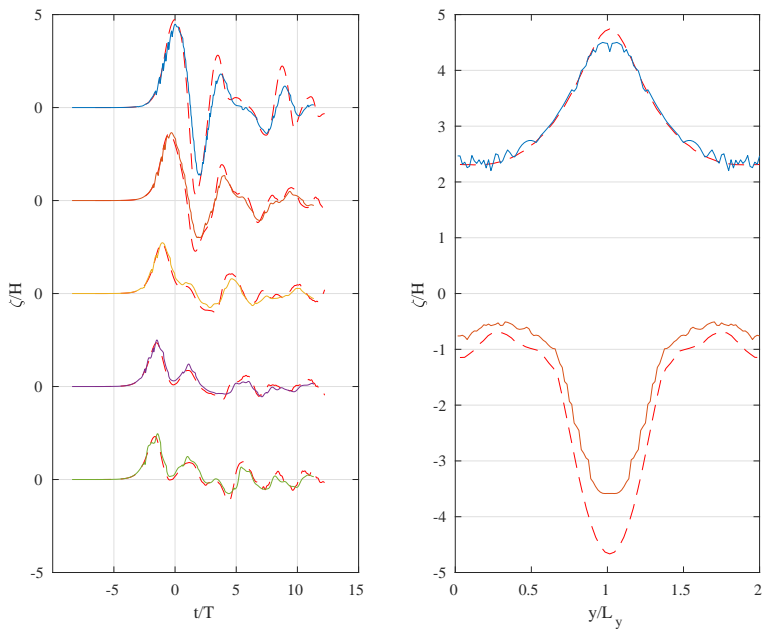


Figure 3.2 Normalized vertical runup in time (panel 1) and maximum and minimum values (panel 2)

The first panel in ?? shows the vertical runup normalized with the offshore wave height H as a function of time, which is normalized by $\sqrt{g h_s} / L_y$ at the 5 cross-sections indicated in Figure 3.1. The solid lines represent the present model results, while the dashed lines denotes Özkan-Haller and Kirby (1997)'s numerical results. The second panel in ?? shows the maximum vertical run-up and run-down, normalized by H , versus the alongshore coordinate y . ?? presents error statistics of the model run with respect to the measurements.

Table 3.1 Error statistics Zelt Case 1

	R^2	Sci	Rel. bias	BSS
Timeseries (min)	0.11	0.26	-0.15	-6.40
Timeseries (max)	0.96	2.49	0.15	0.92
Max. runup	0.99	0.03	-0.01	0.98

3.3

Surfbeat

3.3.1

High- and low-frequency wave transformation over barred beach Experiment description

Boers (1996) performed experiments with irregular waves in the physical wave flume at Delft University of Technology. The flume has a length of 40 meters and a width of 0.8 m. The fixed concrete beach profile represents the beach profile of the LIP 11D-experiment 1B (excluding mega-ripples), on a scale of 1:28 with respect to prototype. This profile has a breaker bar and a surf zone trough. The still water level during the experiments is $z = 0.75$ m above the bottom of the wave flume. The flume is equipped with a hydraulically driven, piston type wave generator with second-order wave generation and Active Reflection Compensation. Measurements were taken at 20 Hz. Three irregular wave conditions were studied (See Table 3.5). The surface elevation was measured at 70 locations shown in Figure 3.13. It is important to note

that the waves are breaking from the start in Tests 1A and 1B. In addition, not a complete jonswap spectrum could be imposed at the boundary due to restrictions with the waveboard. Therefore, the XBeach model is forced with measured timeseries, rather than with a jonswap spectrum.

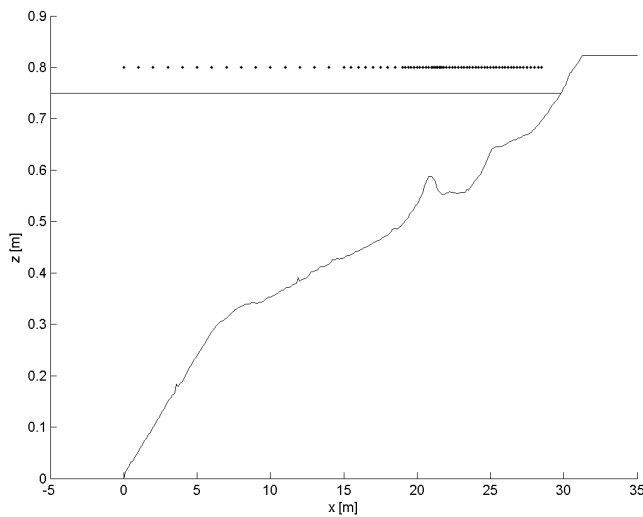


Figure 3.3 Locations of surface eleveation measurements

Test	H_{m0} [m]	T_p [s]
1A	0.157	2.1
1B	0.206	2.1
1C	0.103	3.4

Table 3.2 The Boers (1996) wave conditions.

Results

The comparison between the model and the observations for the wave height transformation of the short waves, the infragravity waves and the setup is shown in [Figure 3.4](#), [Figure 3.5](#) and [Figure 3.6](#). The short-wave height and infragravity wave height are shown in the upper panel. The setup is shown in the second panel and the bathymetry is shown in the last panel. The XBeach boundary is located at the 9th wave gauge since this location contains velocity and surface elevation measurements and the model is forced with the incoming measured wave signal. Note that the setup for these small-scale tests is very small (maximum of several millimetres), which causes the scatter in the observations.

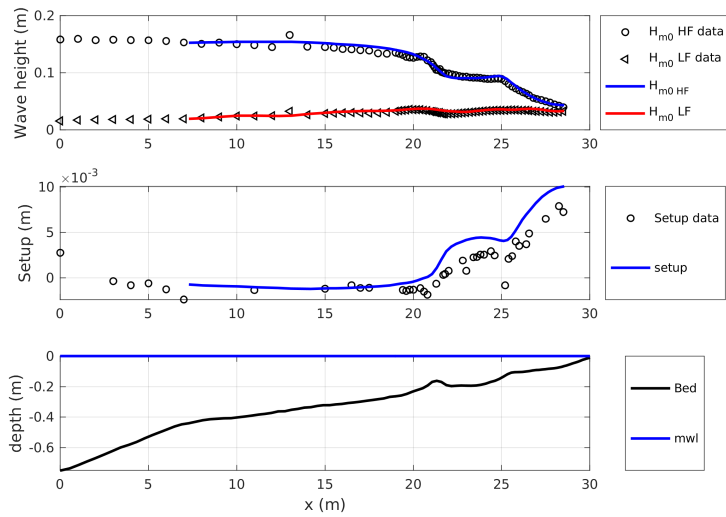


Figure 3.4 Wave hydrodynamics during experiment 1A. The observed short-wave height (dots) and observed infragravity wave height (triangles) are compared to the XBeach results (blue and red line) in the upper panel. The observed setup (dots) is compared to the setup computed with XBeach (blue line) in the second panel and the bathymetry is shown in the third panel.

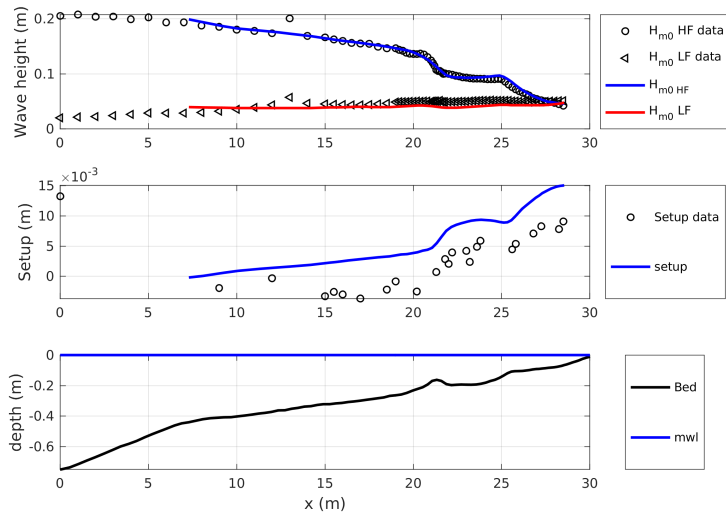


Figure 3.5 Wave hydrodynamics during experiment 1B. The observed short-wave height (dots) and observed infragravity wave height (triangles) are compared to the XBeach results (blue and red line) in the upper panel. The observed setup (dots) is compared to the setup computed with XBeach (blue line) in the second panel and the bathymetry is shown in the third panel.

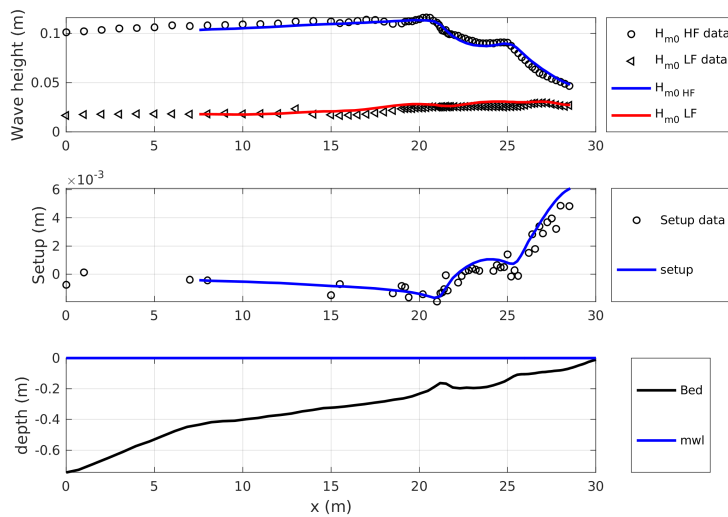


Figure 3.6 Wave hydrodynamics during experiment 1C. The observed short-wave height (dots) and observed infragravity wave height (triangles) are compared to the XBeach results (blue and red line) in the upper panel. The observed setup (dots) is compared to the setup computed with XBeach (blue line) in the second panel and the bathymetry is shown in the third panel.

Overview

An overview of the skill scores is shown in [Figure 3.7](#) and [Table 3.3](#), where the relative bias and scatter index of the short-wave height, infragravity-wave height and setup are shown for the different Boers experiments.

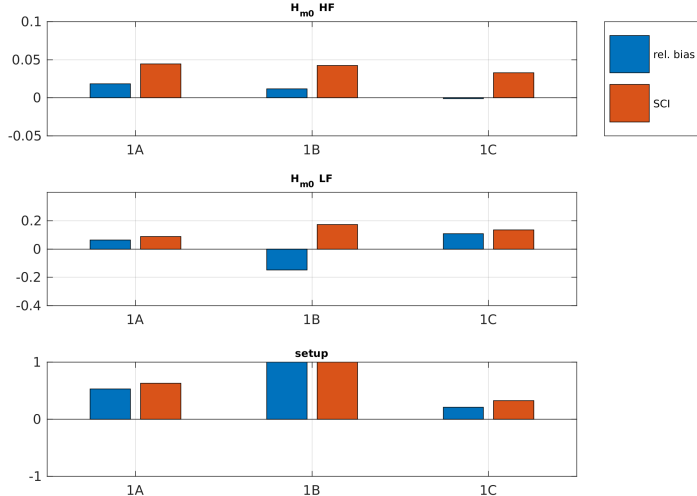


Figure 3.7 Overview of the statistical scores of the Boers experiments. The relative error and scatter index for the short-wave height (upper panel), infragravity wave height (second panel) and setup (third panel) are shown for the different Boers experiments.

Table 3.3 The statistical scores for the Boers experiments. The scatter index (SCI) and relative bias (rel. bias) are shown for the short-wave height, infragravity wave height and setup.

	1A	1B	1C
$H_{m0,HF}$ Rel. bias	0.02	0.01	-0.00
$H_{m0,HF}$ SCI	0.04	0.04	0.03
$H_{m0,LF}$ Rel. bias	0.06	-0.15	0.11
$H_{m0,LF}$ SCI	0.09	0.17	0.13
setup Rel. bias	0.53	1.07	0.21
setup SCI	0.63	1.10	0.33

3.3.2

High- and low-frequency wave transformation over sloping beach

Experiment description

The laboratory data set was obtained during the GLOBEX project (Ruessink *et al.*, 2013). The experiments were performed in the Scheldegoot in Delft, The Netherlands, in April 2012. The flume is 110 m long, 1 m wide and 1.2 m high and has a piston-type wave maker equipped with an Active Reflection Compensation (ARC) to absorb waves coming from the flume and hence prevent their re-reflection from the wave maker. A fixed, mild-sloping (1:80) concrete beach was constructed over almost the entire length of the flume (with a fixed sandy upper layer), except for the first 16.6 m that were horizontal and where the mean water level was 0.85 m (Fig. 3.8). At the cross-shore position $x = 16.6$ m ($x = 0$ m is the wave-maker position at rest), the sloping bed started and intersected with the mean water level at $x \approx 84.6$ m. The profile, and the conditions were on a 1:20 scale with respect to prototype. As detailed in Ruessink *et al.* (2013), the experimental program comprised 8 wave conditions.

Here we will focus on the 3 irregular-wave cases: an intermediate energy sea-wave condition ($A1; H_s = 0.1$ m, $T_p = 1.58$ s), a high-energy sea-wave condition ($A2; H_s = 0.2$ m, $T_p = 2.25$ s), and a narrow-banded swell condition ($A3; H_s = 0.1$ m, $T_p = 2.25$ s). All wave-paddle steering signals included second-order wave generation, and were based on a JONSWAP spectrum with a peak enhancement factor γ of 3.3 for $A1$ and $A2$, and 20 for $A3$. Each condition had a duration of 75 minutes with 21 wave gauges and 5 flow meters sampling at 128 Hz, followed by a rest period of about 15 minutes. After all wave conditions were completed, most instruments were repositioned and the conditions were repeated with the same wave paddle signal. Altogether, the conditions were each repeated 10 times, resulting in a total of 190 positions with water level (η) data and 43 positions with cross-shore flow-velocity (u) data, with an instrument spacing varying from 2.2 m offshore, to 0.55 m in the middle section and 0.37 m inshore, see Figure 3.8. See Ruessink *et al.* (2013) for further details and initial data processing.

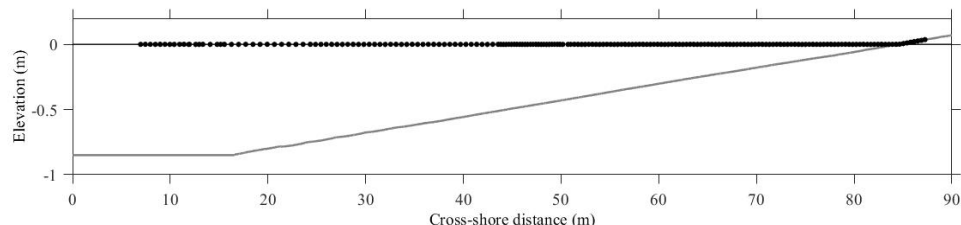


Figure 3.8 Elevation z versus cross-shore distance x in the Scheldegoot during the GLOBEX project. Here, $x = 0$ is the location of the wave-maker at rest, and $z = 0$ corresponds to the still water level. At $x = 84.6$ m the still water level intersected with the bed. The 190 dots are the positions of the wave gauges.

Results

The comparison between the model and the observations for the wave height transformation of the short waves, the infragravity waves and the setup is shown in Figure 3.9, Figure 3.10 and Figure 3.11.

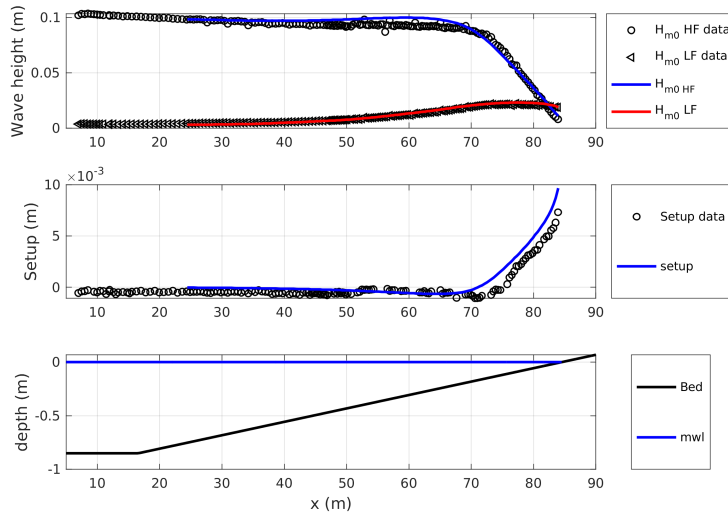


Figure 3.9 Wave hydrodynamics during experiment A1. The observed short-wave height (dots) and observed infragravity wave height (triangles) are compared to the XBeach results (blue and red line) in the upper panel. The observed setup (dots) is compared to the setup computed with XBeach (blue line) in the second panel and the bathymetry is shown in the third panel.

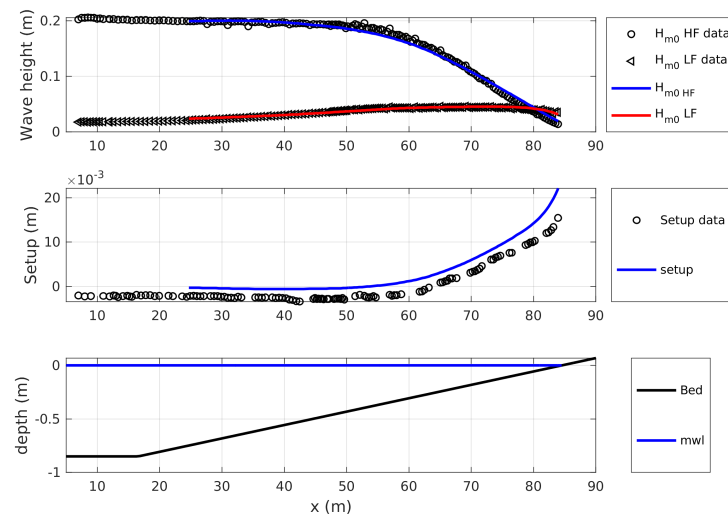


Figure 3.10 Wave hydrodynamics during experiment A2. The observed short-wave height (dots) and observed infragravity wave height (triangles) are compared to the XBeach results (blue and red line) in the upper panel. The observed setup (dots) is compared to the setup computed with XBeach (blue line) in the second panel and the bathymetry is shown in the third panel.

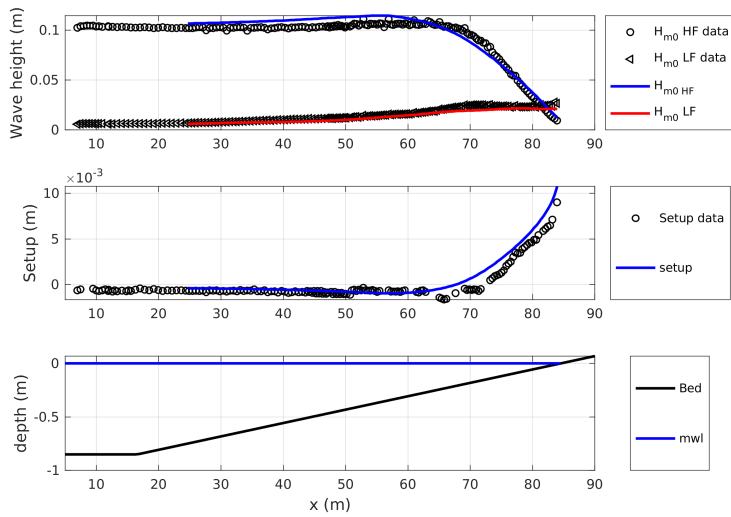


Figure 3.11 Wave hydrodynamics during experiment A3. The observed short-wave height (dots) and observed infragravity wave height (triangles) are compared to the XBeach results (blue and red line) in the upper panel. The observed setup (dots) is compared to the setup computed with XBeach (blue line) in the second panel and the bathymetry is shown in the third panel.

Overview

An overview of the statistical scores is shown in [Figure 3.12](#) and [Table 3.4](#), where the relative bias and scatter index of the short-wave height, infragravity wave height and setup are shown for the different GLOBEX experiments.

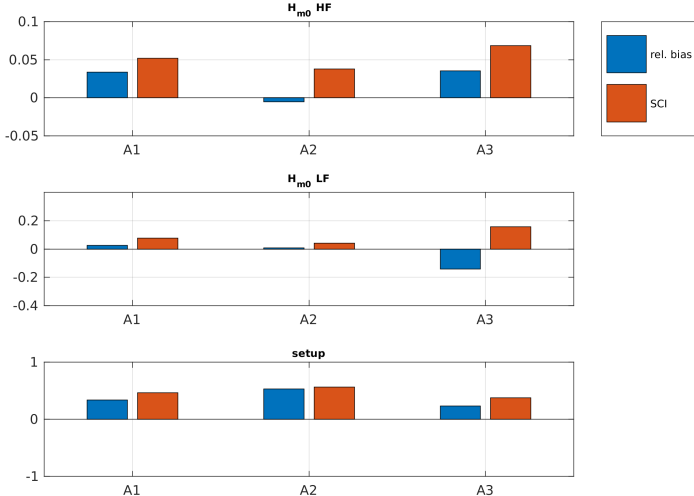


Figure 3.12 Overview of the statistical scores of the GLOBEX experiments. The relative error and scatter index for the short-wave height (upper panel), infragravity wave height (second panel) and setup (third panel) are shown for the different GLOBEX experiments.

Table 3.4 The statistical scores for the GLOBEX experiments. The scatter index (SCI) and relative bias are shown for the short-wave height, infragravity wave height and setup.

	A1	A2	A3
$H_{m0,HF}$ Rel. bias	0.03	-0.01	0.04
$H_{m0,HF}$ SCI	0.05	0.04	0.07
$H_{m0,LF}$ Rel. bias	0.03	0.01	-0.14
$H_{m0,LF}$ SCI	0.08	0.04	0.16
setup Rel. bias	0.34	0.53	0.23
setup SCI	0.46	0.56	0.38

3.4 Nonhydrostatic

3.4.1 High- and low-frequency wave transformation over barred beach

Experiment description

Boers (1996) performed experiments with irregular waves in the physical wave flume at Delft University of Technology. The flume has a length of 40 meters and a width of 0.8 m. The fixed concrete beach profile represents the beach profile of the LIP 11D-experiment 1B (excluding mega-ripples), on a scale of 1:28 with respect to prototype. This profile has a breaker bar and a surf zone trough. The still water level during the experiments is $z = 0.75$ m above the bottom of the wave flume. The flume is equipped with a hydraulically driven, piston type wave generator with second-order wave generation and Active Reflection Compensation. Measurements were taken at 20 Hz. Three irregular wave conditions were studied (See Table 3.5). The surface elevation was measured at 70 locations shown in Figure 3.13. It is important to note that the waves are breaking from the start in Tests 1A and 1B. In addition, not a complete Jonswap spectrum could be imposed at the boundary due to restrictions with the waveboard. Therefore, the XBeach model is forced with measured timeseries, rather than with a Jonswap spectrum.

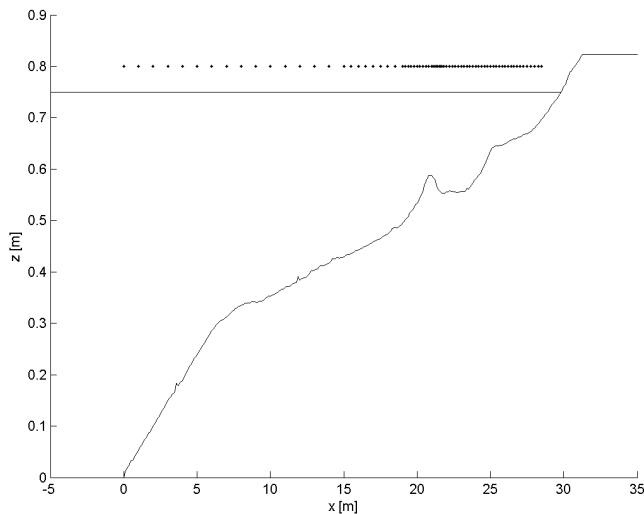


Figure 3.13 Locations of surface elevation measurements

Results

Test	H_{m0} [m]	T_p [s]
1A	0.157	2.1
1B	0.206	2.1
1C	0.103	3.4

Table 3.5 The Boers (1996) wave conditions.

The comparison between the model and the observations for the wave height transformation of the short waves, the infragravity waves, the setup, spectral period, mean period, skewness and asymmetry is shown in Figure 3.14, Figure 3.15 and Figure 3.16. An overview of the statistical scores is given in Table 3.6.

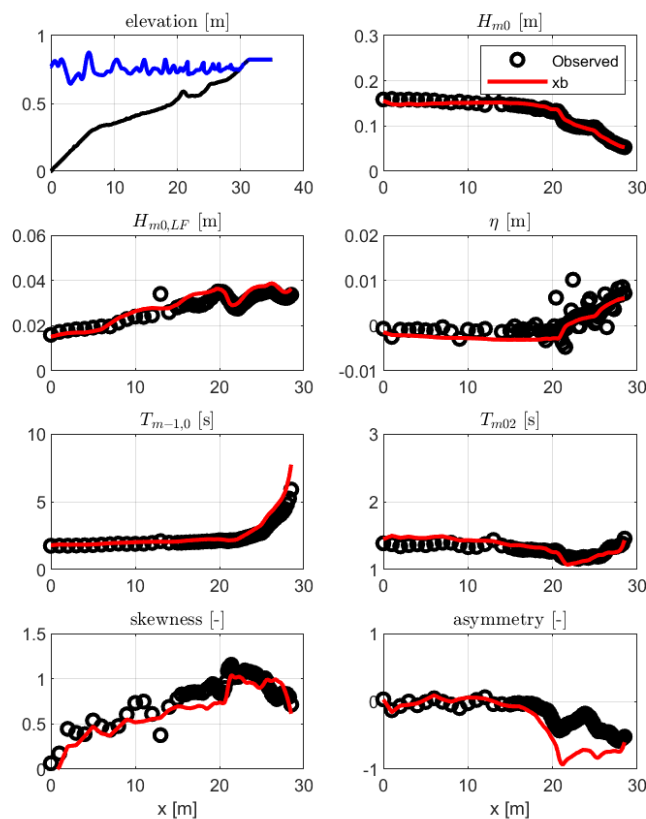


Figure 3.14 Wave hydrodynamics during test 1A. The top-left panel shows the model set-up. The other plots show the performance of XBeach (red) compared to the observations during the experiments (blue).

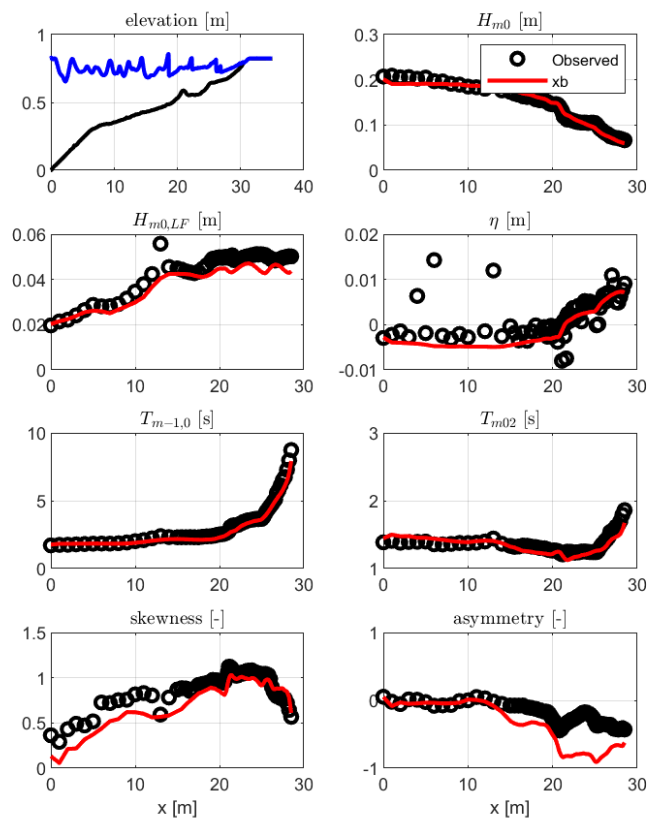


Figure 3.15 Wave hydrodynamics during test 1B. The top-left panel shows the model set-up. The other plots show the performance of XBeach (red) compared to the observations during the experiments (blue).

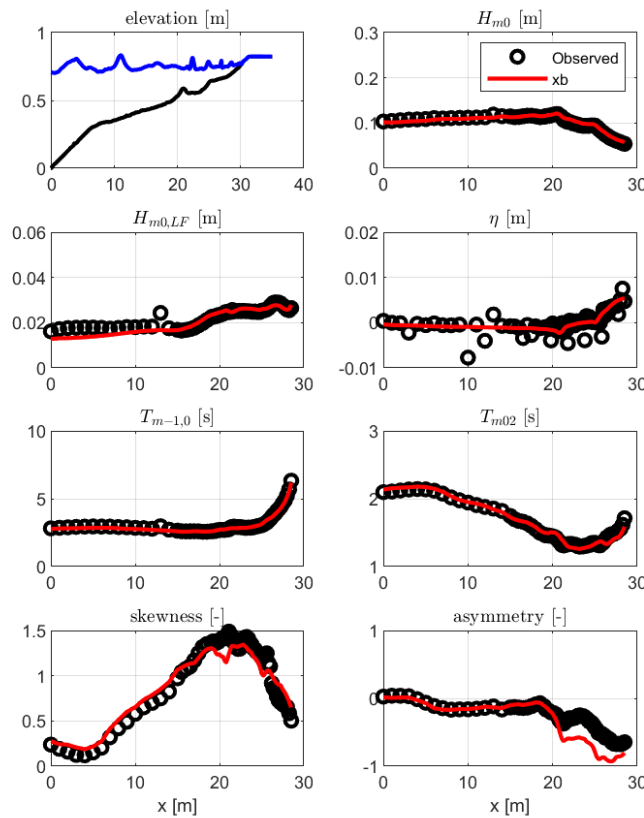


Figure 3.16 Wave hydrodynamics during test 1C. The top-left panel shows the model set-up. The other plots show the performance of XBeach (red) compared to the observations during the experiments (blue).

Table 3.6 The statistical scores for the Boers experiments. The scatter index (SCI) and relative bias (rel. bias) are shown for the short-wave height, infragravity wave height and spectral period.

	$1A_n h$	$1B_n h$	$1C_n h$
$H_{m0,HF}$ Rel. bias	0.00	-0.01	0.02
$H_{m0,HF}$ SCI	0.05	0.05	0.03
$H_{m0,LF}$ Rel. bias	0.06	-0.10	-0.01
$H_{m0,LF}$ SCI	0.09	0.11	0.08
$T_{m-1,0}$ Rel. bias	0.12	-0.06	-0.01
$T_{m-1,0}$ SCI	0.20	0.08	0.03

3.4.2 High- and low-frequency wave transformation over fringing reef Experiment description

Buckley *et al.* (2015) performed experiments with irregular waves in the physical wave flume at Deltires (Eastern Scheldt flume). The flume has a length of 55 meters, a width of 1.0 m and a height of 1.2 m. The reef profile was constructed from marine plywood and had a 1:5 reef slope, a 14-m horizontal reef flat, and a 1:12 beach (Figure 3.17). Based on the 1:36 geometric scaling assumed in this study, this represents a 500-m-long reef flat in field (prototype) scale. Waves were generated with

a piston-type wave maker with second-order wave generation and active reflection compensation of any seaward-propagating waves reflected back to the wave maker from the reef slope and beach. Irregular waves were generated with a TMA-type spectrum. A total of 16 runs were conducted with varying still water depths on the reef flat $h_{0,r}$ and offshore wave conditions. From these 16 runs, 4 runs are considered in this document (Table 3.7). Water levels were measured using resistance wave gauges sampling synchronously at 40 Hz at 17 locations, with the highest density of measurements in the surfzone region near the reef crest at $x = 0$ m (Figure 3.17). Horizontal velocities were also measured synchronously at 40 Hz using programmable electromagnetic current sensors (P-EMS, Deltas) at six locations collocated with wave gauges (Figure 3.17).

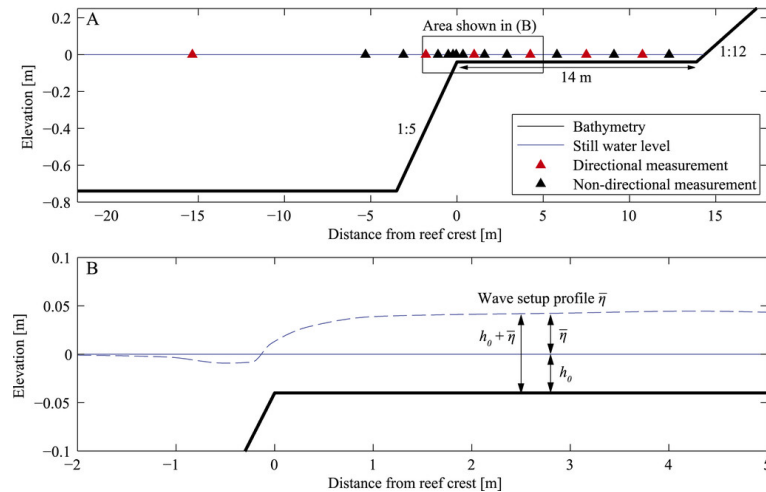


Figure 3.17 Schematic of the fringing reef showing the reef slope (1:5), reef flat length (14 m; 500-m field scale), beach slope (1:12), and instrument locations. Directional measurement sites have collocated water level and velocity measurements, whereas other nondirectional sites have only water level measurements. (b) An example of the wave setup profile in the vicinity of the reef crest, defining the still water depth h_0 and the total water depth.

Test	$H_{rms,0}$ (m)	T_p (s)	$h_{0,r}$ (m)
1	0.03	2.26	0.04
2	0.06	2.26	0.04
9	0.06	2.26	0.00
12	0.06	2.26	0.09

Table 3.7 Specifics for considered test within XBeach testbed

Results

The comparison between the model and the observations for the wave height transformation of the short waves, the infragravity waves, the setup, spectral period, mean period, skewness and asymmetry is shown in Figure 3.18, Figure 3.19, Figure 3.20 and Figure 3.21. An overview of the statistical scores is given in Table 3.8.

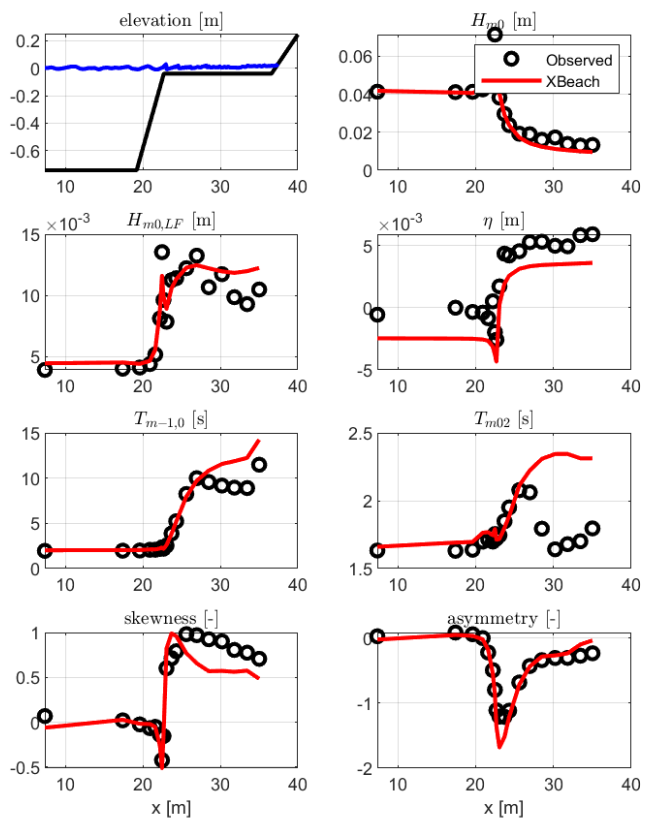


Figure 3.18 Wave hydrodynamics during test 1. The top-left panel shows the model set-up. The other plots show the performance of XBeach (red) compared to the observations during the experiments (blue).

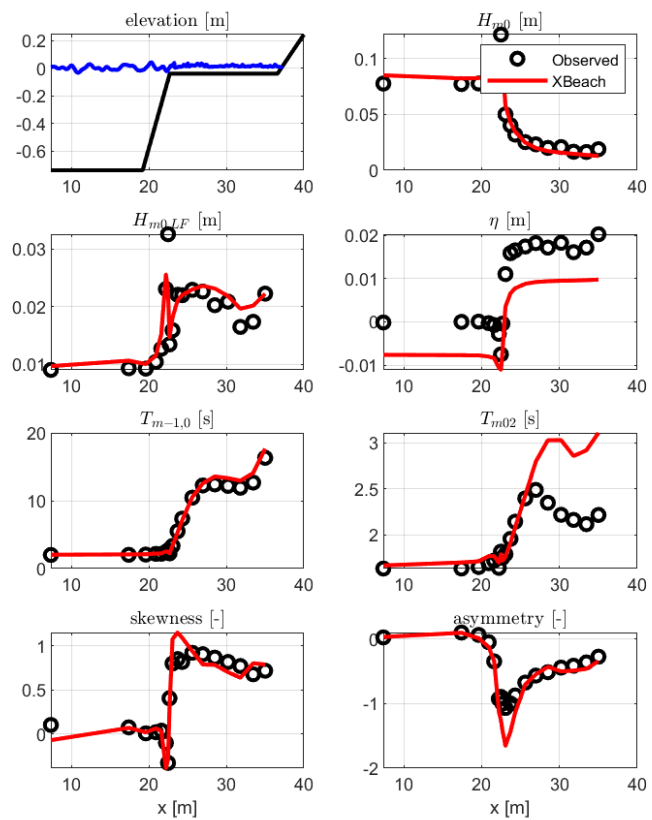


Figure 3.19 Wave hydrodynamics during test 2. The top-left panel shows the model set-up. The other plots show the performance of XBeach (red) compared to the observations during the experiments (blue).

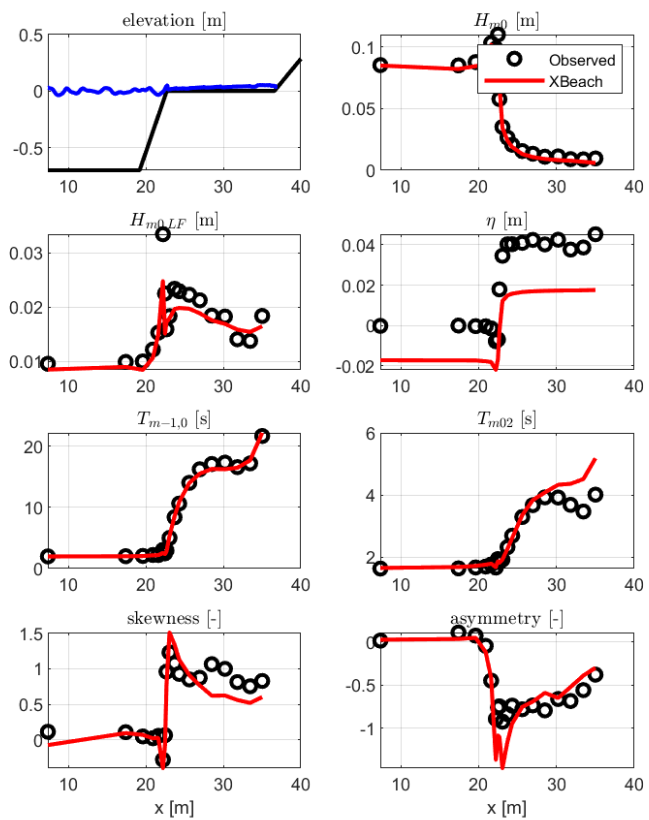


Figure 3.20 Wave hydrodynamics during test 9. The top-left panel shows the model set-up. The other plots show the performance of XBeach (red) compared to the observations during the experiments (blue).

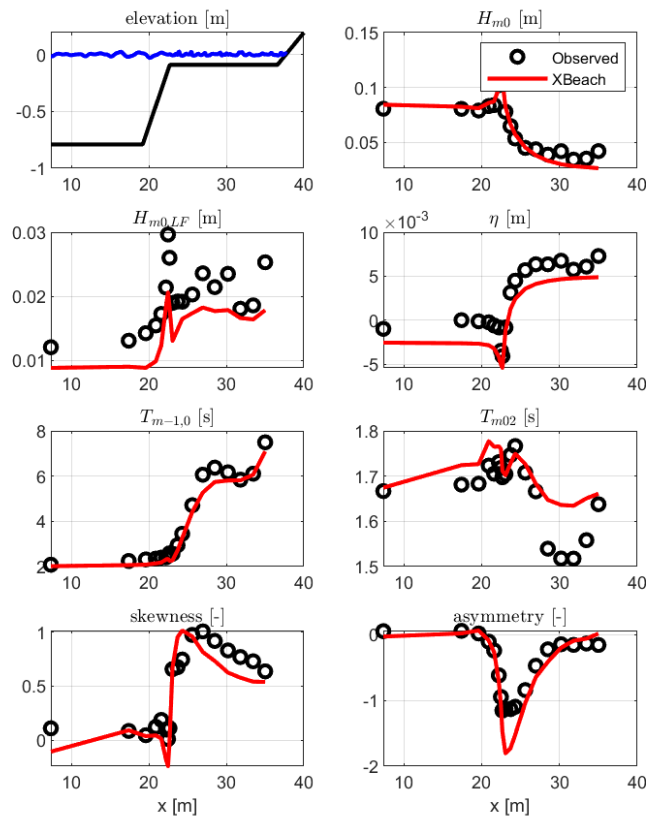


Figure 3.21 Wave hydrodynamics during test 12. The top-left panel shows the model set-up. The other plots show the performance of XBeach (red) compared to the observations during the experiments (blue).

Table 3.8 The statistical scores for the Buckley experiments. The scatter index (SCI) and relative bias (rel. bias) are shown for the short-wave height, infragravity wave height and setup.

	sim1	sim2	sim9	sim12
$H_{m0,HF}$ Rel. bias	+0.04	+0.02	+0.05	+0.04
$H_{m0,HF}$ SCI	+0.10	+0.11	+0.09	+0.11
$H_{m0,LF}$ Rel. bias	+0.03	+0.02	+0.11	+0.25
$H_{m0,LF}$ SCI	+0.09	+0.16	+0.18	+0.27
setup Rel. bias	+0.15	+0.02	+0.14	+0.14
setup SCI	+0.21	+0.11	+0.19	+0.20

3.4.3

Bichromatic waves

In the Van Noorloos (2003) experiment bichromatic waves on a plane beach are studied. A 40 meter long flume with a 1/35 slope sloping beach is used. At 80 locations the water level was measured. The waves are generated with a piston type of wave board which includes second order wave steering. Eight different bichromatic waves are studied with varying frequency and amplitude. In this report test A1, A4 and B4 are simulated with XBeach. In test A1 most of the low frequency waves are dissipated whereas in test A4 most of the low frequency waves are reflected. Additionally, B4 is modelled, because this test contains the largest amplitude of the

bound long wave. In table 3.9 an overview of the three tests is given. The model is forced with a time series of these bichromatic waves including the second order bound waves (super and sub-harmonics).

Table 3.9 Wave conditions for the three tests (Van Noorloos, 2003) which are modelled with XBeach. f_1 and f_2 are the primary wave frequency, f_b is the bound wave frequency and kd the maximum normalized water depth

Test	f_1 (Hz)	f_2 (Hz)	f_b (Hz)	a_1 (m)	a_2 (m)	kd
A1	0.67	0.48	0.19	0.06	0.012	2.00
A4	0.62	0.53	0.09	0.06	0.012	1.81
B4	0.65	0.50	0.15	0.06	0.036	1.95

To show the generation of the bound long wave, the time series is filtered by applying a band filter. The filter is applied to all the higher components of the difference frequency ($m\Delta f = m(f_1 - f_2)$). In this way the higher harmonics of the bound waves are included. In figures 3.22, 3.23 and 3.24 the results for respectively test A1, A4 and B4 are plotted. The upper panel shows the total wave height and the lower panel the filtered bound long wave. An overview of the statistical scores is given in ??.

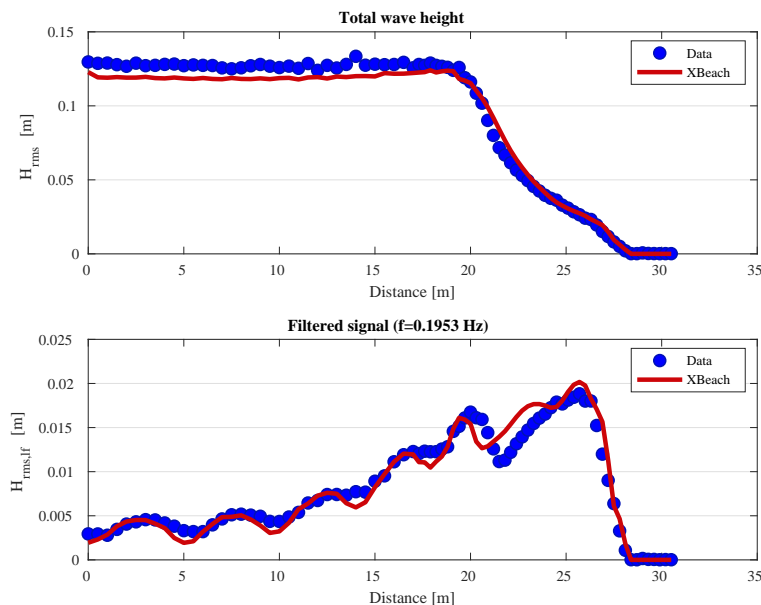


Figure 3.22 The upper panel shows the measured (blue dots) and modeled (red line) total wave height. The lower panel shows the filtered bound long wave of the measurements (blue dots) and the XBeach results (red line).

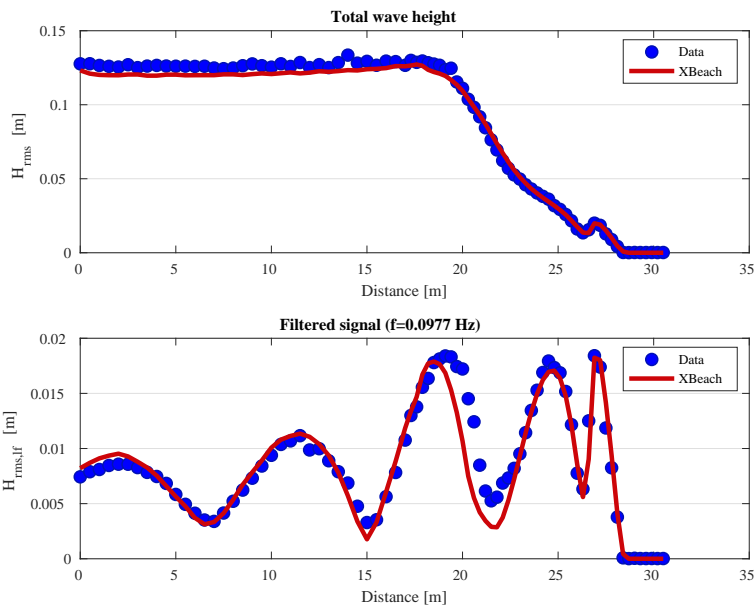


Figure 3.23 The upper panel shows the measured (blue dots) and modeled (red line) total wave height. The lower panel shows the filtered bound long wave of the measurements (blue dots) and the XBeach results (red line).

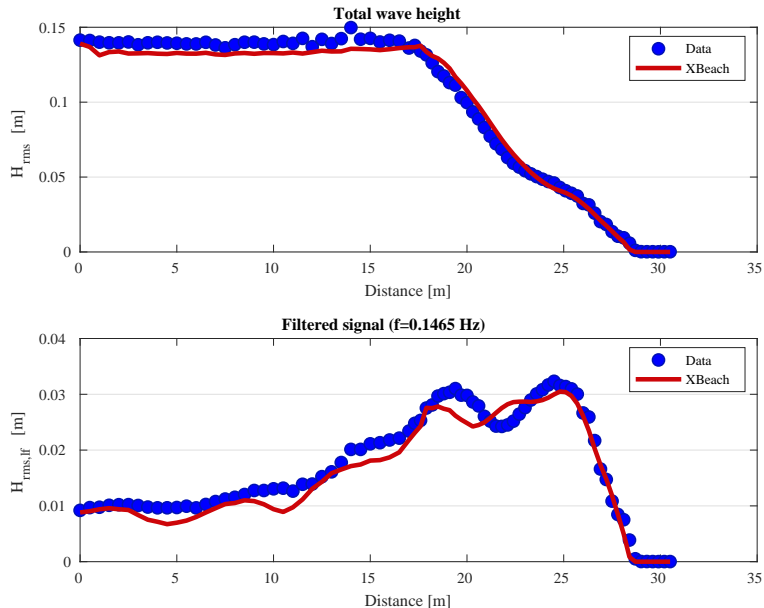


Figure 3.24 The upper panel shows the measured (blue dots) and modeled (red line) total wave height. The lower panel shows the filtered bound long wave of the measurements (blue dots) and the XBeach results (red line).

Table 3.10 The statistical scores for the Van Noorloos experiments. The scatter index (SCI) and relative bias (rel. bias) are shown for the short-wave height, infragravity wave height and spectral period.

	A1	A4	B4
$H_{m0,HF}$ Rel. bias	-0.03	-0.02	-0.02
$H_{m0,HF}$ SCI	0.06	0.04	0.05
$H_{m0,LF}$ Rel. bias	0.02	-0.04	-0.07
$H_{m0,LF}$ SCI	0.02	-0.04	-0.07

4 Hydrodynamic field cases

4.1 Ningaloo Reef

Ningaloo Reef is a large fringing reef on the northwest coast of Australia and consists of a series of reef-channel cells, exposed to tropical cyclones and Southern Ocean swells. A field data set of wave transformation on a shore-normal transect (Figure 4.1) taken at Sandy Bay in June 2009 is described in (Pomeroy *et al.*, 2012). The transect is composed of a steep fore reef, a shallow reef flat (1 – 2m depth) that is separated from the shore by a slightly deeper lagoon (2 – 3m average depth). Instrument C1 was deployed on the forereef slope, C3 and C4 were located on the reef flat, while C5 and C6 were located inside the lagoon behind the reef. The wave field exhibits a dramatic decay in the incident swell band on the fore reef section with a transfer of part of the energy to infragravity waves which are dissipated due to bottom friction over the reef flat and lagoon.

The XBeach model formulations have been extended with a friction dissipation term in the wave action equation (Dongeren *et al.* (2013), which also describes the following case). For this site, optimum friction coefficient values ($f_w = 0.6$, $c_f = 0.1$) were determined for a 1D version of the model based on conditions at the peak of the swell event. These settings were subsequently used to simulate the entire swell event from June 14 12:00 hours to June 19 00:00 hours (109 hours in total) when wave conditions varied significantly. Good agreement was generally observed throughout the simulation and at all sites (Figure 4.2; Figure 5 in Dongeren *et al.* (2013)). The model reproduced the spatial variability in wave heights across the reef, as well as temporal changes in the response to the varying offshore wave conditions and tidal variations. The short wave height predictions matched the data reasonably well (Figure 4.2 a-e), except for a small positive bias of a few centimeters. The IG wave heights were slightly under predicted (negative bias) at C1, but were generally in very good agreement for sites on the reef (Figure 4.2 f-j). The time series of the predicted mean water level residuals (the time-averaged difference between the observed water level on the reef and the observation at C1, $\overline{\Delta z_s} = \overline{z_s - z_{s,C1}}$, thus describing wave setup) followed the observed residuals reasonably well, albeit that the model over predicts the observations by about 0.1 m. (Figure 4.2 l-o) Note that at C1 the observed and predicted water levels rather than the residuals are shown (Figure 4.2 k). A summary of the model skill (bias and the RMS error) for the short wave heights, IG heights and mean water level is shown in Figure 4.3 (Figure 6 in Dongeren *et al.* (2013)).

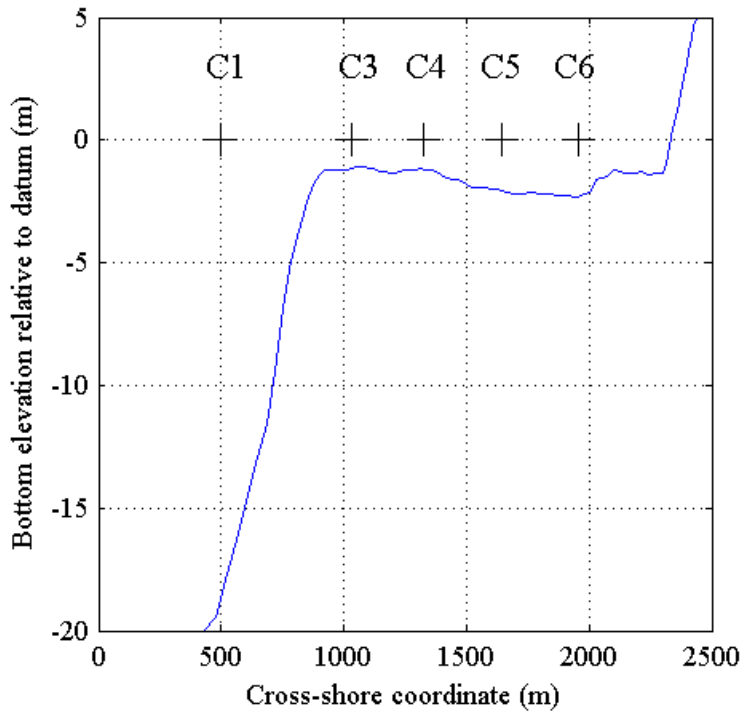


Figure 4.1 Cross-shore profile of the bathymetry along the main measurement transect with instrument locations shown.

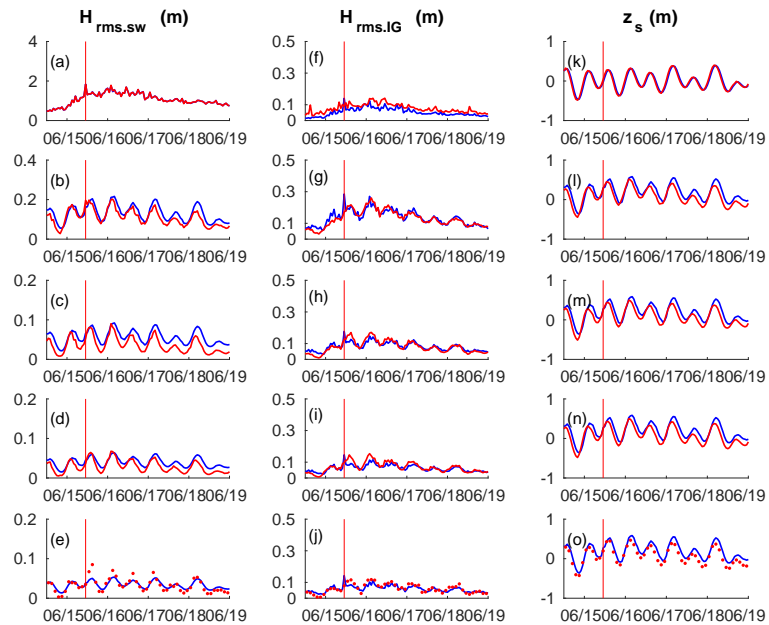


Figure 4.2 Comparison between the 1D model results (blue) and measured data (red) for the duration of the 5 day swell event. (a,f,k) are for instrument C1, (b,g,l) C3, (c,h,m) C4, (d,i,n) C5 and (e,j,o) C6. The peak of the storm is indicated by the red vertical line. Note the large reduction in vertical scale between C1 and the reef sites C3-C6.

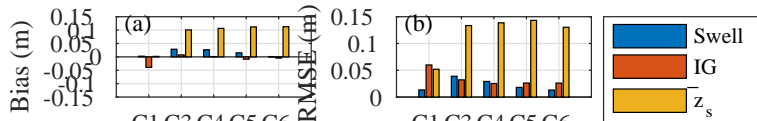


Figure 4.3 Bias and RMS error from the 1D swell duration (5 day) model results compared with the measured data at each site, based on the short wave heights, IG wave heights, and mean water levels.

4.2 DELILAH

In order to verify the 2DH hydrodynamics of XBeach when forced by directionally-spread short waves, a simulation is set up to compare model results to field measurements. In this case the DELILAH field experiment at Duck, North Carolina is selected as a suitable test location. The period that is modeled is October 13th 1990, which was a stormy day, between 16:00 and 17:00 hours. The significant wave height at 8 m water depth was 1.81 m, with a peak period of 10.8 s and a mean angle of incidence of -16° relative to the shoreward normal. This period is selected because the wave conditions are energetic enough to generate a significant infragravity wave component and the incident wave spectrum is sufficiently narrow-banded to justify the assumptions in the model boundary conditions. The model is forced with the wave spectrum measured at 8 m water depth (Birkemeier *et al.*, 1997). A measured tidal signal is imposed on the model boundaries of which the mean level is 0.69 m above datum. The slope of the wave front in the roller model is set to 0.05, which is found to be a slight improvement over the value of 0.10 used in the previous sections. A constant grid size of 5 m in cross shore and 10 m in longshore direction is used. The resolution of the wave model in directional space is 15° . The model is set to generate output at the location of the primary cross shore measurement array, gauge numbers 10, 20, 30, 40, 50, 60, 70, 80 and 90 (Figure 4.4).

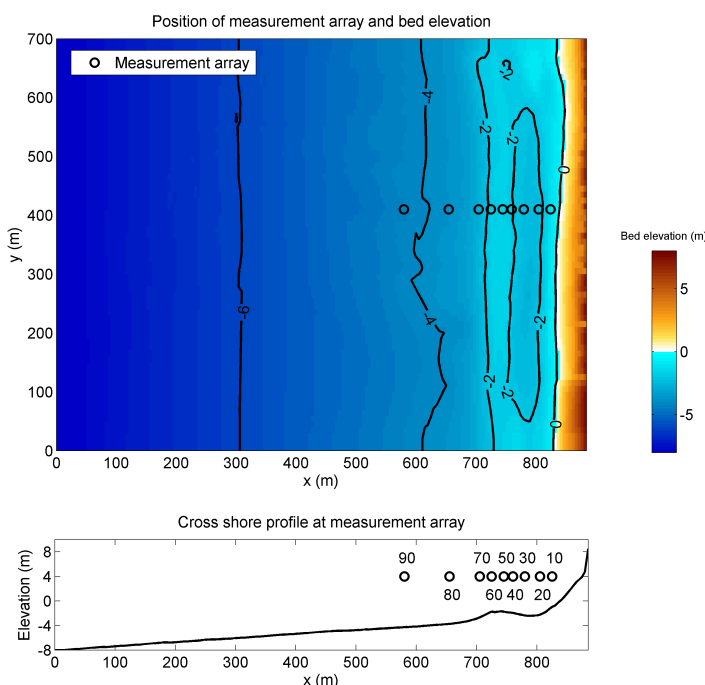


Figure 4.4 Bathymetry and measurement locations

The modeled time-averaged wave heights of the short waves are compared to the time-averaged wave heights measured at the gauges. These results are shown in the first panel of Figure 4.5. Unfortunately, no data exist for gauge number 60.

The infragravity wave height is calculated as follows (Van Dongeren *et al.*, 2003):

$$H_{rms,low} = \sqrt{8 \int_{0.005Hz}^{0.05Hz} Sdf}$$

Figure 4.5 shows the infragravity wave height. The measured and modelled time-averaged longshore current are shown in the second panel of Figure 4.5. The correlation coefficient, scatter index, relative bias and Brier Skill Score for the simulation are shown in Table 4.1.

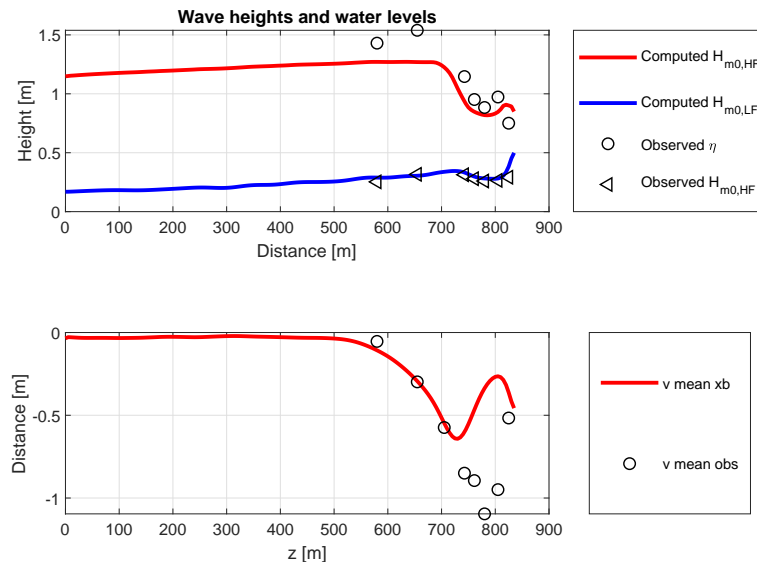


Figure 4.5 Wave height transformation and flow velocities during the DELILAH field experiment 1990

Table 4.1

	R^2	Sci	Rel. bias	BSS
$Hrms_{lf}$	0.73	0.08	0.06	0.46
$Hrms_{hf}$	0.95	0.16	-0.15	0.91
$vmean$	0.51	0.53	0.33	0.26

4.3 Schiermonnikoog

Experiment description

Hydrodynamic data were obtained along a cross-shore transect at the tail of the Dutch barrier island Schiermonnikoog in the Wadden Sea during a measurement campaign of the department Physical Geography of Utrecht University (UU) in the winter of 2014-2015. The campaign was part of the PhD research of Anita Engelstad and Daan Wesselman. The measurements are used for the validation of the hydrodynamics in the BOI-version of the dune erosion model XBeach, with a focus on the validation of simulated infragravity waves.

The location of the measurements is indicated in Figure 4.6. The beach and nearshore morphology near the transect is alongshore almost uniform. The cross-shore profile is a typical Wadden Sea profile, with a mildly sloping foreshore (about 1:100) and three offshore bars. In the intertidal zone, two to three bars are present, which is also visible in the aerial photograph (Figure 4.6). The highest point along the transect the beach crest is at less than 1.8 m +NAP: no dunes are present at the tail and the tail is completely inundated several times per year. At the landward side of the beach crest, the profile gently slopes towards the Wadden Sea. The elevation along the intertidal and subtidal part of the transect has been measured with a RTK-GPS system at the beginning and the end of the field campaign. For the subtidal part, open-source yearly Jarkus transects and Vaklodingen data of RWS are available.

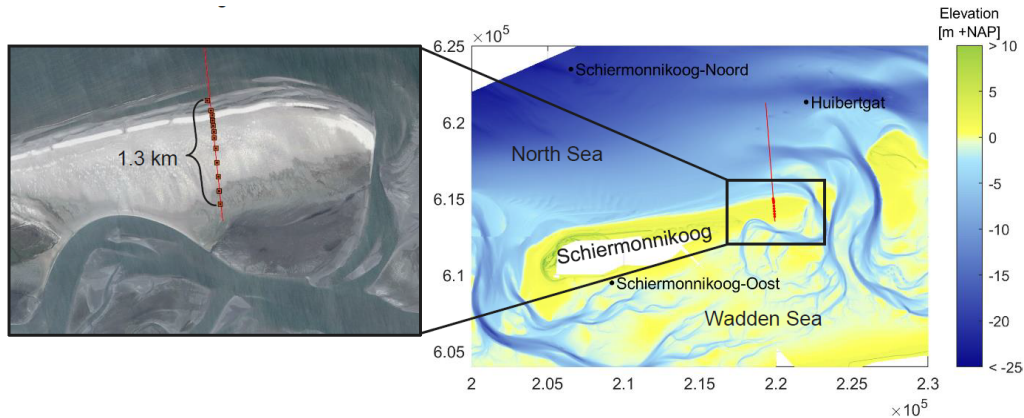


Figure 4.6 Overview of the Schiermonnikoog study area. Right: elevation at and surrounding Schiermonnikoog (mosaic of the Vaklodingen of 2012-2015) and the location of the (offshore) hydraulic stations of RWS (black dots) and the transect (red line) with measurement equipment locations (red dots). Left: aerial photograph of the tail of Schiermonnikoog at 04-20-2014 (Google Earth). The coordinates are in meter (RD-new projection).

The conditions at the case site are mesotidal, mixed-energy and tide-dominated. Generally, the offshore high water levels are about 0.7 m +NAP during neap tide and 1.2 m +NAP during spring tide, while the highest storm surge level in the last 25 years reached 3.5 m +NAP (Wesselman *et al.*, 2018). The mean offshore significant wave height ranges from 0.5 - 1 m in summer to 1 - 2 m in winter, and can increase to 8 - 11 m during (northwestern) storm events. The highest recorded storm setup at this location is approximately 3.5-4 m (Engelstad *et al.*, 2017).

During the observation period, the island tail was flooded 11 times during high water due to storm setup. The highest water levels and wave heights were observed during the storm at 10 and 11-01-2015, with local wind speeds of about 19 m/s from the west and waves from the northwest. This storm is used for the XBeach simulation with BOI-settings for the hydrodynamic validation. The offshore conditions are based on RWS data shared by the UU: offshore water level data at the North Sea (Huibertgat station) and in the Wadden Sea (Schiermonnikoog-Oost station), and wave height, period and directional spreading at the North Sea (Schiermonnikoog-Noord wave buoy) with a 10-min data interval.

The storm peak is defined as the moment with highest water levels (WL = 2.7 m +NAP at the North Sea at Huibertgat and 2.9 m +NAP in the Wadden Sea at Schiermonnikoog-Oost) and coincides with high tide. At this moment, the Hs was about 6.0 m and Ts 12 s. The highest offshore significant wave height (Hs) at the

station Schiermonnikoog-Noord was 7.1 m, and occurred during the low tide (about -0.3 m NAP) in advance of the storm peak. The corresponding significant wave period (T_s or $T_{1/3}$) was 13 s. The wave heights remained higher than 5 m for a full day. During the storm, the waves were more focused: the directional wave spreading decreased from more than 35° to about 23° during the storm peak and about 29° afterwards. Based on the water level, the return period of this storm is about 10 years.

During the field campaign, measurements along the transect from the North Sea to the Wadden Sea (red dots in [Figure 4.6](#)) were performed using among others ten stand-alone pressure transducers (PTs) from 04-11-2014 to 31-01-2015. The PTs recorded the water level continuously at 10 Hz with an accuracy of 1 mbar (approximately 1 cm). Short and infragravity wave heights were determined for 15 min blocks by multiplying the standard deviation of the second-order detrended sea surface elevation with four, using a highpass filter (0.05-1 Hz) for short waves and a lowpass filter (0.005-0.05 Hz) for infragravity waves. More information on the data can be found in [Wesselman et al. \(2018\)](#) and [Engelstad et al. \(2017\)](#). The processed data was made available by the UU in order to compare this with the XBeach model output.

Results

[Figure 4.7](#) shows the spatial patterns in the water depth and wave heights (H_{m0}) along the cross-section during the storm peak. [Figure 4.8](#) shows an example timeseries of the water depth and wave heights during the three tidal cycles just before and during the storm for the first measurement location at the beach (P1). The dots represent the measured values and the blue line the modelled values. [Figure 4.9](#) shows the measured versus the modelled water depth and wave height of the short and infragravity waves for the entire model period and all locations. A quantitative comparison between the model results and the measurements is presented in [Table 4.2](#) by means of goodness-of-fit indicators.

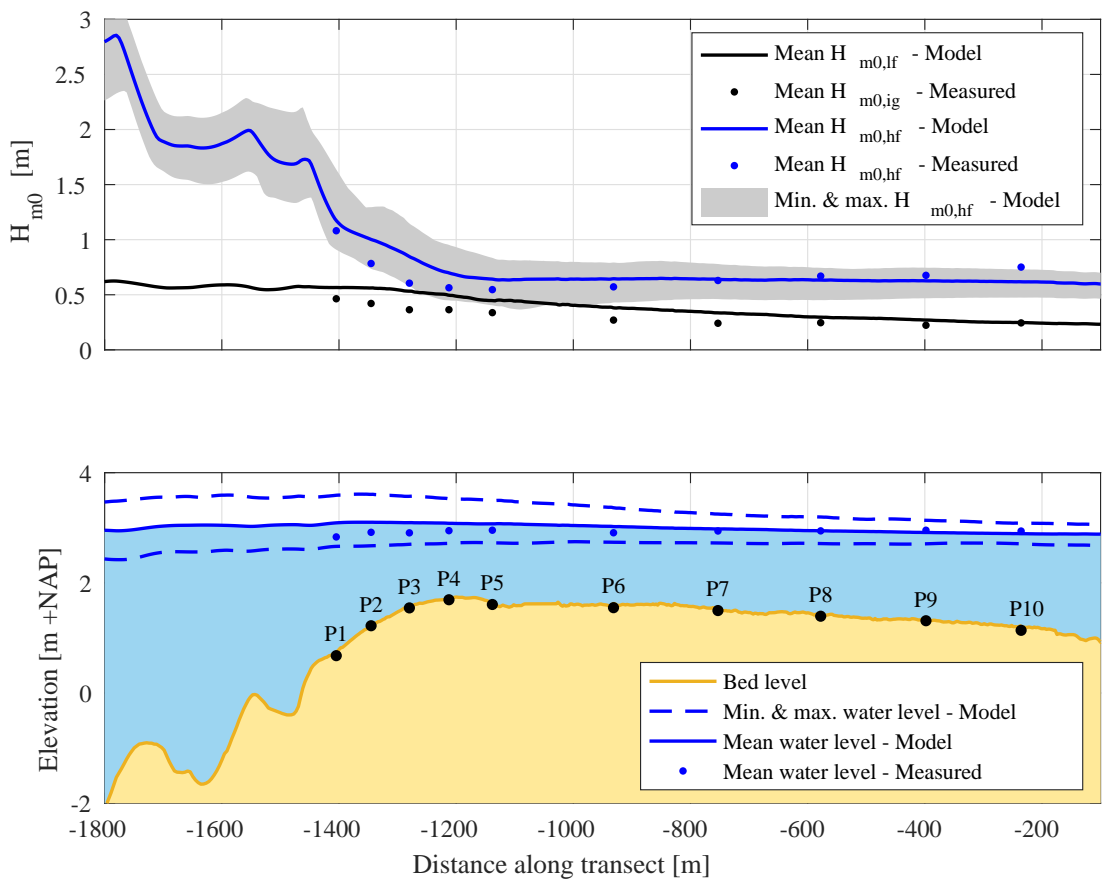


Figure 4.7 Cross-section with the modelled and measured water level and spectral significant wave height (H_{m0}) of high and low frequency waves during the storm peak (11-01-2015 13:00-13:30). The grey zone around the modelled $H_{m0,hf}$ indicates the minimum and maximum $H_{m0,hf}$. Note the difference between the modelled low frequency H_{m0} (no frequency domain filter) (black line) and the measured infragravity H_{m0} (0.005 and 0.05 Hz) at the point locations (grey-green dots).

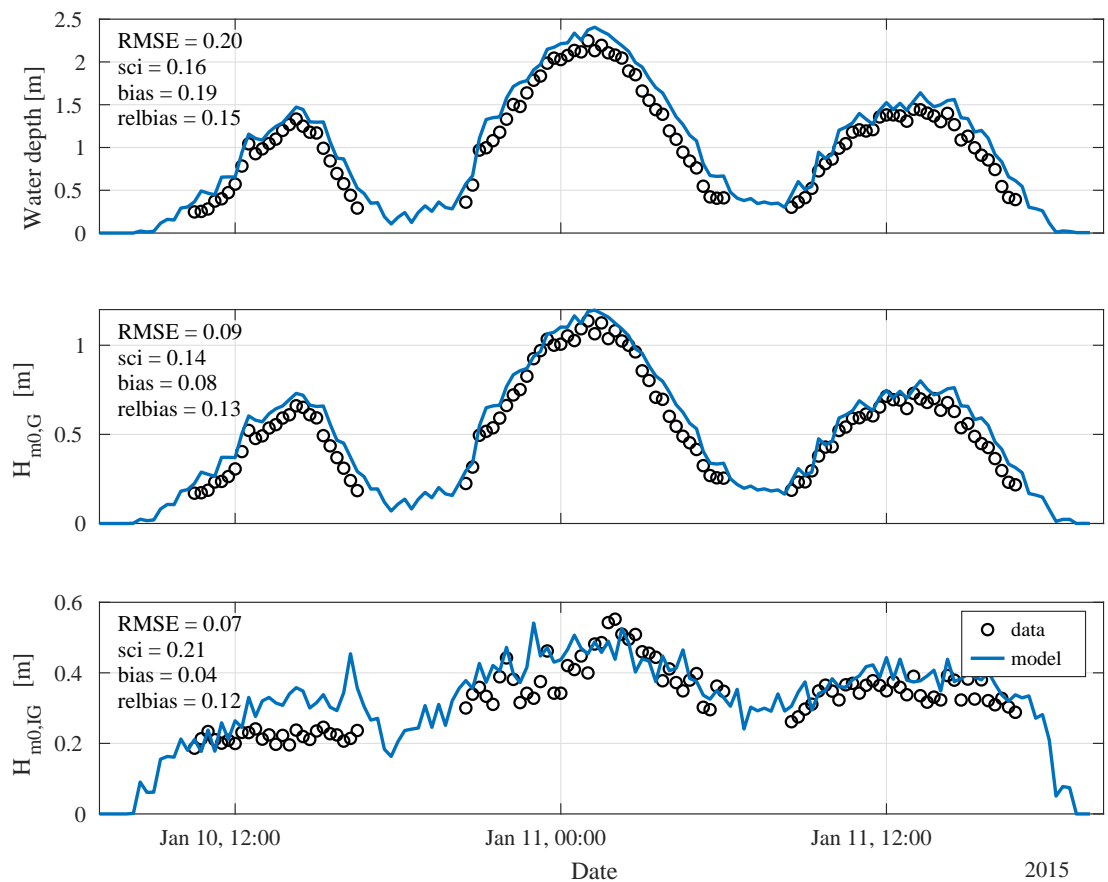


Figure 4.8 Timeseries of measured and modelled water depth, short and infragravity spectral significant wave height including goodness-of-fit indicators for measurement location P1.

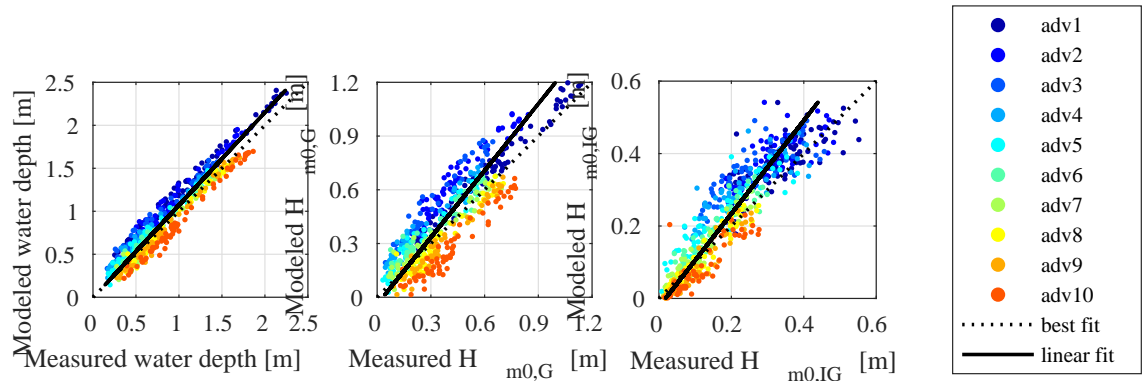


Figure 4.9 Scatter plot of the measured versus modelled water depth, spectral significant wave height (H_{m0}) of short waves (G) and infragravity waves (IG) for all measurement locations at Schiermonnikoog. The dashed line indicates a perfect fit, the continuous line represents a linear fit through the point cloud

Table 4.2 Goodness-of-fit (GoF) indicators for the modelled water depth [m] and the spectral significant wave height [m] for high frequency and infragravity waves compared to the measurements.

	<i>WL</i> <i>RMSE</i>	<i>WL</i> <i>SCI</i>	<i>WL</i> <i>bias</i>	<i>WL</i> <i>relbias</i>	<i>HF</i> <i>RMSE</i>	<i>HF</i> <i>SCI</i>	<i>HF</i> <i>bias</i>	<i>HF</i> <i>relbias</i>	<i>IG</i> <i>RMSE</i>	<i>IG</i> <i>SCI</i>	<i>IG</i> <i>bias</i>	<i>IG</i> <i>relbias</i>
P1	0.20	0.16	0.19	0.15	0.09	0.14	0.08	0.13	0.07	0.21	0.04	0.12
P2	0.20	0.19	0.19	0.18	0.21	0.43	0.21	0.42	0.09	0.28	0.07	0.23
P3	0.18	0.24	0.17	0.22	0.20	0.58	0.19	0.56	0.11	0.41	0.10	0.35
P4	0.12	0.17	0.10	0.15	0.13	0.42	0.12	0.40	0.09	0.38	0.08	0.31
P5	0.09	0.12	0.07	0.09	0.08	0.29	0.07	0.25	0.06	0.32	0.05	0.26
P6	0.06	0.07	0.03	0.03	0.08	0.23	0.07	0.20	0.05	0.27	0.04	0.21
P7	0.05	0.06	-0.00	-0.00	0.04	0.12	0.01	0.04	0.03	0.18	0.01	0.10
P8	0.06	0.06	-0.04	-0.04	0.06	0.14	-0.04	-0.10	0.02	0.16	-0.01	-0.05
P9	0.07	0.07	-0.06	-0.06	0.08	0.20	-0.07	-0.17	0.03	0.24	-0.02	-0.15
P10	0.14	0.13	-0.13	-0.12	0.15	0.32	-0.14	-0.31	0.05	0.35	-0.03	-0.22
Mean	0.14	0.14	0.06	0.06	0.12	0.29	0.05	0.12	0.07	0.29	0.04	0.15

4.4

Saint-Trojan

Experiment description

The field dataset of Saint Trojan in France is used for hydrodynamic validation of the BOI-version of dune erosion model XBeach, in particular regarding the infragravity-wave behavior. The field campaign took place in February 2017 on the gently sloping Saint-Trojan Beach during an energetic storm. [Bertin et al. \(2020\)](#) compared observations to a 2DH XBeach model and presented detailed analysis on infragravity-wave behavior.

The field site is a dissipative sandy beach located in the central part of the French Atlantic coast ([Figure 4.10](#)), along the southwestern coast of Oléron Island. The continental shelf in front of the study area is about 150 km wide, with a very gently sloping shoreface, the 20 m isobath being some 10 km away from the shoreline. The beach slope typically ranges from about 0.0015 at the shoreface to 0.015 in the intertidal area, and the beach is mainly composed of fine and well-sorted sands ($D_{50} = 0.180.22$ mm). The tidal regime in this region is semidiurnal and macrotidal, with a tidal range varying between about 1.5 m during neap tides and 5.5 m during spring tides. Tidal currents are weak at the studied beach, and the impact of tides on short waves remains mostly restricted to water level variations.

The storm Kurt generated very long swell waves that reached the coast between the 2nd and 3rd of February 2017. At the deep-water buoy of Biscay ([Figure 4.10a](#)), the mean wave period increased from 8.0 to 13.0 s, and Hs rapidly increased from 3.0 m to almost 10.0 m, which corresponds to a return period on the order of 1 year ([Lerma et al., 2015](#)). The wave hindcast described in [Guérin et al. \(2018\)](#) suggests that the peak wave period T_p exceeded 20 s.

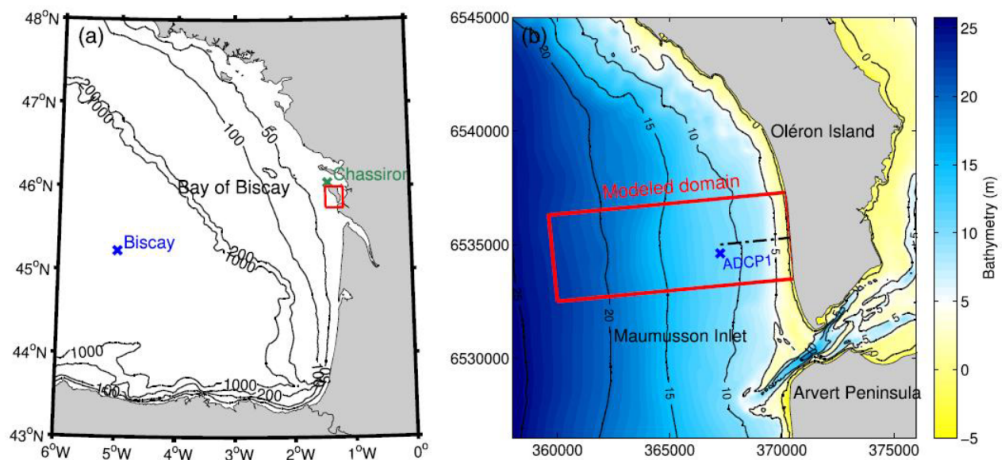


Figure 4.10 Location of the Saint Trojan study area in the Bay of Biscay, with the Biscay buoy (OE) and Chassiron Meteorological station (OE). (b) Detailed bathymetry of the study area (m relative to mean sea level), showing the location of the offshore ADCP1 (OE) and the instrumented cross-shore profile (dashed line). The coordinates are in meter (Lambert-93 projection). Source: [Bertin et al. \(2020\)](#)

The measurement period of the field campaign encompassed four tidal cycles, from the 1st of February 2017 to the 3rd of February 2017, and is characterized by a tidal range of 3.5 to 4 m. An Acoustic Doppler Current Profiler (ADCP1) equipped with a pressure sensor was deployed about 3 km offshore (Figure 4.10b). In the intertidal zone, nine pressure transducers (PT) sampling at 4 Hz were deployed, as well as a second ADCP at the location of PT3. For each sensor, bottom pressure measurements were first corrected for sea level atmospheric pressure measured at the nearby meteorological station of Chassiron. The entire record was then split into consecutive bursts of 30 min, and only the bursts in which the sensor was continuously submerged were considered. PT9 was never continuously submerged for more than 30 min and data from this PT was therefore discarded. Bottom pressure power density spectra $E_p(f)$ were computed using Fast Fourier Transforms, with 10 Hanning windowed, 50% overlapping segments (20 degrees of freedom). These pressure spectra were subsequently converted into elevation spectra considering linear wave theory. The spectral significant wave height (H_{m0}) was computed as $H_{m0} = 4\sqrt{m_0}$ where the upper threshold frequency was set to 0.4 Hz. The threshold frequency between the high-frequency waves and the lower infragravity waves is time-varying and defined following Roelvink and Stive (1989) and Hamm and Peronnard (1997) as half the continuous peak frequency f_p . It is important to note that in processing of the observations the infragravity-wave frequency band was not delimited by a lower threshold, and therefore also covers the VLF (very low frequency) waves. For more information on the field campaign and data processing please refer to [Bertin et al. \(2020\)](#).

Results

The observed and predicted water level, short- and long-wave heights during the peak of the storm are presented in Figure 4.11. The local timeseries of observed and modeled water level and wave-height variations of measurement locations PT3 and PT7 are depicted in Figure 4.12 and Figure 4.13 respectively. Goodness-of-fit indicators are presented in each subplot (per location), and additionally assembled for all locations in Table 4.3. An aggregated scatter plot of observed versus modelled water levels and wave heights is presented in Figure 4.14.

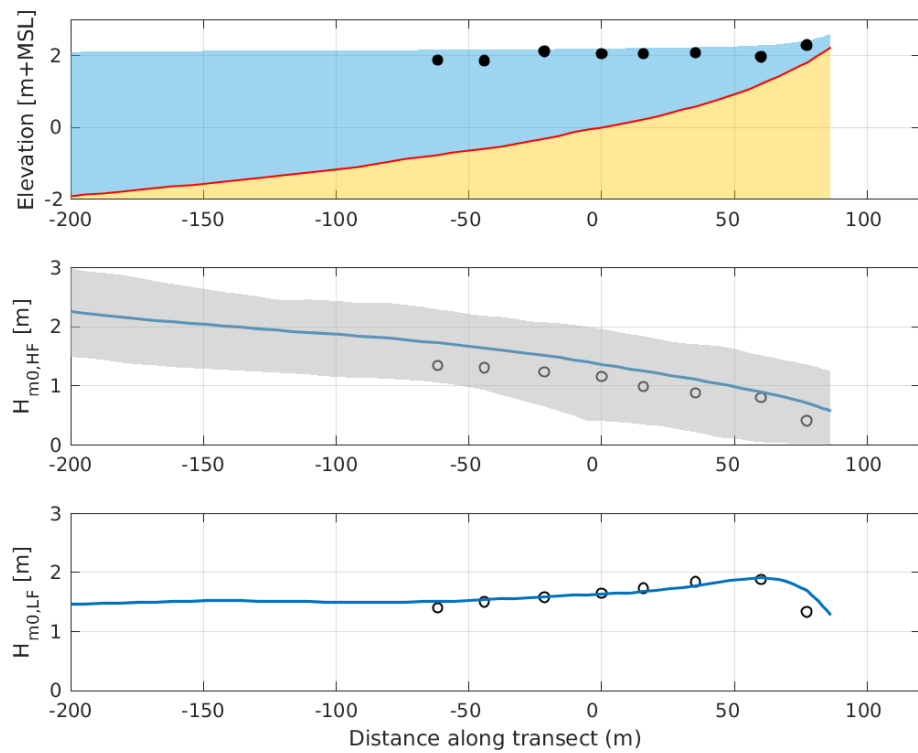


Figure 4.11 Cross-section at the transect location during storm peak (3rd of February 2017 at 8 AM) of the water level (upper panel), short-wave height (middle panel) and low-frequency (IG and VLF) wave height (middle panel). In blue the model results, and the observations are represented by circles. In grey the predicted minimum and maximum short-wave heights during the half hour around the peak of the storm.

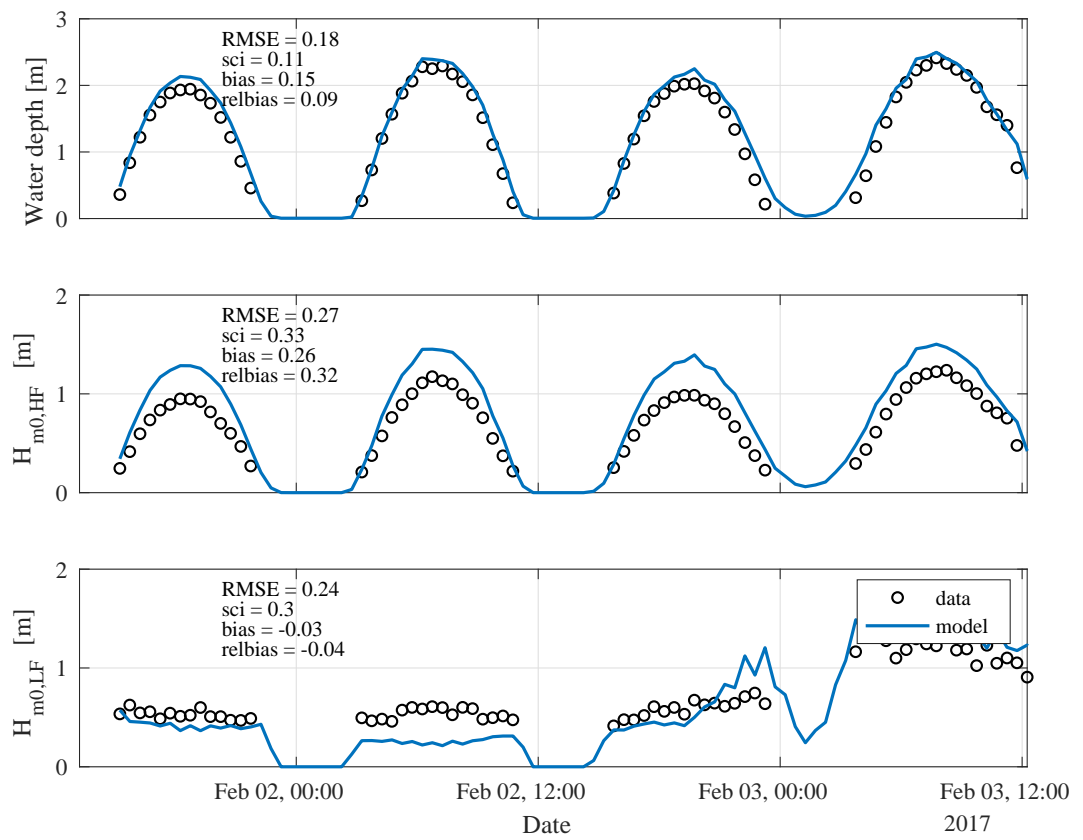


Figure 4.12 Modeled (blue line) against observed (circles) water depth (top), short-wave height (middle) and low-frequency wave height (bottom) at PT3.

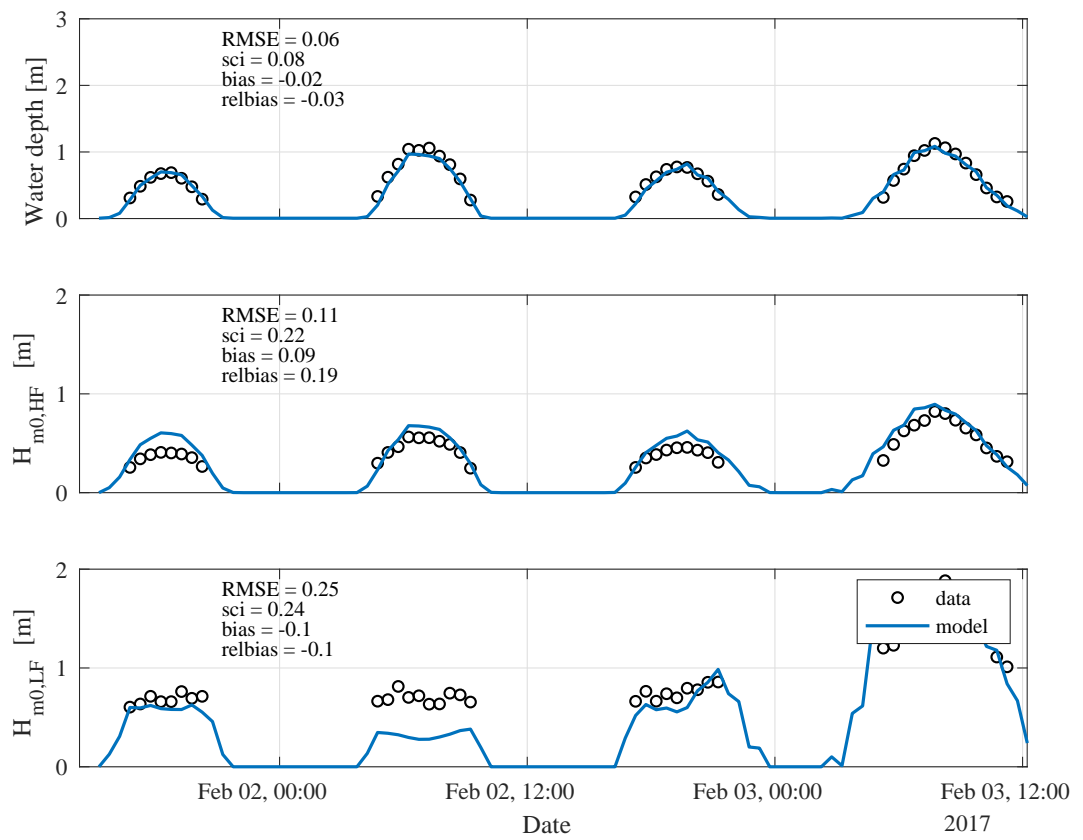


Figure 4.13 Modeled (blue line) against observed (circles) water depth (top), short-wave height (middle) and low-frequency wave height (bottom) at PT7.

Table 4.3 Goodness-of-fit (GoF) indicators for the modelled water depth [m] and the high- and low frequency wave heights [m] compared to the measurements at the PT1 to PT8 (seaward to landward side of measurement transect).

	<i>WL</i>	<i>WL</i>	<i>WL</i>	<i>WL</i>	<i>HF</i>	<i>HF</i>	<i>HF</i>	<i>HF</i>	<i>IG</i>	<i>IG</i>	<i>IG</i>	<i>IG</i>
	<i>RMSE</i>	<i>SCI</i>	<i>bias</i>	<i>relbias</i>	<i>RMSE</i>	<i>SCI</i>	<i>bias</i>	<i>relbias</i>	<i>RMSE</i>	<i>SCI</i>	<i>bias</i>	<i>relbias</i>
PT1	0.13	0.06	0.08	0.04	0.21	0.21	0.19	0.19	0.24	0.33	0.02	0.02
PT2	0.25	0.15	0.24	0.14	0.35	0.41	0.33	0.39	0.23	0.31	0.03	0.04
PT3	0.18	0.11	0.15	0.09	0.27	0.33	0.26	0.32	0.24	0.30	-0.03	-0.04
PT4	0.10	0.07	0.05	0.03	0.24	0.32	0.22	0.29	0.22	0.27	-0.02	-0.03
PT5	0.22	0.18	0.18	0.15	0.28	0.46	0.27	0.44	0.23	0.26	-0.03	-0.03
PT6	0.21	0.22	0.20	0.21	0.19	0.33	0.18	0.31	0.26	0.28	-0.06	-0.06
PT7	0.06	0.08	-0.02	-0.03	0.11	0.22	0.09	0.19	0.25	0.24	-0.10	-0.10
PT8	0.15	0.33	-0.13	-0.29	0.18	0.75	0.16	0.66	0.26	0.33	0.04	0.04

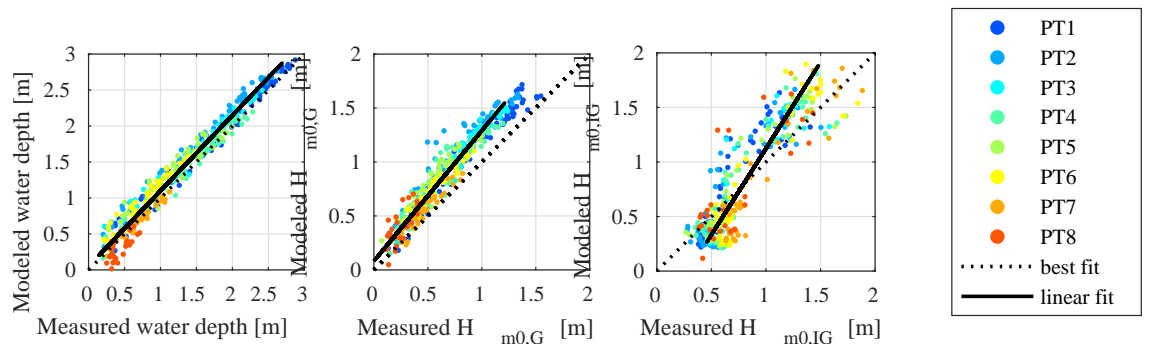


Figure 4.14 Observed versus predicted (left) water levels, (middle) short-wave height $H_{m0,HF}$ and (right) low-frequency wave-height $H_{m0,LF}$.

5 Morphological laboratory tests

In this chapter, the performance of XBeach is compared to results obtained from physical model tests performed in a variety experiments. Research took place at different laboratory scales, mainly depending on the size of the facility used.

The accuracy of XBeach is quantitatively verified for three indicators of the morphology (see [?](#)). Based on the profiles on several moments in time (t), the berm slope indicator, dune retreat indicator and erosion volume are compared to the observed indicator (See [Figure 5.1](#), [Figure 5.2](#) and [Figure 5.3](#)). The definition of these indicators is given in [??](#). The relative error of these indicators is computed for every moment in time where observations are available,

$$V_{rel} = (V_{xb,t} - V_{data,t})/V_{data,t_{end}} \quad (5.1)$$

$$S_{rel} = (slope_{xb,t} - slope_{data,t})/slope_{data,t} \quad (5.2)$$

$$dx_{rel} = (dx_{xb,t} - dx_{data,t})/dx_{data,t_{end}} \quad (5.3)$$

where V is the erosion volume above maximum still water level, $slope$ the berm slope and dx the dune retreat. The quantities computed with XBeach are indicated with xb and the observed quantities are indicated with $data$. Next to the relative error with respect to the last timestep for the erosion volumes and dune retreat, the relative errors with the corresponding time is also computed:

$$V_{rel,t} = (V_{xb,t} - V_{data,t})/V_{data,t} \quad (5.4)$$

$$dx_{rel,t} = (dx_{xb,t} - dx_{data,t})/dx_{data,t} \quad (5.5)$$

The root-mean-squared value of these series of relative errors is used to obtain a single error measure per indicator for all moments in time (except for the data points in the first hour of an experiment). The relative errors in the first hour are ignored since this relative error can be large compared to the other moments in time and the fact that these initial errors are not important for the dune assessment (similar as described in [?](#)).

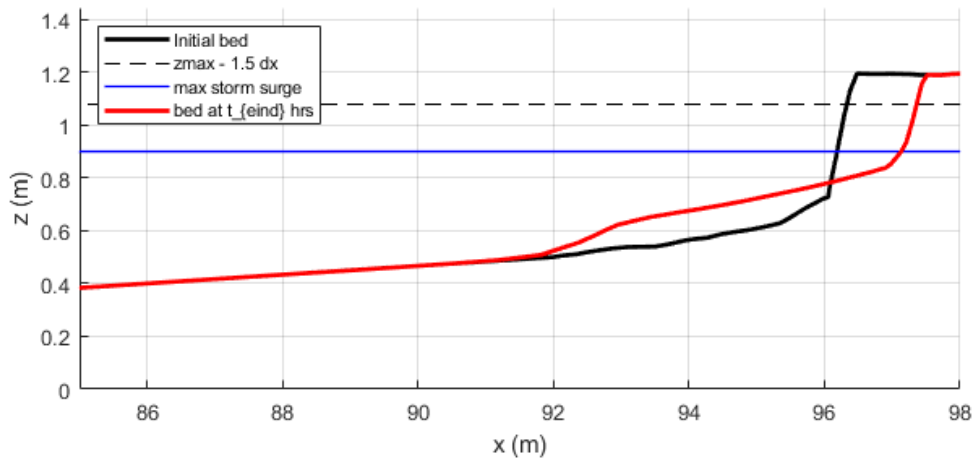


Figure 5.1 Dune retreat indicator. See the Appendix for the definition of this indicator.

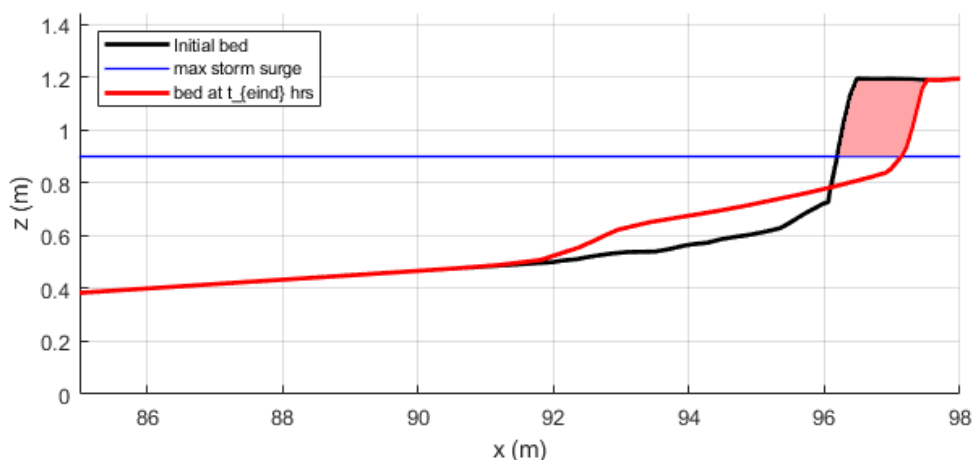


Figure 5.2 Definition of erosion volume. See the Appendix for the definition of this indicator.

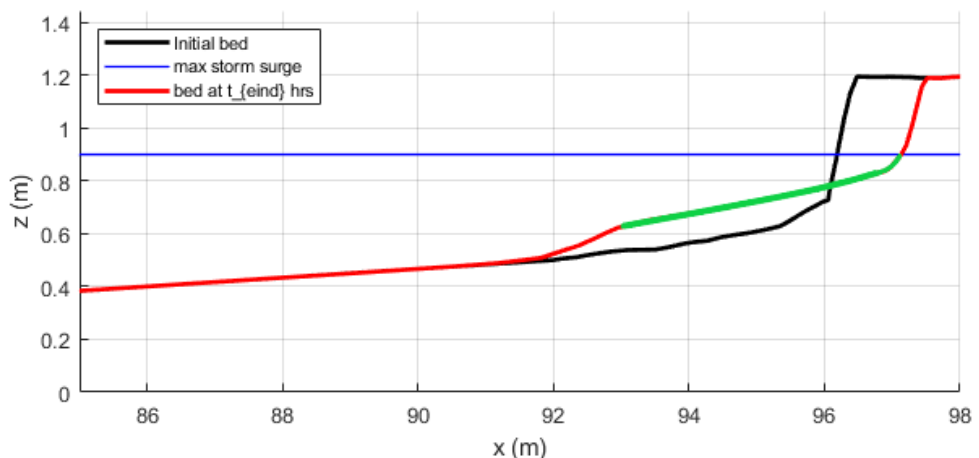


Figure 5.3 Berm slope indicator. See the Appendix for the definition of this indicator.

5.1

M1263 III: Delta Flume 1980-1981

Experiment description

The purpose of research programme M1263-3 was to verify the scale relations and the reliability of the deterministic dune erosion method according to Vellinga (1986), (Vellinga, 1984). In total 5 tests were performed in the Delta Flume of WL | Delft Hydraulics in the period of November 1980 till May 1981. Test 1 and Test 2 were performed at a depth scale of 5 and with a constant water level. In Test 1 the Dutch reference profile (see Figure 1.1) was used as initial profile with a geometric contraction of $S_0 = 3$, while in Test 2 a geometric contraction of $S_0 = 2$ was applied. Test 3 was performed at the same depth scale as Test 2 and with the same initial profile, but with a varying water level. In Test 4 the storm surge of 1953 in The Netherlands was reproduced at a depth scale 3.27. Test 5 can be considered as a full-scale replica 1:1 of a moderate storm in nature; the reference profile was used with a steepness factor of $S_0 = 2.47$. The Delta Flume is approximately 230 m long, 5 m wide and 7 to 9 m deep. At the time these tests were performed the wave board in the Delta flume was not yet equipped with active reflection compensation (ARC) nor with second-order wave steering.

The five experiments are presented in Table 5.1. Tests 1, 2 and 5 had a constant surge level, while tests 3 and 4 had a variable surge level with a course depicted in Figure 5.4 and Figure 5.5 respectively.

Table 5.1 Overview of experiments

Experiment	Depth-scale	Profile contraction	Sediment diameter	Water depth	Wave height	Wave period
1	5	1.91	225	4.2	1.50	5.4
2	5	1.27	225	4.2	1.50	5.4
3	5	1.27	225	4.2	1.50	5.4
4	3.27	1.91	225	4.2	1.85	5.0
5	1	1	225	5.0	2.00	7.6

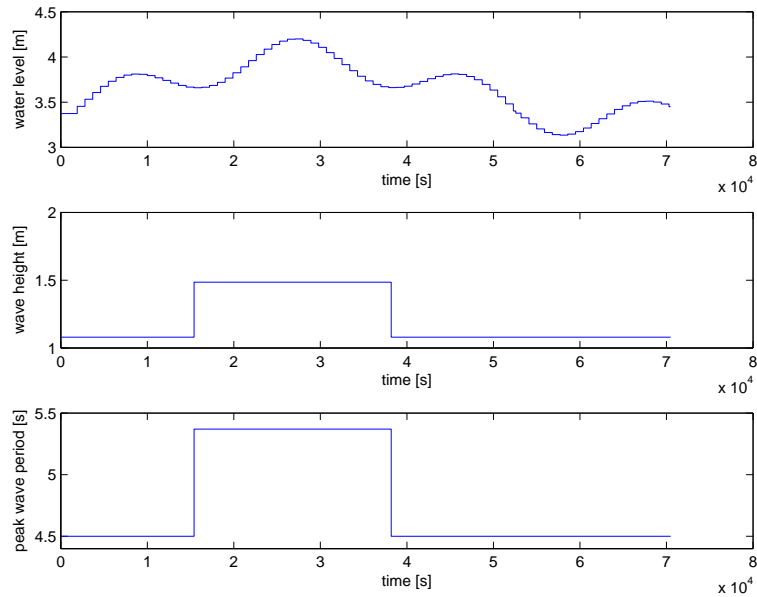


Figure 5.4 Boundary conditions for test 3. The storm development is shown for the water level (upper panel), the wave height (second panel) and the peak period (lower panel) as a function of time.

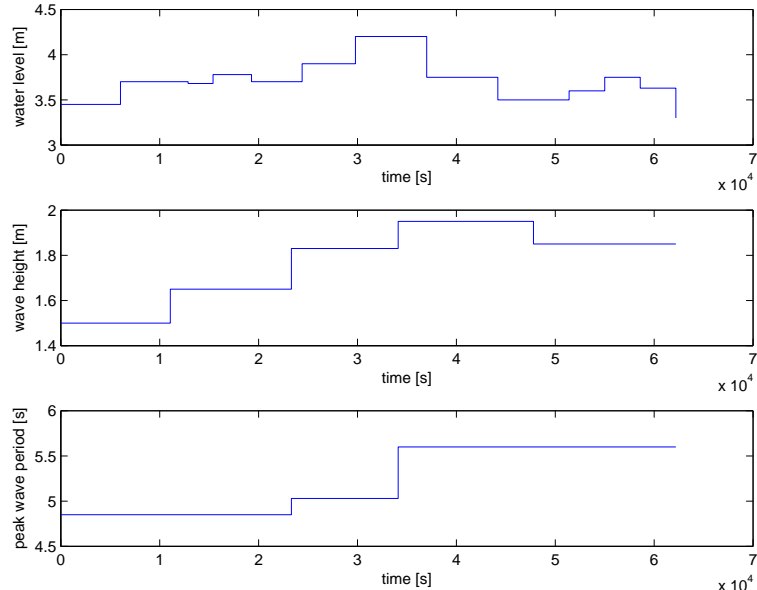


Figure 5.5 Boundary conditions for test 4. The storm development is shown for the water level (upper panel), the wave height (second panel) and the peak period (lower panel) as a function of time.

Results

The profile developments are shown in Figure 5.6 to Figure 5.14. In Table 5.2 to Table 5.6, the indicators for different moments in time are shown. Next to the profiles, the relative errors as a function of time are shown in Figure 5.7, Figure 5.9, Figure 5.11, Figure 5.13 and Figure 5.15. Note that the depth-scale factor is relatively small for Test-4 and Test-5. This means that the grid resolution is also relatively large compared to the others tests, which affects the dune retreat indicator since the dune retreat is defined as the 1.5 grid cell below the maximum dune height. Therefore, the

dune retreat indicator is not shown for these two tests since it does not represent correctly dune retreat.

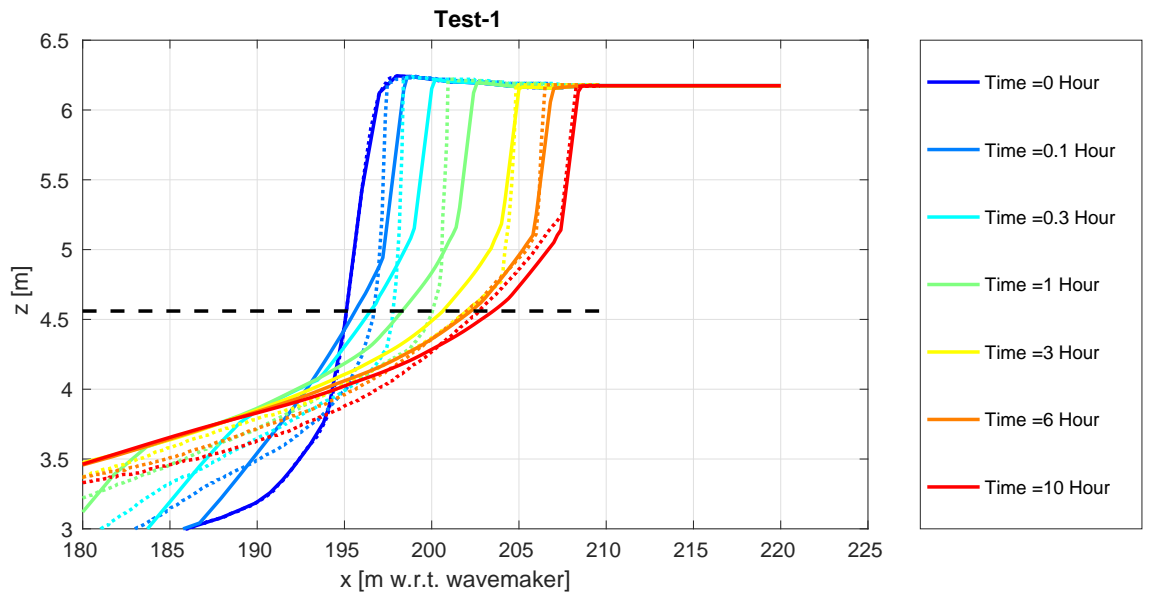


Figure 5.6 Comparisons of profiles from experiment Test-1 for different moments in time. Observed profiles are shown with a dashed line and the XBeach profiles with a solid line. The storm surge level is shown with a black dashed line.

Table 5.2 The computed and observed volume (V) and berm slopes (S) for Test-1. Volumes (V) are given in m^3/m . The relative error is expressed in a percentage. Both the relative error in terms of the same time (rel, t) and the final time are shown (rel).

Time[hour]	V_{xb} [m^3/m]	V_{data} [m^3/m]	V_{rel} [%]	$V_{rel,t}$ [%]	S_{xb} [-]	S_{data}	S_{rel} [%]	dx_{xb} [m]	dx_{data} [m]	dx_{rel} [%]	$dx_{rel,t}$ [%]
0.1	2.44	1.85	3	32	0.18	0.12	53	1.40	0.60	7	133
0.3	4.81	3.52	7	37	0.11	0.08	34	3.00	1.60	12	88
1	8.65	7.70	5	12	0.08	0.07	14	5.40	4.20	11	29
3	12.75	13.67	-5	-7	0.06	0.05	6	8.00	8.00	0	0
6	15.75	15.66	1	1	0.05	0.05	-2	10.00	9.60	4	4
10	18.13	17.69	2	2	0.04	0.04	-3	11.40	11.40	0	0

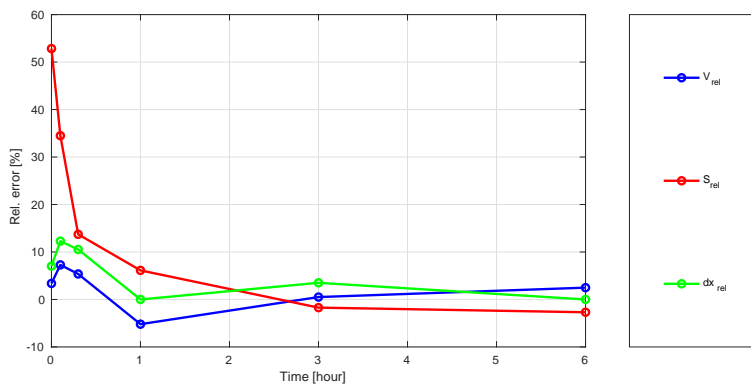


Figure 5.7 Temporal development of the relative error for the three indicators.

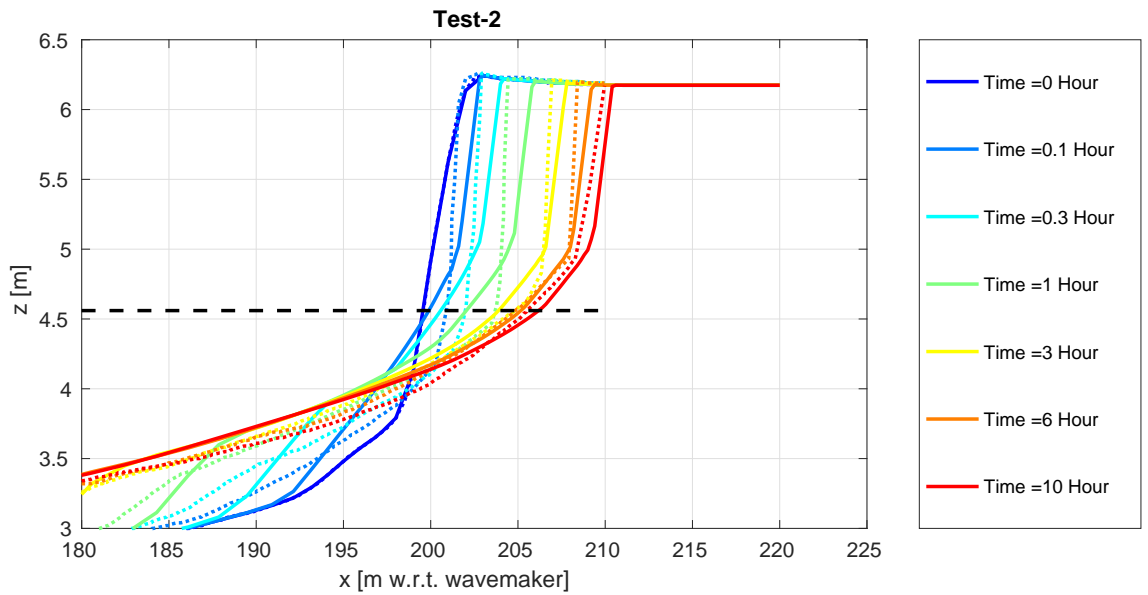


Figure 5.8 Comparisons of profiles from experiment Test-2 for different moments in time. Observed profiles are shown with a dashed line and the XBeach profiles with a solid line. The storm surge level is shown with a black dashed line.

Table 5.3 The computed and observed volume (V) and berm slopes (S) for Test-2. Volumes (V) are given in m^3/m . The relative error is expressed in a percentage. Both the relative error in terms of the same time (rel, t) and the final time are shown (rel).

Time[hour]	V_{xb} [m^3/m]	V_{data} [m^3/m]	V_{rel} [%]	$V_{rel,t}$ [%]	S_{xb} [-]	S_{data} [-]	S_{rel} [%]	dx_{xb} [m]	dx_{data} [m]	dx_{rel} [%]	$dx_{rel,t}$ [%]
0.1	1.80	1.00	6	81	0.17	0.11	56	0.80	0.00	10	Inf
0.3	3.68	2.92	6	26	0.11	0.08	36	2.00	1.40	7	43
1	6.66	5.64	8	18	0.07	0.06	15	3.80	2.80	13	36
3	9.83	9.55	2	3	0.05	0.05	-1	5.80	5.40	5	7
6	12.16	11.61	4	5	0.05	0.05	-6	7.20	6.80	5	6
10	14.00	13.26	6	6	0.04	0.04	1	8.40	8.00	5	5

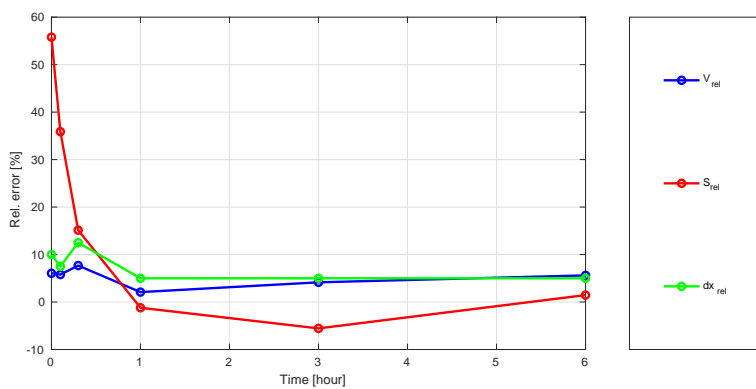


Figure 5.9 Temporal development of the relative error for the three indicators.

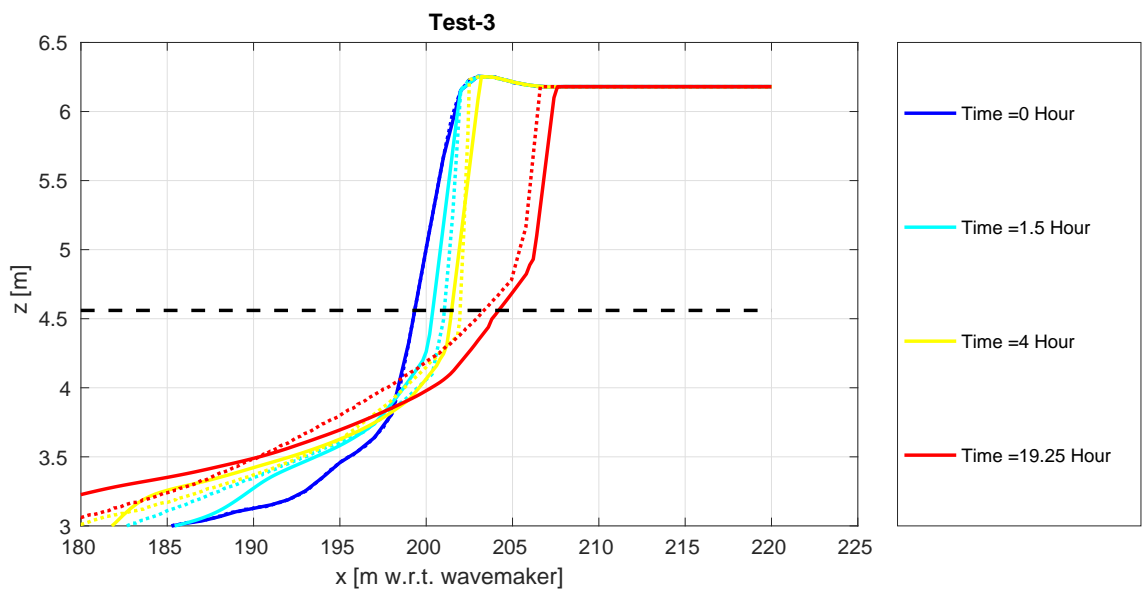


Figure 5.10 Comparisons of profiles from experiment Test-3 for different moments in time. Observed profiles are shown with a dashed line and the XBeach profiles with a solid line. The storm surge level is shown with a black dashed line.

Table 5.4 The computed and observed volume (V) and berm slopes (S) for Test-3. Volumes (V) are given in m^3/m . The relative error is expressed in a percentage. Both the relative error in terms of the same time (rel, t) and the final time are shown (rel).

Time[hour]	V_{xb} [m^3/m]	V_{data} [m^3/m]	V_{rel} [%]	$V_{rel,t}$ [%]	S_{xb} [-]	S_{data}	S_{rel} [%]	dx_{xb} [m]	dx_{data} [m]	dx_{rel} [%]	$dx_{rel,t}$ [%]
1.5	0.97	1.58	-7	-38	0.11	0.09	23	0.20	0.40	-4	-50
4	2.78	2.62	2	6	0.07	0.06	17	1.40	1.00	8	40
19.25	9.74	8.67	12	12	0.04	0.05	-11	5.60	4.80	17	17

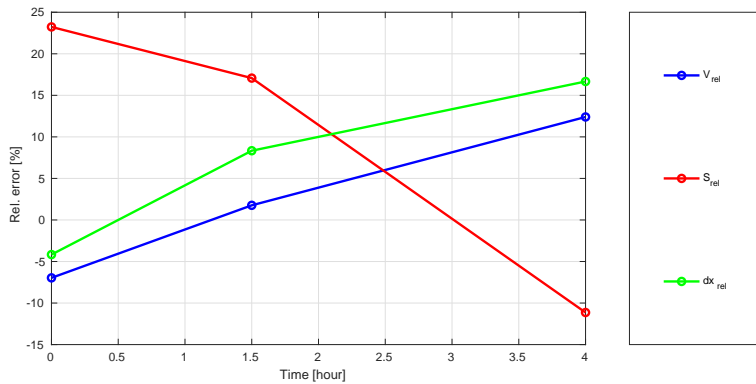


Figure 5.11 Temporal development of the relative error for the three indicators.

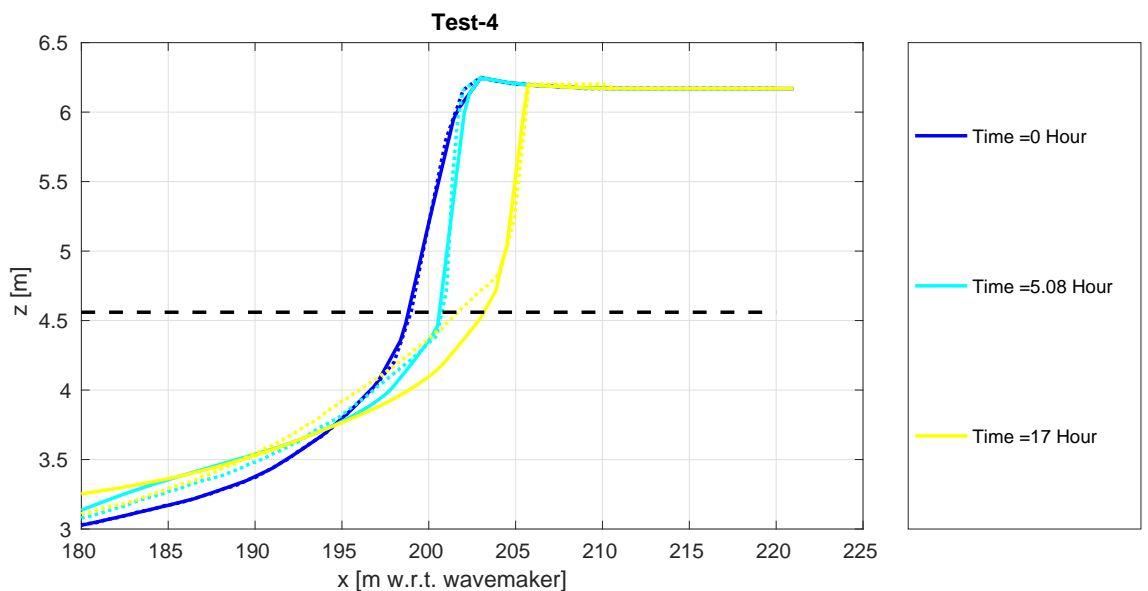


Figure 5.12 Comparisons of profiles from experiment Test-4 for different moments in time. Observed profiles are shown with a dashed line and the XBeach profiles with a solid line. The storm surge level is shown with a black dashed line.

Table 5.5 The computed and observed volume (V) and berm slopes (S) for Test-4. Volumes (V) are given in m^3/m . The relative error is expressed in a percentage. Both the relative error in terms of the same time (rel, t) and the final time are shown (rel).

Time[hour]	V_{xb} [m^3/m]	V_{data} [m^3/m]	V_{rel} [%]	$V_{rel,t}$ [%]	S_{xb} [-]	S_{data} [-]	S_{rel} [%]
5.08	1.71	1.57	2	9	0.06	0.05	36
17	7.20	7.52	-4	-4	0.04	0.04	-4

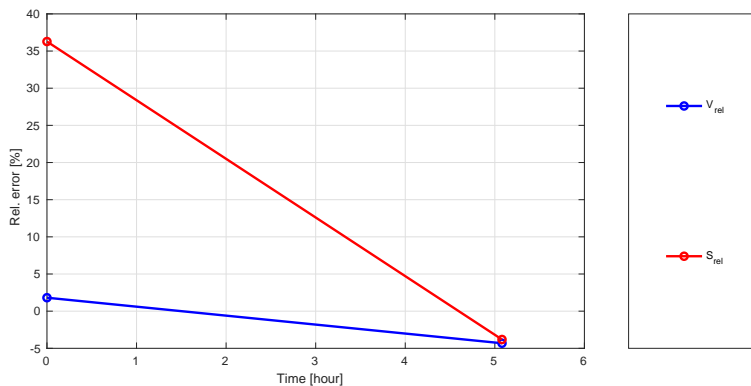


Figure 5.13 Temporal development of the relative error for the three indicators.

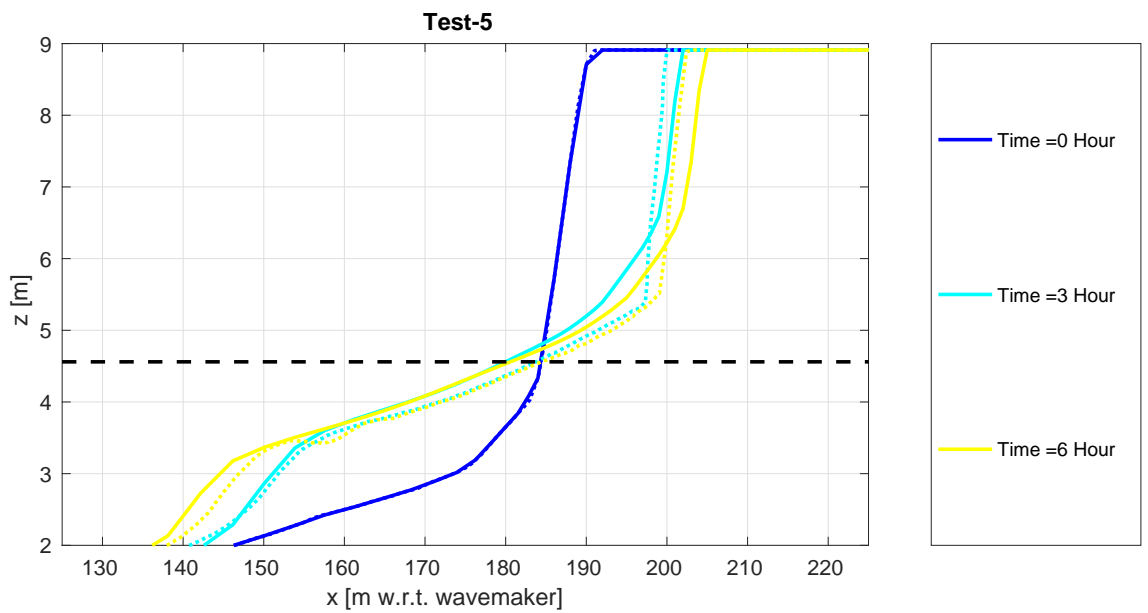


Figure 5.14 Comparisons of profiles from experiment Test-5 for different moments in time. Observed profiles are shown with a dashed line and the XBeach profiles with a solid line. The storm surge level is shown with a black dashed line.

Table 5.6 The computed and observed volume (V) and berm slopes (S) for Test-5. Volumes (V) are given in m^3/m . The relative error is expressed in a percentage. Both the relative error in terms of the same time (rel, t) and the final time are shown (rel).

Time[hour]	V_{xb} [m^3/m]	V_{data} [m^3/m]	V_{rel} [%]	$V_{rel,t}$ [%]	S_{xb} [-]	S_{data} [-]	S_{rel} [%]
3	40.93	42.13	-2	-3	0.06	0.05	6
6	51.88	50.99	2	2	0.05	0.04	11

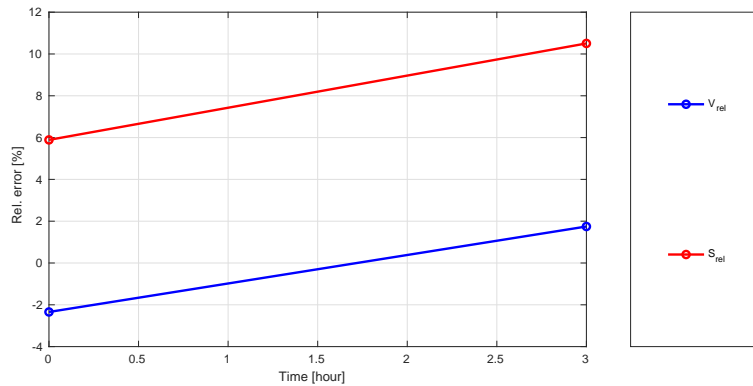


Figure 5.15 Temporal development of the relative error for the three indicators.

Overview

The statistical scores for all experiments are shown Figure 5.16 in Table 5.7.

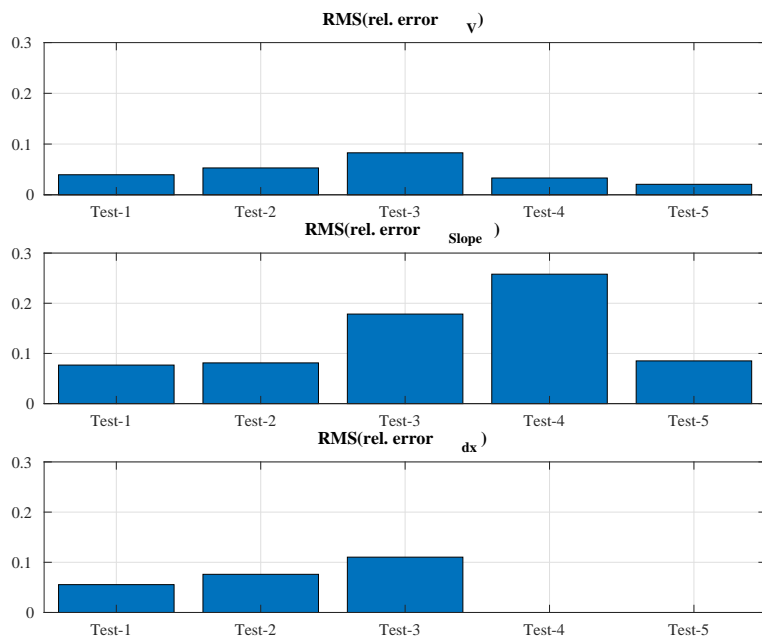


Figure 5.16 Overview of the statistical scores for M1263 experiments.

Table 5.7 M1263 III statistical scores.

	Test-1	Test-2	Test-3	Test-4	Test-5
$RMS(\text{rel.} \nu)$	0.04	0.05	0.08	0.03	0.02
$RMS(\text{rel.} S)$	0.08	0.08	0.18	0.26	0.09
$RMS(\text{rel.} dx)$	0.06	0.08	0.11	NaN	NaN

5.2

DeltaflumeH298 (Revetments)

Steetzel (1987) describes a series of large scale experiments with revetments of different heights. The experiments are performed in the Deltaflume of Delft Hydraulics, now known as Deltares. A depthscale $n_d = 5$ is used for all experiments (Vellinga, 1986) and the initial profile in the flume corresponds to the reference profile for the Holland coast. At the dune foot, which was located at 193m from the wave board and 3.80m above the flumes floor, a concrete revetment is applied that covers almost the whole dune face with a slope of 1:1.8. The lower end of the revetment is located at 2.5m above the flume floor. The location of the top of the revetment varied in each experiment. The tests were conducted with a constant water level of 4.2m and wave conditions that correspond to a Pierson-Moskowitz spectrum with $H_{m0} = 1.50\text{m}$ and $T_p = 4.20\text{s}$. The sediment applied in the test had a median grain diameter of approximately $D_{50} = 210\mu\text{m}$. An overview of the tests is given in Table 5.8.

Table 5.8 Overview of experiments

Experiment	Revetment height w.r.t. flume floor
T1	6.20m
T2	5.40m
T3	4.80m

The profile developments as measured and computed by XBeach are presented in Figure 5.17 to Figure 5.19.

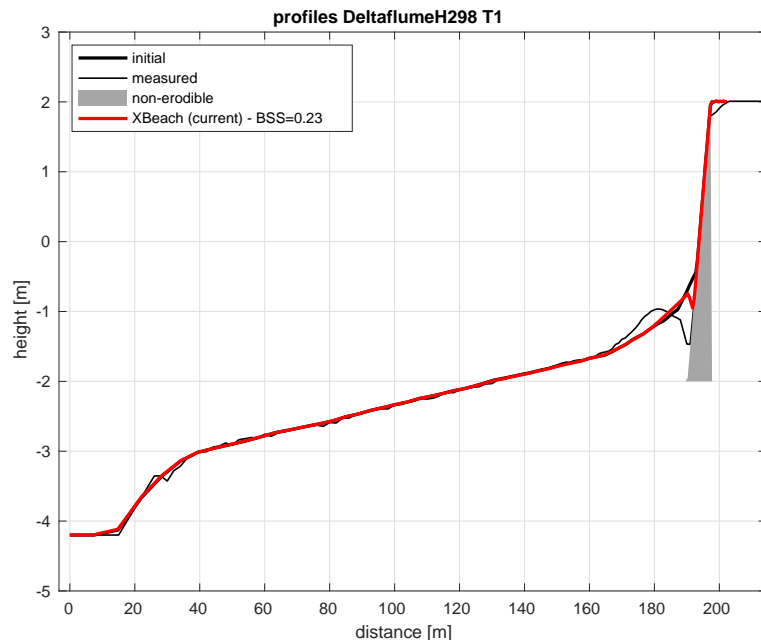


Figure 5.17 Profile development during test T1

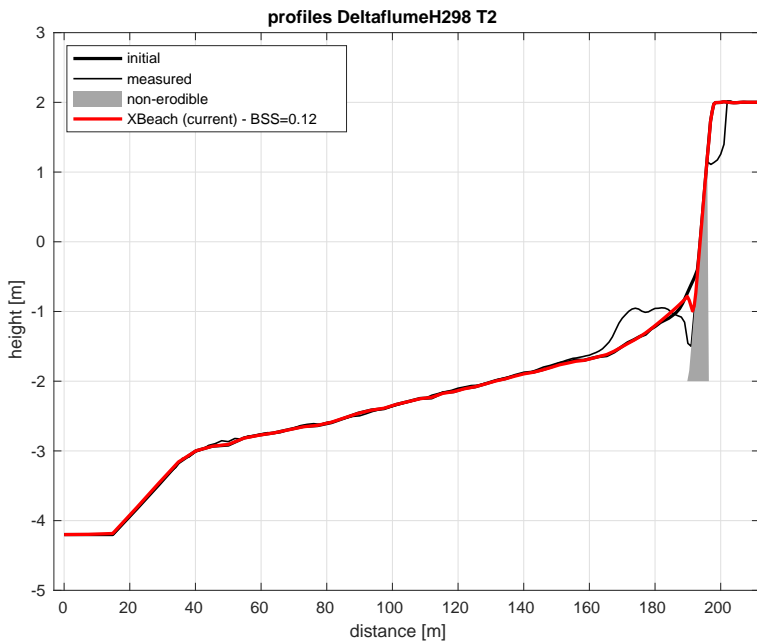


Figure 5.18 Profile development during test T2

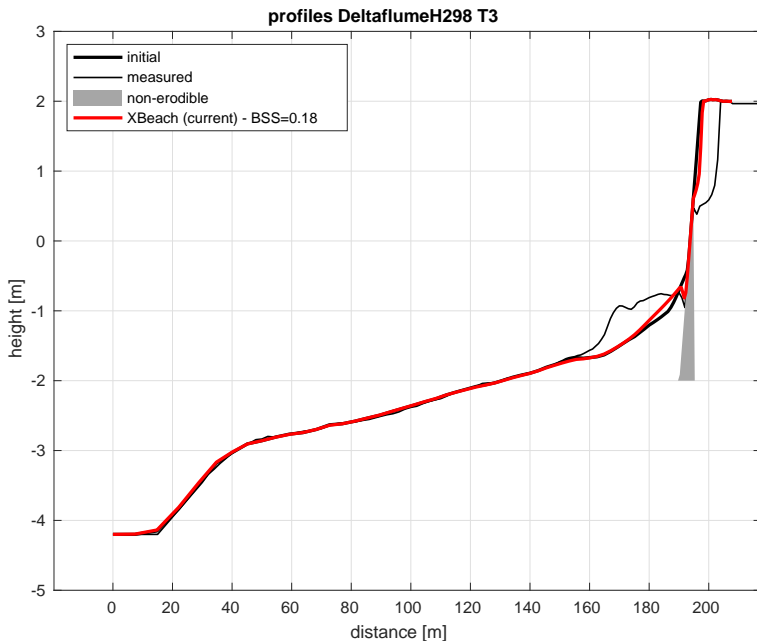


Figure 5.19 Profile development during test T3

5.3 LIP11D: Delta Flume 1994

The purpose of research programme LIP 11D was the generation of high quality and high resolution data on hydrodynamics and sediment transport dynamics on a natural 2DV beach under equilibrium, erosive and accretive conditions. In total 7 tests were performed in the Delta Flume of WL | Delft Hydraulics in the period of April 1993 till June 1993. Test 2E is incorporated in the skillbed, because the profiles and hydraulic conditions in this test correspond rather well to the Dutch situation. Since there is no direct agreement with the reference profile, scale factors or steepness factors cannot be determined in a similar way as in the research programmes in the 1980s. We

assume a scale factor of 1:5. The wave board in the Delta Flume was equipped with active reflection compensation (ARC) at the time these tests were performed, and it is assumed that no second-order wave steering was applied. Waves were measured at a location 20 m from the wave board where the bed level was still horizontal. The sand had a diameter of $D_{50} = 220 \text{ } \mu\text{m}$.

The model test 2E, also described in Arcilla *et al.* (1994), concerns extreme conditions with a raised water level at 4.6 m above the flume bottom, a significant wave height, H_{m0} , of 1.4 m (corresponding to some 7 m on prototype scale) and peak period, T_p , of 5 s (corresponds to 11 s on prototype scale). During the test substantial dune erosion took place.

Based on the integral wave parameters H_{m0} and T_p and a standard Jonswap spectral shape, time series of wave energy were generated and imposed as boundary condition. Since the flume tests were carried out with first-order wave generation (no imposed super-harmonics and sub-harmonics), the hindcast runs were carried out with the incoming, bound long waves set to zero as well. Active wave reflection compensation (ARC) was applied in the physical model, which has a result similar to the weakly reflective boundary condition in XBeach, namely to prevent re-reflecting of outgoing waves at the wave paddle (offshore boundary).

The comparison between the observed profiles and computed profiles is shown in Figure 5.20 and the results for the indicators are shown in Table 5.9. The relative errors from Table 5.9 are also shown in Figure 5.21.

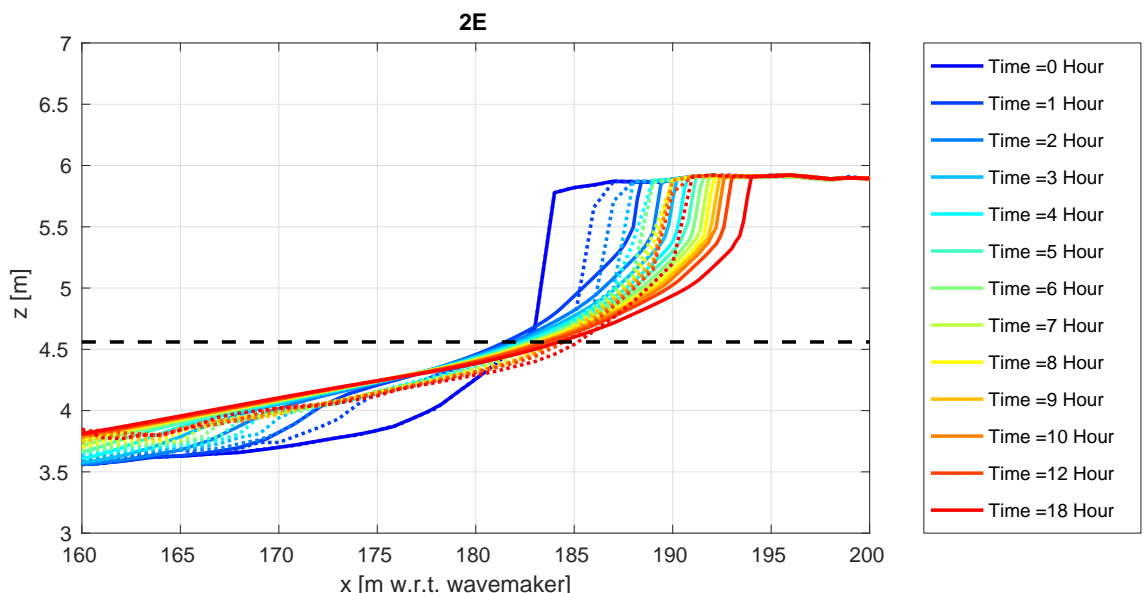


Figure 5.20 Comparisons of profiles from experiment LIP 2E for different moments in time. Observed profiles are shown with a dashed line and the XBeach profiles with a solid line. The storm surge level is shown with a black dashed line.

Table 5.9 The computed and observed volume (V) and berm slopes (S) for 2E. Volumes (V) are given in m^3/m . The relative error is expressed in a percentage. Both the relative error in terms of the same time (rel, t) and the final time are shown (rel).

Time[hour]	V_{xb} [m^3/m]	V_{data} [m^3/m]	V_{rel} [%]	$V_{rel,t}$ [%]	S_{xb} [-]	S_{data} [-]	S_{rel} [%]	dx_{xb} [m]	dx_{data} [m]	dx_{rel} [%]	$dx_{rel,t}$ [%]
1	3.52	2.50	14	41	0.06	0.06	-9	4.20	2.00	33	110
2	4.72	3.50	16	35	0.05	0.06	-10	5.20	3.00	33	73
3	5.53	4.16	19	33	0.04	0.05	-18	6.00	3.80	33	58
4	6.17	4.73	19	30	0.04	0.03	38	6.60	4.60	30	43
5	6.69	4.99	23	34	0.04	0.03	31	7.00	4.80	33	46
6	7.14	5.15	27	39	0.04	0.03	27	7.40	4.80	39	54
7	7.53	5.61	26	34	0.04	0.03	25	7.60	5.60	30	36
8	7.88	5.80	28	36	0.03	0.03	23	7.80	5.60	33	39
9	8.19	5.92	31	38	0.03	0.03	21	8.20	5.80	36	41
10	8.48	6.15	32	38	0.03	0.03	19	8.40	5.80	39	45
12	9.00	6.38	35	41	0.03	0.03	18	8.80	5.80	45	52
18	10.21	7.39	38	38	0.03	0.03	18	9.80	6.60	48	48

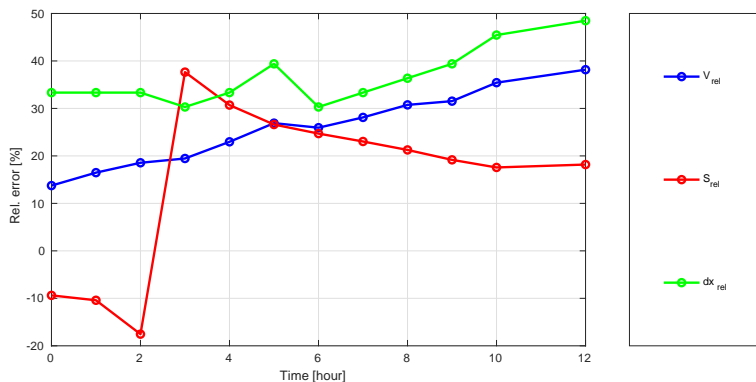


Figure 5.21 Temporal development of the relative error for the three indicators.

5.3.1 Detailed results

This section shows additional detailed comparison of the 2E test of the LIP 11D experiment (Arcilla *et al.*, 1994). The observed and computed wave height transformation and the setup are shown in Figure 5.22. The sedimentation and erosion patterns are shown in Figure 5.23 and the erosion volumes as function of the time are shown in Figure 5.24.

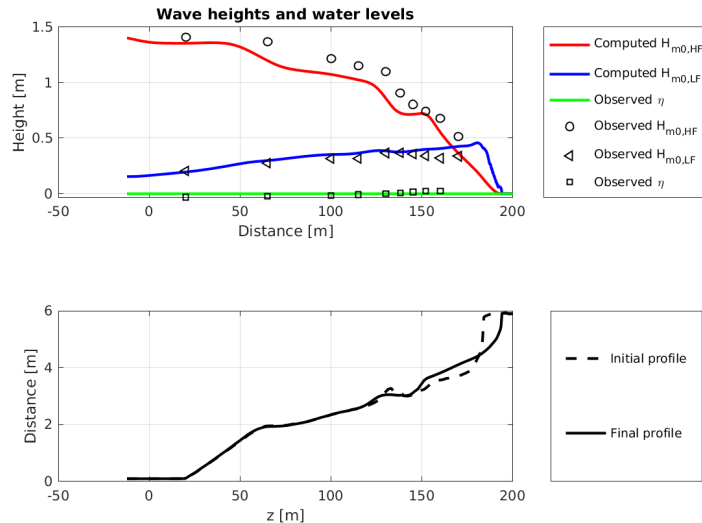


Figure 5.22 Computed and observed short wave height transformation, infragravity wave height transformation and mean water level (upper panel) for test 2E. The lower panel shows the initial and final computed profiles.

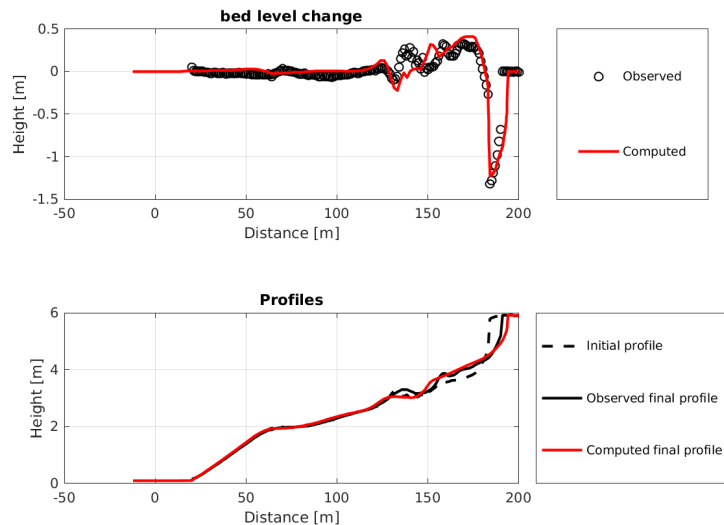


Figure 5.23 Erosion pattern and volumes and retreat distance during test 2E

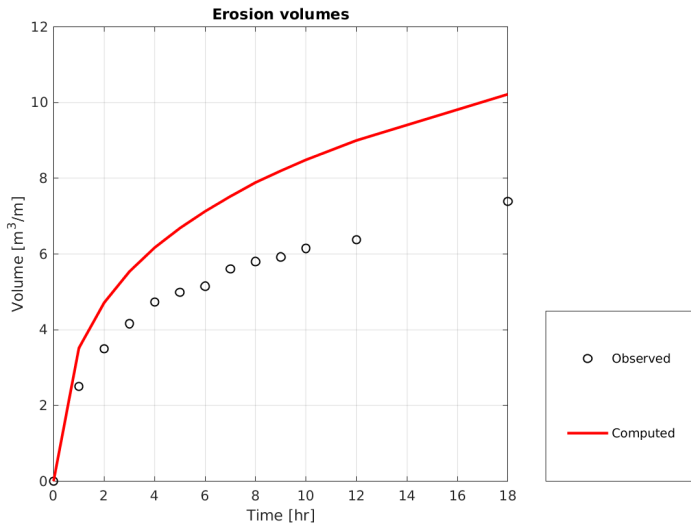


Figure 5.24 Erosion volumes as a function of time for test E2

5.3.2 Bar evolution

In Arcilla *et al.* (1994) two types of profiles and three different dynamic states are investigated: near-equilibrium, erosive and accretive. Also, a test with extreme erosive conditions is performed. In this section the erosive and accretive tests for the first profile are discussed: test 1B and 1C. The two tests are intended to simulate the erosive effects during a storm and the restoring effects afterwards. A clear dune front is absent in the profile used, only a gently sloping beach is present. In Table 5.10 the conditions of these two tests are summarized.

Table 5.10 Overview of experiments

Experiment	H_{m0}	T_p	Water level	Duration
1B	1.4m	5s	4.1m	18h
1C	0.6m	8s	4.1m	13h

In Figure 5.25 and Figure 5.26 the computed and measured morphodynamics are shown.

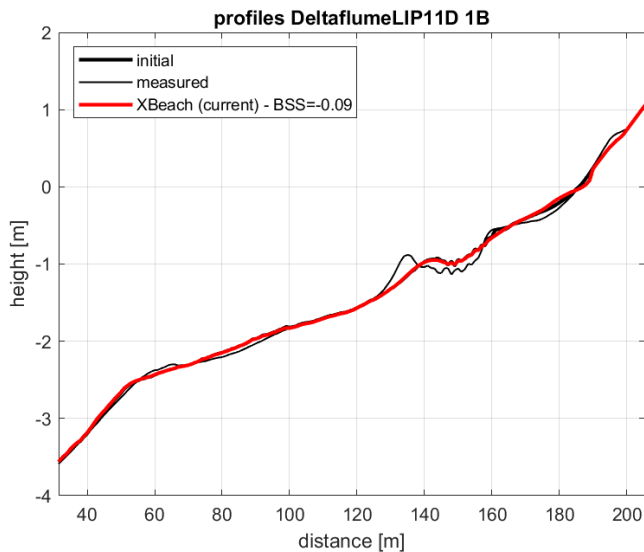


Figure 5.25 Morphodynamics during test 1B

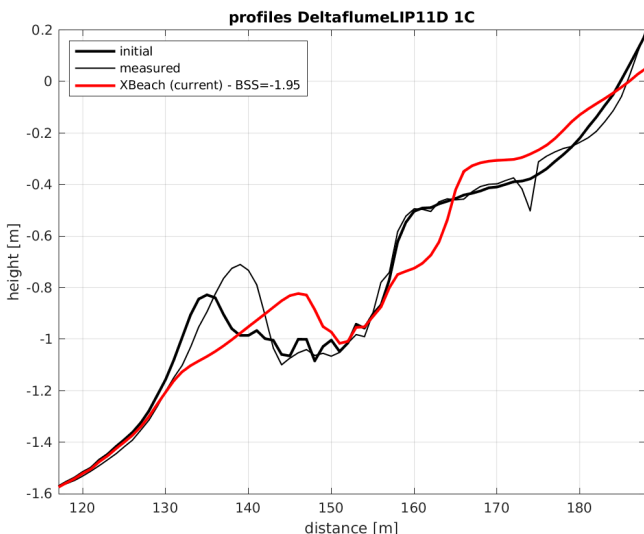


Figure 5.26 Morphodynamics during test 1C

5.4 Deltaflume H4731

In the H4731 Delta flume experiments, it was studied how a collapsed dune revetment affects dune erosion (Van Gent and Coeveld, 2007). Four large-scale experiments were performed in the Delta flume with a depth scale of n_d equals 6. A wave height of 9 m (prototype) and peak period of 12 s (prototype) were forced at the wave maker. The test without a revetment (T14) is modelled with XBeach (Figure 5.27). The results for the indicators for different moments in time are shown in Table 5.11. Note that the observed dune retreat is zero since the dune front does not erode in the observed profiles. This means that the relative error in dune retreat cannot be computed.

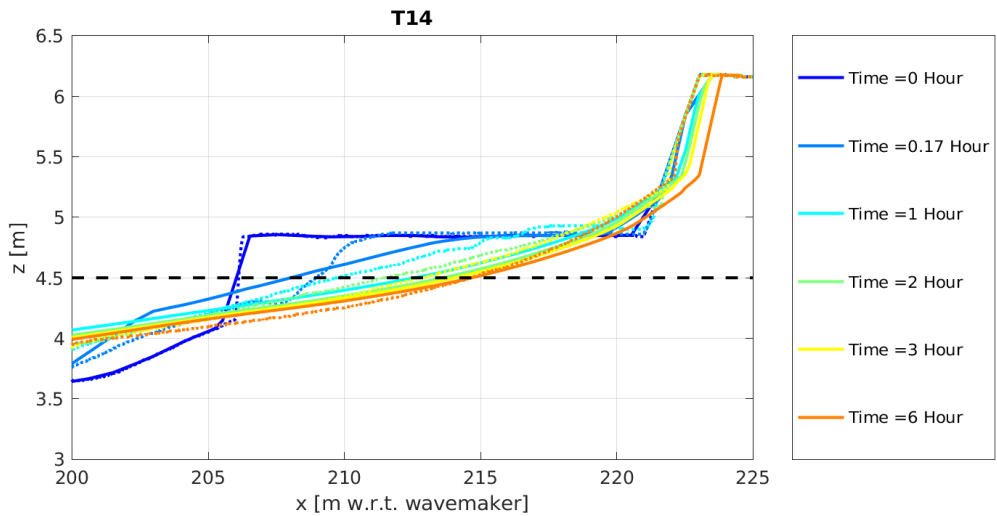


Figure 5.27 Comparison of profile during experiment T14 Observed profiles are shown with a dashed line and the XBeach profiles with a solid line. The storm surge level is shown with a black dashed line.

Table 5.11 The computed and observed volume (V) and berm slopes (S) for T14. Volumes (V) are given in m^3/m . The relative error is expressed in a percentage. Both the relative error in terms of the same time (rel, t) and the final time are shown (rel).

Time[hour]	V_{xb} [m^3/m]	V_{data} [m^3/m]	V_{rel} [%]	$V_{rel,t}$ [%]	S_{xb} [-]	S_{data} [-]	S_{rel} [%]	dx_{xb} [m]	dx_{data} [m]	dx_{rel} [%]	$dx_{rel,t}$ [%]
0.17	1.80	1.28	14	41	0.08	0.08	3	0.00	0.00	NaN	NaN
1	3.53	2.36	31	49	0.04	0.07	-38	0.17	0.00	Inf	Inf
2	3.89	3.04	22	28	0.04	0.05	-26	0.17	0.00	Inf	Inf
3	4.16	3.32	22	25	0.04	0.04	-15	0.33	0.00	Inf	Inf
6	4.89	3.79	29	29	0.04	0.04	1	0.83	0.00	Inf	Inf

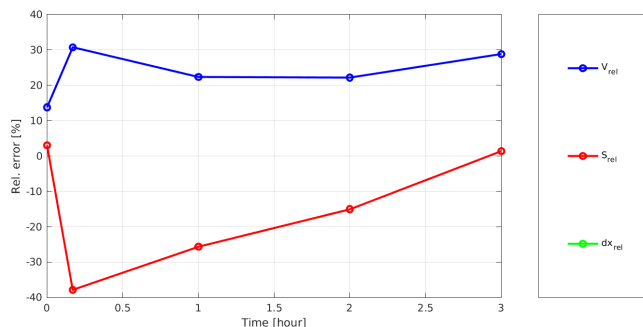


Figure 5.28 Temporal development of the relative error for the three indicators.

5.5

Grosse Wellen Kanal 1998

Experiment description

The purpose of research programme GWK98 was to improve the methods of design and performance assessment of beach nourishments. In total 24 tests were performed in the wave flume in Hannover (Grosse Wellen Kanal) in the period of November 1996 till August 1997.

These tests were not carried out with an initial profile similar to the Dutch reference profile, nor with hydraulic conditions characteristic for the Dutch coast. Scale factors or steepness factors can therefore not be determined in a similar way as in the research programmes in The Netherlands in the 1980s. We assumed wave-height scaling with respect to super-storm conditions for the Dutch coast (wave-height of 9 m), which resulted in a scale of 1:8. In total 8 series of tests were performed with different initial profiles with and without supporting structures. Imposed wave heights for all tests was 1.16 m (estimated as 9 m on prototype scale), with a wave period of 6.4 s (corresponding to 18 s on prototype scale). In total 5 tests without structures are incorporated in the skillbed, which have a dune-type cross-shore profile and hydraulic conditions large enough to cause significant erosion. First order wave steering was applied, and ARC compensation was present.

Results

The profile development is shown in Figure 5.29 to Figure 5.37. The results for the indicators for different moments in time are shown in Table 5.12 to Table 5.16. Note that the profile measurements do not show a clear dune retreat. Therefore, the dune retreat is not included in shown tables.

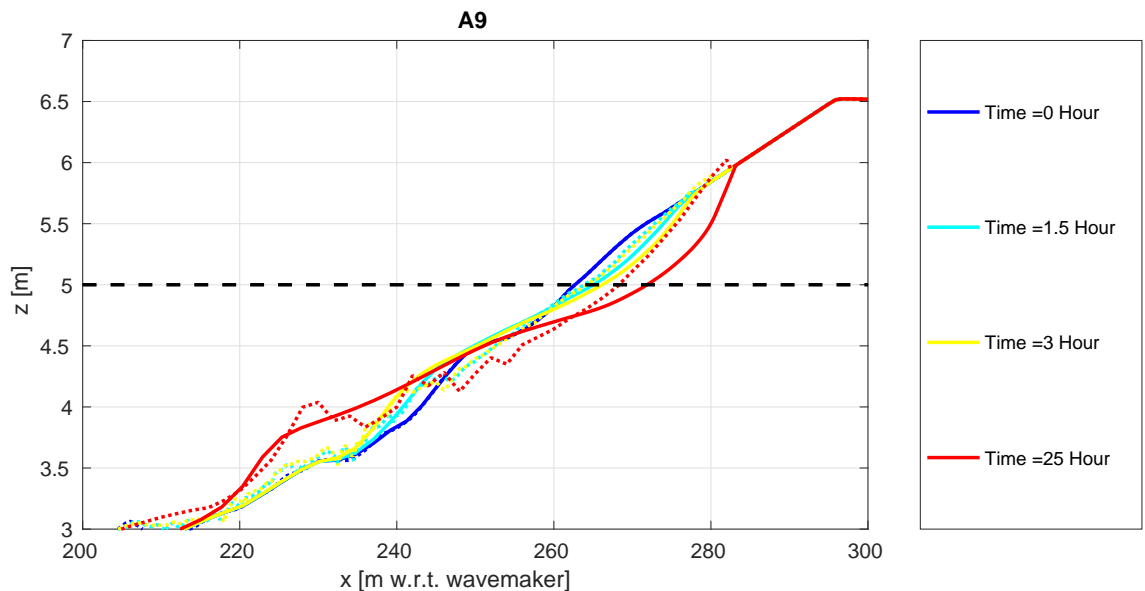


Figure 5.29 Comparisons of profiles from experiment A9 for different moments in time. Observed profiles are shown with a dashed line and the XBeach profiles with a solid line. The storm surge level is shown with a black dashed line.

Table 5.12 The computed and observed volume (V) and berm slopes (S) for A9. Volumes (V) are given in m^3/m . The relative error is expressed in a percentage. Both the relative error in terms of the same time (rel, t) and the final time are shown (rel).

Time[hour]	V_{xb} [m^3/m]	V_{data} [m^3/m]	V_{rel} [%]	$V_{rel,t}$ [%]	S_{xb} [-]	S_{data} [-]	S_{rel} [%]
1.5	1.70	0.90	26	90	0.04	0.04	12
3	2.54	1.15	44	121	0.04	0.04	-12
25	6.75	3.12	116	116	0.03	0.03	-5

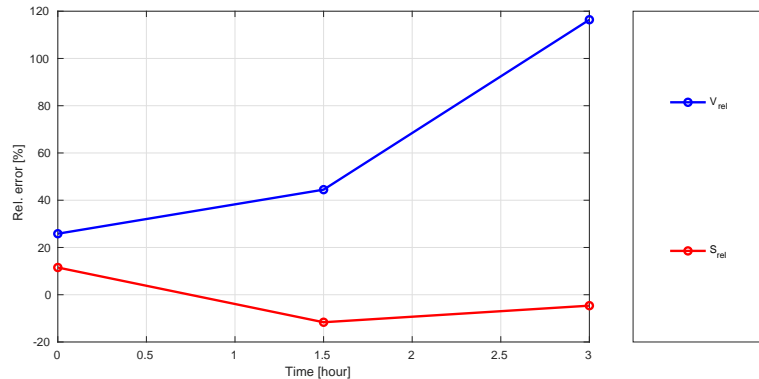


Figure 5.30 Temporal development of the relative error for the three indicators.

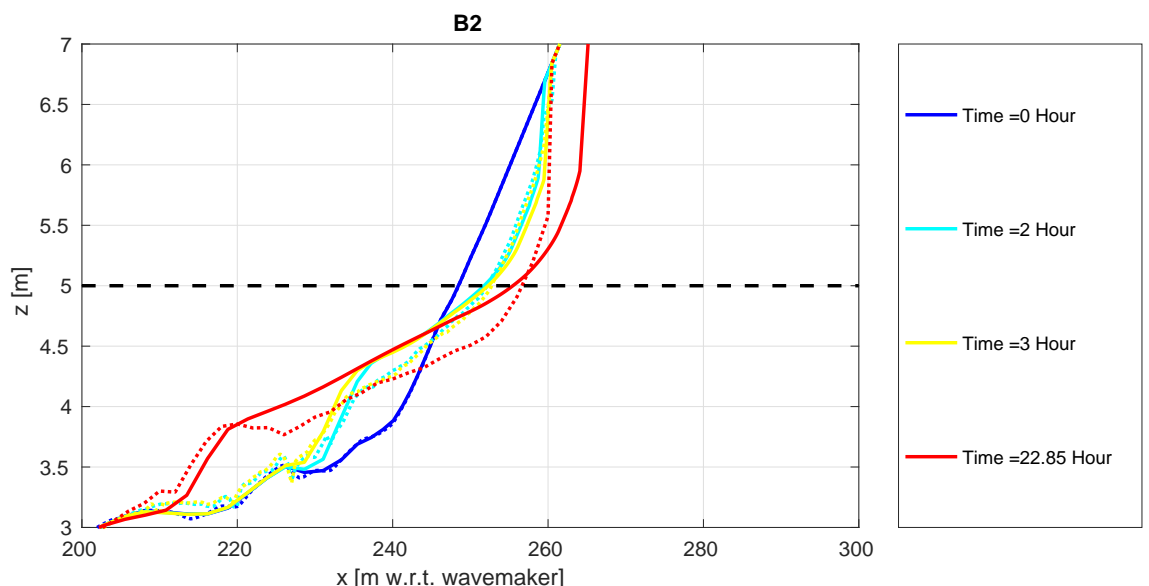


Figure 5.31 Comparisons of profiles from experiment B2 for different moments in time. Observed profiles are shown with a dashed line and the XBeach profiles with a solid line. The storm surge level is shown with a black dashed line.

Table 5.13 The computed and observed volume (V) and berm slopes (S) for B2. Volumes (V) are given in m^3/m . The relative error is expressed in a percentage. Both the relative error in terms of the same time (rel, t) and the final time are shown (rel).

Time[hour]	V_{xb} [m^3/m]	V_{data} [m^3/m]	V_{rel} [%]	$V_{rel,t}$ [%]	S_{xb} [-]	S_{data} [-]	S_{rel} [%]
2	5.71	5.56	2	3	0.06	0.06	-4
3	6.97	5.98	11	17	0.06	0.06	2
22.85	16.83	9.40	79	79	0.04	0.04	2

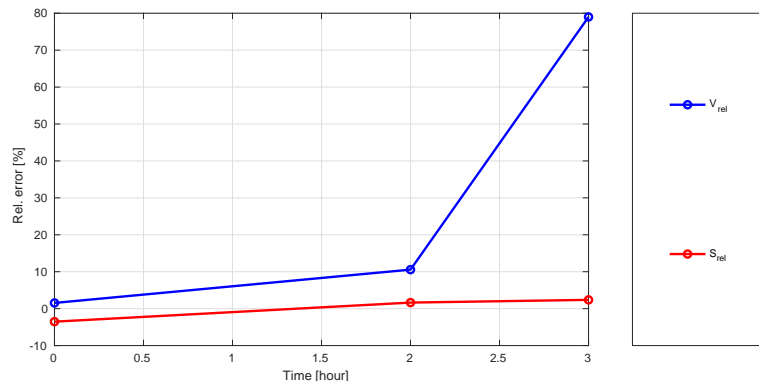


Figure 5.32 Temporal development of the relative error for the three indicators.

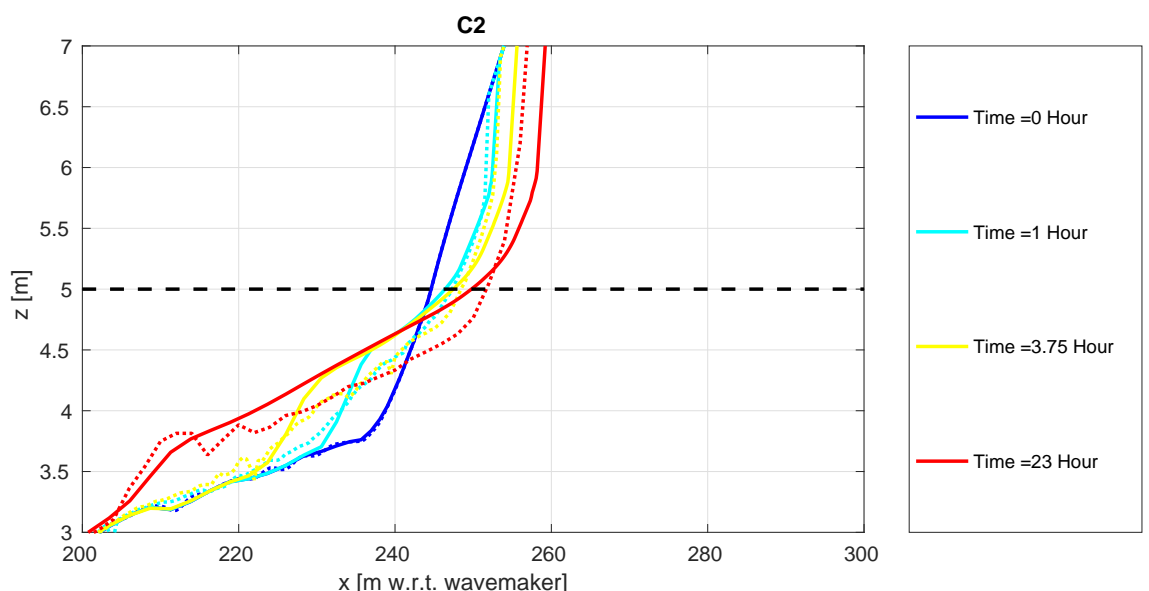


Figure 5.33 Comparisons of profiles from experiment C2 for different moments in time. Observed profiles are shown with a dashed line and the XBeach profiles with a solid line. The storm surge level is shown with a black dashed line.

Table 5.14 The computed and observed volume (V) and berm slopes (S) for C2. Volumes (V) are given in m^3/m . The relative error is expressed in a percentage. Both the relative error in terms of the same time (rel, t) and the final time are shown (rel).

Time[hour]	V_{xb} [m^3/m]	V_{data} [m^3/m]	V_{rel} [%]	$V_{rel,t}$ [%]	S_{xb} [-]	S_{data} [-]	S_{rel} [%]
1	4.93	4.19	6	18	0.07	0.07	-1
3.75	9.25	6.13	23	51	0.05	0.05	-12
23	19.37	13.40	45	45	0.03	0.03	9

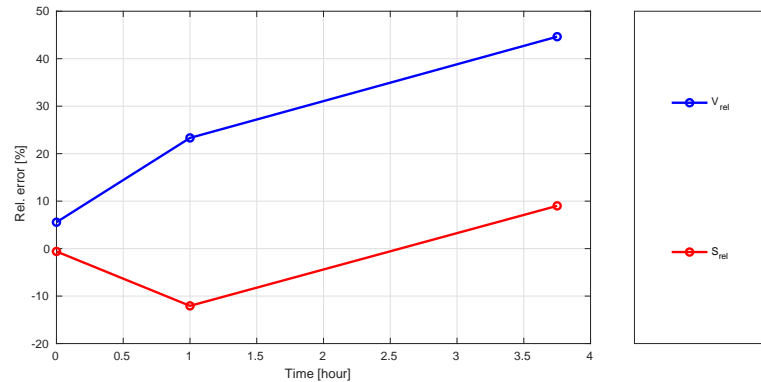


Figure 5.34 Temporal development of the relative error for the three indicators.

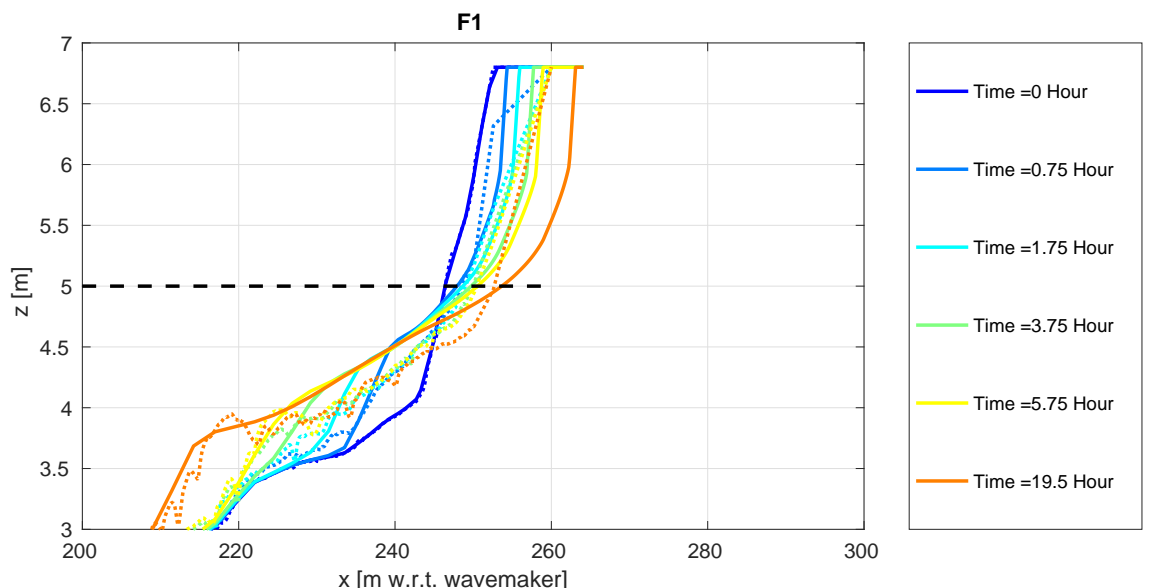


Figure 5.35 Comparisons of profiles from experiment F1 for different moments in time. Observed profiles are shown with a dashed line and the XBeach profiles with a solid line. The storm surge level is shown with a black dashed line.

Table 5.15 The computed and observed volume (V) and berm slopes (S) for F1. Volumes (V) are given in m^3/m . The relative error is expressed in a percentage. Both the relative error in terms of the same time (rel, t) and the final time are shown (rel).

Time[hour]	V_{xb} [m^3/m]	V_{data} [m^3/m]	V_{rel} [%]	$V_{rel,t}$ [%]	S_{xb} [-]	S_{data} [-]	S_{rel} [%]
0.75	4.85	6.88	-12	-30	0.08	0.08	-2
1.75	7.47	12.12	-27	-38	0.06	0.06	-4
3.75	10.49	13.79	-19	-24	0.05	0.05	-3
5.75	12.51	14.75	-13	-15	0.04	0.04	11
19.5	19.68	17.43	13	13	0.04	0.04	1

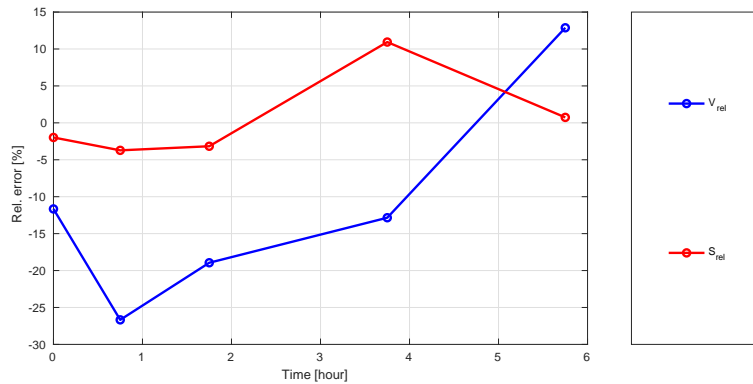


Figure 5.36 Temporal development of the relative error for the three indicators.

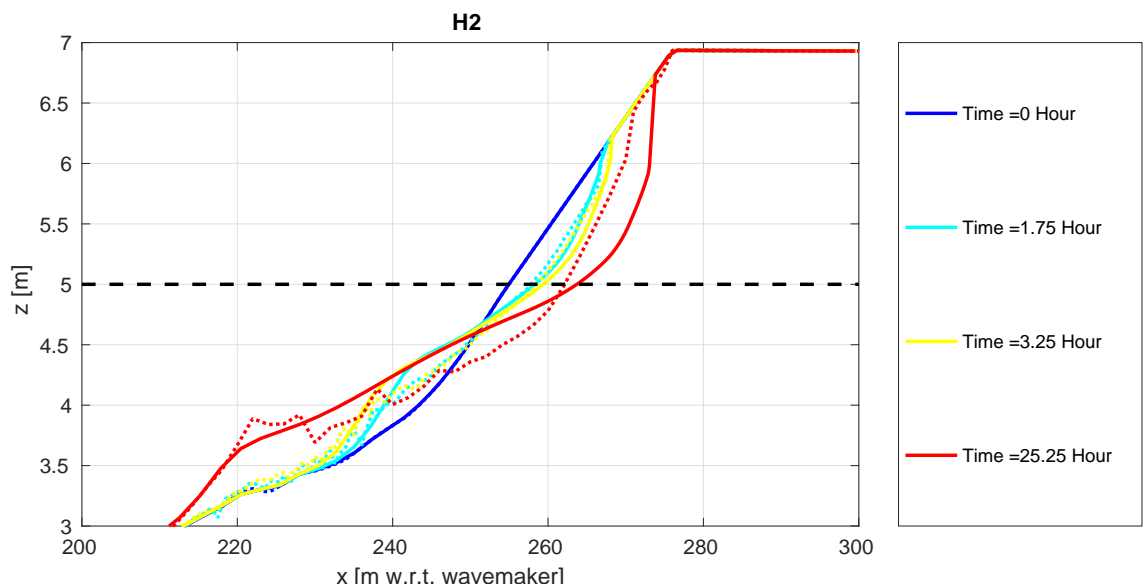


Figure 5.37 Comparisons of profiles from experiment H2 for different moments in time. Observed profiles are shown with a dashed line and the XBeach profiles with a solid line. The storm surge level is shown with a black dashed line.

Table 5.16 The computed and observed volume (V) and berm slopes (S) for H2. Volumes (V) are given in m^3/m . The relative error is expressed in a percentage. Both the relative error in terms of the same time (rel, t) and the final time are shown (rel).

Time[hour]	V_{xb} [m^3/m]	V_{data} [m^3/m]	V_{rel} [%]	$V_{rel,t}$ [%]	S_{xb} [-]	S_{data} [-]	S_{rel} [%]
1.75	3.30	2.80	7	18	0.05	0.05	-7
3.25	4.59	3.68	13	25	0.05	0.05	-6
25.25	12.14	6.95	75	75	0.03	0.03	-4

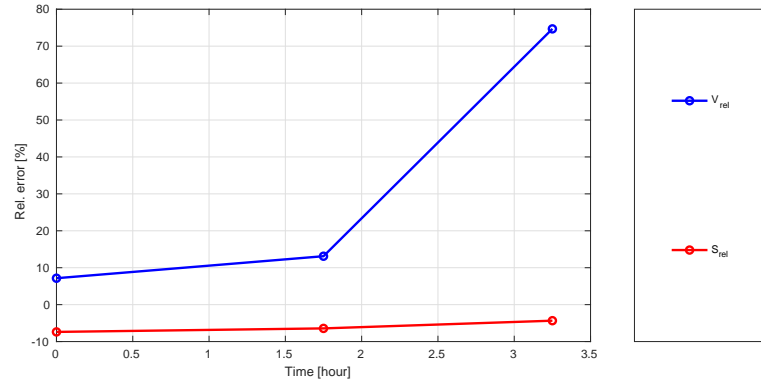


Figure 5.38 Temporal development of the relative error for the three indicators.

Overview

An overview of the statistical scores is shown in [Figure 5.39](#) and [Table 5.17](#). Note that dune retreat is not shown and that only the errors in dune erosion volume and berm slope are shown.

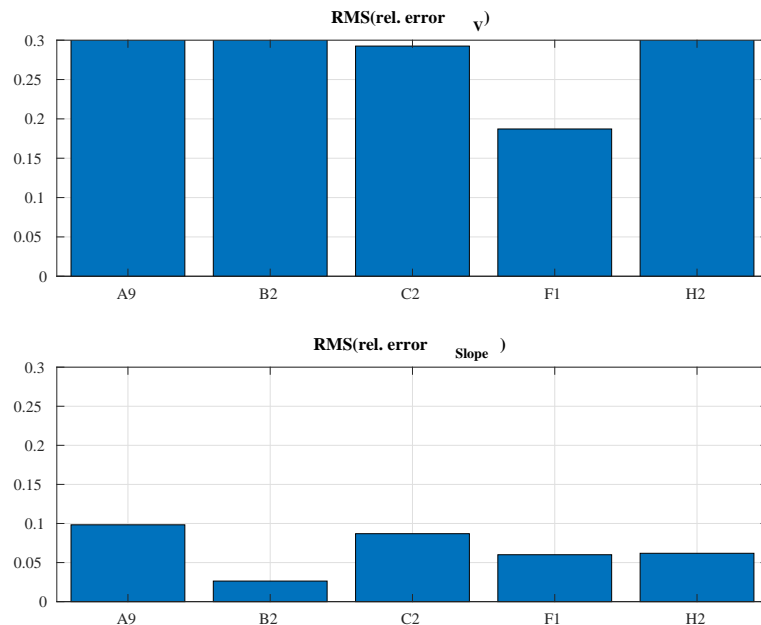


Figure 5.39 GWK overview

Table 5.17 Statistical scores for the Grosse Wellen Kanal experiments.

	A9	B2	C2	F1	H2
$RMS(\text{rel. volume})$	0.73	0.46	0.29	0.19	0.44
$RMS(\text{rel. slope})$	0.10	0.03	0.09	0.06	0.06

5.6

M1797: Delta Flume 1981

In 1981, Delta Flume experiments were performed to gain insight in the effect of a dune revetment on the morphological behaviour of the dune, however, experiments were also carried out without a dune revetment. The profile in question is based on a stretch of coast called the Noorderstrand at Schouwen, the Netherlands (Vellinga, 1981). Two large scale experiments (depth scale of 2) were performed, one with and one without dune revetment. The latter is depicted in Figure 5.40. Table 5.18 shows the results for the indicators at different moments in time.

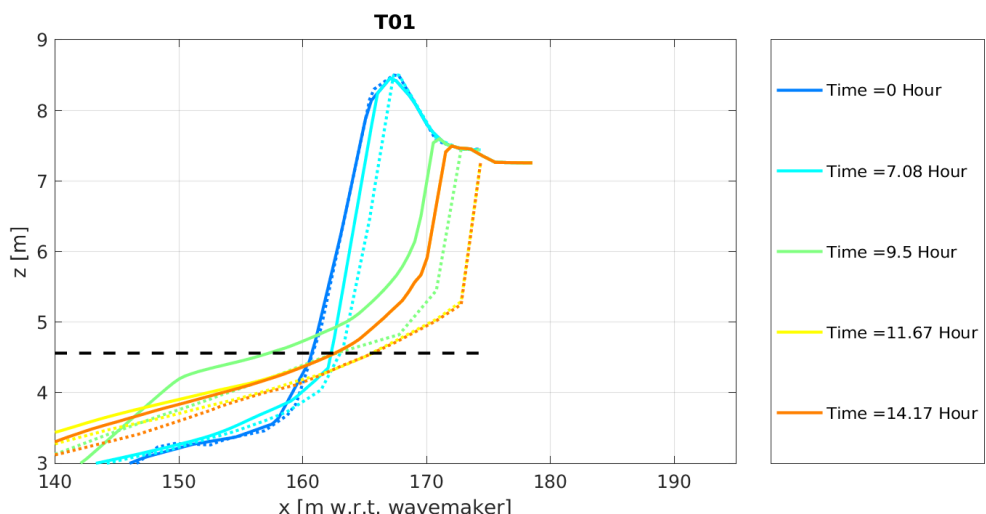


Figure 5.40 Comparison of profile during experiment T01. Observed profiles are shown with a dashed line and the XBeach profiles with a solid line. The storm surge level is shown with a black dashed line.

Table 5.18 The computed and observed volume (V) and berm slopes (S) for T01. Volumes (V) are given in m^3/m . The relative error is expressed in a percentage. Both the relative error in terms of the same time (rel, t) and the final time are shown (rel).

Time[hour]	V_{xb} [m^3/m]	V_{data} [m^3/m]	V_{rel} [%]	$V_{rel,t}$ [%]	S_{xb} [-]	S_{data} [-]	S_{rel} [%]	dx_{xb} [m]	dx_{data} [m]	dx_{rel} [%]	$dx_{rel,t}$ [%]
7.08	3.48	7.24	-11	-52	0.05	0.06	-22	0.50	2.00	-18	-75
9.5	17.54	28.28	-32	-38	0.09	0.06	38	5.00	7.00	-24	-29
11.67	22.76	33.04	-31	-31	0.05	0.06	-10	6.00	8.50	-29	-29
14.17	22.76	33.23	-32	-32	0.05	0.05	4	6.00	8.50	-29	-29

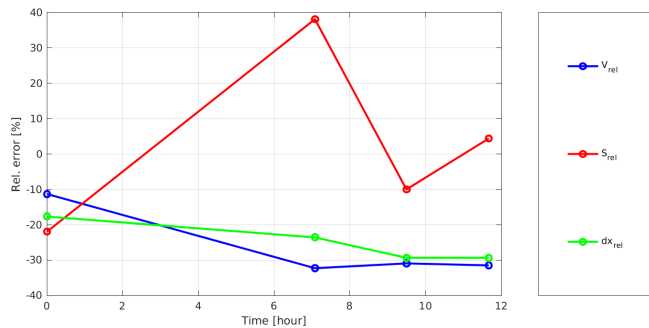


Figure 5.41 Temporal development of the relative error for the three indicators.

5.7 H4357: Delta Flume 2006

Experiment description

Van Gent *et al.* (2008) and Van Thiel de Vries *et al.* (2008) describe large-scale laboratory experiments that have been performed to study the influence of the wave period on the dune erosion process. They concluded that not only short waves, but also (wave group generated) long waves are important in the dune erosion process. Initially, about 30% of the dune erosion is due to long-wave energy, but this amount increases throughout the storm, with the development of an erosion profile. Moreover, an increase of the wave period was seen to increase the resulting dune erosion volumes.

These experiments have been performed in the Deltaflume of Delft Hydraulics, currently known as Deltares, using the reference profile for the Holland coast on a scale of 1:6. This is a schematized profile that is considered representative for the Holland coast. Furthermore, a significant wave height 1.50 m (corresponding to 9 m on proto-type scale) and a water depth of 4.50 m is used. The test programme is given in Table 5.19. During Test T01, T02 and T03 a single dune has been tested, whereas during test T08, the storm impact on a profile with a double dune row was analysed.

Table 5.19 Overview of experiments

Experiment	T_p	$T_{m-1,0}$	Spectrum
T01	4.90	4.45	Pierson-Moskowitz
T02	6.12	5.56	Pierson-Moskowitz
T03	7.35	6.68	Pierson-Moskowitz
T08	7.35	6.68	Pierson-Moskowitz

Results

The comparison between the observed and numerically predicted beach profiles with the BOI parameter settings is shown in Figure 5.42, Figure 5.44, Figure 5.46 and Figure 5.48. The observed profiles are represented by a dashed line and the computed profiles through a solid line. The line color indicates the moment in time. Table 5.20 to Table 5.23 show the results for the different indicators. In Figure 5.43, Figure 5.45, Figure 5.47 and Figure 5.49, the relative error is plotted as a function of

time. Besides a comparison of the observed and predicted beach profiles, also a detailed hydrodynamic and morphodynamic analysis is performed, which is presented in Appendix ??.

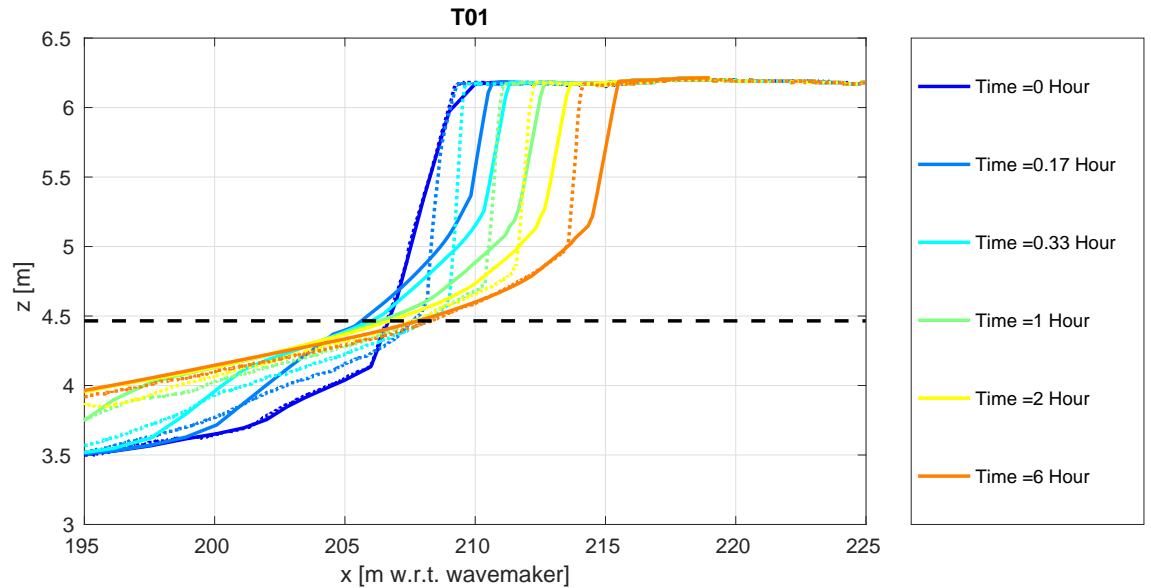


Figure 5.42 Comparisons of profiles from experiment T01 for different moments in time. Observed profiles are shown with a dashed line and the XBeach profiles with a solid line. The storm surge level is shown with a black dashed line.

Table 5.20 The computed and observed volume (V) and berm slopes (S) for T01. Volumes (V) are given in m^3/m . The relative error is expressed in a percentage. Both the relative error in terms of the same time (rel, t) and the final time are shown (rel).

Time[hour]	V_{xb} [m^3/m]	V_{data} [m^3/m]	V_{rel} [%]	$V_{rel,t}$ [%]	S_{xb} [-]	S_{data} [-]	S_{rel} [%]	dx_{xb} [m]	dx_{data} [m]	dx_{rel} [%]	$dx_{rel,t}$ [%]
0.17	1.89	0.96	11	98	0.13	0.09	39	1.50	0.00	30	Inf
0.33	2.90	2.21	8	31	0.08	0.07	19	2.17	0.50	33	333
1	5.05	4.29	9	18	0.06	0.06	-2	3.50	2.00	30	75
2	6.64	5.94	8	12	0.05	0.05	4	4.50	3.17	27	42
6	9.71	8.68	12	12	0.04	0.04	-8	6.33	5.00	27	27

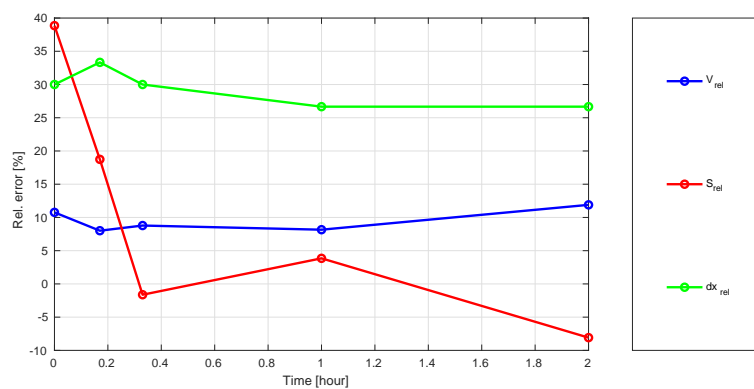


Figure 5.43 Temporal development of the relative error for the three indicators.

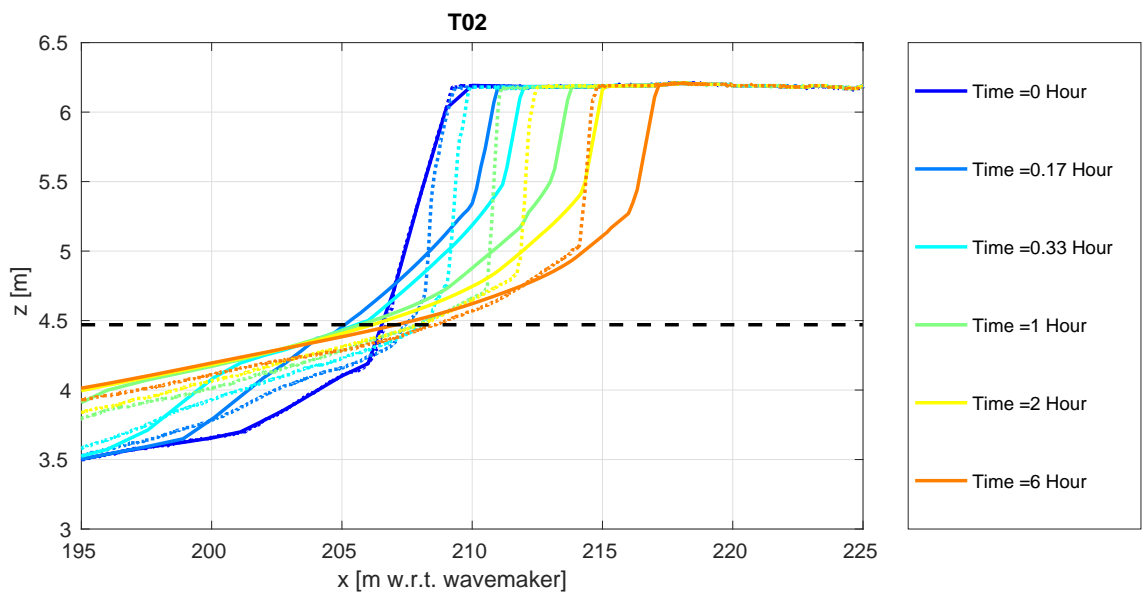


Figure 5.44 Comparisons of profiles from experiment T02 for different moments in time. Observed profiles are shown with a dashed line and the XBeach profiles with a solid line. The storm surge level is shown with a black dashed line.

Table 5.21 The computed and observed volume (V) and berm slopes (S) for T02. Volumes (V) are given in m^3/m . The relative error is expressed in a percentage. Both the relative error in terms of the same time (rel, t) and the final time are shown (rel).

Time[hour]	V_{xb} [m^3/m]	V_{data} [m^3/m]	V_{rel} [%]	$V_{rel,t}$ [%]	S_{xb} [-]	S_{data} [-]	S_{rel} [%]	dx_{xb} [m]	dx_{data} [m]	dx_{rel} [%]	$dx_{rel,t}$ [%]
0.17	2.21	1.04	12	113	0.13	0.09	49	1.83	0.17	29	1000
0.33	3.44	2.34	11	47	0.08	0.07	23	2.83	0.83	35	240
1	6.25	4.63	17	35	0.05	0.05	1	4.67	2.00	47	133
2	8.18	6.37	19	28	0.05	0.05	-1	5.83	3.33	44	75
6	11.70	9.63	22	22	0.04	0.04	2	8.00	5.67	41	41

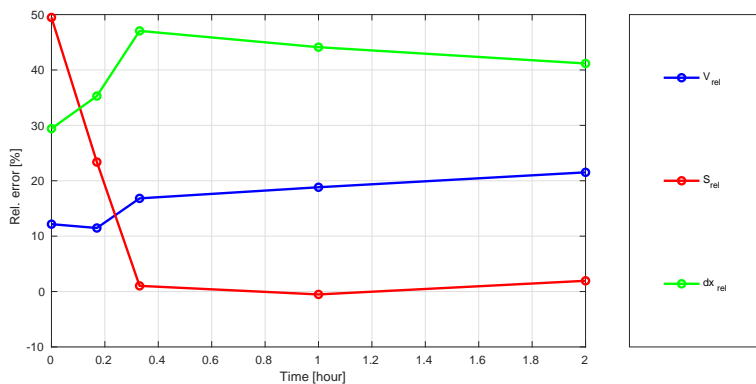


Figure 5.45 Temporal development of the relative error for the three indicators.

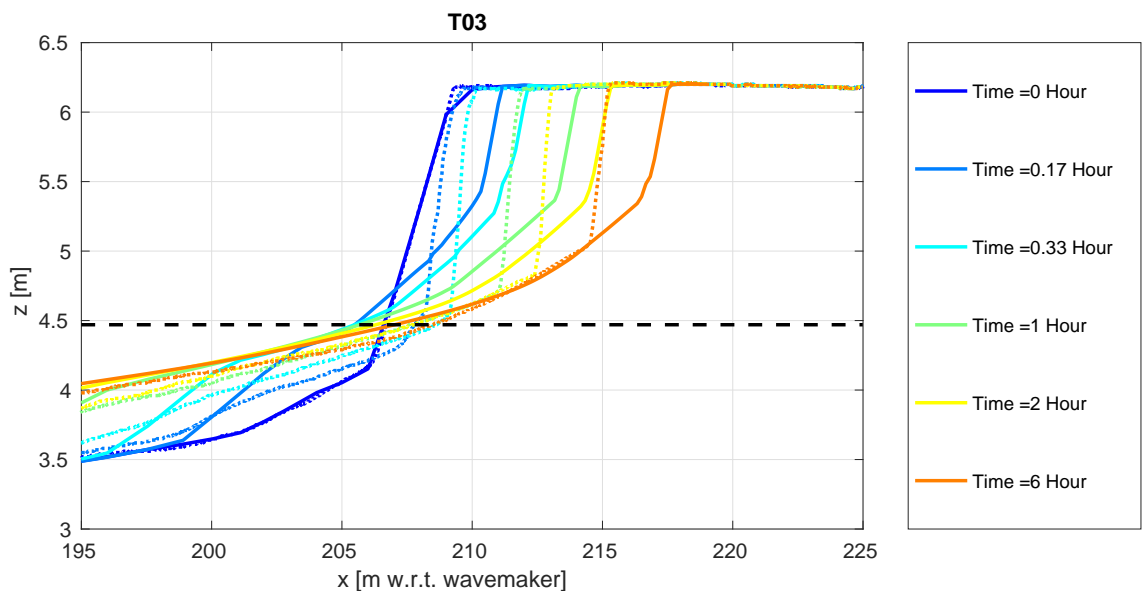


Figure 5.46 Comparisons of profiles from experiment T03 for different moments in time. Observed profiles are shown with a dashed line and the XBeach profiles with a solid line. The storm surge level is shown with a black dashed line.

Table 5.22 The computed and observed volume (V) and berm slopes (S) for T03. Volumes (V) are given in m^3/m . The relative error is expressed in a percentage. Both the relative error in terms of the same time (rel, t) and the final time are shown (rel).

Time[hour]	V_{xb} [m^3/m]	V_{data} [m^3/m]	V_{rel} [%]	$V_{rel,t}$ [%]	S_{xb} [-]	S_{data} [-]	S_{rel} [%]	dx_{xb} [m]	dx_{data} [m]	dx_{rel} [%]	$dx_{rel,t}$ [%]
0.17	2.33	1.22	11	91	0.11	0.08	37	2.00	0.33	27	500
0.33	3.73	2.60	11	43	0.08	0.06	26	3.00	0.83	35	260
1	6.53	5.41	11	21	0.06	0.05	10	5.00	2.83	35	76
2	8.52	7.21	13	18	0.05	0.05	3	6.17	4.00	35	54
6	11.84	9.96	19	19	0.04	0.04	11	8.33	6.17	35	35

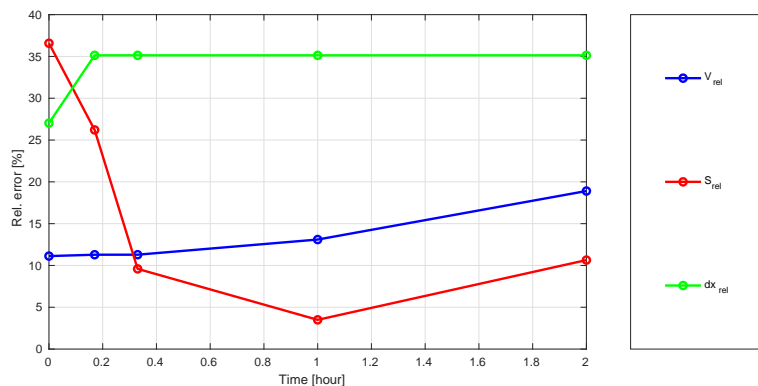


Figure 5.47 Temporal development of the relative error for the three indicators.

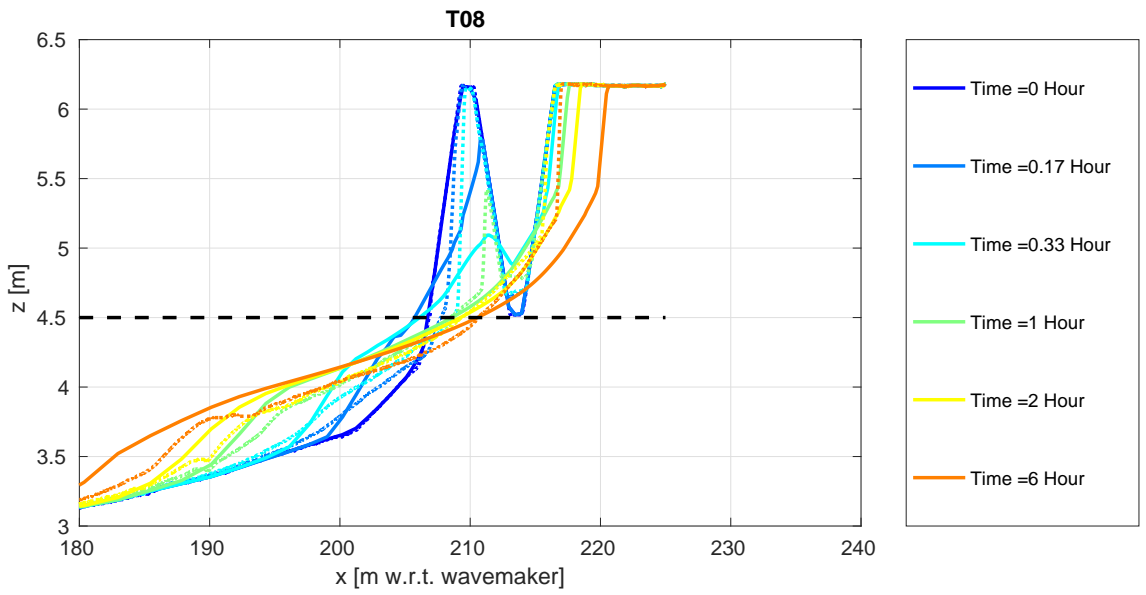


Figure 5.48 Comparisons of profiles from experiment T08 for different moments in time. Observed profiles are shown with a dashed line and the XBeach profiles with a solid line. The storm surge level is shown with a black dashed line.

Table 5.23 The computed and observed volume (V) and berm slopes (S) for T08. Volumes (V) are given in m^3/m . The relative error is expressed in a percentage. Both the relative error in terms of the same time (rel, t) and the final time are shown (rel).

Time[hour]	V_{xb} [m^3/m]	V_{data} [m^3/m]	V_{rel} [%]	$V_{rel,t}$ [%]	S_{xb} [-]	S_{data} [-]	S_{rel} [%]	dx_{xb} [m]	dx_{data} [m]	dx_{rel} [%]	$dx_{rel,t}$ [%]
0.17	2.13	1.19	13	79	0.12	0.09	40	7.17	0.17	88	4200
0.33	4.31	2.29	29	89	0.08	0.07	22	7.50	0.67	85	1025
1	6.60	4.84	25	36	0.04	0.06	-23	8.33	7.33	12	14
2	7.89	5.88	29	34	0.04	0.05	-9	9.17	7.33	23	25
6	10.93	7.03	55	55	0.04	0.04	-7	11.17	8.00	40	40

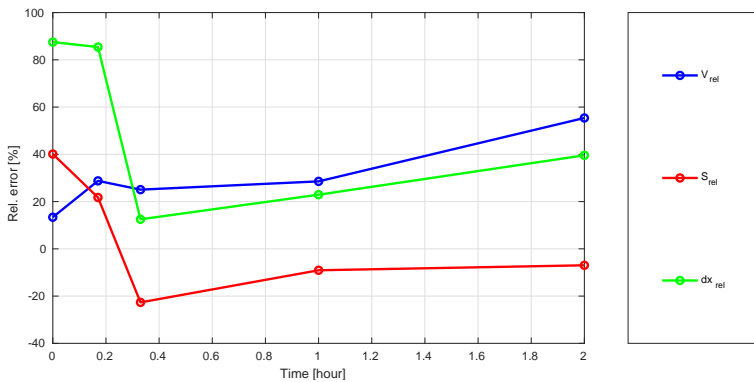


Figure 5.49 Temporal development of the relative error for the three indicators.

Overview

An overview of the statistical scores is shown in Figure 5.50 and Table 5.24.

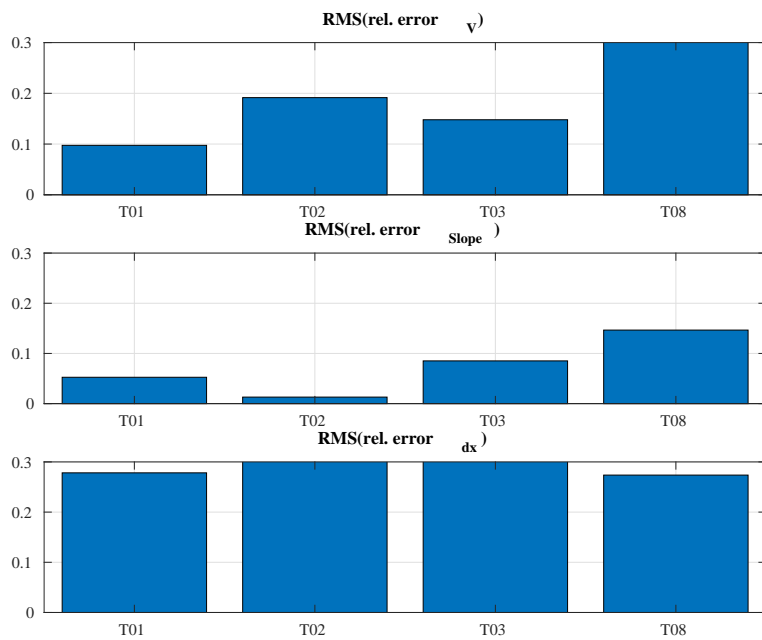


Figure 5.50 Overview of statistical scores for the Deltagoot 2006 experiments.

Table 5.24 Deltagoot 2006 statistical scores.

	T01	T02	T03	T08
<i>RMS(rel. volume)</i>	0.10	0.19	0.15	0.39
<i>RMS(rel. slope)</i>	0.05	0.01	0.09	0.15
<i>RMS(rel. retreat)</i>	0.28	0.44	0.35	0.27

5.7.0.1 Spectral shape

Test DP01 and DP02 were conducted with a double-peaked wave spectrum to investigate what (spectral) wave period is best qualified to describe dune erosion (Van Gent *et al.*, 2008). In this document the tests are discussed to obtain further insight in the capability of the model to simulate dune erosion for various wave spectra. The simulations are performed on a regular grid with $dx = 1\text{ m}$ and input to the model are time series of short wave varying energy (low pass filtered on the wave group time scale) and incoming (bound) long waves. The time series are constructed from pressure and flow measurements at $x = 41\text{ m}$ from the wave board. The short wave group velocity (associated with advection of wave action) is based on the $T_{m-1,0}$ wave period. Settings for the wave energy dissipation model are found in Table 5.25.

Table 5.25 Wave dissipation parameter settings

Experiment	α	γ	n
DP01	1.0	0.50	10
DP02	1.0	0.48	10

Simulated and measured profile evolution and dune erosion volumes for test DP01 and DP02 are compared in Figure 5.51 to Figure 5.54 respectively. For test DP01 the

profile evolution is accurately reproduced and results for test DP02 are reasonable even though the erosion rate during the last interval is overestimated.

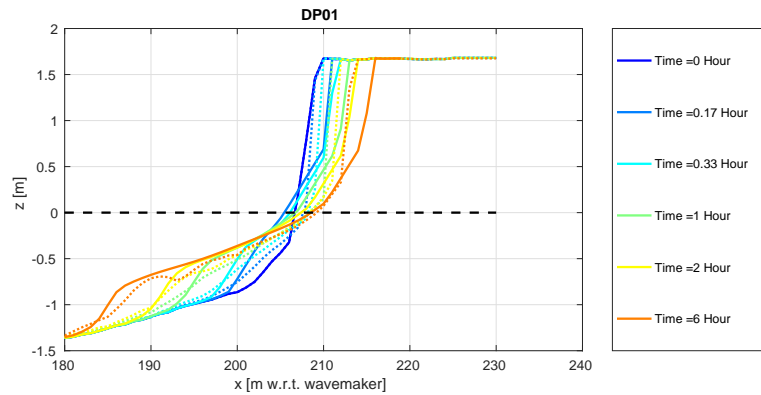


Figure 5.51 Profile development during test DP01

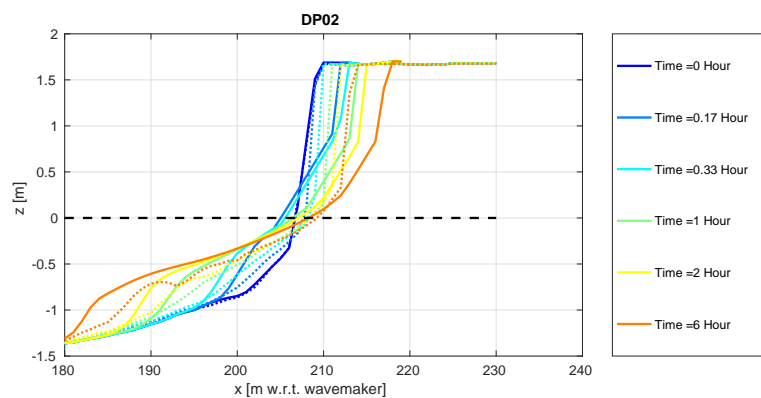


Figure 5.52 Profile development during test DP02

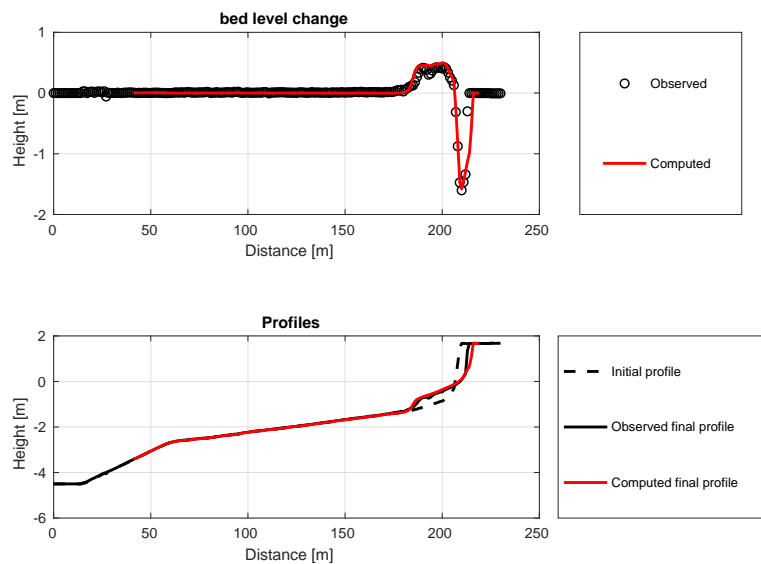


Figure 5.53 Erosion pattern and volumes and retreat distance during test DP01

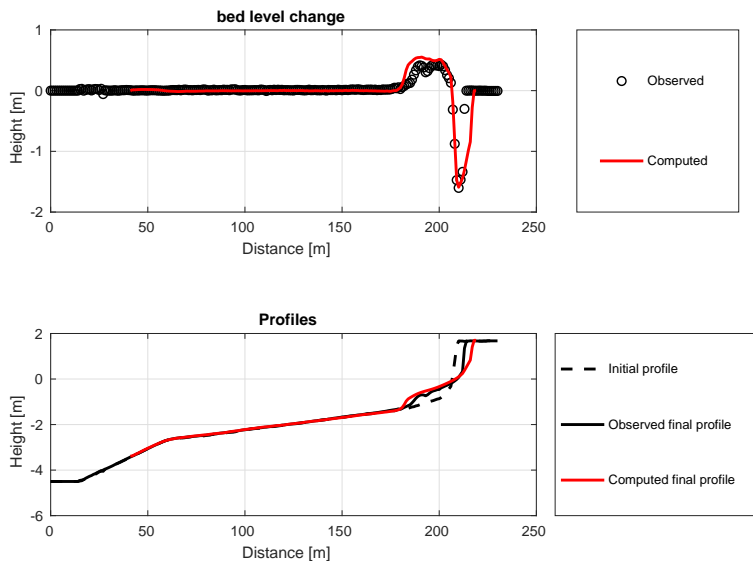


Figure 5.54 Erosion pattern and volumes and retreat distance during test DP02

The imposed double-peaked wave spectra affect the time scale and amplitude of the simulated wave groups. Consequently, the interaction of simulated long waves with the short wave groups is different and hydrodynamics in front of the dune face are expected to have other characteristics. In Figure 5.55 and Figure 5.56 the simulated wave transformation, flows and sediment concentrations are favourably compared with measurements obtained during test DP01. It seems the model is capable to take into account the effect of various wave spectra on near dune hydrodynamics and sediment transports.

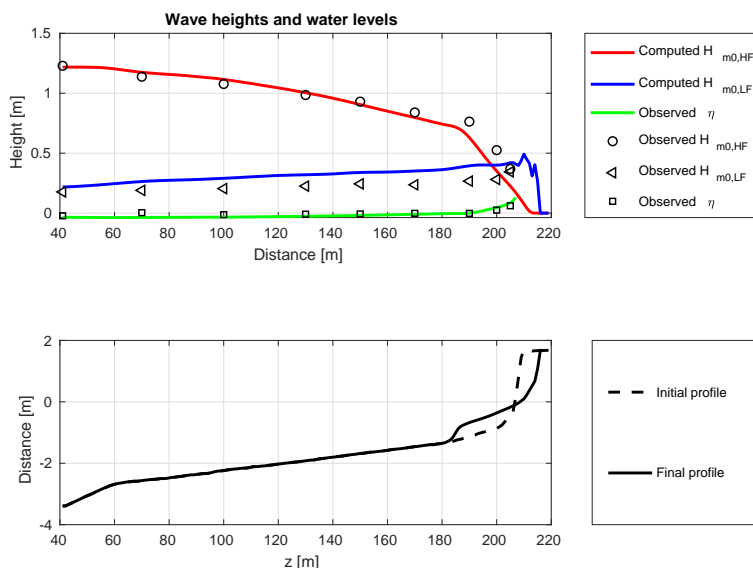


Figure 5.55 Hydrodynamics during test DP01

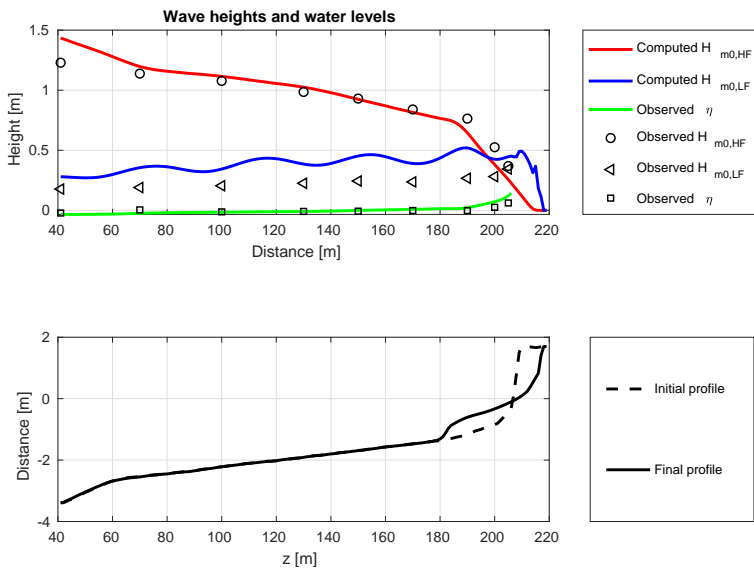


Figure 5.56 Hydrodynamics during test DP02

It is concluded that the effect of the wave spectral shape on dune erosion and dune face retreat is favourably predicted with the model. The time averaged simulated wave transformation, flow and sediment concentration compare well with the mobile frame measurements obtained during test DP01.

In Van Gent *et al.* (2008) the spectral mean wave period $T_{m-1,0}$ is argued to be more qualified to describe dune erosion than the peak wave period T_p . The simulations presented in this subsection are performed with the $T_{m-1,0}$ wave period and show satisfying results suggesting the spectral mean wave period proposed by Van Gent *et al.* (2008) is indeed a good measure to describe dune erosion. It is remarked though that any firm conclusion would require extra simulations in which the peak wave period T_p is applied instead of the $T_{m-1,0}$ wave period. In addition this would demand for a new model optimization and most likely different settings for the wave dissipation model.

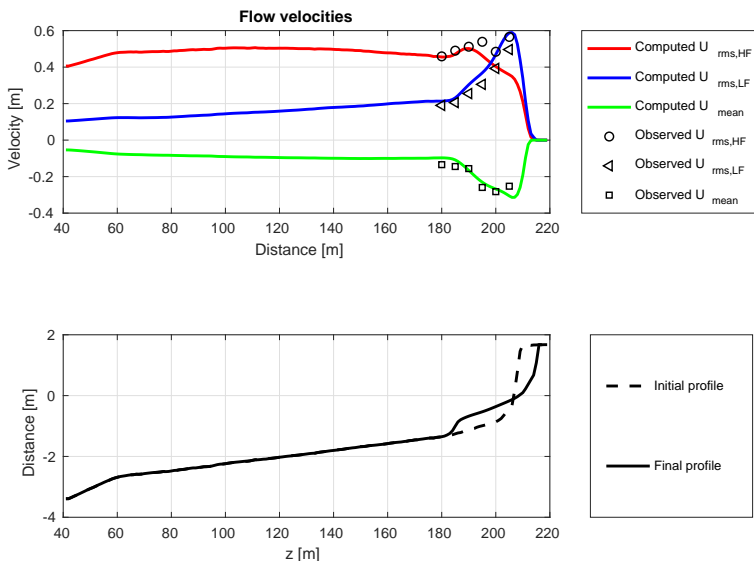


Figure 5.57 Velocities during test DP01

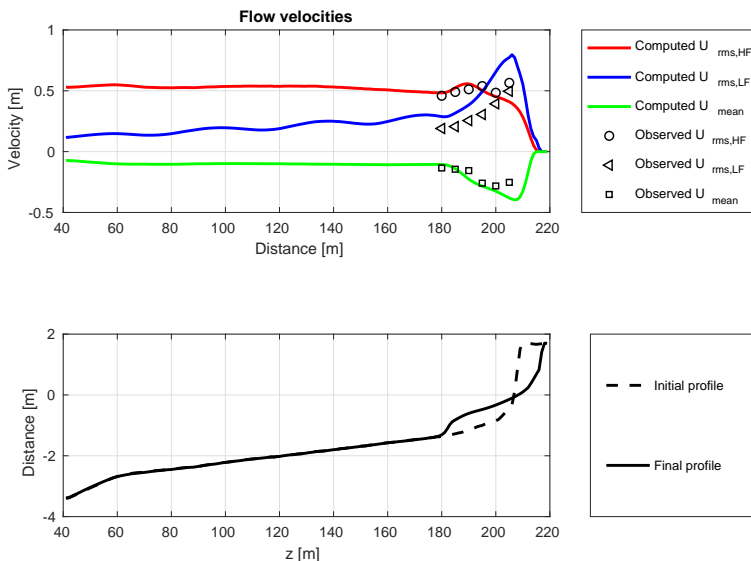


Figure 5.58 Velocities during test DP02

5.7.1 Double dune system

Test T04 of the Deltaflume experiment 2006 (Van Gent *et al.*, 2008) is carried out with an initial profile that contains a small dune in front of a larger volume dune that collapses after approximately one hour of waves (interval C and D). After breaching of the small dune, the foreshore is already very efficient in reducing wave impacts on the dune face resulting in small erosion rates over the remaining test intervals. In this test it is examined to what extent the dune breach can be reproduced with the XBeach model and whether the (substantially smaller) erosion rate at the end of a storm is correctly predicted. The simulations is performed on a regular grid with $dx = 1$ m and input to the model are time series of short wave varying energy (low pass filtered on the wave group time scale) and incoming (bound) long waves. The time series are constructed from pressure and flow measurements at $x = 41$ m from the wave board. The short wave group velocity (associated with advection of wave action) is based on the $T_{m-1,0}$ wave period. Settings for the wave energy dissipation model are equal to the settings for the T03 test.

Simulated profile evolution and dune erosion volumes are shown in Figure 5.59 and Figure 5.60 respectively. The simulated hydrodynamics are presented in Figure 5.61. For the first three intervals (the small dune breaches in interval 3) the dune erosion rate is slightly overestimated but the profile evolution compares favourably with the measured profiles. Considering the last two intervals, erosion rates and dune face retreat are too large.

Breaching of a small dune in front of a larger volume dune causes that suddenly the foreshore is significantly closer to equilibrium with the storm surge conditions. As a result near shore hydrodynamics, near shore sediment transports and wave impacts on the dune face are less severe. It is concluded that the feedback between profile evolution and near dune processes is not sufficiently well included in the model at the end of test T04, which is representative for conditions at the end of a storm. More insight in the model performance at the end of a storm could possibly be obtained by comparing the evolution of simulated driving processes (undertow, sediment concentrations and avalanching) with measurements.

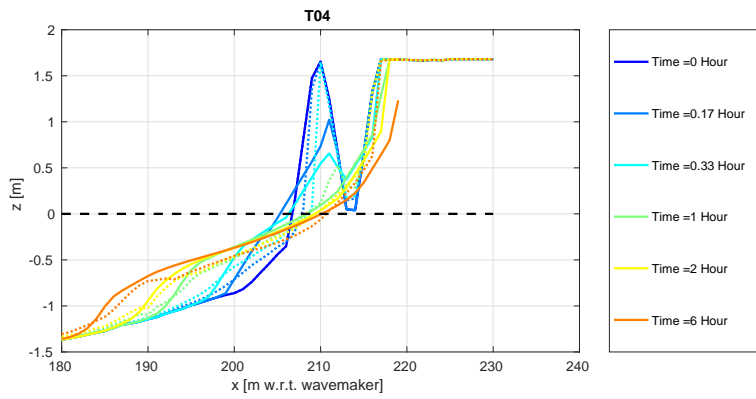


Figure 5.59 Profile development during test T04

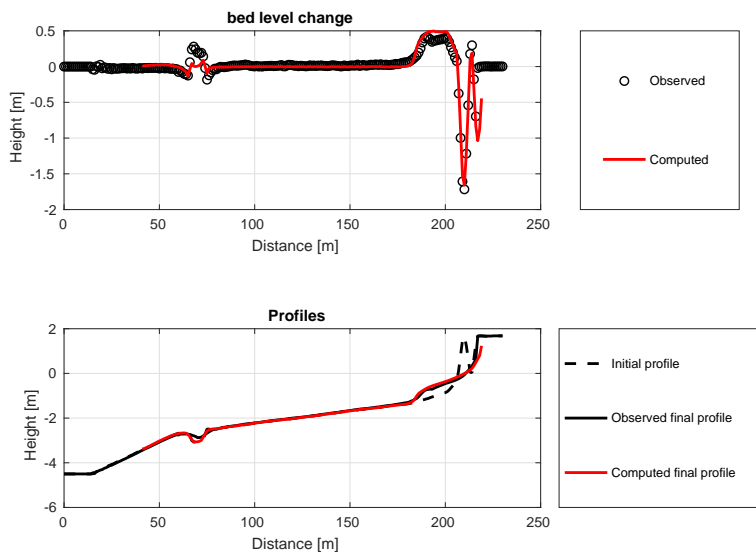


Figure 5.60 Erosion pattern and volumes and retreat distance during test T04

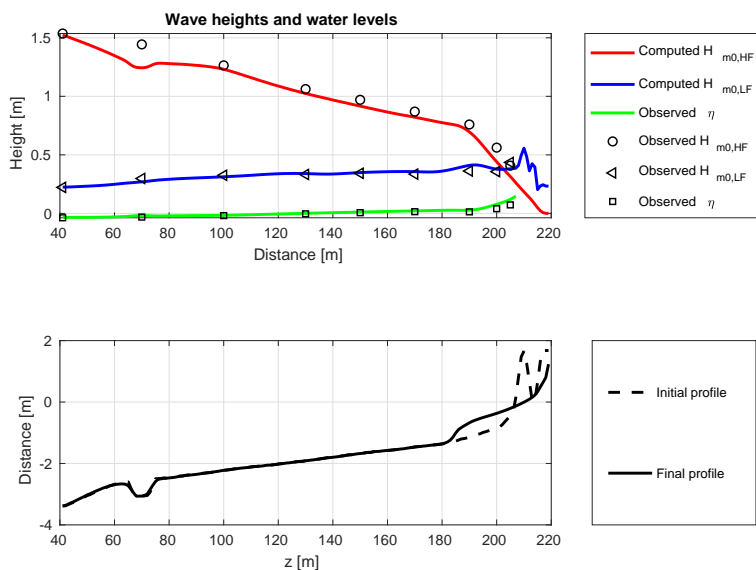


Figure 5.61 Hydrodynamics during test T04

6 Field validation

6.1 Egmond

Experiment description

The field dataset collected at Egmond aan Zee in the Netherlands is used for both hydrodynamic and morphodynamic validation of the BOI-version of XBeach. Egmond aan Zee is located along the Dutch Holland coast [Figure 6.1](#), where tides are semi-diurnal, with a neap and spring tidal range of 1.4 and 1.8 m. Annual mean offshore wave height $Hm0 = 1.3$ m and wave period $Tm02 = 4.5$ s ([Wijnberg, 2002](#)). During northwesterly storms, significant wave heights can reach up to 7 m and storm surges can raise the water level by more than 1 m ([Ruessink et al., 2019](#)). The coastal zone of the field site is characterized by 2-3 subtidal bars and an intertidal bar on a gently sloping intertidal (1:40) beach. The dune toe is located at 3 m + MSL and changes into a steep fore dune with a 1:2,5 slope. Around 14 to 17 m + MSL, the profile abruptly changes in slope and continues gently to the foredune crest at a height of 20 to 25 m+ MSL. Alongshore variability in foredune shape and height is small. During multiple years without dune erosion, embryo dunes can develop at the toe of the foredune ([De Winter et al., 2015](#)). The well-sorted quartz sand at the study site has a medium grain size of 250300 µm, with a tendency to decrease in the landward direction.

A quick reaction force was set up to collect field data directly preceding, during and following storms. The dune erosion event on 8-9 January 2019 is selected for validation. The offshore water level at the study site reached 2 m + MSL and the maximum significant wave height (Hs) was just below 5 m and maximum peak period (Tp) was 15 s. The waves arrived obliquely incident, from west-southwest during the beginning of the storm and the direction changed to the northwest for the remainder of the storm.

During the winter of 2018/2019 7 pairs of pressure sensors were deployed spaced 250 - 750 m apart, along a 1.5 - 3 km stretch of beach south of Egmond aan Zee ([Figure 6.1](#), right panel). The pairs consist of a seaward and a landward sensor (40m distance in cross-shore direction). The landward sensors were located above the high tide water level, each at different elevation levels (maximum 1 m difference). The surface elevations were collected at a frequency of 5 Hz and post-processed into consecutive bursts of 30 min, only the bursts in which the sensor was continuously submerged were considered, to calculate mean water levels and significant wave heights in the sea-swell (HS,SS) and infragravity (Hs,IG) frequency band.

Full bathymetric (sonar-equipped jetski) and topographic (mobile laser scanner) surveys provided pre and post the storm observations. Bathymetric data was collected on 23 November 2018 and 22 January 2019, while topographic survey was collected directly preceding (7 January 2019) and post (10 January 2019) the storm event. The bed level measurements show that the storm did not result in large erosion volumes, but erosion of the lower dune face did occur along the entire field site. Due to the northwesterly wave incidence during the largest storms, the outer crescentic bar mostly rotated clock-wise, leading to an alternation of onshore and offshore migration alongshore.

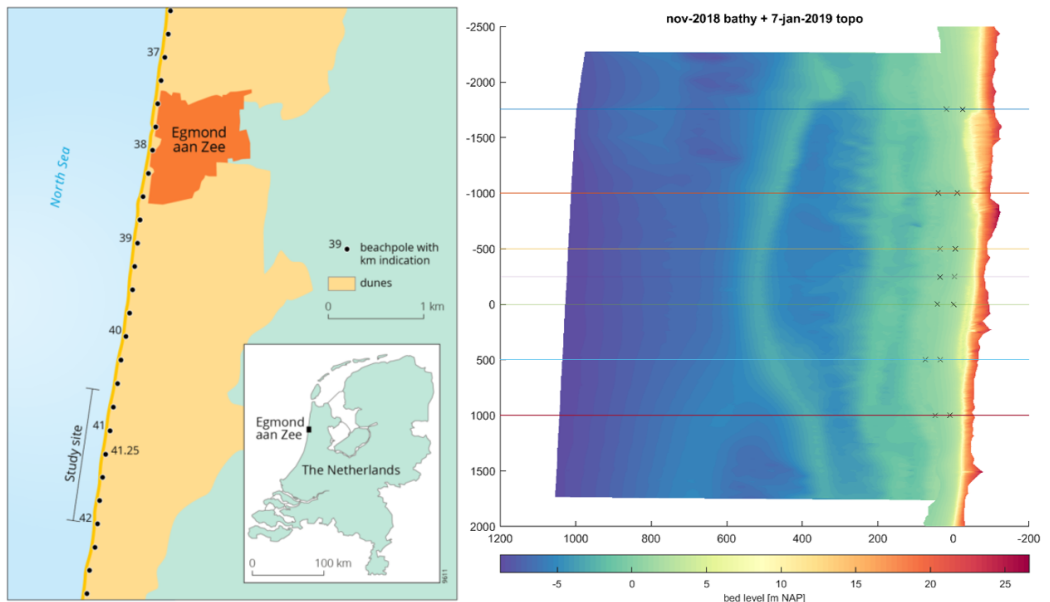


Figure 6.1 Location of study site (left panel). The beach poles form an alongshore reference line, with the km number referring to the distance to the zero point at the northern end of the Holland coast. The origin of the local coordinate system used (right panel) here is beach pole 41.25, with positive x and y in the seaward and southern direction, respectively. The crosses (x) indicate the different pressure sensors.

Results Hydrodynamics

The timeseries of observed and modeled water levels, high frequency and infragravity wave heights for all pressure sensors are presented in [Figure 6.2](#), [Figure 6.3](#) and [Figure 6.4](#) respectively. Some of the sensors run dry during lower water elevations, especially the sensors closer to the beach (right column in the figures), explaining the gaps in the observations. The modelled surface elevations are collected at a frequency of 10 Hz and post-processed into consecutive bursts of 30 min to calculate mean water levels and significant wave heights in the sea-swell (HS,SS) and infragravity (Hs,IG) frequency band. Only the bursts for which the sensor was continuously submerged are considered.

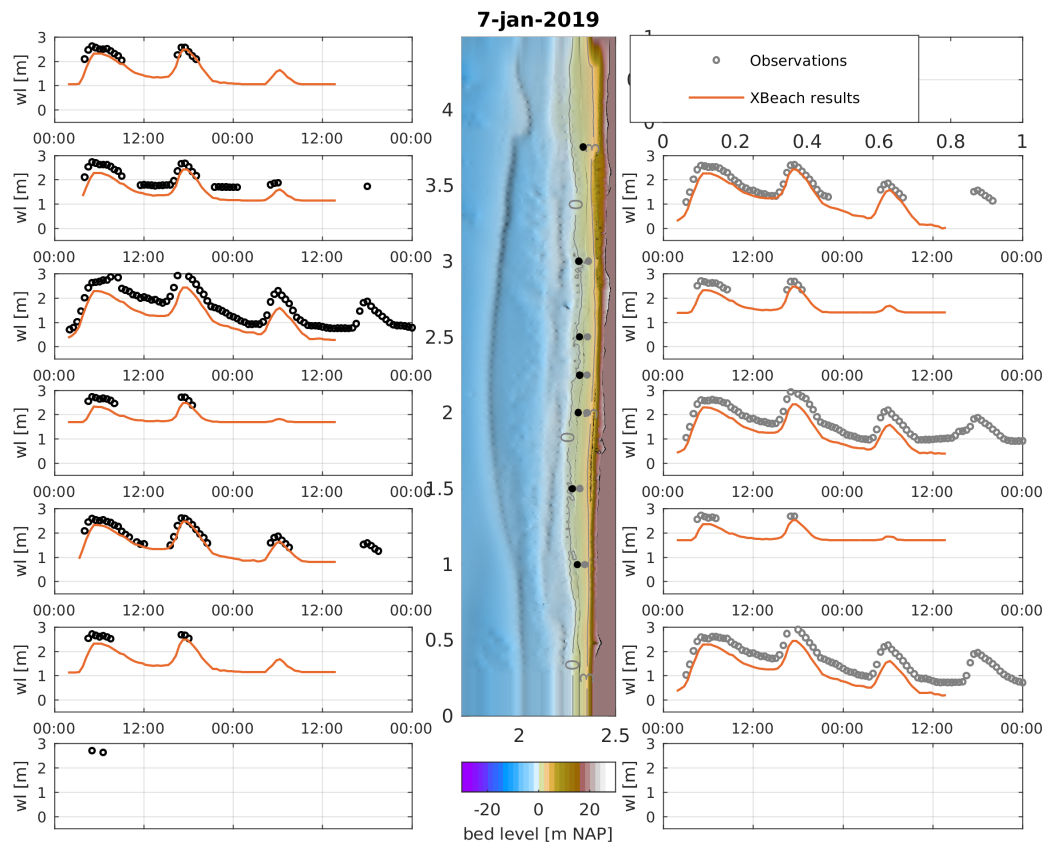


Figure 6.2 Observed water levels (black circles) against the modelled water levels (orange) for all pressure sensors. The panel in the middle shows the location of the pressure sensors, and the surrounding subpanels follow the order from North to South (top to bottom) and from sea (left) to the beach (right).

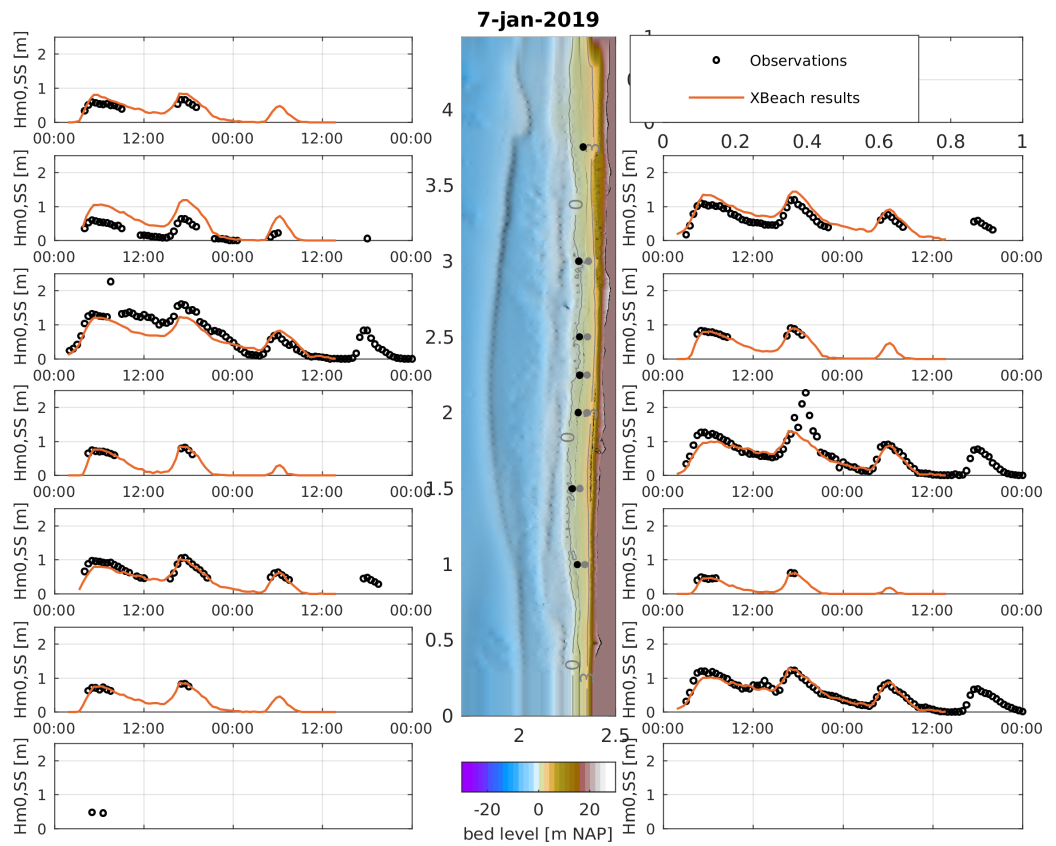


Figure 6.3 Observed short-wave heights (black circles) against the modelled short-wave heights (orange) for all pressure sensors. The panel in the middle shows the location of the pressure sensors, and the surrounding subpanels follow the order from North to South (top to bottom) and from sea (left) to the beach (right).

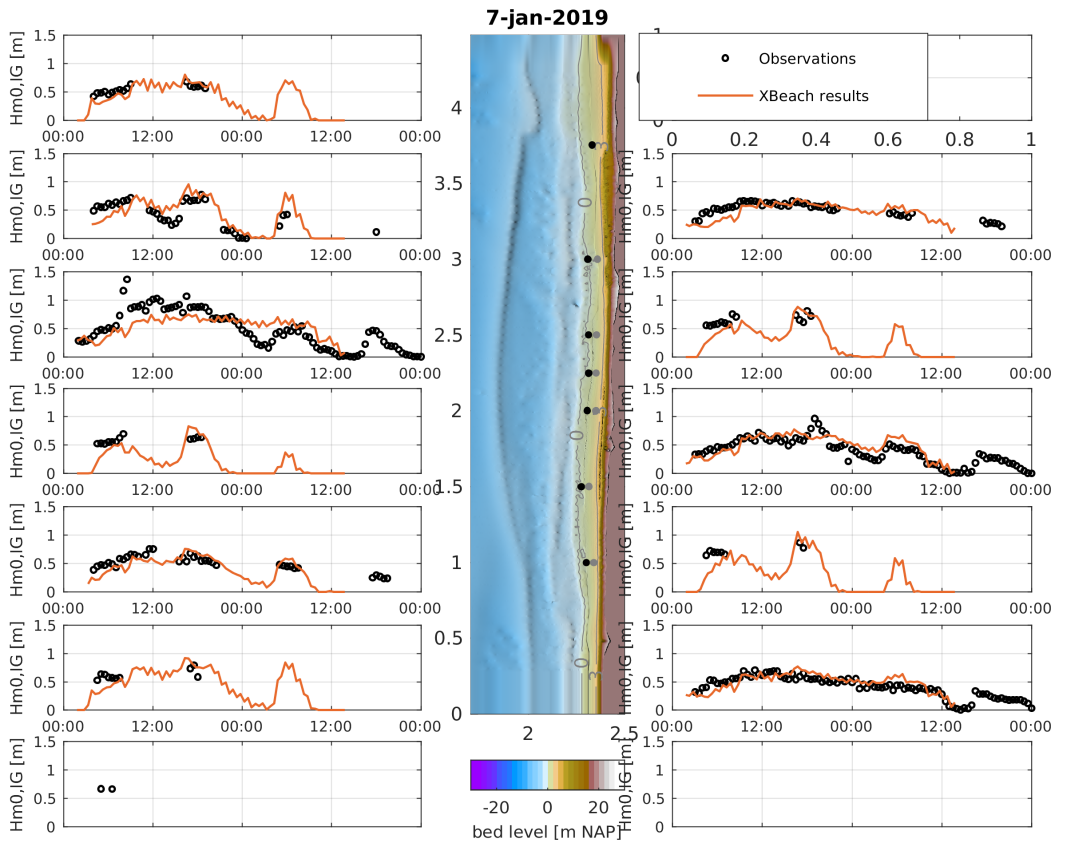


Figure 6.4 Observed infragravity wave heights (black circles) against the modelled infragravity wave heights (orange) for all pressure sensors. The panel in the middle shows the location of the pressure sensors, and the surrounding subpanels follow the order from North to South (top to bottom) and from sea (left) to the beach (right).

Results Morphodynamics

The morphological model results are validated using the topography measurements of the beach and dunes, collected on January 10th. The vertical reference level of maximum dune retreat is determined at NAP + 3 m, based on the observed pre- and post-storm topography. A quantitative comparison between observed and modelled erosion volumes and dune retreat is presented in [Table 6.1](#). For transects T(y=0) and T(y=-1755), graphical comparisons are presented as well in [Figure 6.5](#) and [Figure 6.6](#).

Table 6.1 A quantitative comparison of modelled and observed erosion volumes [m^3/m] and dune retreat [m] at 3m + NAP for all 7 profiles.

	VeroXB	VeroMeas	retreatXB	retreatMeas
T -1001	13.12	1.38	5.40	1.70
T -1755	6.95	0.03	4.86	0.57
T -249	8.22	8.15	2.13	3.75
T -502	7.73	6.22	3.15	4.16
T 0	4.87	3.86	1.52	2.77
T 1001	8.55	5.88	2.56	4.01
T 499	7.16	3.99	3.10	2.63

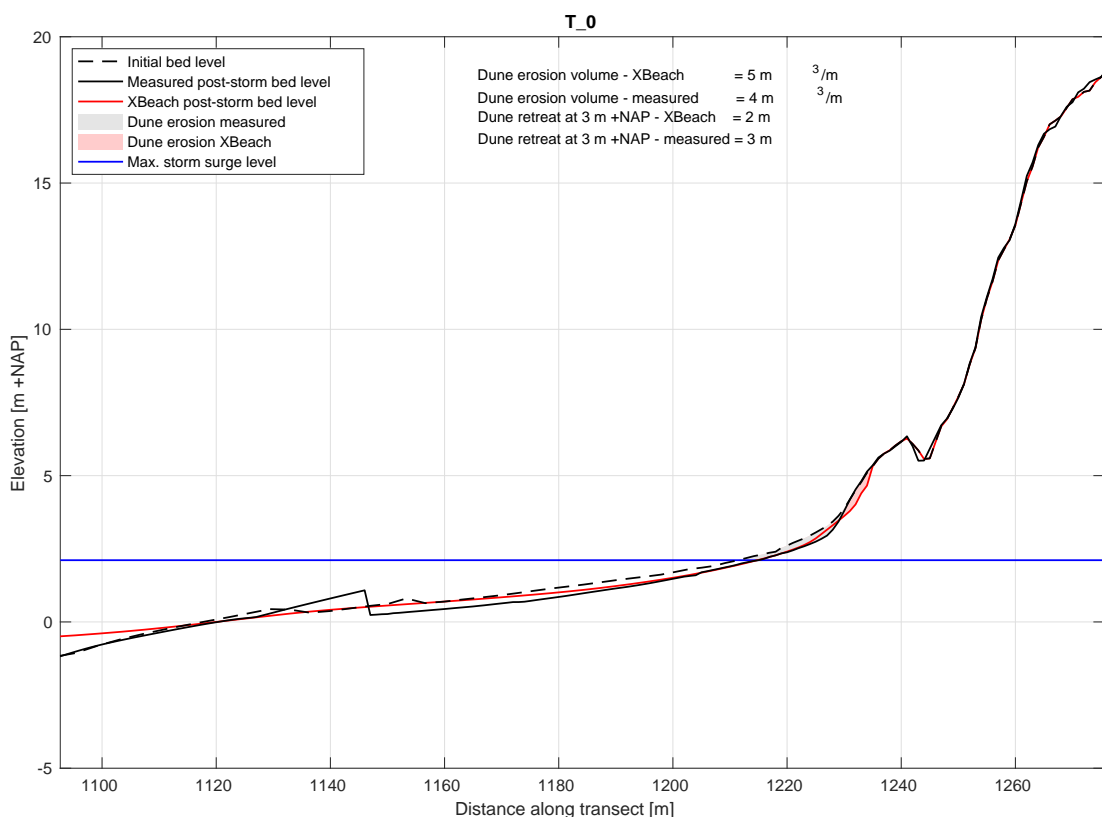


Figure 6.5 XBeach results for cross-shore transect 0 at Egmond aan Zee. Initial bed levels are depicted by the black dotted line, observed post-storm bed levels by the black solid line and XBeach model results are presented in red. The modelled dune erosion is shown by the red shaded area.

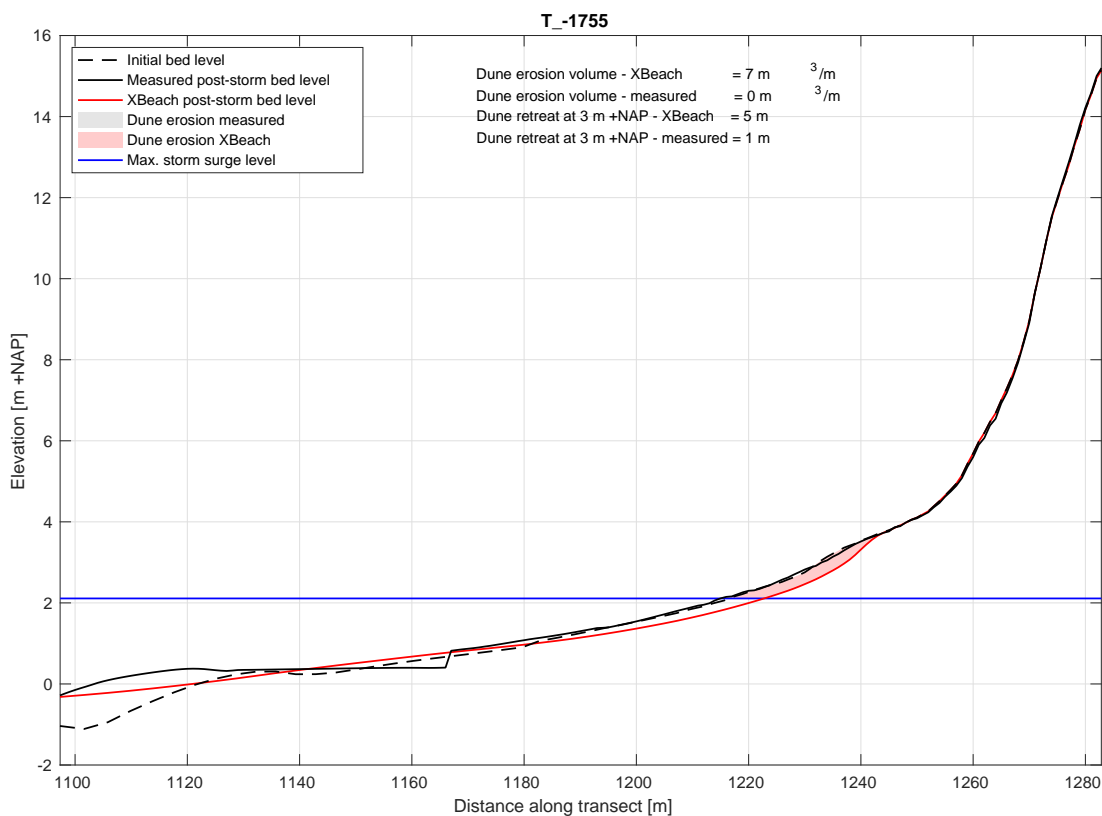


Figure 6.6 XBeach results for cross-shore transect -1755 at Egmond aan Zee. Initial bed levels are depicted by the black dotted line, observed post-storm bed levels by the black solid line and XBeach model results are presented in red. The modelled dune erosion is shown by the red shaded area.

6.2 Vlaanderen

Experiment description

At 5-6 December 2013, the northwestern storm at the North Sea called Storm Xaver or the Sint Nicholas storm (Sinterklaasstorm) with relatively low wind speeds and a long fetch resulted in high surge levels in combination with moderately high waves (Trouw *et al.*, 2015). This resulted in beach and dune erosion along among others the Belgian coast on the order of 8 m³/m (Lanckriet *et al.*, 2015). The Coastal Division of the Flemish Government collected 122 cross-shore profiles of the beach and (first) dune row during a dGPS survey 2-4 days before this storm and based on an airborne lidar survey 4 days after this storm (Trouw *et al.*, 2015). A selection of these pre- and post-storm profiles (Figure 6.7) is being used for the validation of the morphodynamics in the BOI-version of the dune erosion model XBeach, focusing on dune erosion volumes and retreat distances.



Figure 6.7 Overview of the Belgian coastline with the location of the analyzed cross-shore profiles measured before and after the Sint Nicholas storm and the water level (WL) and wave measurement locations used for this case.

Based on the data of the Vlaamse Banken, the offshore storm surge levels reached up to 6.0 m +TAW1 (5 min average) during the Sint Nicholas storm at measurement pole A2 and Scheur Wielingen in front of the Belgian coast (bottom depth respectively about -7 m LAT2 and -10 m LAT). This was the result of a combined high storm setup and spring tide. At the harbor of Ostend, storm surge levels reached 6.19 m TAW (Trouw *et al.*, 2015). The observed water levels were highest since 1953 and were estimated to have a return period of about 40 year in Belgium (IMDC, 2005). Besides, significant wave heights reached up to 3.8 m (20 min average) at the offshore wave buoy ZW-Akkaert at -20 m LAT (Figure 6). The highest peak occurred during rising tide; at the peak water level, the wave height was already about 0.5 m lower. The peak wave period during the storm was about 8 s with a peak to 15 s at the end of the storm at the same location. This corresponds to a return period in the order of 1 year along the Belgian coast (IMDC, 2005). The waves approached approximately shore-normal from the northwest. After more than one day of high waves, the wave height gradually reduced, together with the storm surge.

The Belgian coast has gently sloping, dissipative beaches that are slightly steeper towards the east. They are mainly composed of fine to medium sand (Degraer *et al.*, 2003). The tidal regime along the Belgian coast is semidiurnal and macrotidal, with a of 3.7-3.9 m neap tidal range and 4.5-5 m spring tidal range which slightly decrease from west to east (Degraer *et al.*, 2003). To prevent the beaches from erosion by the strong tidal currents, a large part of the coastline is protected by groynes. Moreover, a concrete dike along the most of the coastline must protect the inland from flooding (Degraer *et al.*, 2003). In the areas with natural beach-dune transitions between Ostend and the Dutch-Belgian border, 15 profiles are selected for this case study (Figure 6.7). The beaches in the selected profiles have a slope of on average 1:45 to 1:65 from the dune toe to the relatively flat zone at -5 m TAW (westernmost profiles) to -7 m TAW (easternmost profiles). Just below mean sea level, 2-4 bars are present in all profiles except the easternmost profiles (117-121). The relatively flat plateau

extends more than 10 km into the sea and contains some sand banks. Further offshore, seaward of the profiles, the bathymetry is characterized by large sand banks at intermediate to deep water.

Results

The dune erosion volumes and retreat distances at 7m + TAW, based on the measured pre- and post-storm profiles and the XBeach simulations for all 15 profiles are tabulated in [Table 6.2](#). As an example, the pre- and post-storm profile for profile nr. 119 based on the measurements and on the XBeach simulation are presented in [Figure 6.8](#).

Table 6.2 Dune erosion volume [m^3/m] and retreat distance [m] at 7 m +TAW for the Sint Nicholas storm in the XBeach simulation and the measured profiles for the 15 selected profiles along the Flemish coast.

	VeroXB	VeroMeas	retreatXB	retreatMeas
T 117	11.73	13.53	5.70	5.88
T 118	12.80	10.06	6.37	4.99
T 119	7.87	8.09	3.95	4.12
T 120	11.54	18.54	4.50	5.56
T 121	4.46	8.47	2.59	3.46
T 60	9.16	12.59	5.63	8.36
T 61	6.75	7.21	3.93	4.85
T 62	7.37	10.00	3.28	3.92
T 63	8.10	10.27	3.99	4.42
T 64	4.74	7.91	2.73	4.43
T 69	9.89	15.22	4.15	5.35
T 71	4.18	6.21	1.84	3.26
T 79	4.76	10.06	2.41	2.89
T 80	4.81	7.13	0.01	1.25
T 83	3.29	3.88	1.97	1.63

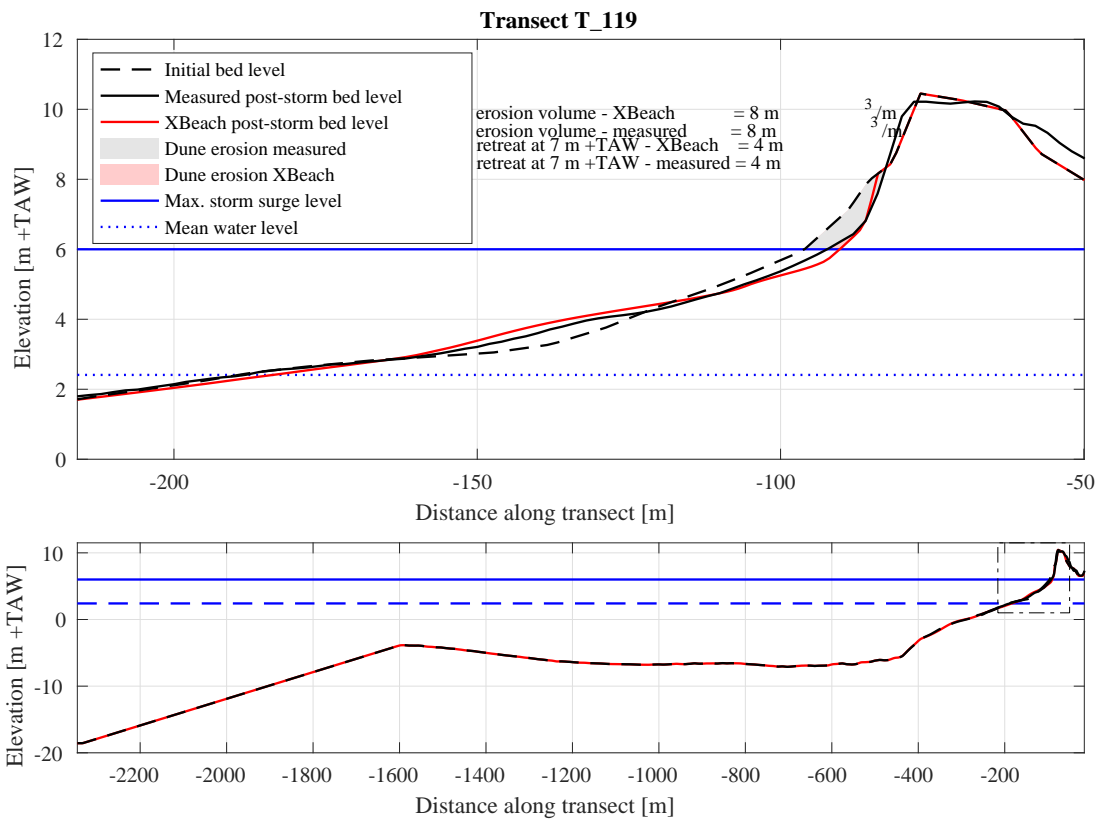


Figure 6.8 Cross-section profile nr. 119 before and after the Sint Nicholas storm based on the measurements and XBeach, including dune erosion volumes and retreat distances. Bottom: entire XBeach profile, top: zoom of beach and dune profile.

6.3

Vedersoe

Experiment description

Vedersoe is located at the Danish North Sea coast. Coastal measurements along multiple transects were obtained before and after a severe storm in January 2005, and reported to the Danish Coastal Authority. The observed dune retreats and erosion volumes show a high variability in alongshore direction. A study by the Danish Coastal Authority (DCA), as a part of the larger EU-InterReg project Building with Nature, considered two 1D transects close to each other (< 500 m) for which the observed dune retreat ranges from 4 to 14 meter, see Figure 6.9 (Kystdirektoratet, 2021). Though the profiles show large similarity, the different erosive behavior is likely due to the presence of a berm (above storm surge level) which reduces the erosion for one of the profiles. The two transects at Vedersoe are used to validate the BOI-XBeach model and settings for morphological changes due to storm impact. Compared to the Dutch coast, the Danish profiles have a similar slope in the lower shoreface, but a steeper surfzone.

According to Saye and Pye (2006) the Danish Southwest coast has a strong alongshore variation in grain size, with grain sizes up to 0.4 mm. However, Clemmensen *et al.* (2006) show that dunes in the southwest of Denmark are mainly formed by aeolian transport of fine-grained sand with a D₅₀ of around 0.2 mm. They also note that the inland dunes are more coarse-grained than the coastal dunes. A D₅₀ of 0.25 mm is used within the BOI project.

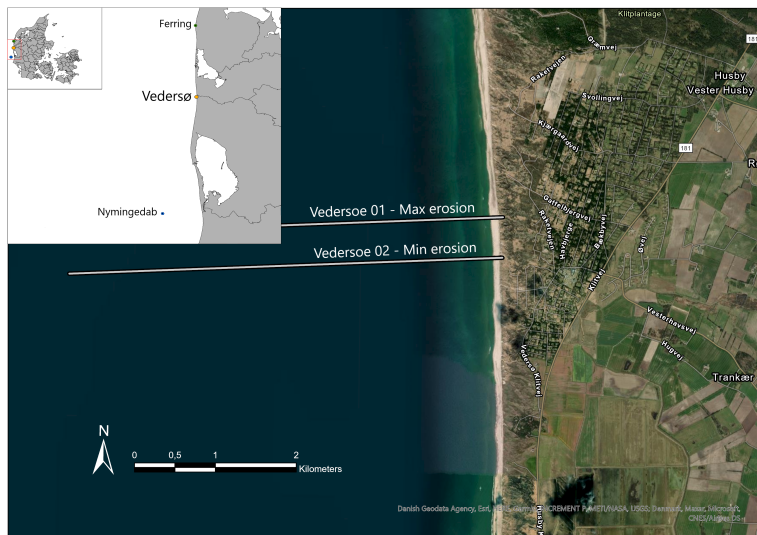


Figure 6.9 Location of the study area near Vedersoe (Denmark). The two different transects considered in this study are located close to each other, but different morphological behaviour is observed. Source: [Kystdirektoratet \(2021\)](#)

The wave climate during the storm in 2005 is measured by wave buoys located outside Nymingedab (50 km southward of Vedersoe at 17.5 m depth). At the deep-water wave buoy, the peak wave period T_p increased from 9.0 to 13.3 s, and H_s rapidly increased from 2.9 to 6.6 m. Water levels during the storm are obtained at a tidal gauge on one of the headlands of Ferring (30 km to the North from Vedersoe), and reached up to 3 m +MSL during the 2005 storm.

Results

Although the two transects are located within 500 m of each other and were exposed to the same hydrodynamic forcing, their morphological response differs significantly. The results for Vedersoe 01 are presented in [Figure 6.10](#) and the results for Vedersoe 02 are presented in [Figure 6.11](#). In addition, he dune erosion volumes and retreat distances at 5m + MSL, based on the measured pre- and post-storm profiles and the XBeach simulations are tabulated for both profiles in [Table 6.3](#).

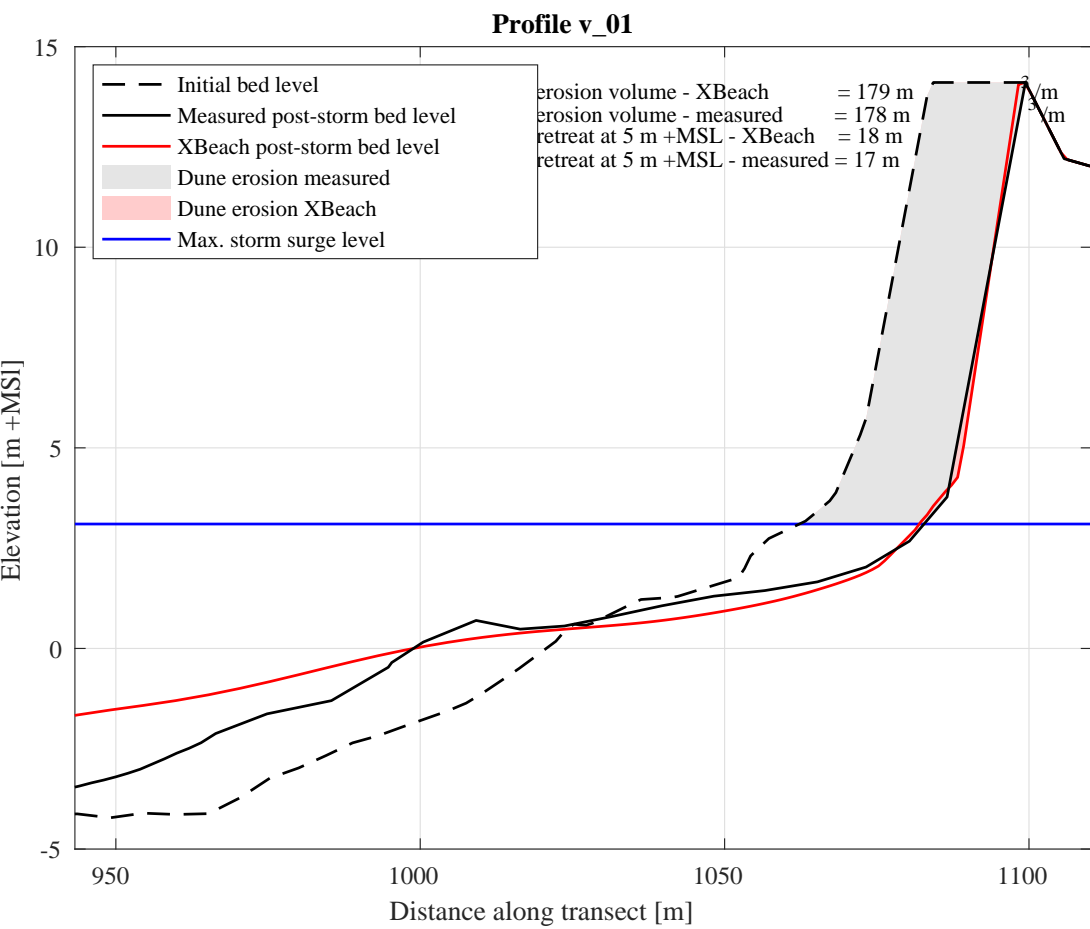


Figure 6.10 XBeach results for cross-shore transect Vedersoe 01. Initial bed levels are depicted by the black dashed line, observed post-storm bed levels by the black solid line and XBeach model results are presented in red. The modelled dune erosion is shown by the red shaded area, whereas the observed dune erosion is depicted with the grey shaded area.

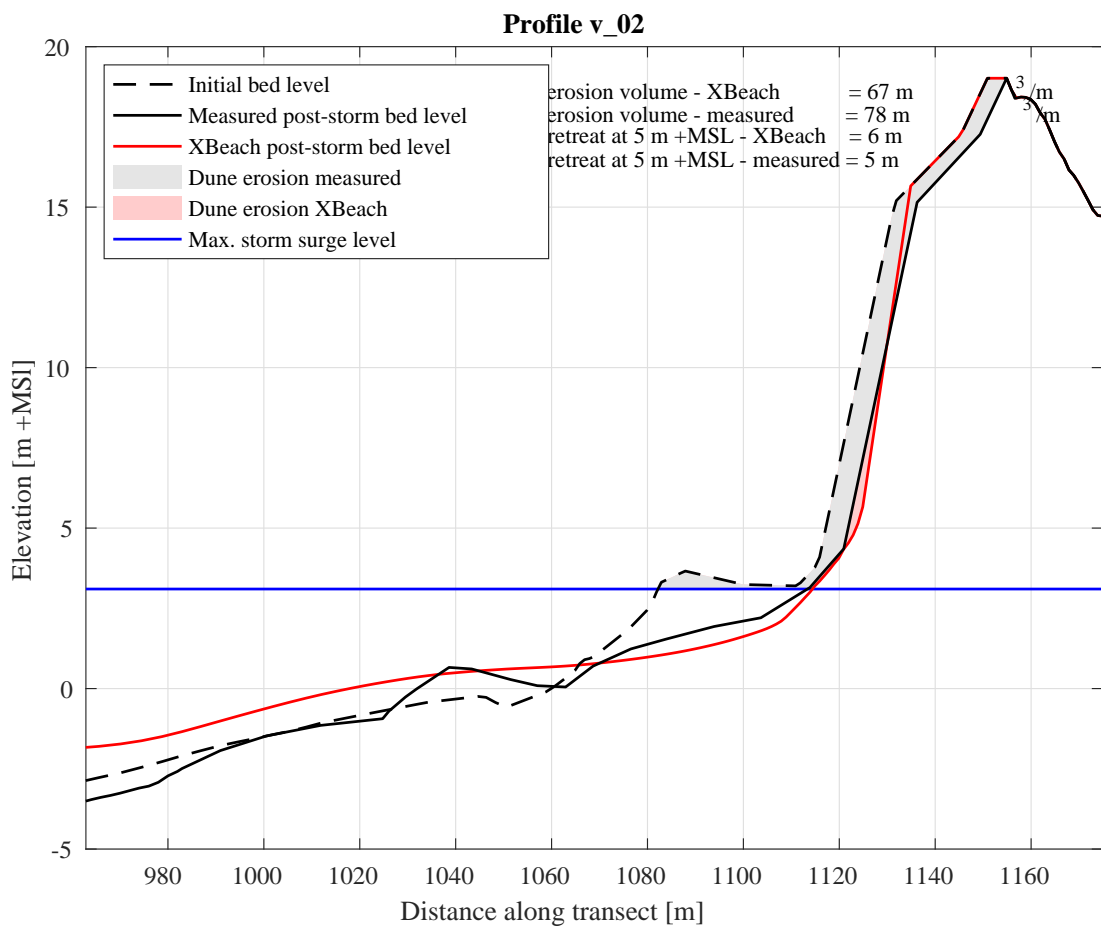


Figure 6.11 XBeach results for cross-shore transect Vedersoe 02. Initial bed levels are depicted by the black dashed line, observed post-storm bed levels by the black solid line and XBeach model results are presented in red. The modelled dune erosion is shown by the red shaded area, whereas the observed dune erosion is depicted with the grey shaded area.

Table 6.3 A quantitative comparison of modelled and observed erosion volumes [m^3/m] and dune retreat [m] at 5m + MSL for both profiles

	VeroXB	VeroMeas	retreatXB	retreatMeas
v 01	178.68	178.12	17.83	16.69
v 02	66.61	78.05	6.33	4.67

6.4 Fire-Island

Experiment description

Hurricane Sandy made landfall as a Category 1 post-tropical storm on the New Jersey Coast on October 29, 2012. The storm severely impacted the Fire Island barrier island off the Long Island, New York, coast, where profile volume loss along the entire barrier island varied from 25% to 75% (Hapke et al., 2013). Off the coast of Bellport (NY, Figure 6.12), an uninhabited section of the barrier island Wilderness Area breached during Sandy. Dune crests were lowered, and large wash-over fans developed in the area around the breach. Prior to the storm, the area was covered by dune grass, wetland- and woody vegetation. The sea floor offshore of Fire Island shows shoreface-connected sand ridges in the western part and smaller, sorted bedforms

along the eastern part of the island that includes the Wilderness area (Schwab *et al.*, 2013). The cross-shore profiles are characterized by a steeply sloped beach (1 in 20 slope), a pronounced alongshore-uniform breaker bar, and a foreshore slope that gradually becomes less steep (1 in 85 slope) up to the wide continental shelf at a depth of 25 m.

During Sandy, maximum water levels (surge and tide) ranged 1.8 m (Montauk) to 3.5 m NAVD881 (The Battery) along the barrier island and offshore significant wave heights reached 10 m with periods up to 14 s. LiDAR surveys of the island were flown pre-Sandy in May 2012 (Fredericks, 2016) and post-Sandy on November 5, 2012. A median grain size of 400 m was reported at Wilderness (Buster *et al.*, 2018) with a grading of D90/D50 = 1.5.

Comparison of pre- and post-storm observations of bed elevations (Figure 1) shows that the initial dune crest heights were ranging from only 2 to 6 m, much lower than generally found in the Netherlands. The observed cumulative erosion-sedimentation patterns show that the dune front eroded several meters along the entire stretch of coast. A breach developed between kilometer marks (KM) 1 and 1.2 where originally a high dune was located. Large overwash deposits were observed east of the breach (KM 1.22). West of the breach the dune crests were initially higher, and impact remained in the collision regime with little overwash deposits.

Van der Lught et al. (2019) setup a 2DH morphodynamic XBeach model with hydrodynamic forcing extracted from a regional coupled D-Flow FM/SWAN model, and showed that the model predicted erosion volumes, dune-crest lowering and breach-formation well. The model bathymetry and boundary conditions of this 2DH model is used to set-up 1D transects and validate the BOI-XBeach settings for morphological storm impact.

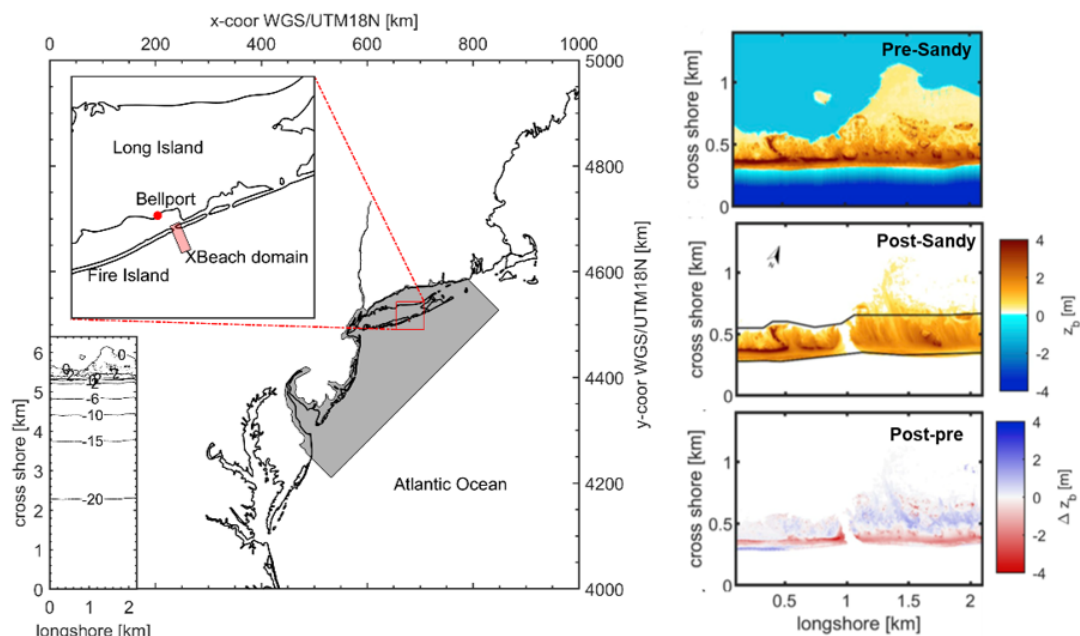


Figure 6.12 Left: Model domain extent of the nested regional D-Flow FM/SWAN model (in grey) and the XBeach model (in red): Wilderness breach. Right: observed pre- (top) and post- (middle) bathymetry and sedimentation/erosion (bottom).

Results

The XBeach model results are validated using the post-Sandy LiDAR data obtained on November 5, 2012. The dune erosion volumes and retreat distances at 3 m +NAVD88, based on the measured pre- and post-storm profiles and the XBeach simulations for all 6 profiles are tabulated in [Table 6.4](#). Furthermore, the pre- and post-storm profile for profiles 5, 305 and 405 based on the measurements and on the XBeach simulation are presented in [Figure 6.13](#), [Figure 6.14](#) and [Figure 6.15](#) respectively.

Table 6.4 Modeled and measured erosion volumes [m^3/m] and retreat distances [m] at 3 m +NAVD88 in absolute values. NaN means that no dune retreat could be determined, i.e. the dune has breached.

	VeroXB	VeroMeas	retreatXB	retreatMeas
005	51.29	51.29	NaN	NaN
105	51.61	44.73	NaN	NaN
205	74.23	75.29	NaN	NaN
305	54.33	68.17	13.01	28.61
365	19.23	24.86	3.44	5.85
405	24.42	55.81	11.87	23.08

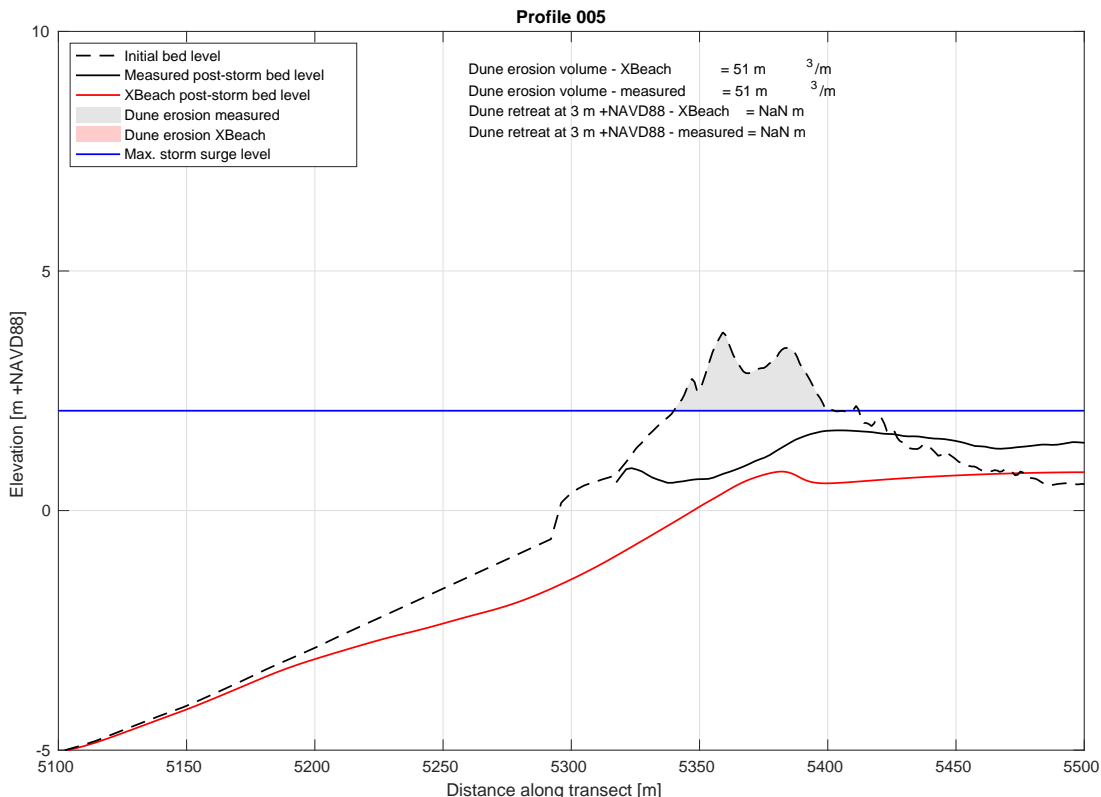


Figure 6.13 XBeach results for cross-shore transect 005 at Fire Island. Initial bed levels are depicted by the black dotted line, observed post-storm bed levels by the black solid line and XBeach model results are presented in red. The modelled dune erosion is shown by the red shaded area.

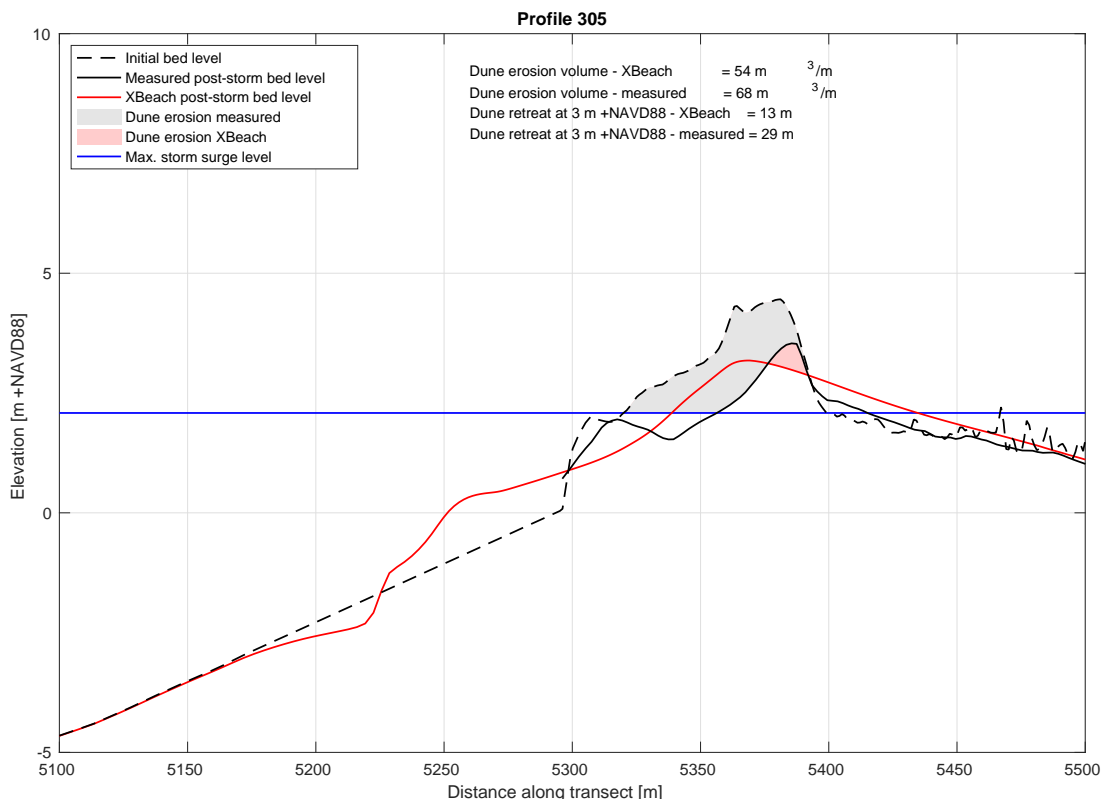


Figure 6.14 XBeach results for cross-shore transect 305 at Fire Island. Initial bed levels are depicted by the black dotted line, observed post-storm bed levels by the black solid line and XBeach model results are presented in red. The modelled dune erosion is shown by the red shaded area.

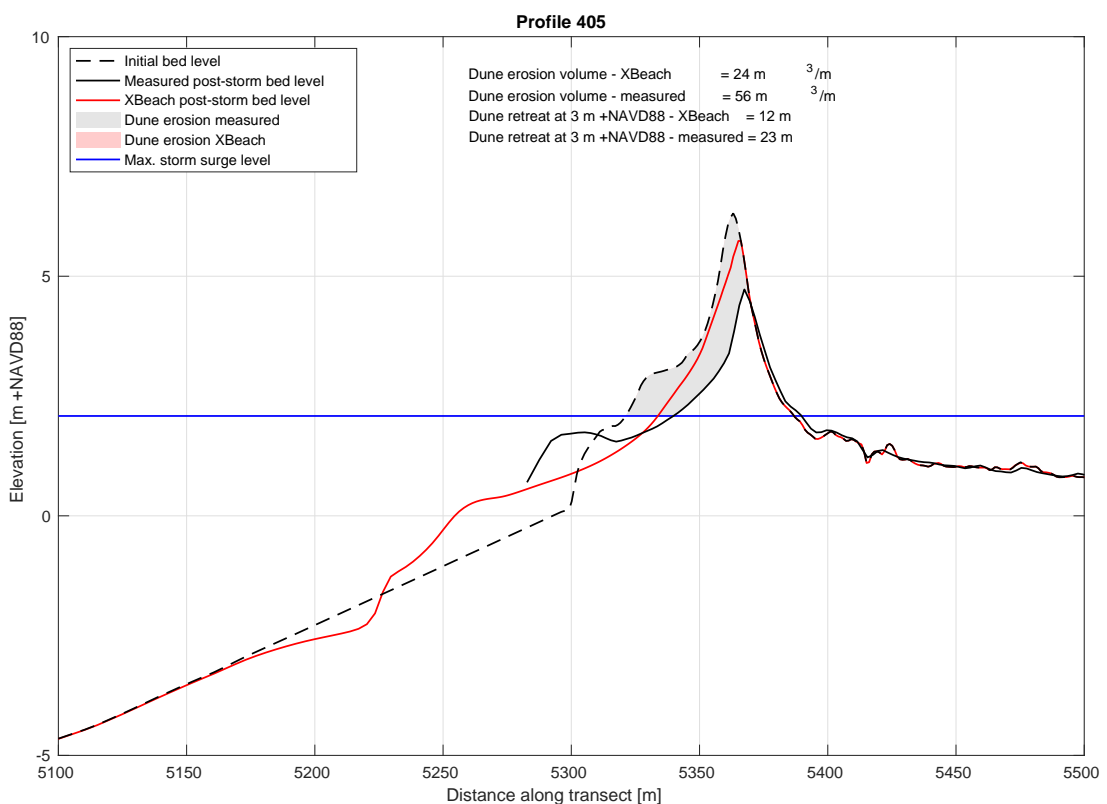


Figure 6.15 XBeach results for cross-shore transect 405 at Fire Island. Initial bed levels are depicted by the black dotted line, observed post-storm bed levels by the black solid line and XBeach model results are presented in red. The modelled dune erosion is shown by the red shaded area.

6.5 Langeoog

Experiment description

The island of Langeoog is one of seven inhabited barrier islands situated along the East Frisian German North Sea coast (Figure 6.16). The shoreface of Langeoog can be characterized by migrating sand shoals through the ebb-tidal delta and a breaker bar system that migrates in eastern direction, comparable to the morphological configuration for the Dutch Wadden Sea Islands. The mildly sloping and shallow shoreface extends to deeper water with a slope of 1:300. On Langeoog approximately 3.9 million m³ of sand have been nourished since 1971 to protect the inhabited areas landwards of the dunes. This coastal area can be classified as mesotidal with semidiurnal tides with a mean tidal range of about 2.7 m at the Langeoog gauge. The mean grain size (D50) for Langeoog northern beaches is in the order of 0.25 mm (Hillmann, 2021). The upper beach and dune foot area has a mean grain size of 0.20 mm, whereas in the surf zone it is in the order of 0.30 mm.

Storm Xaver passed Langeoog from 5 to 7 December 2013, in the Netherlands referred to as Sinterklaasstorm, and led to an extreme maximum storm surge level of NHN1 +3.95 m at Langeoog gauge station. Offshore of Langeoog a maximum wave height of Hs = 7 m and period Tp = 15 s was observed. The storm caused significant dune erosion at the Northern side of the island. Two months prior to the storm, October 2013, a beach nourishment was deployed on the North-Western part of the island (Figure 6.16). A large part of the beach nourishment was eroded due to the storm, and the observed dune erosion landwards of the nourishment was considerably less compared to the adjacent dunes.

Topographic measurements of the beach/dunes were collected after the beach nourishment placement, on October 18th, 2013, 2 months prior to Storm Xaver. Post-storm topography was collected on December 13th, 2013 for the area around the beach nourishment and April 30th, 2014 for the Eastern part of the island. Bathymetric data of the shoreface was collected in August 2013.

In the Interreg VB North Sea Region Building with Nature project a 2D XBeach model of Langeoog was set-up and validated for the 2013 storm ([Hillmann and Frederiksen, 2021](#)). The 2D model domain is 4km in longshore and 4.5km in cross-shore direction, and covers the area where the beach nourishment was located (Figure 6.16). The initial model bathymetry was constructed by combining the August 2013 shoreface measurements and October 18th, 2013 topographic measurements. From this 2D model bathymetry and accompanying forcing conditions, six transects were extracted to use for the morphological validation of the BOI-XBeach model and settings.

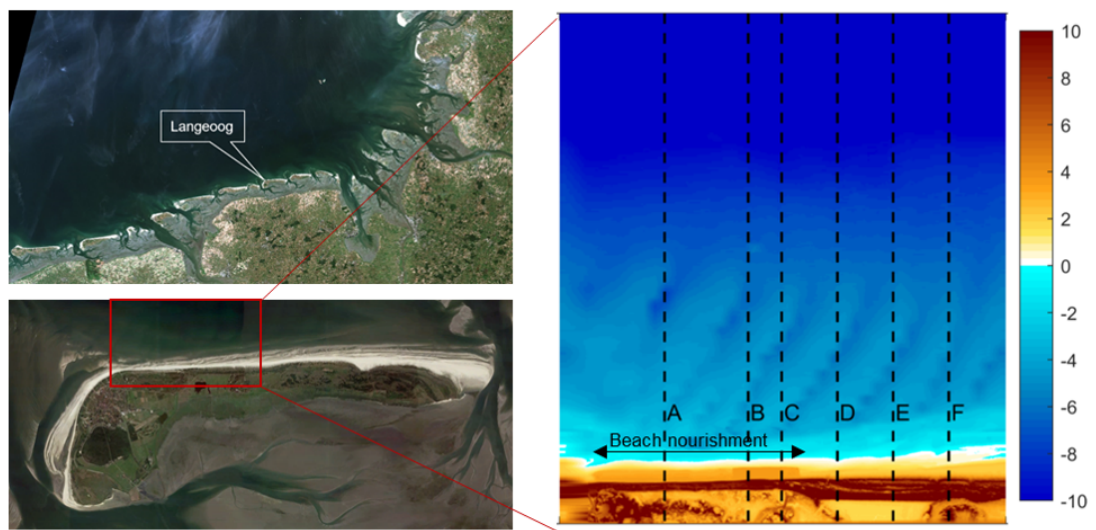


Figure 6.16 Location of the study site in Langeoog, Germany and location of the XBeach model. Model input bathymetry (right panel) with the location of the beach nourishment and the six transects A to F. Source: [Hillmann and Frederiksen \(2021\)](#)

Results

The model results are validated using the topography measurements of the beach and dunes, collected on December 13th, 2013 for the area around the beach nourishment and April 30th, 2014 for the Eastern part of the island. The dune erosion volumes and retreat distances at 5 m +NHN, based on the measured pre- and post-storm profiles and the XBeach simulations for all 6 profiles are tabulated in [Table 6.5](#). Furthermore, the pre- and post-storm profile for profiles A and D based on the measurements and on the XBeach simulation are presented in [Figure 6.17](#) and [Figure 6.18](#) respectively.

Table 6.5 A quantitative comparison of modelled and observed erosion volumes [m^3/m] and dune retreat [m] at 5 m +NHN for all 6 profiles

	VeroXB	VeroMeas	retreatXB	retreatMeas
profile A	16.33	0.97	-2.65	0.52
profile B	14.57	12.76	-2.32	3.53
profile C	10.56	10.13	-1.87	4.01
profile D	32.28	17.97	4.73	6.49
profile E	28.99	13.85	5.60	7.03
profile F	26.79	10.81	6.94	4.52

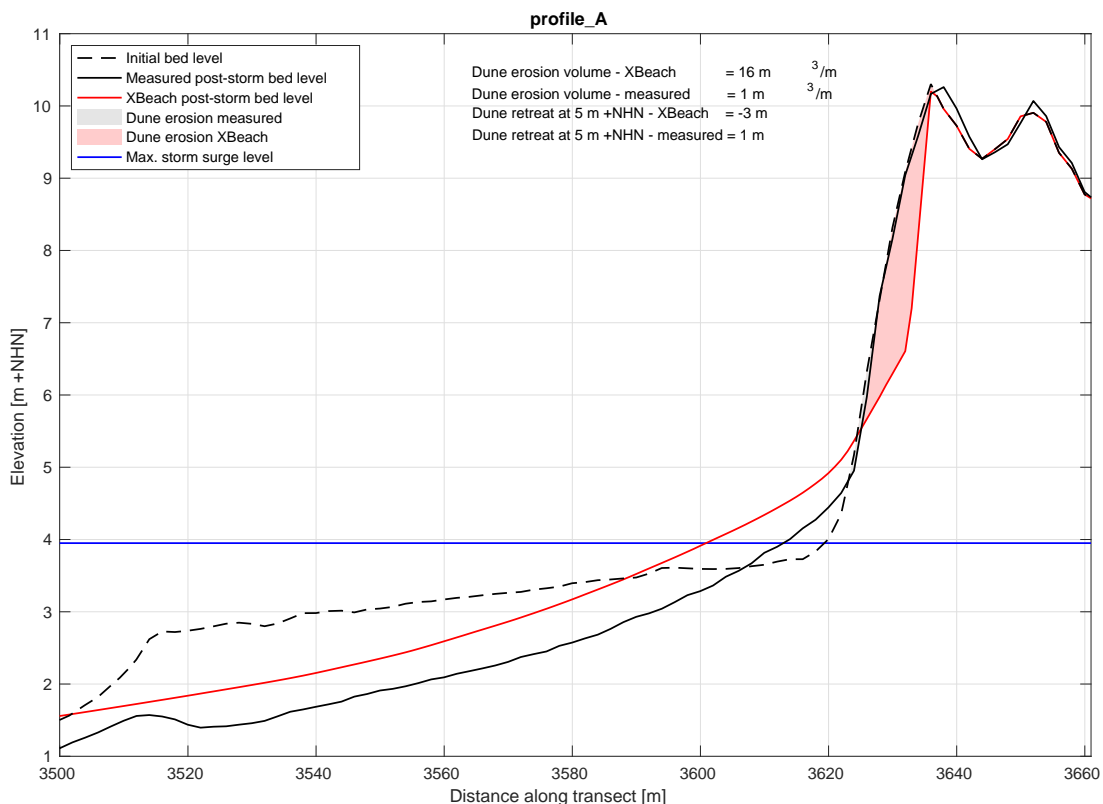


Figure 6.17 XBeach results for cross-shore transect A at Langeoog. Initial bed levels are depicted by the black dotted line, observed post-storm bed levels by the black solid line and XBeach model results are presented in red. The modelled dune erosion is shown by the red shaded area.

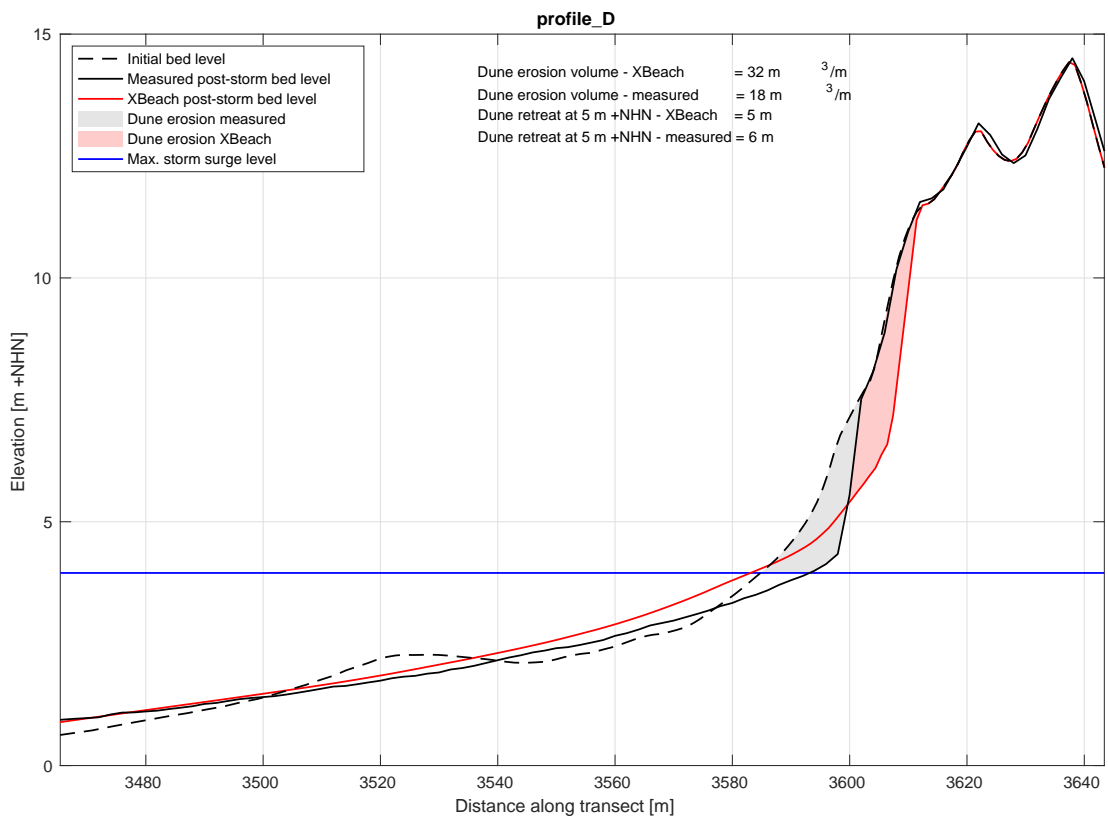


Figure 6.18 XBeach results for cross-shore transect D at Langeoog. Initial bed levels are depicted by the black dotted line, observed post-storm bed levels by the black solid line and XBeach model results are presented in red. The modelled dune erosion is shown by the red shaded area.

6.6 Holland 1976

Experiment description

The storm that hit the Dutch coast in the night between the 2nd and 3rd of February 1976 is classified as a violent storm (zeer zware storm); 11 at the Beaufort scale. A storm event severity that is very rarely experienced in the Netherlands. While the storm surge and high waves impacted the entire Dutch coast, the Delta coast (Zeeland) was hit the hardest with a peak storm surge level of 4.1 m +NAP at Vlissingen: the highest water level since the 1953 storm surge (4.5 m +NAP). The Belgian coast was also impacted heavily, including major flooding in the province of Antwerp. This led to the initiation of the Sigmaplan, designed to better protect the Scheldt basin from flooding during storm surges.

For this validation case the impact of the 1976 storm surge on the northern part of the Dutch coast (the coastal section between Noordwijk and Den Helder) is compared to observations. For the hydraulic boundary conditions, the [Van der Werf et al. \(2011\)](#) study is used as a starting point. This validation case then focusses more on the morphodynamic comparison between simulated and observed dune erosion and dune retreat, which is available for a set of 30 profiles in the considered coastal section (between profile 568 in the north and profile 7100 in the south, as shown in Figure 6.19). Most profiles have a profile with high dunes, multiple bars up above -9 m NAP and slopes similar to the representative Holland coast profile.

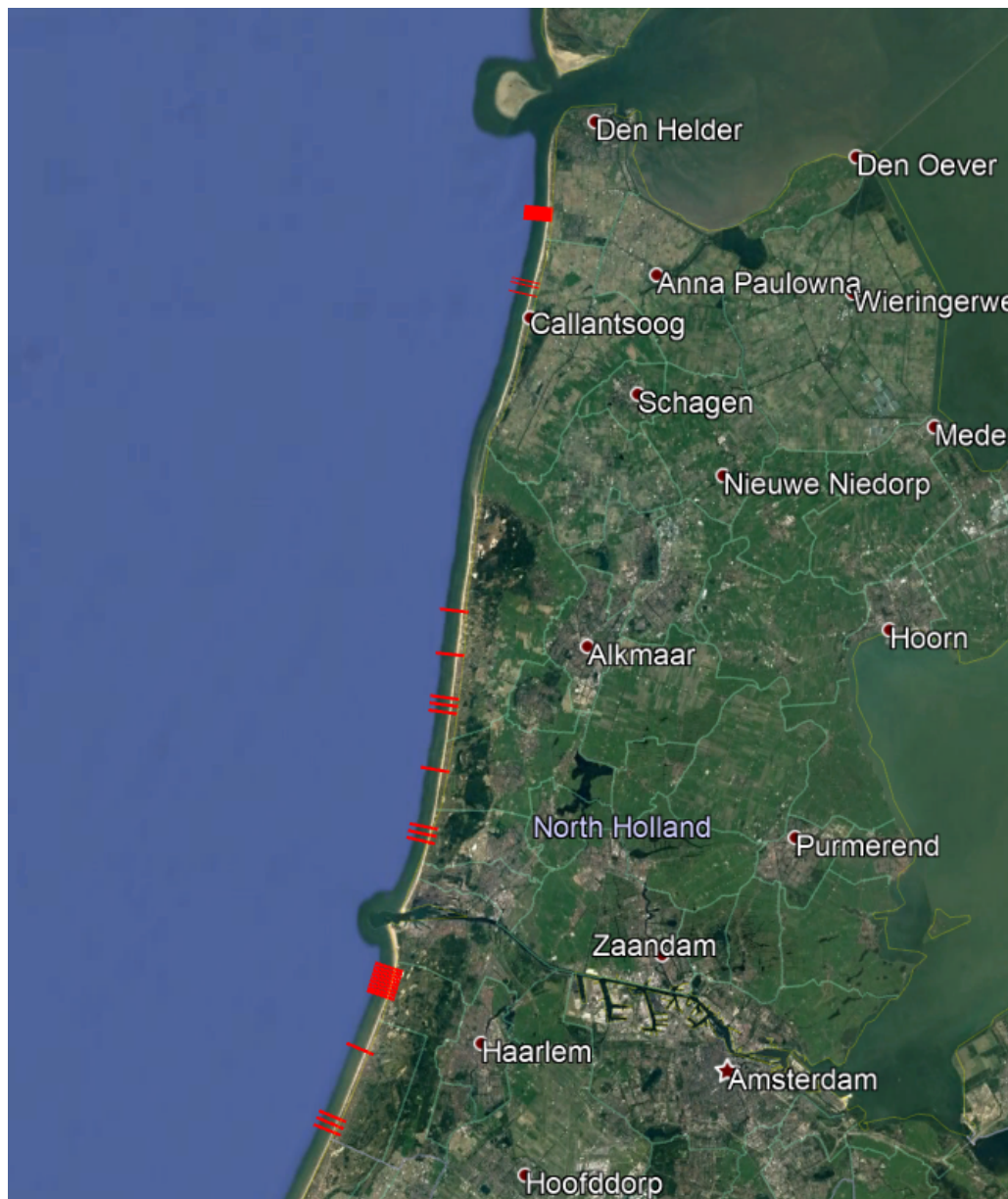


Figure 6.19 Indication of assessed coastal profiles in red, from 568 in the north to 7100 in the south.

The hydraulic boundary conditions are as follows:

- The peak surge level consisting of tide and storm surge is 2.99 m +NAP.
- The peak significant wave height H_s during the storm is 6.1 meters.
- The maximum wave peak period T_p is 10.8 seconds.

Results

The dune erosion volumes and retreat distances at 4m + NAP, based on the measured pre- and post-storm profiles and the XBeach simulations for all 30 profiles are tabulated in [Table 6.6](#). To provide some more insight in the results, the pre- and post-storm profiles for profiles 648, 5000 and 7100 are presented in [Figure 6.20](#), [Figure 6.21](#) and [Figure 6.22](#).

Table 6.6 Dune erosion volume [m^3/m] and retreat distance [m] for the 1976 storm in the XBeach simulation and the measured profiles for the 30 profiles along the northern Dutch coast. The Veromeas of profiles with insufficient measured data is indicated with NaN.

	VeroXB	VeroMeas	retreatXB	retreatMeas
Raai1085	32.53	NaN	4.53	NaN
Raai1115	40.15	NaN	5.58	NaN
Raai1175	40.52	NaN	8.18	NaN
Raai3400	19.31	24.00	7.14	10.20
Raai3700	13.29	NaN	2.18	NaN
Raai4000	53.64	49.00	7.43	8.40
Raai4050	19.39	26.00	6.66	10.80
Raai4100	41.21	34.00	4.94	6.60
Raai4500	38.30	46.00	4.99	9.30
Raai4900	40.53	NaN	4.76	NaN
Raai4950	19.31	NaN	5.01	NaN
Raai5000	47.72	62.00	4.70	7.60
Raai568	39.45	NaN	5.93	NaN
Raai588	41.93	NaN	7.33	NaN
Raai5900	37.61	24.00	5.63	6.00
Raai5925	43.60	30.00	4.11	5.80
Raai5950	43.44	43.00	4.78	6.90
Raai5975	52.80	70.00	5.33	8.40
Raai6000	51.38	67.00	4.39	7.10
Raai6025	51.98	20.00	4.57	4.30
Raai6050	48.21	49.00	5.15	7.30
Raai6075	58.75	39.00	5.16	5.40
Raai608	40.00	NaN	5.57	NaN
Raai6100	58.04	50.00	4.31	4.80
Raai628	29.31	NaN	4.90	NaN
Raai648	19.01	19.00	25.50	24.00
Raai6500	25.94	25.00	12.48	12.80
Raai7000	40.73	28.00	5.38	6.90
Raai7050	33.06	24.00	4.92	7.40
Raai7100	32.85	18.00	6.62	6.30

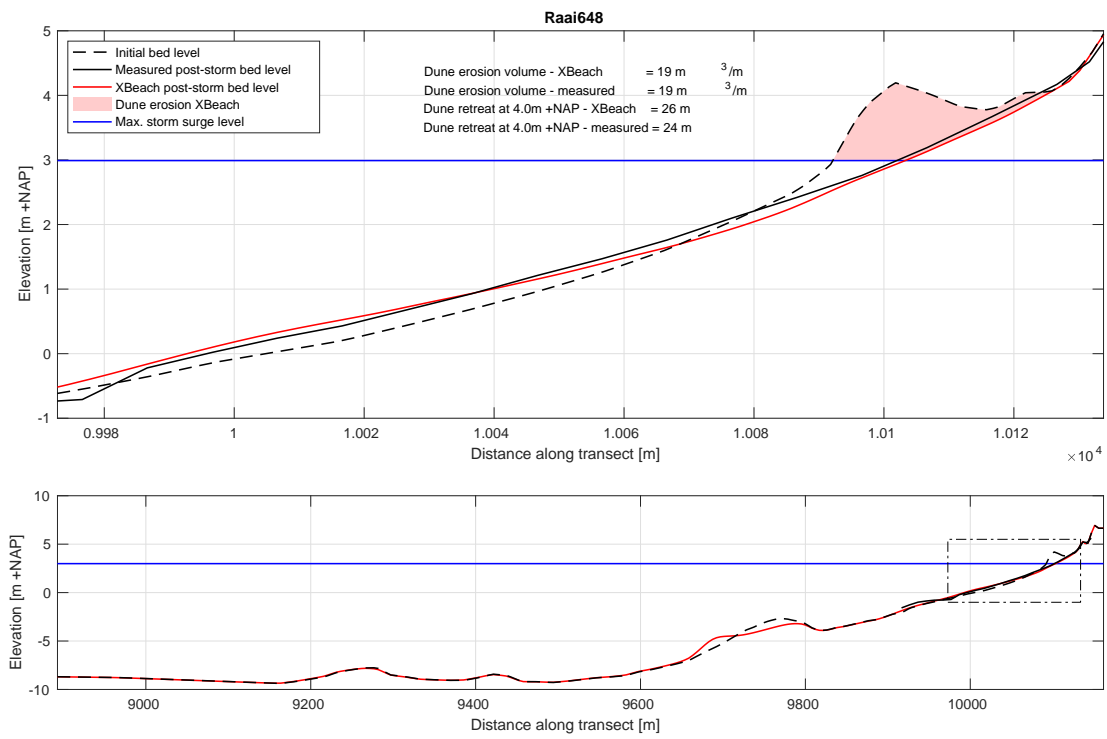


Figure 6.20 Cross-section for JarKus profile 648 before and after the 1976 storm based on the measurements and XBeach, including dune erosion volumes and retreat distances.

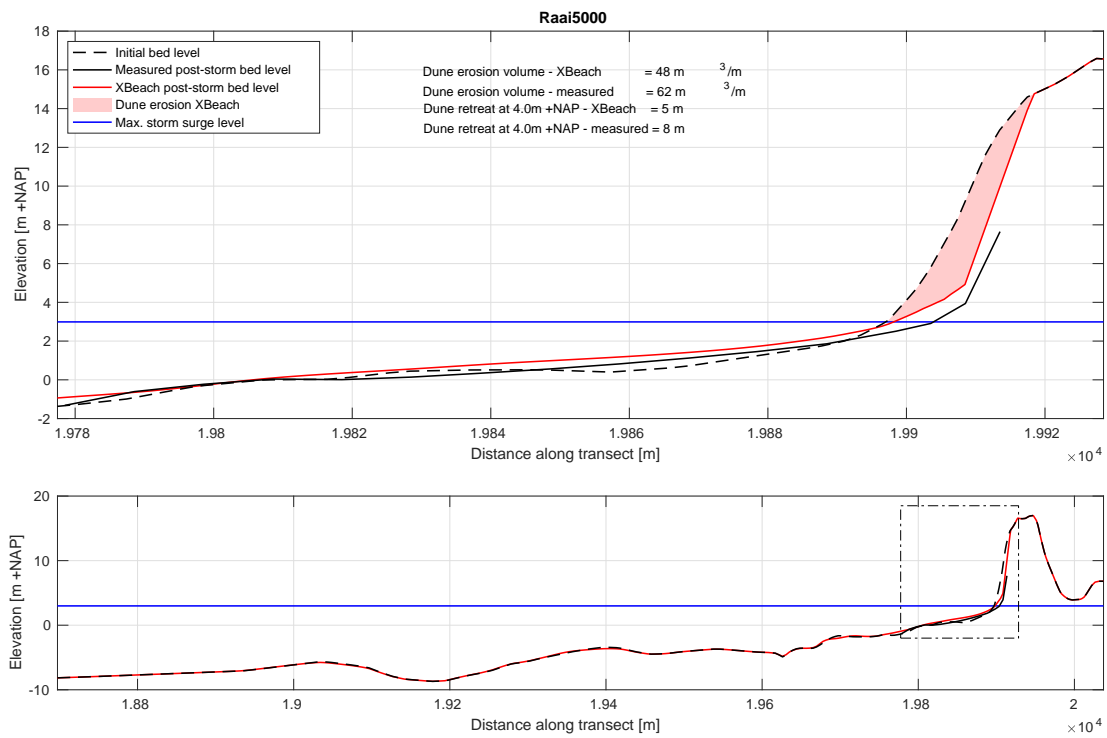


Figure 6.21 Cross-section for JarKus profile 5000 before and after the 1976 storm based on the measurements and XBeach, including dune erosion volumes and retreat distances.

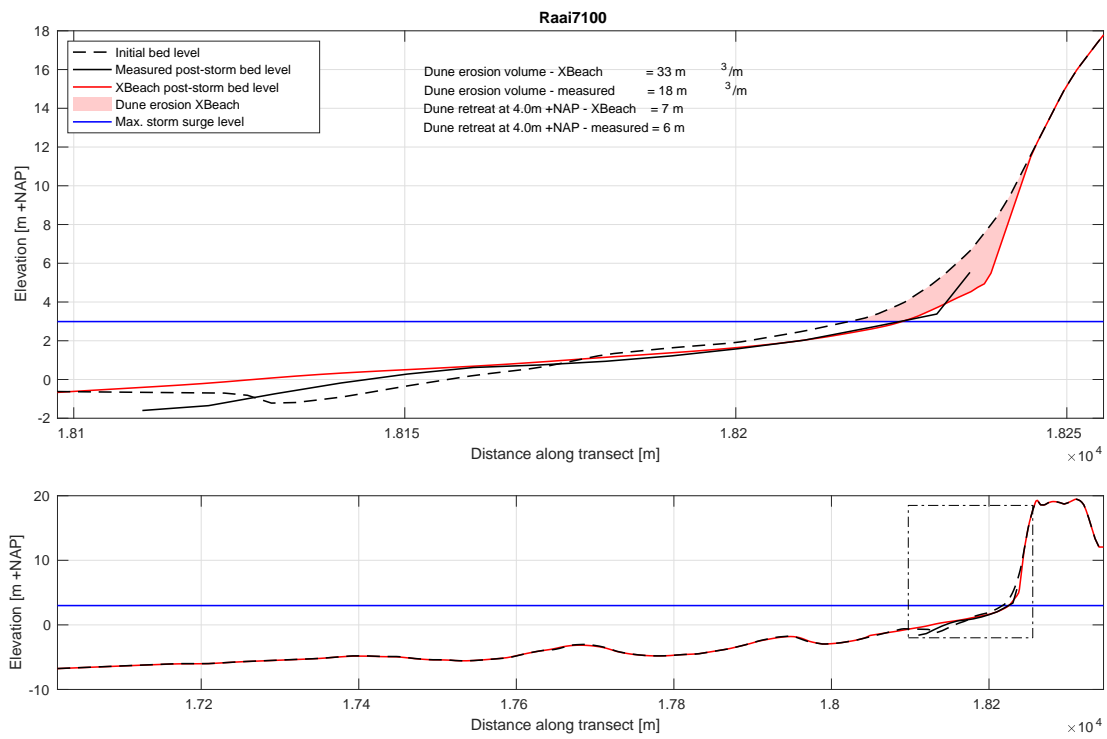


Figure 6.22 Cross-section for JarKus profile 7100 before and after the 1976 storm based on the measurements and XBeach, including dune erosion volumes and retreat distances.

6.7 Holland 1953

Experiment description

One of the most memorable storm surges in recent history, is the storm surge in early February of 1953, leading up to the flooding of large areas in the southwest of the Netherlands and resulting in hundreds of casualties. The storm surge was especially disastrous because of the occurrence of the worst case scenario where a storm surge coincides with spring tide. A very strong northwesterly storm and spring tide led to one of the largest natural disasters (called the Watersnoodramp). It was one of the main causes for the initiation of the Dutch Delta plan, with the primary goal to increase and regulate the water security of the Dutch coast.

Because the event occurred in 1953, the amount of available data is limited. As such, a coastal profile representative for the Dutch coast is applied as pre-storm profile. For the hydrodynamic conditions, a combination of satellite derived reanalysis data, ERA5 (Bell, 2020) and literature (Gerritsen, 2005) is used. Finally, the properties of the simulated post-storm profile will be compared to reported dune erosion (Van thielen de Vries, 2009), reported at around 90 m³/m and changes in dune foot location that are available from Ruessink and Jeuken (2002), ranging from 8 to 16 meters along the Dutch coast. Because of this, the main focus of this validation case will be the morphological in nature.

Using the available data, as explained in more detail in the following sections, boundary conditions are reconstructed, representative for the coastal section between Hoek van Holland Scheveningen (Figure 6.23).

The resulting hydraulic boundary conditions, explained in more detail below, are as follows:

- The peak surge level consisting of high (spring) tide and storm surge is 4.0 m +NAP.
- The peak significant wave height Hs during the storm is 7.3 meters.
- The maximum wave peak period Tp is 14.1 seconds.



Figure 6.23 Overview of the extent of the southern part of the Dutch coast (Hoek van Holland to IJmuiden) and the location of the ERA5 data.

Results

Just like the pre-storm profile data, the post-storm data for the 1953 storm event is fairly limited. From [Van thielen de Vries \(2009\)](#), a representative range for the dune erosion above storm surge level along the Dutch coast is available: $90 \pm 26 \text{ m}^3/\text{m}$ (with $90 \text{ m}^3/\text{m}$ being the mean of all observations and $26 \text{ m}^3/\text{m}$ being equal to 1 standard deviation). From [Ruessink and Jeuken \(2002\)](#), the cross-shore displacement of the dunefoot along the Dutch coast through the years is available. Looking at the 1953 timeframe specifically, a noticeable negative displacement (i.e. erosion) can be observed for all locations along the Delta coast (Walcheren and Schouwen) and the Dutch coast (Hoek van Holland to Den Helder). The displacement at Vlieland and Terschelling is less pronounced. Assuming that the entire displacement within this specific measurement interval is the result of the 1953 storm surge, the resulting dunefoot erosion can be deduced. An uncertainty range of $\pm 1.5 \text{ m}$ is added due to the visual deduction method. The southern-most coastal sections show the largest dune foot erosion of up to $16.5 \pm 1.5 \text{ m}$. Towards the north, the dunefoot erosion gradually reduces, down to $8.5 \pm 1.5 \text{ m}$ at Den Helder, possibly due to the increasing time difference between the peak waves and the peak water level, as was previously discussed. The source does not specifically mention the height at which the retreat is measured, a height of 1 meter above maximum storm surge level (i.e. 5 m +NAP) is assumed.

In [Figure 6.24](#), the predicted dune erosion due to the 1953-storm is presented and compared to the ranges of observed dune erosion and retreat.

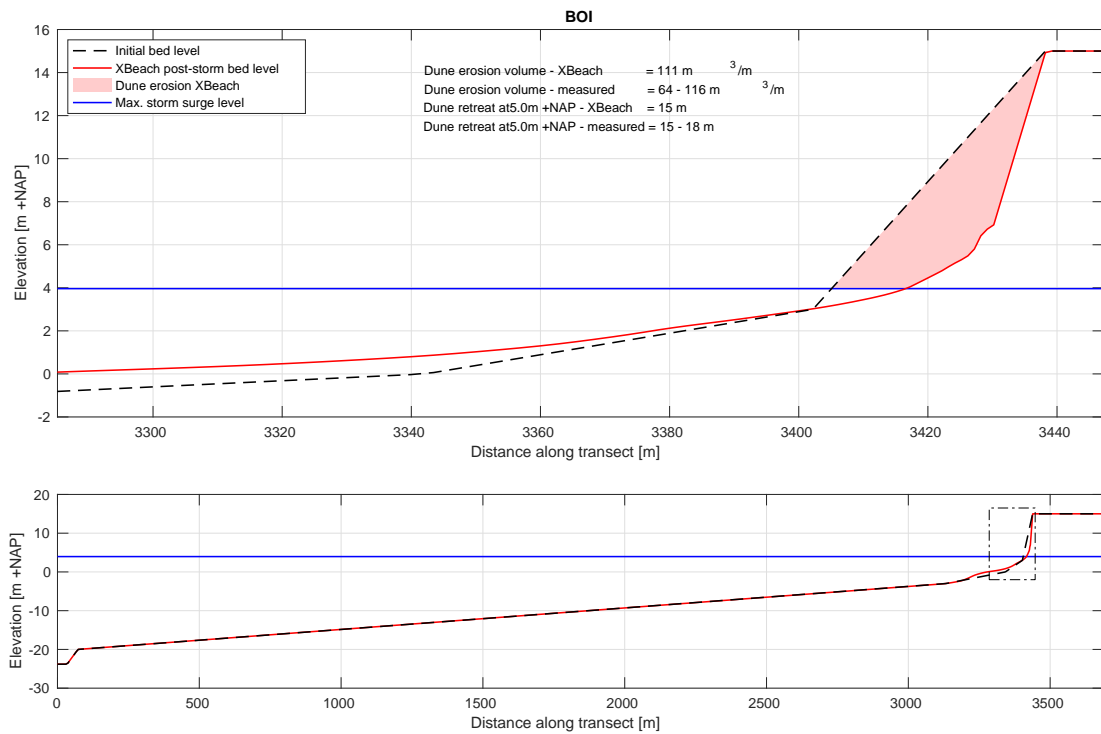


Figure 6.24 Pre and post storm surge profile as computed by XBeach. Upper frame shows the dune erosion section, the lower frame shows the entire XBeach profile.

6.8

Erosion and overwash of Assateague Island

This test concerns the morphodynamic response of sandy dunes to extreme storm impacts at Assateague Island, Maryland, USA, which was analyzed before by [Jimenez et al. \(2006\)](#). Two consecutive North Easters attacked the barrier island during late January and early February, 1998. The bathymetry was measured using LIDAR in September 1997 and again February 9th and 10th, 1998 after the two storms had subsided.

Three types of dunes were identified by [Jimenez et al. \(2006\)](#), shown in Figure 6.25. Profile A (upper left panel) is initially characterized by a steep faced dune, where the maximum run-up exceeded the dune crest height and the mildly sloped back of the dune. The morphological response is characterised by profile lowering, decrease of the beach face slope and landward barrier displacement, while retaining barrier width.

Profile type B is a double-peaked dune profile and has two different shapes. Profile B1 (upper right panel) is initially characterized by a primary and secondary dune, both of which are lower than the maximum run-up height and which are separated by a valley. Profile B2 (bottom left panel) initially has two peaks of which the seaward one is lower. The backside of the barrier of either type is therefore either characterized by a secondary dune line (profile B1) or a taller crest of the dune (profile B2) which prevents the eroded sand from being transported to the backside of the dune. The main morphological response for these profile types is a decrease of the beach face slope, outer shoreline retreat and narrowing of the barrier.

The height of the dune crest of profile C (lower right panel) exceeds the maximum run-up height and so little overwash is observed. The morphological response of this type of profile is crest lowering due to slumping, decrease of the beach face slope and

retreat of the outer shoreline. The width of the barrier is seen to decrease.

The storm impact of the two North Easters on Assateague Island were modelled with XBeach for the four profiles described by Jimenez *et al.* (2006). The profiles were extended with a shallow foreshore and a 1:100 slope in seaward direction till a water depth of 9 m below NAVD88. As XBeach has not been shown to accurately simulate morphological change during very long storm durations, the simulations were run for a total of 20 hours. The measured wave and surge conditions were parameterized for each storm by a constant surge level and a constant wave spectrum (Pierson-Moskowitz) (see Table 6.7). This approach assumes that two 72 hour storms with varying surge and wave conditions can be approximated by two 10 hour simulations with constant maximum surge and wave conditions following a similar approach as Vellinga (1986). This approach also facilitates further sensitivity studies into the effect of varying hydraulic forcing conditions. The calculation grid size varies from 18 m at the offshore boundary to 2 m on the islands. A morphological acceleration factor of 5 is applied. The final simulated bed profiles are shown in Figure 6.25.

Table 6.7 Hydrodynamic boundary conditions XBeach simulations

	Storm 1	Storm 2
Surge level [m +NAVD]	0.8	1.0
H_s [m]	4.1	3.9
T_p [s]	8.5	8.5

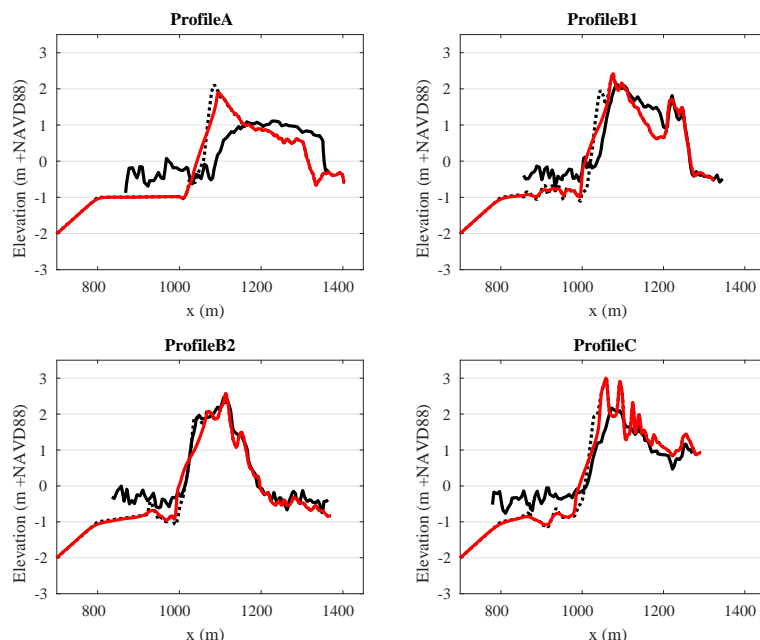


Figure 6.25 Pre-storm profiles (black dotted line), measured post-storm profiles (black solid line) and modelled post-storm profiles (red solid line). Upper left panel: profile A. Upper right panel: profile B1. Lower left panel: profile B2. Lower right panel: profile C. The seaward side is on the left in all panels. Note that the measured post-storm profiles contain only the sea surface and emerged topography and no submerged topography.

6.9

Breach growth at Zwin

This test is based on the Zwin breach growth experiment, as reported by Visser (1998). In the mouth of the Zwin, a tidal inlet located at the border between the Netherlands and Belgium, an artificial dam was constructed with a crest height of 3.3 m +N.A.P. (Dutch datum, approx. MSL), crest width 8 m, inner slope 1:3 outer slope 1:1.6 and length 250 m. An initial depression of 0.8 m was made in the middle of the dam having a width of 1 m and a side slope of 1:1.6 to ensure that the breach initiated at this location. The level of the surrounding sea bed was about 0.7 m + N.A.P. The mean tidal prism of the Zwin is about 350,000 m³. The polder area A_p as a function of the water level behind the dam is given by:

$$A_p = 170.000m \cdot z_s - 100.000m^2, \quad 0.6m < z_s < 2.3m + NAP$$
$$A_p = 2.100.000m \cdot z_s - 4.540.000m^2, \quad z_s \geq 2.3m + NAP$$

At t = 0, about 10 minutes prior to high water, the water level at the seaside was 2.72m+NAP. At t = 10 minutes a water level of 2.75m+NAP. was reached. For the remainder of the test, which had a total duration of 1 hour, the water level marginally decreased. After 1 hour the breach growth became nil, as the water level of the polder area behind the breached equaled the sea level. The wave height near the dam was negligible during the experiment. The wind speed was about 2 m/s. Until t = 6.5 minutes the breach depth grew whereas the breach width remained constant. At t = 6.5 minutes the original dike structure had nearly completely disappeared over the initial depression width of 1 m. Near t = 6.5 minutes the onset of lateral breach growth was observed. The scour hole developed further down to a depth of -1.6m+NAP. (4.9 m below the original dam crest level). The rate of lateral breach growth was about 2 cm/s. After approximately 40 minutes the process slowed down considerably and after approximately 1 hour the water levels at both sides were equal. A schematized representation of the Zwin test was created in XBeach, with at the sea side a uniform bed level at 0.7m+NAP, and inside the basin a prismatic profile with the deepest point at 0.7m+NAP and sloping sides, such that the polder area as a function of the water level was in accordance with the equations above. The grid is non-equidistant with grid sizes gradually varying from 0.5 m near the breach to approx. 50 m far away from it. The median grain diameter D_{50} of the bed material was set to 0.3 mm in accordance with the prototype test conditions for the artificial dam. The applied critical slopes for avalanching are the same as in other tests and standard settings were applied for the transport formulations. Waves were negligible in the test and were set to zero. The model was run with a CFL of 0.5 and remained smooth and stable despite the steep slopes and supercritical flows.

In ?? a sequence of 3D images is shown depicting the various stages in the breaching process: the initial overflowing, the cutting back of the breach, the deepening and finally the widening of the breach.

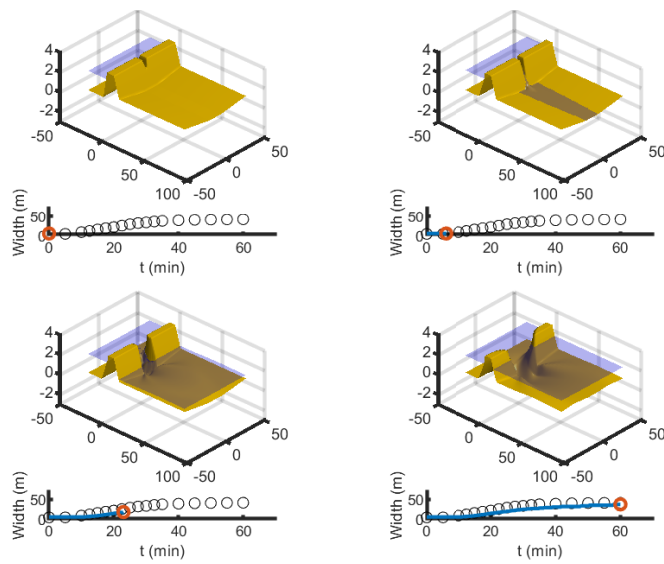


Figure 6.26 Growth of breach width

In ?? a comparison is given between measured and simulated water levels, flow velocities and development of the breach width in time. Observation point MS2 is 30 m upstream of the centre point of the breach and MS4 is 30 m downstream of it. In MS4 there was some ambiguity in the measured initial water level, which explains the initial discrepancy between measurements and simulations.

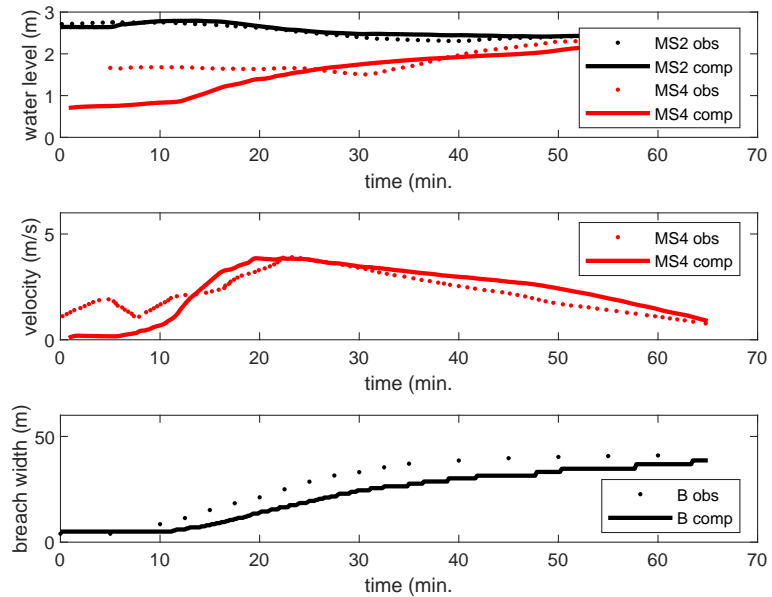


Figure 6.27 Breach width related to water level and flow velocities

7 Specific functionalities

In the previous chapters, the core functionalities are discussed: hydro- and morphodynamics on different scales. However, XBeach is equipped with a variety of additional functionalities that facilitate more complex computations. One example already discussed is hard elements in the profiles. This chapter discusses a variety of other functionalities, like discharges, drifters and multiple sediment fractions.

7.1 Gravel (XBeach-G)

The gravel cases are setup to test the implementation of XBeach-G. Two field cases: Slapton Sands, a fine gravel barrier ($D_{50} = 6\text{mm}$) with a crest height approximately 7 meters above ODN (approximately equal to 0.4 m below MSL) and Chesil Beach, a coarse ($D_{50} = 40\text{mm}$) gravel barrier with a crest height approximately 10 meters above ODN (Ordnance Datum Newlyn; approximately equal to 0.2m below mean sea level MSL) including a seawall. On top of that, experiment E10 from the Bardex experiments (Turner and Masselink, 2012) has been validated. NB: Model setups have been carried by Robert McCall as part of his PhD thesis. For more information on XBeach-G, download the PhD thesis of [McCall \(2015\)](#) on URL: <http://hdl.handle.net/10026.1/3929>.

Measurements and model results for Slapton Sands (Figure 7.1), Chesil Beach (Figure 7.2) and BARDEX E10 (Figure 7.3) show that XBeach-G is successfully incorporated in the main version of XBeach. Users can apply XBeach-G settings by including "*useXBeachGSettings = 1*" in the params.txt file.

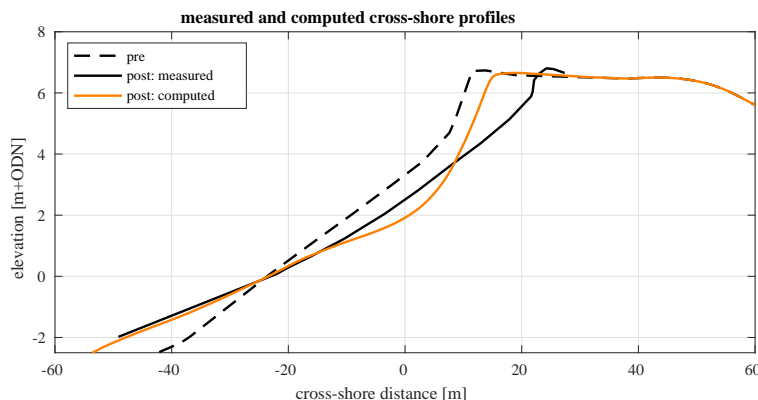


Figure 7.1 Profile development for Slapton Sands

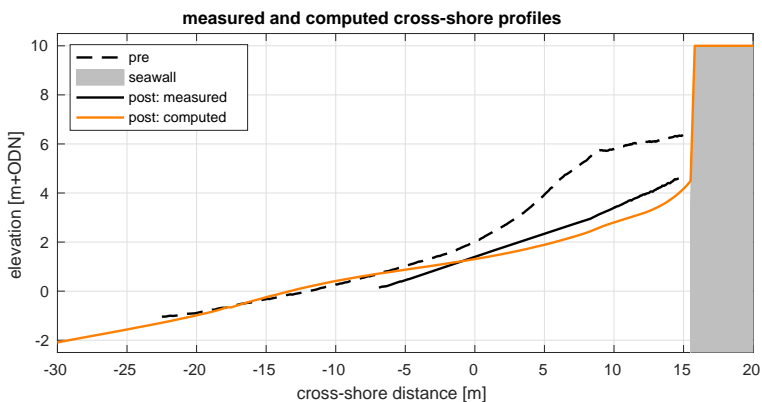


Figure 7.2 Profile development for Chesil Beach

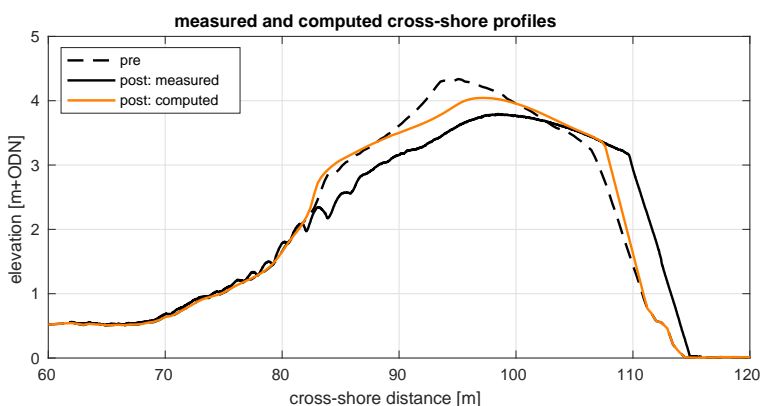


Figure 7.3 Profile development for test E10 of the Bardex experiment

7.2

Vegetation

The vegetation case is set up to test the XBeach vegetation module and is based on an experiment described by Lovas (2000). The experiments were carried out in a 40 m long wave tank with an underwater slope of 1/30 (see Figure 7.4, bottom panel), and several runs were carried out with and without vegetation. The flexible vegetation mimics were placed in about 0.3 - 0.5 m water depth and had an effective height of about 0.09 m. The vegetation density was 1200 units/m². The test program included random waves with two peak wave periods and two wave heights. In addition, two experiments were carried out in which the water depth was lowered, resulting in a total of six different experiments.

Figure 7.4 shows the measurements and model results for both the XBeach nonhydrostatic (top panel) and surfbeat (middle panel) mode for case 4 of the experiments. The test presented considers the effect of the vegetation on the high-frequency (sea-swell) wave height (solid lines) and the low-frequency (infragravity) waves (dotted). Results for the other cases as well as the overall validation of the vegetation module of XBeach is described in more detail in Van Rooijen *et al.* (2016).

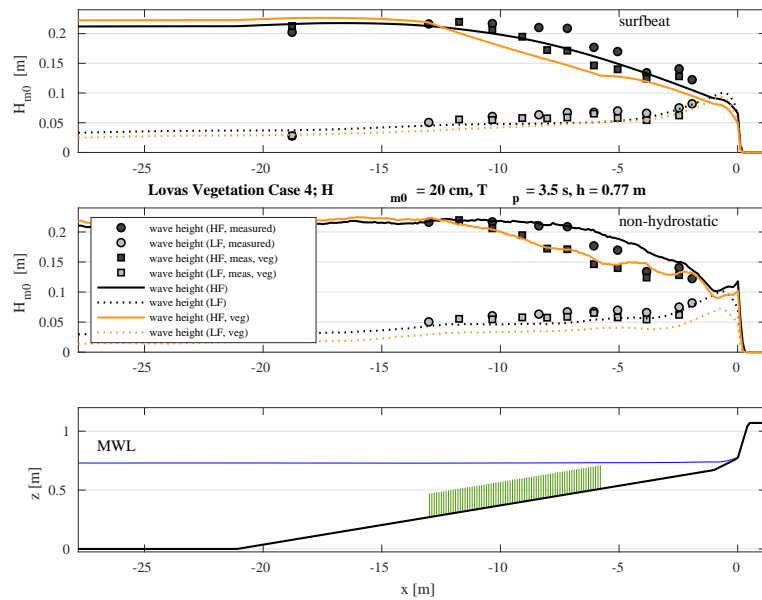


Figure 7.4 Significant high-frequency (sea-swell) and low-frequency (infragravity) wave height computed with XBeach nonhydrostatic (top panel) and surfbeat mode (middle panel) without (black) and with vegetation (orange) for case 4 reported by Lovas (2000). Measurements are indicated with the black and grey symbols (respectively, without and with vegetation)

References

- Arcilla, A. S., J. A. Roelvink, B. A. O'Connor, A. Reniers and J. A. Jimenez, 1994. "The Delta flume '93 experiment." In *Coastal Dynamics*, pages 488–502.
- Bell, H. H. B. P. D. P. H. A. M. S. J. T. J.-N., B., 2020. "ERA5 hourly data on single levels from 1950 to 1978 (preliminary version)." Retrieved from <https://cds.climate.copernicus-climate.eu/cdsapp!/dataset/reanalysisera5-single-levels-preliminary-back-extension?tab=overview>.
- Bertin, X., K. Martins, A. de Bakker, T. Chataigner, T. Guérin, T. Coulombier and O. de Viron, 2020. "Energy transfers and reflection of infragravity waves at a dissipative beach under storm waves." *Journal of Geophysical Research: Oceans* 125 (5): e2019JC015714.
- Birkemeier, W. A., C. Donoghue, C. E. Long, K. K. Hathaway and C. F. Baron, 1997. *1990 DELILAH Nearshore Experiment: Summary report*. Tech. Rep. CHL-97-4-24, U.S. Army Corps of Engineers. Field Research Facility.
- Boers, M., 1996. *Simulation of a Surf Zone with Barred Beach, Part 1: Wave heights and Wave breaking*. Communications on Hydraulic and Geotechnical Engineering 69-5, Delft University of Technology. 116 p.
- Buckley, M. L., R. J. Lowe, J. E. Hansen and A. R. Van Dongeren, 2015. "Dynamics of wave setup over a steeply sloping fringing reef." *Journal of Physical Oceanography* 45 (12): 3005–3023.
- Buster, N. A., J. C. Bernier, O. T. Brenner, K. W. Kelso, T. M. Tuten, J. L. Miselis and P. looking approximately east along Fire, 2018. *Sediment Data From Vibracores Collected in 2016 From Fire Island, New York*. US Department of the Interior, US Geological Survey.
- Carrier, G. F. and H. P. Greenspan, 1958. "Water waves of finite amplitude on a sloping beach." *Journal of Fluid Mechanics* 4: 97–109.
- Chanson, H., 2006. "Analytical solutions of laminar and turbulent dam break wave." *River Flow* (1955): 465–474. ISBN 0415408156.
- Clemmensen, L. B., K. Pedersen, A. Murray and J. Heinemeier, 2006. "A 7000-year record of coastal evolution, Vejers, SW Jutland, Denmark." *Bulletin of the Geological Society of Denmark* 53: 1–22.
- Damgaard, J., N. Dodd, L. Hall and R. Chesher, 2002. "Morphodynamic modelling of rip channel growth." *Coastal Engineering* 45: 199–221.
- De Winter, R., F. Gongrip and B. Ruessink, 2015. "Observations and modeling of alongshore variability in dune erosion at Egmond aan Zee, the Netherlands." *Coastal Engineering* 99: 167–175.
- Degraer, S., A. Volckaert and M. Vincx, 2003. "Macrofaunal zonation patterns along a morphodynamical continuum of macrotidal, low tide bar/rip and ultra-dissipative sandy beaches." *Estuarine, Coastal and Shelf Science* 56 (3-4): 459–468.
- Dongeren, A. V., R. Lowe, A. Pomeroy, D. M. Trang, D. Roelvink, G. Symonds and R. Ranasinghe, 2013. "Numerical modeling of low-frequency wave dynamics over a fringing coral reef." *Coastal Engineering* 73 (0): 178 - 190.

- Engelstad, A., B. Ruessink, D. Wesselman, P. Hoekstra, A. Oost and M. van der Vegt, 2017. "Observations of waves and currents during barrier island inundation." *Journal of Geophysical Research: Oceans* 122 (4): 3152–3169.
- Erikson, L., M. Larson and H. Hanson, 2005. "Prediction of swash motion and run-up including the effects of swash interaction." *Coastal Engineering* 52: 285–302.
- Feddersen, F., R. T. Guza, S. Elgar and T. C. Herbers, 2000. "Velocity moments in alongshore bottom shear stress parameterizations." *Journal of Geophysical Research* 105: 8673–8688.
- Fredericks, H. C. L. E., X., 2016. "Coastal Topography - Fire Island, New York, 07 May 2012 U.S. Geological Survey data release."
- Gerritsen, H., 2005. "What happened in 1953? The Big Flood in the Netherlands in retrospect." *Philosophical Transactions of the Royal Society A: Mathematical, Physical and Engineering Sciences* 363 (1831): 1271–1291.
- Guérin, T., X. Bertin, T. Coulombier and A. de Bakker, 2018. "Impacts of wave-induced circulation in the surf zone on wave setup." *Ocean Modelling* 123: 86–97.
- Hamm, L. and C. Peronnard, 1997. "Wave parameters in the nearshore: A clarification." *Coastal Engineering* 32 (2-3): 119–135.
- Hapke, C. J., O. Brenner, R. Hehre and B. Reynolds, 2013. *Coastal Change from Hurricane Sandy and the 2012-13 Winter Storm Season: Fire Island, New York*. US Department of the Interior, US Geological Survey Reston, Virginia.
- Hillmann, H. T. F., Simon; Blum, 2021. *National Analysis. Germany / Lower Saxony NLWKN - Interreg VB NSR BwN*. Tech. rep., <https://building-with-nature.eu/publications/monitoring-evaluation/>.
- Hillmann, K. Q. E. H. R., S.; Geertsen and B. Frederiksen, 2021. *Influencing the SPR forstorm surge events. A cross-border XBeach application. Interreg North Sea Region VB Ū Building with Nature report*. Tech. rep.
- Huntley, D. A., R. T. Guza and E. B. Thornton, 1981. "Field observations of surf beats, 1, progressive edge waves." *Journal of Geophysical Research* 86: 6451–6466.
- IMDC, 2005. *Hydraulisch Randvoorwaardenboek Vlaamse Kust*. Tech. Rep. I/RA/11226/03.041/KTR, IMDC. In Dutch.
- Jimenez, J. A., A. H. Sallenger and L. Fauver, 2006. "Sediment transport and barrier island changes during massive overwash events." In *30th International Conference on Coastal Engineering*. ASCE, San Diego, California, USA.
- Kroon, J., 2009. *Implementation of a wetting and drying algorithm in a finite element model*. Master's thesis, Delft University of Technology.
- Kystdirektoratet, 2021. *Calculation of cliff retreat on sandy coasts in Denmark using XBeach*. Tech. rep., Kystdirektoratet.
- Lanckriet, T., K. Trouw, N. Zimmermann, L. Wang, B. De Maerschalck, R. Delgado, T. Verwaest and F. Mostaert, 2015. "Scientific support regarding hydrodynamics and sand transport in the coastal zone: hindcast of the morphological impact of the 5-6 December 2013 storm using XBeach." *WL Rapporten*.
- Larson, M., L. Erikson and H. Hanson, 2004. "An analytical model to predict dune erosion due to wave impact." *Coastal Engineering* 51 (8–9): 675–696.

- Leatherman, S. P., A. T. Williams and J. S. Fisher, 1977. "Overwash sedimentation associated with a large-scale northeaster." *Marine Geology* 24: 109–121.
- Lerma, A. N., T. Bulteau, S. Lecacheux and D. Idier, 2015. "Spatial variability of extreme wave height along the Atlantic and channel French coast." *Ocean Engineering* 97: 175–185.
- List, J. H., 1992. "A model for two-dimensional surfbeat." *Journal of Geophysical Research* 97: 5623–5635.
- Lovas, S., 2000. *Hydro-physical conditions in kelp forests and the effect on wave damping and dune erosion: A case study on Laminaria hyperborea*. Ph.D. thesis, Norwegian Univ. of Science and Technology, Trondheim, Norway.
- Lugt, M. A. van der, E. Quataert, A. van Dongeren, M. van Ormondt and C. R. Sherwood, 2019. "Morphodynamic modeling of the response of two barrier islands to Atlantic hurricane forcing." *Estuarine, Coastal and Shelf Science* 229: 106404.
- McCall, R., 2015. *Process-based modelling of storm impacts on gravel coasts*. Ph.D. thesis, University of Plymouth.
- Murphy, A. H. and E. S. Epstein, 1989. "Skill scores and correlation coefficients in model verification." *Monthly Weather Review* 117: 572–581.
- Nairn, R. B., J. A. Roelvink and H. N. Southgate, 1990. "Transition zone width and implications for modelling surfzone hydrodynamics." In B. L. Edge, ed., *22th International Conference on Coastal Engineering*, pages 68–81. ASCE, Reston, Virginia, USA.
- Nishi, R. and N. C. Kraus, 1996. "Mechanism and calculation of sand dune erosion of storms." In *25th International Conference on Coastal Engineering*, pages 3034–3047. ASCE, Orlando, Florida, USA.
- Overton, M. F. and J. S. Fisher, 1988. "Laboratory investigation of dune erosion." *Journal of Waterway, Port, Coastal and Ocean Engineering* 114 (3): 367–373.
- Özkan-Haller, H. T. and J. T. Kirby, 1997. "A Fourier-Chebyshev collocation method for the shallow water equations including shoreline runup." *Applied Ocean Research* 19: 21–34.
- Phillips, O. M., 1977. *The Dynamics of the Upper Ocean*. Cambridge University Press, New York, 2nd ed.
- Pomeroy, A., R. Lowe, G. Symonds, A. V. Dongeren and C. Moore, 2012. "The dynamics of infragravity wave transformation over a fringing reef." *Journal of Geophysical Research* 117 (C11022): 1 - 17.
- Raubenheimer, B. and R. T. Guza, 1996. "Observations and predictions of run-up." *Journal of Geophysical Research* 101 (C10): 25,575–25,587.
- Reniers, A. J. H. M., J. MacMahan, E. B. Thornton and T. P. Stanton, 2006. "Modelling infragravity motions on a rip-channel beach." *Coastal Engineering* 53: 209–222.
- Reniers, A. J. H. M., J. A. Roelvink and E. B. Thornton, 2004a. "Morphodynamic modelling of an embayed beach under wave group forcing." *Journal of Geophysical Research* 109 (C01030). DOI: [10.1029/2002JC001586](https://doi.org/10.1029/2002JC001586).
- Reniers, A. J. H. M., E. B. Thomas, T. P. Stanton and J. A. Roelvink, 2004b. "Vertical flow structure during Sandy Duck: observations and modeling." *Coastal Engineering* 51 (3): 237–260.

- Ritter, A., 1892. "Die fortpflanzung de wasserwellen." *Zeitschrift Verein Deutscher Ingenieure* 36 (33): 947–954.
- Roelvink, J. A., 1993a. "Dissipation in random wave groups incident on a beach." *Coastal Engineering* 19: 127–150.
- Roelvink, J. A., 1993b. *Surf beat and its effect on cross-shore profiles*. Ph.D. thesis, Delft University of Technology.
- Roelvink, J. A., A. J. H. M. Reniers, A. R. Van Dongeren, J. S. M. Van Thiel de Vries, R. T. McCall and J. M. Lescinski, 2009. "Modelling storm impacts on beaches, dunes and barrier islands." *Coastal Engineering* 56 (11-12): 1133–1152. DOI: [10.1016/j.coastaleng.2009.08.006](https://doi.org/10.1016/j.coastaleng.2009.08.006).
- Roelvink, J. A. and M. J. F. Stive, 1989. "Bar-generating cross-shore flow mechanisms on a beach." *Journal of Geophysical Research* 94 (C4): 4785–4800.
- Roelvink, J. A., T. Van Kessel, S. Alfageme and R. Canizares, 2003. "Modelling of barrier island response to storms." In *Coastal Sediments '03*. Clearwater, Florida, USA.
- Ruessink, B. and M. Jeuken, 2002. "Dunefoot dynamics along the Dutch coast." *Earth Surface Processes and Landforms: The Journal of the British Geomorphological Research Group* 27 (10): 1043–1056.
- Ruessink, B. G., H. Michallet, P. Bonneton, D. Mouazé, J. Lara, P. A. Silva and P. Wellens, 2013. "Globex: wave dynamics on a gently sloping laboratory beach." *Proceedings Coastal Dynamics 2013* pages 1351–1362.
- Ruessink, B. G., J. R. Miles, F. Feddersen, R. T. Guza and S. Elgar, 2001. "Modeling the alongshore current on barred beaches." *Journal of Geophysical Research* 106: 22,451–22,462.
- Ruessink, G., C. S. Schwarz, T. D. Price and J. J. Donker, 2019. "A multi-year data set of beach-foredune topography and environmental forcing conditions at Egmond aan Zee, The Netherlands." *Data* 4 (2): 73.
- Sallenger, A. H., 2000. "Storm impact scale for barrier islands." *Journal of Coastal Research* 16 (3): 860–895.
- Saye, S. E. and K. Pye, 2006. "Variations in chemical composition and particle size of dune sediments along the west coast of Jutland, Denmark." *Sedimentary Geology* 183 (3-4): 217–242.
- Schaeffer, H. A., 1994. "Edge waves forced by short-wave groups." *Journal of Fluid Mechanics* 259: 125–148.
- Schwab, W. C., W. E. Baldwin, C. J. Hapke, E. E. Lentz, P. T. Gayes, J. F. Denny, J. H. List and J. C. Warner, 2013. "Geologic evidence for onshore sediment transport from the inner continental shelf: Fire Island, New York." *Journal of Coastal Research* 29 (3): 526–544.
- Soulsby, R. L., 1997. *Dynamics of Marine Sands*. Thomas Telford, London.
- Soulsby, R. L., L. Hamm, G. Klopman, D. Myrhaug, R. R. Simons and G. P. Thomas, 1993. "Wave-current interaction within and outside the bottom boundary layer." *Coastal Engineering* 21: 41–69.

- Steetzel, H. J., 1987. *Systematic research on the effectiveness of dune toe revetments - Large scale model investigation*. Tech. Rep. H298-I, Delft Hydraulics.
- Steetzel, H. J., 1993. *Cross-shore transport during storm surges*. Ph.D. thesis, Delft University of Technology.
- Stelling, G. S. and S. P. A. Duinmeijer, 2003. "A staggered conservative scheme for every Froude number in rapidly varied shallow water flows." *International Journal for Numerical Methods in Fluids* 43: 1329–1354.
- Stive, M. J. F. and H. J. De Vriend, 1994. "Shear stresses and mean flow in shoaling and breaking waves." In B. L. Edge, ed., *24th International Conference on Coastal Engineering*, pages 594–608. ASCE, Reston, Virginia, USA.
- Stockdon, H. F., R. A. Holman, P. A. Howd and A. H. Sallenger, 2006. "Empirical parameterization of setup, swash, and runup." *Coastal Engineering* 53: 573–588.
- Sutherland, J., A. H. Peet and R. L. Soulsby, 2004. "Evaluating the performance of morphological models." *Coastal Engineering* 51 (8–9): 917–939.
- Svendsen, I. A., 1984. "Wave heights and set-up in a surf-zone." *Coastal Engineering* 8: 303–329.
- Thornton, E. B., J. MacMahan and A. H. Sallenger, 2007. "Rip currents, mega-cusps, and eroding dunes." *Marine Geology* 240 (1–4): 151–167. DOI: [10.1016/j.margeo.2007.02.018](https://doi.org/10.1016/j.margeo.2007.02.018).
- Trouw, K., R. Houthuys, T. Lanckriet, N. Zimmermann, L. Wang, B. De Maerschalck, R. Delgado, T. Verwaest and F. Mostaert, 2015. "Wetenschappelijke bijstand zanddynamica: inventarisatie randvoorwaarden en morfologische impact van de Sinterklaasstorm op 6 december 2013." *WL Rapporten*.
- Tucker, M. J., 1954. "Surfbeats: sea waves of 1 to 5 minutes' period." In *Proceedings of Royal Society*, no. A in 202, pages 565–576. London.
- Turner, I. L. and G. Masselink, 2012. "Coastal gravel barrier hydrology – Observations from a prototype-scale laboratory experiment (BARDEX)." *Coastal Engineering* 63: 13 - 22. DOI: <https://doi.org/10.1016/j.coastaleng.2011.12.008>, ISSN 0378-3839, URL <http://www.sciencedirect.com/science/article/pii/S0378383911002006>.
BARDEX: a large-scale laboratory study of gravel barrier dynamics.
- Van Dongeren, A. R., A. J. H. M. Reniers, J. A. Battjes and I. A. Svendsen, 2003. "Numerical modeling of infragravity wave response during DELILAH." *Journal of Geophysical Research* 108 (C9): 3288. DOI: [10.1029/2002JC001332](https://doi.org/10.1029/2002JC001332).
- Van Dongeren, A. R. and I. A. Svendsen, 1997. "Absorbing-generating boundary condition for shallow water models." *Journal of Waterway, Port, Coastal and Ocean Engineering* pages 303–313.
- Van Gent, M. R. A. and E. M. Coeveld, 2007. *Influence of collapsed revetments on dune erosion*. Tech. Rep. H4731, Delft Hydraulics.
- Van Gent, M. R. A., J. S. M. Van Thiel de Vries, E. M. Coeveld, J. H. De Vroeg and J. Van de Graaff, 2008. "Large-scale dune erosion tests to study the influence of wave periods." *Coastal Engineering* 55 (12).
- Van Noorloos, J. C., 2003. *Energy transfer between short wave groups and bound long waves on a plane slope*. Master's thesis, Delft University of Technology.

- Van Rijn, L. C., D. J. R. Walstra, B. Grasmeijer, J. Sutherland, S. Pan and J. P. Sierra, 2003. "The predictability of cross-shore bed evolution of sandy beaches at the time scale of storms and seasons using process-based profile models." *Coastal Engineering* 47 (3): 295–327. DOI: 10.1016/S0378-3839(02)00120-5. ISSN 0378-3839.
- Van Rooijen, A. A., R. T. McCall, J. S. M. Van Thiel de Vries, A. R. Van Dongeren, A. J. H. M. Reniers and J. A. Roelvink, 2016. "Modeling the effect of wave-vegetation interaction on wave setup." *J. Geophys. Res. Oceans* 121: 4341–4359. DOI: 10.1002/2015JC011392.
- Vellinga, P., 1981. *The functioning of dune revetments during a super storm surge.* Tech. Rep. M1797, Delft Hydraulics. In Dutch.
- Vellinga, P., 1984. *Scale series dune erosion: Large scale tests in Deltaflume.* Tech. Rep. M1263 part III, Delft Hydraulics. In Dutch.
- Vellinga, P., 1986. *Beach and Dune Erosion during Storm Surges.* Ph.D. thesis, Delft University of Technology.
- Visser, P. J., 1998. *Breach growth in sand dikes.* Ph.D. thesis, Delft University of Technology.
- Vries, J. S. M. Van Thiel de, 2009. *Dune erosion during storm surges.* Ph.D. thesis, Delft University of Technology.
- Vries, J. S. M. Van Thiel de, M. R. A. Van Gent, D. J. R. Walstra and A. J. H. M. Reniers, 2008. "Analysis of dune erosion processes in large-scale flume experiments." *Coastal Engineering* 55 (12).
- Wang, P. and M. H. Horwitz, 2007. "Erosional and depositional characteristics of regional overwash deposits caused by multiple hurricanes." *Sedimentology* 54: 545–564.
- Werf, J. Van der, R. Van Santen, M. Van Ormondt, C. Briere and A. Van Dongeren, 2011. "Operational model to simulate storm impact along the Holland Coast." In *Proceedings Coastal Sediments 2011*. Miami, Florida, USA.
- Wesselman, D., R. de Winter, A. Engelstad, R. McCall, A. van Dongeren, P. Hoekstra, A. Oost and M. van der Vegt, 2018. "The effect of tides and storms on the sediment transport across a Dutch barrier island." *Earth Surface Processes and Landforms* 43 (3): 579–592.
- Wijnberg, K. M., 2002. "Environmental controls on decadal morphologic behaviour of the Holland coast." *Marine Geology* 189 (3-4): 227–247.
- Zelt, J. A., 1986. *Tsunamis: the response of harbours with sloping boundaries to long wave excitation.* Ph.D. thesis, W.M. Keck Laboratory of Hydraulics and Water Resources, Division of Engineering and Applied Science, California Institute of Technology. 318 p.

A Model Performance Statistics

A.1 Introduction

In this Appendix the theory behind the Model Performance Statistics (MPS) used in the XBeach skillbed is explained. The MPS are used to quantify the performance of model results based on a comparison with measurement data. Different MPS parameters are used as each parameter has its own characteristics.

First an overview is given of the MPS parameters used in the XBeach skillbed, summarized in table form including some basic characteristics. Consequently, each MPS parameters listed in the overview table is further explained in separate sections.

A.2 MPS parameters

An overview of the MPS parameters used in the XBeach skillbed is given in [Table A.1](#).

Table A.1 MPS parameters

Parameter	Description	Ranges
ME & STD	Mean Error & Standard Deviation	0: perfect prediction
R	Correlation coefficient (range: [0 1])	1: perfect correlation
Rel. bias	Systematic error relative to the mean	low value: good performance
Sci	Scatter Index	low values: performance
BSS	Brier Skill Score (Sutherland et al., 2004)	see below
BSS	Brier Skill Score (Murphy and Epstein, 1989)	see below

Each parameter listed in the table is further explained in the following paragraphs.

A.3 Mean Error & Standard Deviation

The Mean Error (ME) and the Standard Deviation (STD) of the error of a time series are a useful measure to quantify model performance for parameters such as wave heights or water levels. The SD is in general not so useful when applied to morphological parameters such as the bed level evolution.

$$ME = \frac{1}{N} \sum_{i=1}^N (f_{comp,i} - f_{meas,i}) \quad (A.1)$$

$$STD = \sqrt{\frac{1}{N-1} \sum_{i=2}^N (f_{comp,i} - f_{meas,i} - ME)^2} \quad (\text{A.2})$$

A.4 Correlation coefficient

The Correlation Coefficient R is a measure quantifying the correlation of the measurements and simulation results, but does not indicate significance because the distributions of the series are not taken into account.

A.5 Relative Bias

The Relative Bias (Rel. Bias) is the systematic error relative to the mean. Relative low values of the mean can cause high values of the Rel. Bias.

$$Rel.Bias = \frac{\sum_{i=1}^N (f_{comp,i} - f_{meas,i})}{\sum_{i=1}^N \bar{f}_{meas.}} \quad (\text{A.3})$$

A.6 Scatter Index

The Scatter index (Sci) is the standard deviation relative to the mean value of the measured signal. Relative low values of the mean can cause high values of the Sci.

$$Sci = \frac{\sqrt{\frac{1}{N-1} \sum_{i=2}^N (f_{comp,i} - f_{meas,i} - ME)^2}}{\bar{f}_{meas.}} \quad (\text{A.4})$$

A.7 Brier Skill Score

The Brier Skill Score (BSS) calculates the performance of the prediction relative to a baseline prediction. The BSS calculates the mean square difference between the prediction and observation with the mean square difference between baseline prediction and observation.

$$BSS = 1 - \frac{\frac{1}{N} \sum_{i=1}^N (z_{b,c} - z_{b,m})^2}{\frac{1}{N} \sum_{i=1}^N (z_{b,0} - z_{b,m})^2} \quad (\text{A.5})$$

where $z_{b,c}$ is the computed bottom, $z_{b,m}$ is the measured bottom and $z_{b,0}$ is the initial bottom (variables taken at each cross-shore coordinate i).

Perfect agreement gives a Brier score of 1, whereas modelling the baseline condition gives a score of 0. If the model prediction is further away from the final measured condition than the baseline prediction, the skill score is negative. Van Rijn *et al.* (2003) proposed a classification for the Brier Skill Score as shown in Table A.2.

The BSS is very suitable for the prediction of bed evolution. The baseline prediction for morphodynamic modelling will usually be that the initial bed remains unaltered. In other words, the initial bathymetry is used as the baseline prediction for the final bathymetry. A limitation of the BSS is that it cannot account for the migration direction of a bar; it just evaluates whether the computed bed level (at time t) is closer to the measured bed level (at time t) than the initial bed level. If the computed bar migration is in the wrong direction, but relatively small; this may result in a higher BSS compared to the situation with bar migration in the right direction, but much too large. The BSS will even be negative, if the bed profile in the latter situation is further away from the measured profile than the initial profile. The limitation shown here is that position and amplitude errors are included in the BSS. Distinguishing position errors from amplitude errors, requires a visual inspection of measured and modelled profiles or the calculation of further statistics ([Murphy and Epstein, 1989](#)). The BSS can be extremely sensitive to small changes when the denominator is low, in common with other non-dimensional skill scores derived from the ratio of two numbers.

Table A.2 Brier Skill Score quantification ([Van Rijn et al., 2003](#))

Qualification	Brier Skill Score
Excellent	1.0 - 0.8
Good	0.8 - 0.6
Reasonable fair	0.6 - 0.3
Poor	0.3 - 0.0
Bad	<0.0

A.8 Brier Skill Score ([Murphy and Epstein, 1989](#))

[Murphy and Epstein \(1989\)](#) decomposed the BSS, leading to contributions due to errors in predicting the amplitude (α), the phase (β) and the mean (γ) as presented in [Table A.3](#). The decomposition facilitates linking performance quantifications to model processes and accordingly bringing the model performance to a higher level.

$$BSS = \frac{\alpha - \beta - \gamma + \epsilon}{1 + \epsilon} \quad (\text{A.6})$$

$$\alpha = r_{Y'X'}^2; \beta = (r_{Y'X'} - \frac{\sigma_{Y'}}{\sigma_{X'}})^2; \gamma = (\frac{\langle Y' \rangle - \langle X' \rangle}{\sigma_{X'}})^2; \epsilon = \frac{\langle X' \rangle^2}{\sigma_{X'}} \quad (\text{A.7})$$

Table A.3 Brier Skill Score decomposition factors (Murphy and Epstein, 1989)

Factor	Indication	Perfect modelling
phase error (α)	transport locations	$\alpha = 1$
amplitude error (β)	transport volumes	$\beta = 0$
map mean error (γ)	-	$\gamma = 0$
normalization term (ϵ)	-	-

Van Rijn *et al.* (2003) also proposed a classification for the decomposed Brier Skill Score as shown in Table A.4.

Table A.4 Brier Skill Score (Murphy and Epstein, 1989) quantification (Van Rijn *et al.*, 2003)

Qualification	Brier Skill Score
Excellent	1.0 - 0.5
Good	0.5 - 0.2
Reasonable fair	0.2 - 0.1
Poor	0.1 - 0.0
Bad	<0.0

B Overview

In the table below, the statuses of all tests found in the skillbed are summarized. The first three columns identify the test with a combination of a binary, test and run name. The following three columns provide information on the status of that specific run. These columns indicate whether the model ran, the analysis ended successfully and whether the run used default or custom settings. An empty status means the run or analysis is ignored, a cross indicates failure and a checkmark indicates success. The other columns in the table provide information on the model configuration.

Tests can be run multiple times using different settings. Different runs are identified by a run name, which follows after the test name. If a test runs once only, it is common use to name the run *default*. This is not the same as running a test with default settings, which is indicated in the “Default settings” column.

The table provides all tests ran in a single skillbed run. This report not necessarily uses all available tests. Therefore, not all tests in the table are necessarily found in the continuation of this report.

Table B.1 Status overview skillbed tests

Test	Run	Status	Matlab	Default settings	Configuration	Waves*	Water levels**	Fractions	Morphology	Hard layers	Groundwater flow
Assateague_Island	profA	✓	✓	✓	1D	ST	C	1	✓		
Assateague_Island	profB1	✓	✓	✓	1D	ST	C	1	✓		
Assateague_Island	profB2	✓	✓	✓	1D	ST	C	1	✓		
Assateague_Island	profC	✓	✓	✓	1D	ST	C	1	✓		
Bardex	E10	✓	✓	✓	1D	WG	C	1			
Boers	1A_SB_BOI	✓	✓	✓	1D	WG	C	1			
Boers	1B_SB_BOI	✓	✓	✓	1D	WG	C	1			
Boers	1C_SB_BOI	✓	✓	✓	1D	WG	C	1			
Boers_nh	1A_nh	✓	✓	✓	1D	WG	C	1			
Boers_nh	1B_nh	✓	✓	✓	1D	WG	C	1			
Boers_nh	1C_nh	✓	✓	✓	1D	WG	C	1			
Buckley	sim1	✓	✓	✓	1D	WG	C	1			
Buckley	sim12	✓	✓	✓	1D	WG	C	1			
Buckley	sim2	✓	✓	✓	1D	WG	C	1			
Buckley	sim9	✓	✓	✓	1D	WG	C	1			
CarrierGreenspan	default	✓	✓	✓	1D	ST	C	1			
Chesil	default	✓	✓	✓	1D	ST	C	1			

Table B.1 Status overview skillbed tests

Test	Run	Status	Matlab	Default settings	Configuration	Waves*	Water levels**	Fractions	Morphology	Hard layers	Groundwater flow
Curvi_Island	default	✓	✓	✓	2D	WG	C	1			
DamBreak	1D_dry...	✓	✓	✓	1D	WG	C	1			
DamBreak	1D_dry...	✓	✓	✓	1D	WG	C	1			
DamBreak	1D_wet...	✓	✓	✓	1D	WG	C	1			
DamBreak	1D_wet...	✓	✓	✓	1D	WG	C	1			
DamBreak	2D_dry...	✓	✓	✓	1D	WG	C	1			
DamBreak	2D_dry...	✓	✓	✓	1D	WG	C	1			
DamBreak	2D_wet...	✓	✓	✓	1D	WG	C	1			
DamBreak	2D_wet...	✓	✓	✓	1D	WG	C	1			
Delilah_199010131000	default	✓	✓	✓	2D	WG	C	1			
Deltaflume2006	DP01	✓	✓	✓	1D	WG	C	2	✓		
Deltaflume2006	DP02	✓	✓	✓	1D	WG	C	2	✓		
Deltaflume2006	T01_BOI	✓	✓	✓	1D	WG	C	2	✓		
Deltaflume2006	T01_BO...	✓	✓	✓	1D	WG	C	2	✓		
Deltaflume2006	T01_zebra	✓	✓	✓	1D	WG	C	2	✓		
Deltaflume2006	T02_BOI	✓	✓	✓	1D	WG	C	2	✓		
Deltaflume2006	T03_BOI	✓	✓	✓	1D	WG	C	2	✓		
Deltaflume2006	T04	✓	✓	✓	1D	WG	C	2	✓		
Deltaflume2006	T08_BOI	✓	✓	✓	1D	WG	C	2	✓		
DeltaflumeH298	T1	✓	✓	✓	1D	WG	C	1	✓	✓	
DeltaflumeH298	T2	✓	✓	✓	1D	WG	C	1	✓	✓	
DeltaflumeH298	T3	✓	✓	✓	1D	WG	C	1	✓	✓	
DeltaflumeLIP11D	1B	✓	✓	✓	1D	WG	C	1	✓		
DeltaflumeLIP11D	1C	✓	✓	✓	1D	WG	C	1	✓		
DeltaflumeLIP11D	2E_BOI	✓	✓	✓	1D	WG	C	1	✓		
Deltaflume_H4731	T14_BOI	✓	✓	✓	1D	WG	C	1	✓	✓	
Deltaflume_M1263_III	Test-1_BOI	✓	✓	✓	1D	WG	C	1	✓		
Deltaflume_M1263_III	Test-2_BOI	✓	✓	✓	1D	WG	C	1	✓		
Deltaflume_M1263_III	Test-3_BOI	✓	✓	✓	1D	WG	C	1	✓		
Deltaflume_M1263_III	Test-4_BOI	✓	✓	✓	1D	WG	C	1	✓		
Deltaflume_M1263_III	Test-5_BOI	✓	✓	✓	1D	WG	C	1	✓		
Deltaflume_M1797	T01_BOI	✓	✓	✓	1D	WG	V	1	✓		
Drifters	default	✓	✓	✓	2D	?	C	1			
Egmond	T_-1001	✓	✓	✓	1D	WG	V	1	✓		

Table B.1 Status overview skillbed tests

Test	Run	Status	Matlab	Default settings	Configuration	Waves*	Water levels**	Fractions	Morphology	Hard layers	Groundwater flow
Egmond	T_-1001_MS	✓	✓	✓	1D	WG	V	1	✓		
Egmond	T_-1755	✓	✓	✓	1D	WG	V	1	✓		
Egmond	T_-1755_MS	✓	✓	✓	1D	WG	V	1	✓		
Egmond	T_-249	✓	✓	✓	1D	WG	V	1	✓		
Egmond	T_-249_MS	✓	✓	✓	1D	WG	V	1	✓		
Egmond	T_-502	✓	✓	✓	1D	WG	V	1	✓		
Egmond	T_-502_MS	✓	✓	✓	1D	WG	V	1	✓		
Egmond	T_0	✓	✓	✓	1D	WG	V	1	✓		
Egmond	T_0_MS	✓	✓	✓	1D	WG	V	1	✓		
Egmond	T_1001	✓	✓	✓	1D	WG	V	1	✓		
Egmond	T_1001_MS	✓	✓	✓	1D	WG	V	1	✓		
Egmond	T_499	✓	✓	✓	1D	WG	V	1	✓		
Egmond	T_499_MS	✓	✓	✓	1D	WG	V	1	✓		
FireIsland	005	✓	✓	✓	1D	WG	V	1	✓		
FireIsland	105	✓	✓	✓	1D	WG	V	1	✓		
FireIsland	205	✓	✓	✓	1D	WG	V	1	✓		
FireIsland	305	✓	✓	✓	1D	WG	V	1	✓		
FireIsland	365	✓	✓	✓	1D	WG	V	1	✓		
FireIsland	405	✓	✓	✓	1D	WG	V	1	✓		
GLOBEX	A1_GLOBEX	✓	✓	✓	1D	WG	C	1			
GLOBEX	A2_GLOBEX	✓	✓	✓	1D	WG	C	1			
GLOBEX	A3_GLOBEX	✓	✓	✓	1D	WG	C	1			
GWK86	T01	✓	✓	✓	1D	WG	V	1	✓		
GWK86	T02	✓	✓	✓	1D	WG	V	1	✓		
GWK86	T03	✓	✓	✓	1D	WG	V	1	✓		
GWK86	T04	✓	✓	✓	1D	WG	V	1	✓		
GWK86	T05	✓	✓	✓	1D	WG	V	1	✓		
GWK86	T06	✓	✓	✓	1D	WG	V	1	✓		
GWK98	A9_BOI	✓	✓	✓	1D	WG	C	1	✓		
GWK98	B2_BOI	✓	✓	✓	1D	WG	C	1	✓		
GWK98	C2_BOI	✓	✓	✓	1D	WG	C	1	✓		
GWK98	F1_BOI	✓	✓	✓	1D	WG	C	1	✓		
GWK98	H2_BOI	✓	✓	✓	1D	WG	C	1	✓		
Holland1953	BOI	✓	✓	✓	1D	WG	V	1	✓		

Table B.1 Status overview skillbed tests

Test	Run	Status	Matlab	Default settings	Configuration	Waves*	Water levels**	Fractions	Morphology	Hard layers	Groundwater flow
Holland1976	Raai1085	✓	✓	✓	1D	WG	V	1	✓		
Holland1976	Raai1115	✓	✓	✓	1D	WG	V	1	✓		
Holland1976	Raai1175	✓	✓	✓	1D	WG	V	1	✓		
Holland1976	Raai3400	✓	✓	✓	1D	WG	V	1	✓		
Holland1976	Raai3700	✓	✓	✓	1D	WG	V	1	✓		
Holland1976	Raai4000	✓	✓	✓	1D	WG	V	1	✓		
Holland1976	Raai4050	✓	✓	✓	1D	WG	V	1	✓		
Holland1976	Raai4100	✓	✓	✓	1D	WG	V	1	✓		
Holland1976	Raai4500	✓	✓	✓	1D	WG	V	1	✓		
Holland1976	Raai4900	✓	✓	✓	1D	WG	V	1	✓		
Holland1976	Raai4950	✓	✓	✓	1D	WG	V	1	✓		
Holland1976	Raai5000	✓	✓	✓	1D	WG	V	1	✓		
Holland1976	Raai568	✓	✓	✓	1D	WG	V	1	✓		
Holland1976	Raai588	✓	✓	✓	1D	WG	V	1	✓		
Holland1976	Raai5900	✓	✓	✓	1D	WG	V	1	✓		
Holland1976	Raai5925	✓	✓	✓	1D	WG	V	1	✓		
Holland1976	Raai5950	✓	✓	✓	1D	WG	V	1	✓		
Holland1976	Raai5975	✓	✓	✓	1D	WG	V	1	✓		
Holland1976	Raai6000	✓	✓	✓	1D	WG	V	1	✓		
Holland1976	Raai6025	✓	✓	✓	1D	WG	V	1	✓		
Holland1976	Raai6050	✓	✓	✓	1D	WG	V	1	✓		
Holland1976	Raai6075	✓	✓	✓	1D	WG	V	1	✓		
Holland1976	Raai608	✓	✓	✓	1D	WG	V	1	✓		
Holland1976	Raai6100	✓	✓	✓	1D	WG	V	1	✓		
Holland1976	Raai628	✓	✓	✓	1D	WG	V	1	✓		
Holland1976	Raai648	✓	✓	✓	1D	WG	V	1	✓		
Holland1976	Raai6500	✓	✓	✓	1D	WG	V	1	✓		
Holland1976	Raai7000	✓	✓	✓	1D	WG	V	1	✓		
Holland1976	Raai7050	✓	✓	✓	1D	WG	V	1	✓		
Holland1976	Raai7100	✓	✓	✓	1D	WG	V	1	✓		
Langeoog	profile_A	✓	✓	✓	1D	WG	V	1	✓		
Langeoog	profile_B	✓	✓	✓	1D	WG	V	1	✓		
Langeoog	profile_C	✓	✓	✓	1D	WG	V	1	✓		
Langeoog	profile_D	✓	✓	✓	1D	WG	V	1	✓		

Table B.1 Status overview skillbed tests

Table B.1 Status overview skillbed tests

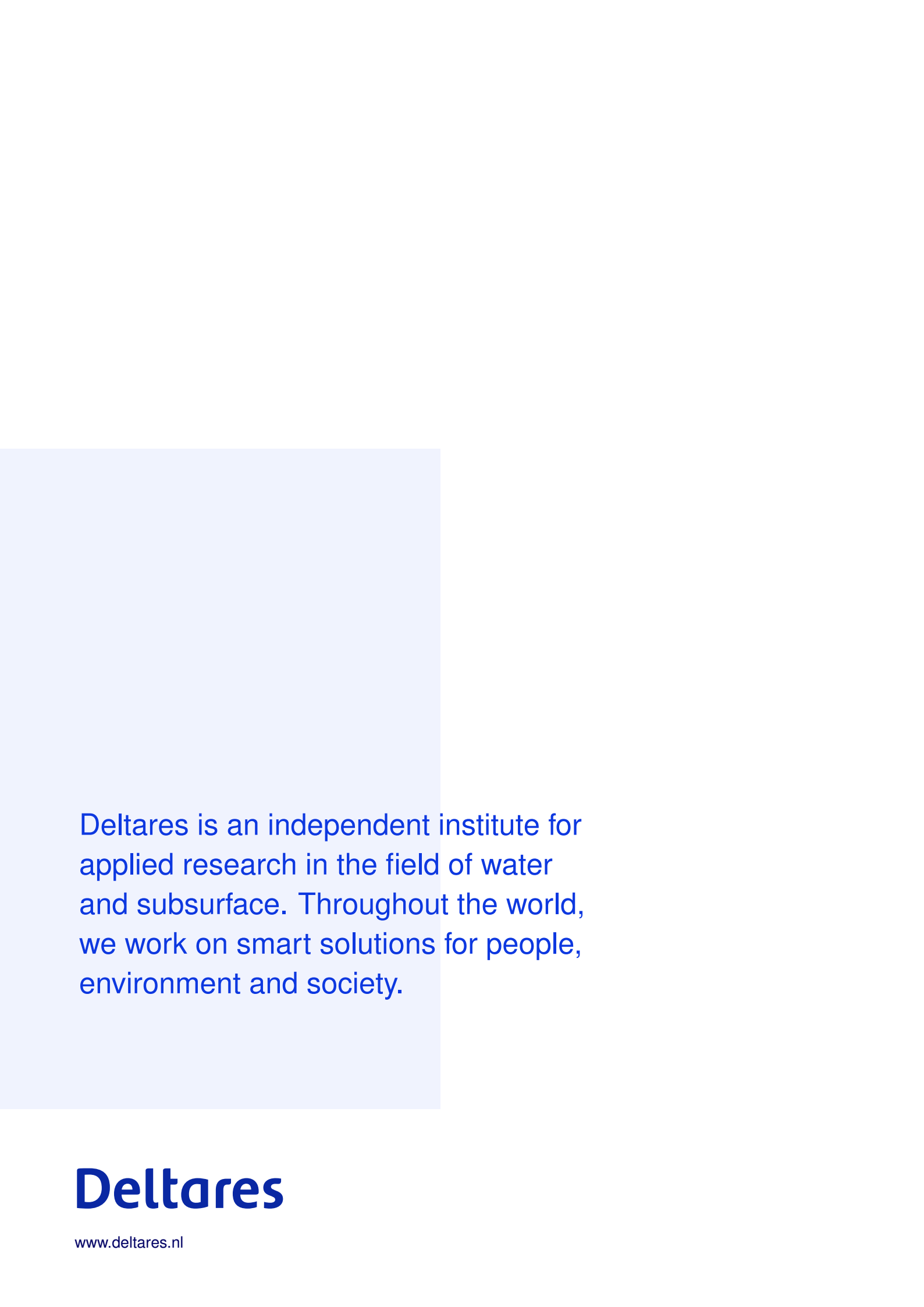
Test	Run	Status	Matlab	Default settings	Configuration	Waves*	Water levels**	Fractions	Morphology	Hard layers	Groundwater flow
Vegetation	lovas_...	✓	✓	✓	1D	WG	C	1			
Vegetation	lovas_...	✓	✓	✓	1D	WG	C	1			
Vegetation	lovas_...	✓	✓	✓	1D	WG	C	1			
Vlaanderen	T_117	✓	✓	✓	1D	WG	V	1	✓		
Vlaanderen	T_118	✓	✓	✓	1D	WG	V	1	✓		
Vlaanderen	T_119	✓	✓	✓	1D	WG	V	1	✓		
Vlaanderen	T_120	✓	✓	✓	1D	WG	V	1	✓		
Vlaanderen	T_121	✓	✓	✓	1D	WG	V	1	✓		
Vlaanderen	T_60	✓	✓	✓	1D	WG	V	1	✓		
Vlaanderen	T_61	✓	✓	✓	1D	WG	V	1	✓		
Vlaanderen	T_62	✓	✓	✓	1D	WG	V	1	✓		
Vlaanderen	T_63	✓	✓	✓	1D	WG	V	1	✓		
Vlaanderen	T_64	✓	✓	✓	1D	WG	V	1	✓		
Vlaanderen	T_69	✓	✓	✓	1D	WG	V	1	✓		
Vlaanderen	T_71	✓	✓	✓	1D	WG	V	1	✓		
Vlaanderen	T_79	✓	✓	✓	1D	WG	V	1	✓		
Vlaanderen	T_80	✓	✓	✓	1D	WG	V	1	✓		
Vlaanderen	T_83	✓	✓	✓	1D	WG	V	1	✓		
Zelt_Case1	default	✓	✓	✓	2D	WG	C	1			
Zwin_T01	default	✓	✓	✓	2D	ST	V	1	✓		
long_wave_propag...	default	✓	✓	✓	1D	ST	C	1			
longcrested_refr...	1bin_a...	✓	✓	✓	2D	WG	C	1			
longcrested_refr...	1bin_a...	✓	✓	✓	2D	WG	C	1			
longcrested_refr...	1bin_a...	✓	✓	✓	2D	WG	C	1			
longcrested_refr...	3bin_a...	✓	✓	✓	2D	WG	C	1			
longcrested_refr...	3bin_a...	✓	✓	✓	2D	WG	C	1			
longcrested_refr...	3bin_a...	✓	✓	✓	2D	WG	C	1			
longcrested_refr...	3bin_a...	✓	✓	✓	2D	WG	C	1			
longcrested_refr...	5bin_a...	✓	✓	✓	2D	WG	C	1			
longcrested_refr...	5bin_a...	✓	✓	✓	2D	WG	C	1			
longcrested_refr...	5bin_a...	✓	✓	✓	2D	WG	C	1			
longcrested_refr...	10deg	✓	✓	✓	1D	ST	C	1			
longcrested_refr...	2p5deg	✓	✓	✓	1D	ST	C	1			
longcrested_refr...	5deg	✓	✓	✓	1D	ST	C	1			
longcrested_refr...	snellius	✓	✓	✓	1D	ST	C	1			

Table B.1 Status overview skillbed tests

Test	Run	Status	Matlab	Default settings	Configuration	Waves*	Water levels**	Fractions	Morphology	Hard layers	Groundwater flow
tideonly	blanke...	✓	✓	✓	2D	ST	V	1			
tideonly	default	✓	✓	✓	2D	ST	V	1			

* ST = stationary, WG = wave groups, NH = non-hydrostatic

** C = constant, V = varying



Deltares is an independent institute for applied research in the field of water and subsurface. Throughout the world, we work on smart solutions for people, environment and society.

Deltares

www.deltares.nl